Tropical Water Quality Hub

National Environmental Science Programme

Final Report

Development and application of automated tools for high resolution gully mapping and classification from lidar data

James Daley, Justin C. Stout, Graeme Curwen, Andrew P. Brooks and John Spencer

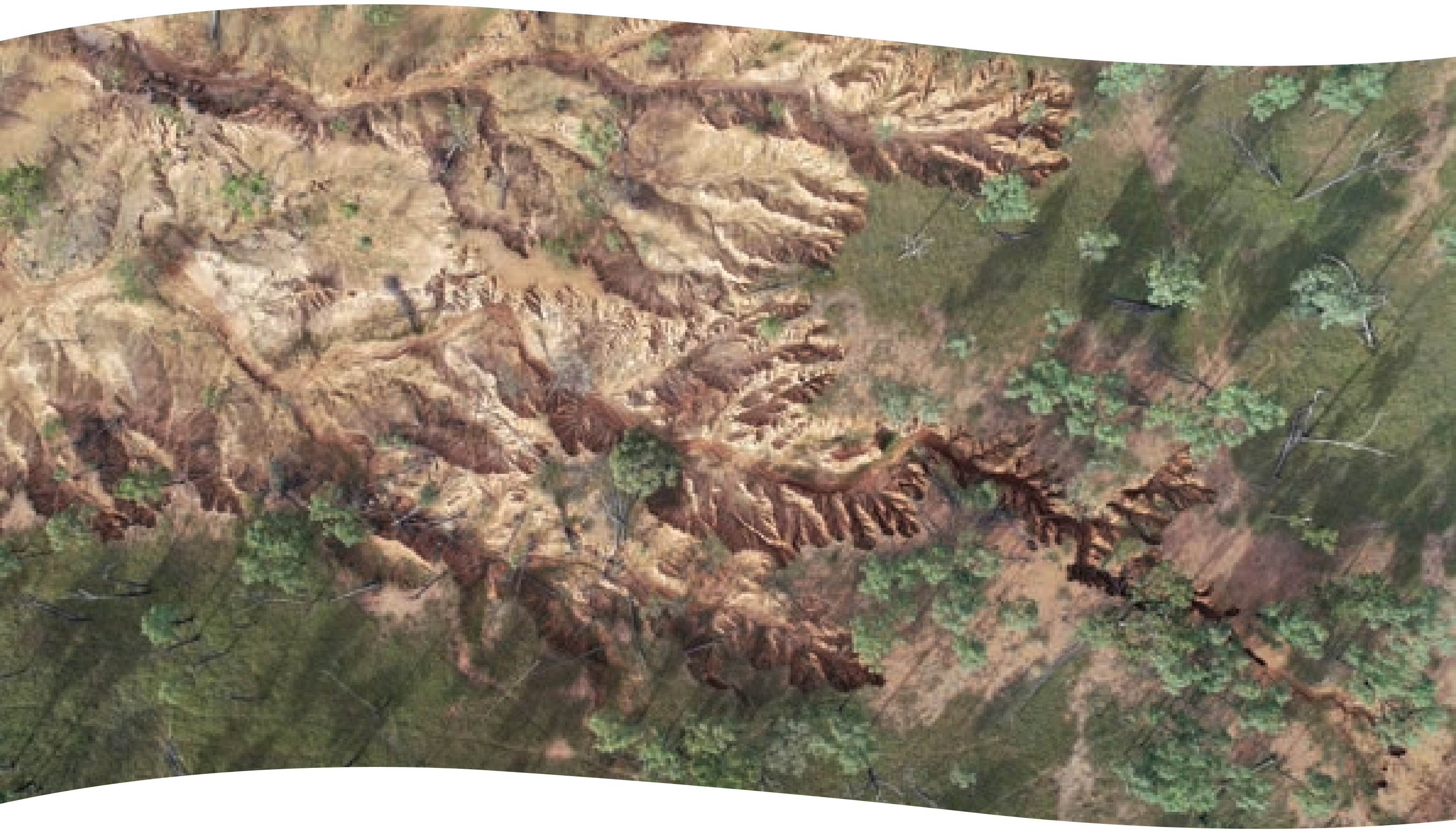

Griffith UNIVERSITY

Development and application of automated tools for high resolution gully mapping and classification from lidar data

James Daley, Justin C. Stout, Graeme Curwen, Andrew P. Brooks and John Spencer

Precision Erosion and Sediment Management Research Group (PrESM),
Coastal and Marine Research Centre, Griffith University

Supported by the Australian Government's
National Environmental Science Program
Project 5.10 Development and application of automated tools for high resolution gully mapping and classification from LiDAR data.

National Library of Australia Cataloguing-in-Publication entry:
978-1-925514-83-4

This report should be cited as:
Daley, J., Stout, J.C., Curwen, G., Brooks, A.P. and Spencer, J. (2021) *Development and application of automated tools for high resolution gully mapping and classification from lidar data.* Report to the National Environmental Science Program. Reef and Rainforest Research Centre Limited, Cairns (169pp.).

Published by the Reef and Rainforest Research Centre on behalf of the Australian Government's National Environmental Science Program (NESP) Tropical Water Quality (TWQ) Hub.

The Tropical Water Quality Hub is part of the Australian Government's National Environmental Science Program and is administered by the Reef and Rainforest Research Centre Limited (RRRC). The NESP TWQ Hub addresses water quality and coastal management in the World Heritage listed Great Barrier Reef, its catchments and other tropical waters, through the generation and transfer of world-class research and shared knowledge.

Cover photographs: (front) An active hillslope gully complex migrating across the landscape in the Bowen catchment. Image: James Daley. (back) View of the Bowen river showing a large alluvial gully complex. Image: Andrew Brooks.

This report is available for download from the NESP Tropical Water Quality Hub website:
http://www.nesptropical.edu.au

CONTENTS

LIST OF TABLES

LIST OF FIGURES

ACRONYMS

AUC .... Area Under the Curve
ASTER .... Advanced Spaceborne Thermal Emission and Reflection Radiometer (satellite imagery)
BBB .... Bowen, Bogie and Broken catchments (sub-catchments of the Burdekin River)
CSIRO .... Commonwealth Scientific and Industrial Research Organisation
CYNRM .... Cape York Natural Resource Management
DEM .... Digital Elevation Model
DES .... Department of Environment and Science (Qld Govt.).
DNRME .... Department of Natural Resources Mines and Energy (Qd Govt.)
DoD .... DEM of Difference (i.e. the net result from subtracting the elevations in one DEM from another).
ECW .... Enhanced Compression Wavelet image. Herein used to refer to 0.1-m aerial imagery acquired alongside the lidar data
ELF .... Eroded Landforms
FBA .... Fitzroy Basin Association
GBR .... Great Barrier Reef
GBRF .... Great Barrier Reef Foundation
GECAT .... Gully Erosion Control Assessment Tool
GMT .... Gully Monitoring Tool
JCU .... James Cook University
MDHS .... Multi-directional hillshading
MrVBF .... Multi Resolution Valley Bottom Flatness index
MSAVI2 .... Modified secondary soil-adjusted vegetation index
NESP .... National Environmental Science Program
NRM .... Natural Resource Management
NQDT .... North Queensland Dry Tropics
OBIA .... object-based image analysis
OOA .... object-oriented image analysis object-based image analysis
P/A .... Presence/absence (gully mapping program)
PAE .... Potential Active Erosion
PLS .... Prior Land Surface
PrESM .... Precision Erosion and Sediment Management research group (Griffith University)
PS .... PlanetScope analytic surface reflectance data
PLS .... Prior Land Surface
QWMN .... Queensland Water Modelling Network
QDAF .... Queensland Department of Agriculture and Fisheries
RMSE .... Root Mean Square Error
ROC .... Receiver Operating Characteristics
ROI .... Region of interest
RRRC .... Reef and Rainforest Research Centre
TRI .... Terrain Ruggedness Index
TWQ .... Tropical Water Quality Hub (NESP Research Hub)
ROI .... Region of interest
TRI .... Terrain Ruggedness Index

ACKNOWLEDGEMENTS

We gratefully acknowledge the ongoing support for this research from the Australian Government's National Environmental Science Program (NESP) Tropical Water Quality (TWQ) Hub with particular thanks to the tireless work of Damian Burrows, Sheriden Morris, Julie Carmody at the Reef and Rainforest Research Centre (RRRC) and James Cook University (JCU) staff who have kept the whole show on the road. We thank the Australian Government Reef Trust Program for the provision of the lidar data, and we thank John Gallant for his efforts in coordinating the lidar acquisition and processing. We also thank Robin Thwaites for fruitful discussion on the framework for defining gullies at the conception of this project.

We thank Dr. Tim Pietsch, Dr. James Grove and Dr. Greg Pasternack for their thoughtful and thorough reviews of this report. The final report was greatly improved as a result of their input.

EXECUTIVE SUMMARY

Given the significance of gully erosion as one of the dominant sources of fine sediment and particulate nutrient pollution to the Great Barrier Reef (GBR) Lagoon, there is now a major focus on the remediation of gullies in order to meet the Reef Water quality targets for the GBR Lagoon by 2030 and 2050. To ensure water quality targets are met in the most cost-effective manner, there is an increasing need to identify the individual gullies that are a priority for remediation. The existing one ha presence/absence mapping that has to date been the primary dataset available for prioritising resources in the GBR, cannot provide sufficient detail to enable management prioritisation at the required gully scale.

This project addresses this issue by providing a method to enable gullies to be consistently mapped from lidar at four orders of magnitude higher resolution than the previous one ha resolution mapping (i.e. 1 m^2).

Through this project we have developed methods for mapping and characterising gullies in GBR catchments, which will have wider application in identifying other sediment sources (e.g. stream bank erosion). It provides a repeatable method by which gullies have been mapped across ~5,300 km^2 and has produced the largest and most complete inventory of gullies in a subset of the GBR catchment, albeit in areas targeted for having a high concentration of gullies (Table 1). The methods developed in this report map eroded landforms (ELFs) and within these features, actively eroding gullies, across a large spatial area using a one meter-resolution Digital Elevation Model (DEM) derived from air-borne lidar and largely existing tools in ArcGIS. Mapping gullies is not as straight forward as it may seem as there are many “gully like” features in the landscape, and a key aspect of this project was the development of methods to filter the features that are not gullies (including small ephemeral stream channels). Tools developed for the filtering process also provide the means to determine the relative activity of the mapped gullies. These gully activity maps can then be used by managers and researchers to help locate and prioritise gullies for remediation.

Of the 5,300 km^2 mapped in the three catchments, the total area of gullies represents between 0.26% and 1.32% of the landscape, comprising around 26,000 gullies (Table 1). As more lidar data becomes available it will now be feasible to carry out similar mapping at this resolution across large areas.

Table 1: Summary statistics of gullies within each study area.

	BBB	Fitzroy	Normanby	**Total**
Area of analysis (km^2)	3,507	1,210	571	**5,288**
No. gullies	22,311	1,785	1,820	**25,916**
Gully area (ha)	4,621	312	563	**5,496**
Proportion of land gullied (%)	1.32	0.26	0.99	**1.04**
Proportion alluvial:hillslope (%)	43	60	91	**49**

Key features of the method developed through the project:

- Validation of the gully mapping was conducted at two levels of analysis. Firstly, validation of boundary mapping against both 22 hand digitised and 12 field tracking data indicates a high correlation between datasets. Root Mean Square Errors (RMSE) of 3.66 m and 3.29 m, respectively, were found in the difference between absolute boundary positions. Secondly, validation of the semi-automated ELF-gully filtering approach against manual observation and selection yielded a high accuracy of 0.86, an F1 statistic of 0.7 and Cohen's Kappa of 0.61.
- We have developed an index of Potential Active Erosion (PAE) that enables the identification of actively eroding gullies from a single lidar DEM (i.e. without the need for repeat lidar).
- When correlated against measured erosion pixel data measured from repeat lidar DoD data (based on data from 645 gullies) PAE was able to predict eroding pixels within gullies with a high level of certainty (R^2~0.7 across all landscapes; R^2 up to 0.89 in local areas).
- We have developed an objective method for modelling the pre—erosion land surface in gullied landscapes. This allows us to accurately determine the gully volume, and hence total of gully life sediment production. Current methods used in the gully toolbox (Wilkinson et al., 2019) implicitly assume a flat prior land surface which potentially over-estimates gully volume significantly.
- The prior land surface (PLS) reconstruction method also allows us to quantify the primary gully dimensions (e.g. average gully width and length, mean and maximum gully depth) as well as a suite of additional gully metrics for the database of ~ 26,000 gullies mapped to date (e.g. Figure 4).

Key findings from the mapping include:

- In the Fitzroy and Laura catchments the majority of gullies are alluvial (60% and 90% respectively), while in the BBB alluvial gullies are outnumbered by colluvial gullies (43:57%)
- Alluvial gullies dominate when comparing the total estimated gully volumes by gully type (Figure 3), which means that lifetime sediment yields are evened up between the gully types in the BBB.
- Given the fundamental differences in gully dimensions according to gully type (i.e. alluvial vs hillslope) it is no longer tenable to apply average gully dimensions at the catchment scale (Figure 4). The outliers in the gully dimensional plots represent the gullies which yield a disproportionate amount of the total sediment load. Hence if the mean conditions are applied to all gullies in the presence/absence dataset, this will bias the spatial distribution of priority gully areas.
- In each catchment the gully lifetime sediment yield is highly skewed, with a relatively small number of gullies contributing a large proportion of the net gully lifetime sediment yield (Figure 5).
    - in the BBB 2% of gullies contribute 30% of the total sediment yield; whereas 6% contribute 50%.
    - In the Fitzroy 1.5% of gullies produce 30% of the sediment yield whereas 4% of the gullies produce 50% of the yield.
    - In the Laura 3.5% of gullies produce 30% of the sediment yield and 10% of the gullies produce 50% of the yield.

- The highly skewed nature of the gully population in terms of lifetime sediment yield is also reflected in the dimension data (e.g. widths and depth) (Figure 4).
- Cumulatively the gullies mapped in this 5,300km area have eroded a total of 156M m^3 of sediment which is equivalent of approximately 470 t/ha (gully area) on average across their lifetime.
- The net volume of this erosion is equivalent to 0.28 SydHarbs (i.e. 28% of the volume of Sydney Harbour) or about 25% of the volume of Uluru.
- The mapping data shows that when we compare the ratios of the gully soft and hard margin areas to their respective contributing gully catchment area there are significant differences according to gully type and different landscapes (Figure 6, Table 2).
- For the alluvial gullies between 48-67% of gullies have a catchment/ gully area ratio of < 2 (i.e. the catchment area is the same size as the gully or less) based on the soft margins; or 8-26% based on the hard margins.
- For Colluvial gullies the ratios are 0.6-32% for the catchment area/ gully soft margin ratios < 2 and 0-7% for the hard margins; while for the rugged gullies the ratios are 2-20% for the soft margins and 0.3 % for the hard margins;
- This has significant implications for gully remediation strategies that rely on passive management of the gully catchment as the primary mechanism for managing erosion within the gully. It is unlikely that a measurable change in gully sediment yield will be achieved through minor changes to the rainfall/runoff response in circumstances where the catchment area ratio is small (e.g. 2 – 3 times the gully area).

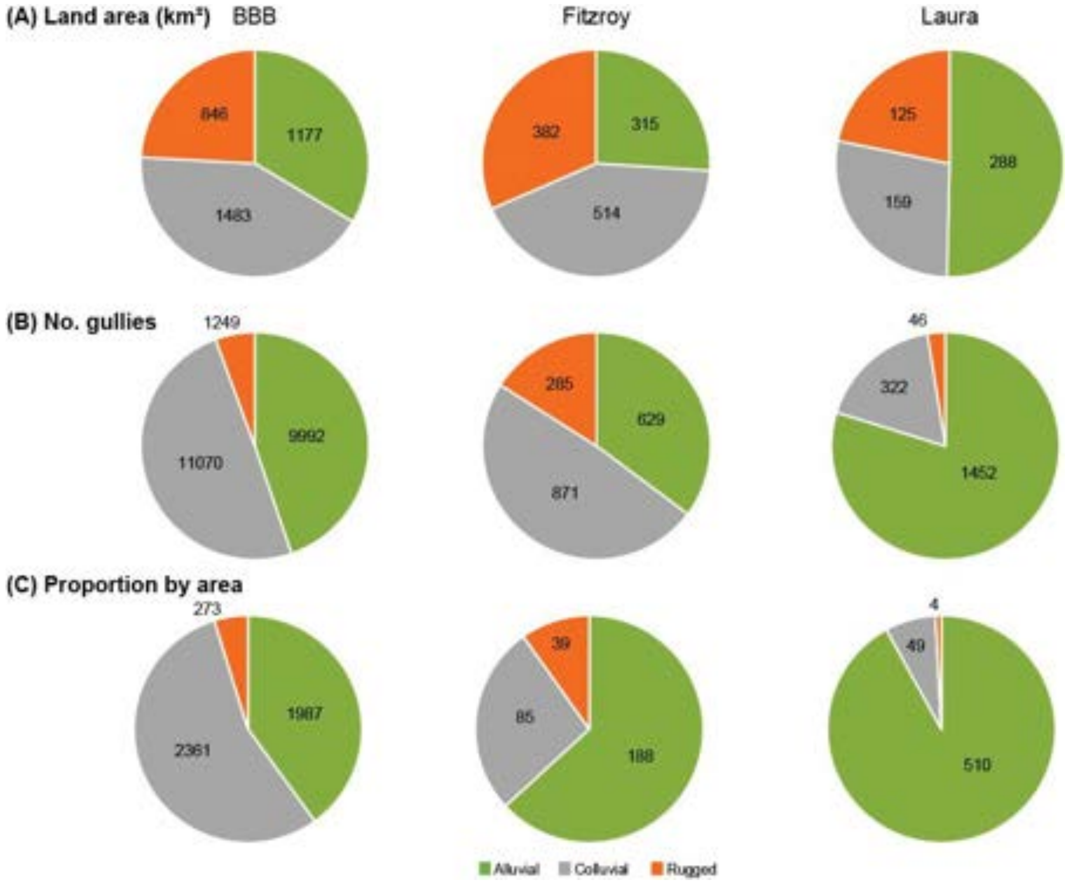

Figure 1: (A) The relative proportion of each landscape type in each catchment lidar block (data labels = ha) and (B) the number of gullies mapped in each landscape unit, (C) the proportion of each landscape area affected by gullying (data labels = gully numbers). In this study we have classified gullies at a very basic level according to their landscape unit: alluvial and colluvial which as the names suggest differentiate the landscape into alluvium and colluvium (within which hillslope gullies are found), while the third category (rugged) is a subset of the colluvial/hillslope category The rugged class delineates gullies found in steeper more rugged hillslopes than the rest of the colluvial category. These are features which tend to have the form of gullies but are in shallow soils and rocky drainage lines and consequently tend to have low sediment yields.

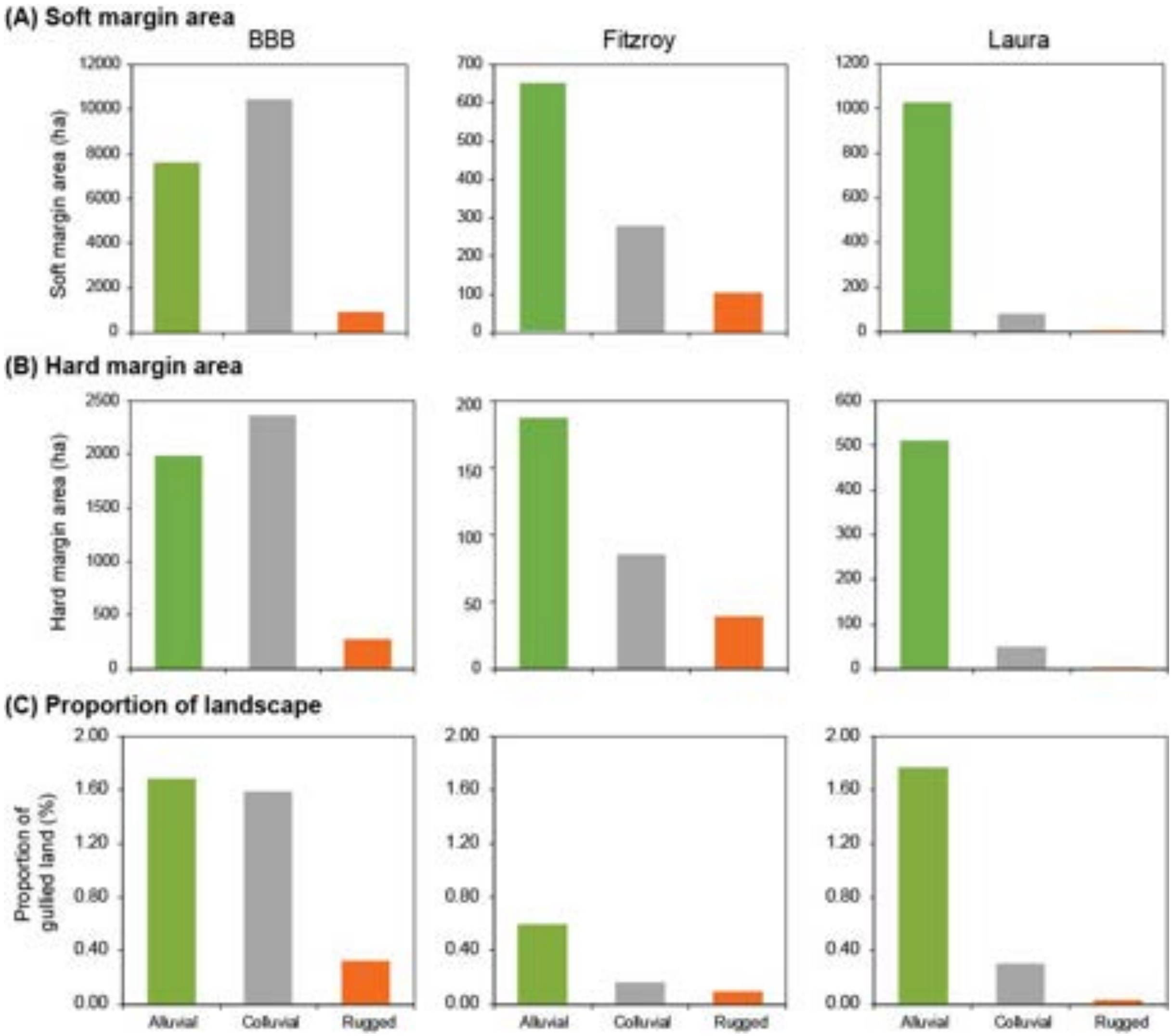

Figure 2: The proportion of gully types in each catchment by area, for both the hard and soft margins, and as a proportion of the landscape (hard margin). As explained in the text the soft margin is a mapping boundary that delineates the eroded landforms (ELFs) while the hard margin defines the area that most observers would regard as the gully proper.

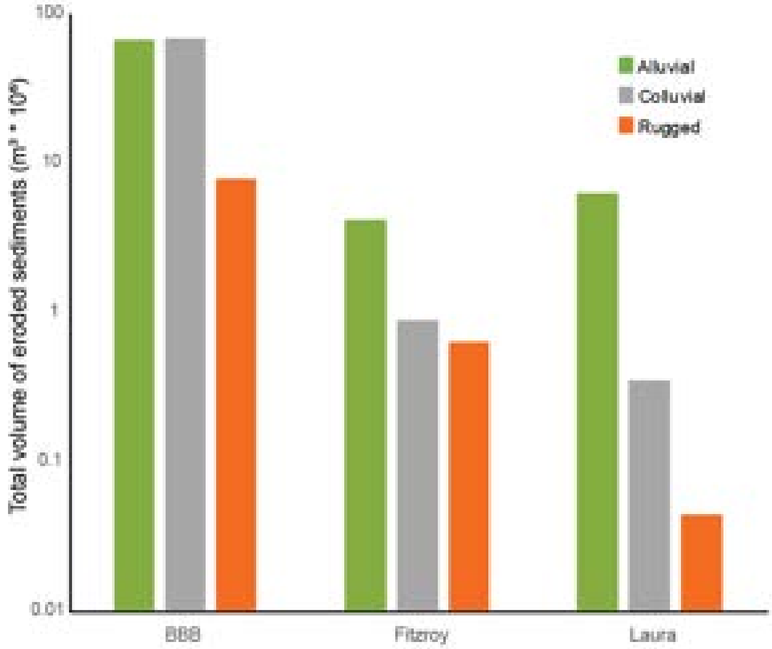

Figure 3: Total volume of sediments eroded from each region split by gully type.

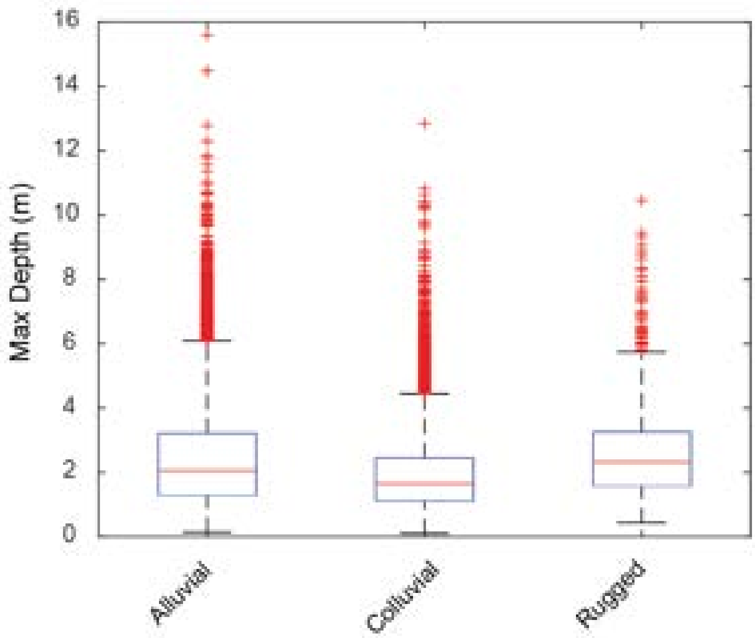

Figure 4: Example of the highly skewed distribution in the gully dimension data (in this case maximum depth). The outliers in these data will likely represent the gullies that are a high priority for remediation.

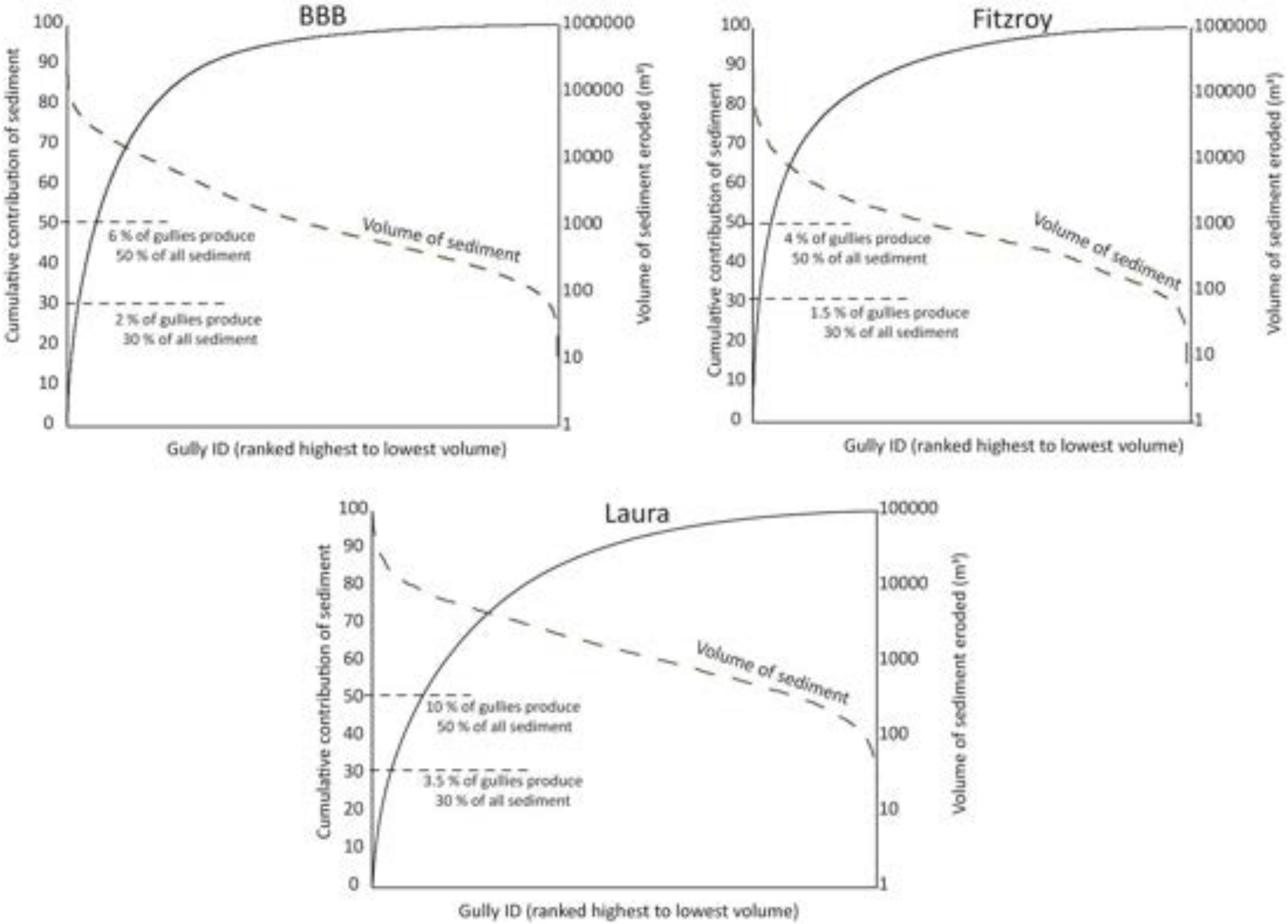

Figure 5: Cumulative proportional lifetime sediment yield curves for ranked gullies in the three catchments. The solid line represents the cumulative proportion of lifetime sediment yield (left axis) delivered by the mapped population of gullies in each lidar block when ranked according to sediment yield - across the X axis (highest on left). N= 22,311 for BBB; 1,785 for Fitzroy and 1,820 for Laura. The dashed line is the eroded volume per gully (show on right axis).

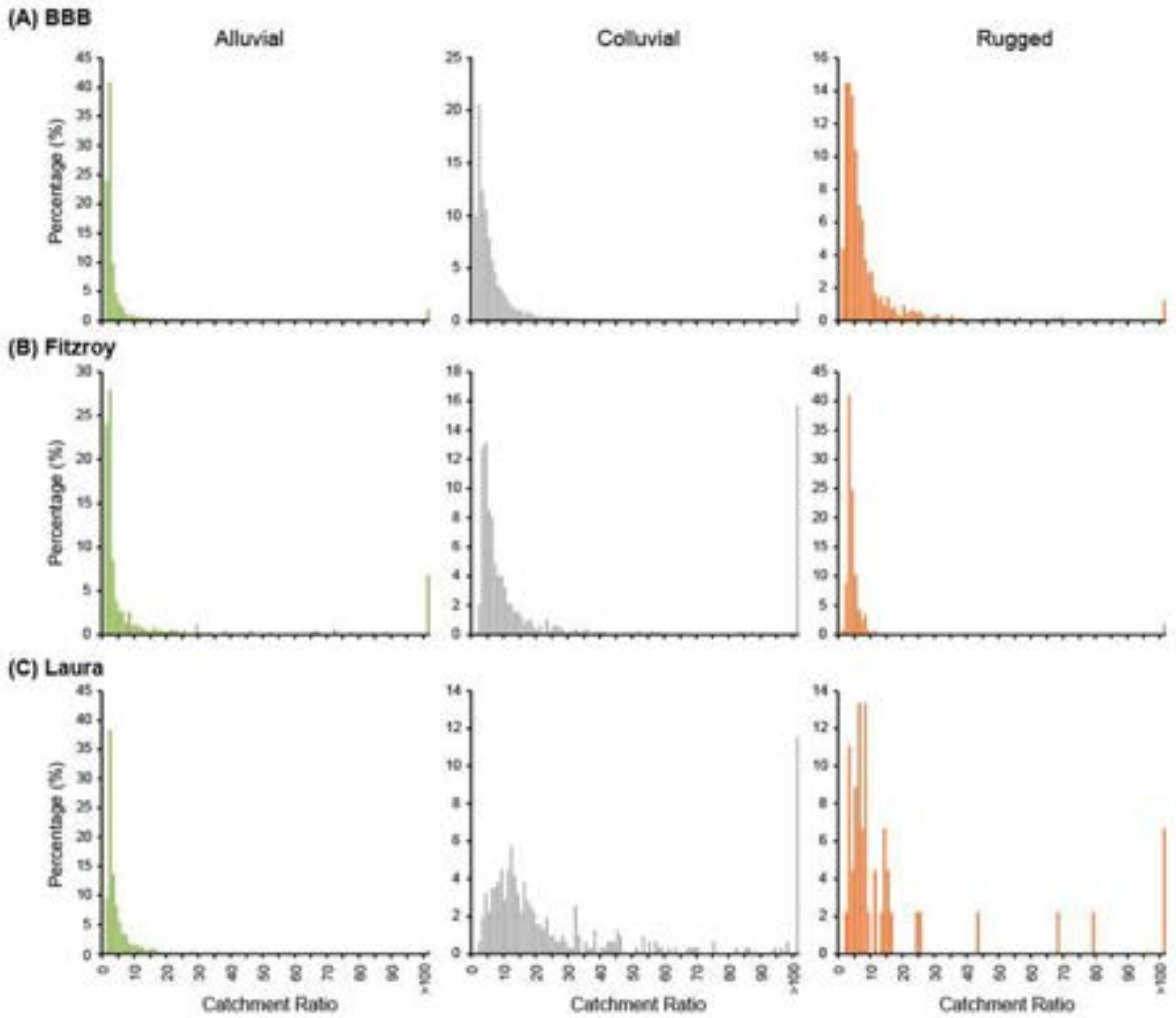

Figure 6: Contributing catchment area at the gully outlet to gully area ratios (soft margin) in the three study catchments broken down by gully type, plotted as percentage of the population in unit ratio categories. A ratio of 2 means the catchment area is the same size as the gully area (i.e. gully catchment area is measured at the gully outlet – so includes the gully area).

Table 2: Percentage of contributing catchment to gully area ratio that is <2, i.e catchment is less than double the area of the gully (or the non gullied part of the catchment is less than or equal to the gully area) , using both hard and soft areas.

		Alluvial%	Colluvial%	Rugged%
BBB	Soft	48.7	18.9	12.9
	Hard	25.9	6.8	3.2
Fitzroy	Soft	52.0	2.2	9.5
	Hard	19.5	0.0	1.1
Laura	Soft	47.9	0.6	2.2
	Hard	23.6	0.0	0.0

RECOMMENDATIONS

1. This project has demonstrated that gullies can now be mapped consistently and cost effectively at a resolution that is 4 orders of magnitude higher than existing presence/absence mapping in the GBR. We recommend that further lidar acquisition should by prioritised in hotspot areas identified through the existing P/A mapping program and further mapping undertaken using the approaches outlined in this report.
2. Inconsistencies between the two approaches due to both the gully conceptual model used and the mapping resolution suggest that prioritisation should no longer be based on the 1 ha P/A data as many of the mapped features are not gullies.
3. There is a need to ensure that all gully field observations and mapping use an updated conceptual model/definition of what a gully actually is, based on geomorphic principles. The current definition in the "yellow book" (NCST, 2009) is too vague, and does not define a gully in a robust manner.
4. There is a need to systematically ground truth the mapped gullies, using a standardised field protocol. We suggest that the field data collection protocols developed for the Queensland gully classification project (see NESP TWQ Hub Project 4.9 and subsequent refinements through QWMN) are a good starting point. These field protocols should be further developed and incorporated into the GECAT and GMT gully apps being developed by Queensland Department of Agriculture and Fisheries (QDAF).
5. There is a particular need to ground truth the rugged and colluvial classes within a diversity of landscapes, as we suspect that the relative activity of these gullies are overestimated by the PLS method. Due to Covid restrictions, adequate ground truthing was not able to be completed through the project.
6. Depending on the outcomes from the ground truth data, there may be a need to modify the approach for these gully types.
7. Notwithstanding the issues raised in points 5 and 6, we recommend that the general principles underpinning the PLS method (i.e. that the prior land surface was very rarely flat) should be adopted for all estimates of gully depth, in particular. As a minimum, gully depth should be adjusted to 80% of the maximum depth estimated from present day bank top estimates.
8. As a way around the problem of gathering data from multiple users in the field, it is suggested that actual gully volumes and sediment yields are provided to end users based on the standardised data once the gullies are mapped and characterised from lidar data. To achieve this a centralised database of prioritised should be developed and end users provided with the data. This could also form the initial component of a centralised monitoring strategy for any gully management works, including Reef Credits, in which baseline sediment yield estimates are supplied, as well as ongoing post-remediation monitoring.
9. Further refinements can be made to the gully filtering procedures, incorporating additional gully attributes including soil materials and gully morphology.

1.0 INTRODUCTION

Gully erosion is one of the major drivers of land and water degradation globally (Castillo and Gomez, 2016; Vanmaerke et al., 2016). In Australia, there has been increasing recognition over the last decade that gully erosion represents a major source of anthropogenically accelerated erosion within Great Barrier Reef (GBR) catchments and consequently a major threatening process to freshwater aquatic ecosystems and a source of sediment and nutrient pollution to the GBR Lagoon (Brooks et al., 2013; Olley., et al., 2013; Wilkinson et al., 2015; Bartley et al., 2017). Current estimates are that on average around 40% of the fine sediment load delivered to the GBR Lagoon is sourced from gully erosion (Wilkinson et. al. 2014; Bartley et al., 2017), although this proportion is only loosely constrained, and varies considerably between catchments. In some catchments (e.g. the Bowen) it is around 60%, and others substantially less.

Consequently, gully remediation and management is a high-priority activity across most GBR Natural Resource Management (NRM) regions. Both the Queensland and Australian Governments have recently invested significant resources into major gully rehabilitation programmes. With these major investments, which to date total more than $100M, including new investments through the Great Barrier Reef Foundation (GBRF) fund, there is a pressing need to identify the location of high-sediment-yielding gullies in the landscape and to prioritise management efforts and resources to reduce the yield from these gullies (an example of a large alluvial gully is illustrated in Figure 7). However, due to the vast expanse of the contributing catchments to the GBR, we first need a method by which we can map and identify active gullies across the landscape, and thereby prioritise management effort.

To fully understand the impact of gully erosion on water quality and landscape degradation it is necessary to identify the location and spatial distribution of gullies, thresholds at which gullies might initiate, and the calibre of sediment being derived from each gully.

Figure 7: Large alluvial gully on Havilah Station (near Collinsville) on the bank of Parrot Creek, tributary to the Bowen River.

1.1 What is a gully?

A commonly accepted definition of gullies is that they are erosion features larger than rills – (erosional features < 0.3 m deep which can be ploughed out or easily crossed (Poesen et al., 2003; NCST, 2009), but smaller than streams, creeks, arroyos, or river channels (Graf, 1983; Wells, 2004). The Australian Soil and Land Survey Handbook (NCST, 2009, p.39), which is the Australian standard for landscape description, defines a gully as a Landform Element that is, "(an) open depression with short, precipitous walls and moderately inclined to very gently inclined floor or small stream channel, eroded by channelled stream flow [emphasis added] and consequent collapse and water-aided mass movement".

The vague definition used as the Australian 'standard' has introduced considerable confusion by referring to gullies as 'channels' and thereby allowing first and second order stream channels to be included in the concept of a gully. This definition, however, includes no reference to what most practitioners would consider to be one of the essential characteristics of a gully, which is the presence of a headwall or scarp.

To clarify the distinction between channels and gullies, and thereby avoid producing mapping that misrepresents the different geomorphic processes that occur in channels and gullies, we have adopted the following definition of gullies in this study and in related gully classification work (see Brooks et al., 2019, Thwaites et al., in review).

***Gullies** are a persistent, incised erosion feature with walls and/or head scarp on average > 0.5 m deep (or that cannot generally be removed by conventional tillage methods for Field Gullies) and cannot be defined as a stream channel (1st order or greater – see below). The feature erodes residual soils, unconsolidated materials and saprolite, but not solid bedrock, and it has multiple modes of expansion. It always includes extension by headward retreat into an otherwise un-dissected landscape by way of a clearly defined head scarp or head wall. It has erosional side walls of at least moderately steep gradient (~ 30^{o} or ~ 60 %). The gully walls are dominantly bare soil materials with a distinct break of slope from the uneroded hillslope or floodplain/terrace surface, that exhibit erosion by means of mass movement, direct rainsplash erosion, with or without tunnelling and/or sapping. The feature overall is typically driven by ephemeral flows associated with direct rainfall into the gully and in the gully catchment. Gully floors are typically fairly uniform in long profile, except when they are undergoing multiple incisional phases and have more than one headcut down the long profile. Alluvial gullies are commonly affected by backwater and in some cases complete over topping by floodwaters from the stream/river they adjoin. The active sediment source delivered from a gully is predominantly from within the gully defined by a clear, bounded (autochthonous) internal erosional zone" (*Figure 8*).*

In contrast, a **stream channel** is considered to be a persistent elongate landscape feature formed by flowing water (either ephemeral or perennial) with a defined bed and banks which may be erosional and/or depositional. Channels may be found in either bedrock, colluvium, or alluvium. Channels often include associated fluvial geomorphic units such as floodplains, terraces, bars, benches, inset floodplains, pools and riffles. Depositional materials tend to be predominantly derived from up-stream (alochthonous) sources. Channel beds are seldom uniform in long profile, often being characterised by rhythmic pool and riffle sequences. Channels also show evidence of intermittent overbank flooding and they have a width/depth ratio that tends to be > 1. The definition overall is by weight of evidence; not all criteria are necessary, nor is each characteristic in isolation a defining feature of a channel (Figure 8).

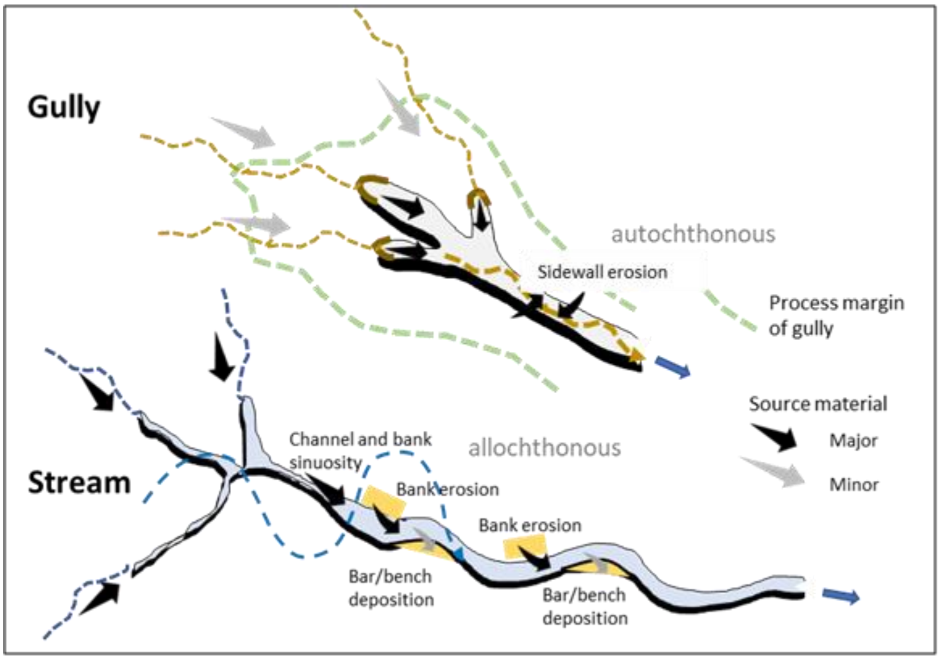

Figure 8: Conceptual model showing the difference between a river channel and an active gully (after Thwaites et al., in review).

1.1.1 Practical Attributes of gullies for mapping

This conceptual understanding is often not directly translatable to extracting metrics from remotely sensed data but relates to forms and processes that fundamentally distinguish gullies from stream channels and other erosional landscapes. For practical mapping purposes in this study, we consider gullies to have:

i. High surface roughness from multiple erosional forms within the gully – e.g. rilling, fluting, block collapse and slumping
ii. Slopes >25% along flow lines
iii. Change in slope range >30% along scarps
iv. Has a definable head scarp
v. Dominantly bare, exposed soil materials on the surface
vi. Does not include ordered fluvial depositional units such as bars, benches and floodplains

1.1.2 What is an ELF?

When analysing lidar-derived DEMs over large areas it is readily apparent that many "gully-like" features are identified in the first pass of any mapping process. Such features are not necessarily gullies, and for the purposes of this exercise we have termed these undifferentiated features as eroded landforms (ELFs). An ELF is a surface depression or swale which is a continuous spatial unit with an area 10^2 - 10^4 m^2, generally occurring along first or second order drainage lines, or as detached depressions elsewhere in the landscape (Figure 9). ELFs feature a break in slope or defined margin from the surrounding residual land surface, based on our experience having a minimum slope of 20 to 30 degrees over a 2 to 3 m in distance. For our mapping purposes we term this margin the soft margin (Figure 9). Upstream of the soft margin, the land surface is relatively stable and doesn't have any erosional forms (i.e. on engineering or management timeframes). The soft margin is a boundary mapping step that defines the local geomorphic context and may contain multiple ELFs. Gullies are a subset of ELFs, but ELFs also include features such as swales, ephemeral channels, palaeochannels, stabilised drainage features and surface depressions that may not be gullies. Gullies may also be located within a larger ELF of which the soft margin is not representative of the gully (Figure 9).

In contrast to this, we use the term hard margin to describe the principle erosional zone of a gully. Indeed, to be a gully or contain a gully, an ELF must have, or contain, a hard margin, which is indicative of active erosion (defined below). The hard margin represents the boundary most practitioners would determine to be the gully margin. The hard margin typically represents the sharp, visible scarps that form the boundary of a gully and features landscape elements such as scarps, rills, mass failure, bare soil, etc. The soft margin of an ELF and hard margin of gully may align, particularly at the headwall of such a feature. However, some gullies demonstrate a tendency to grade out toward the downstream limit due to diffusion mechanisms in the evolution of that landform. In such circumstances, the hard margin may not be continuous or contiguous with an ELF and thus poses a considerable challenge to mapping individual gully units as a continuous polygon. In such areas, the soft margin is still necessary to constrain the hard margin to a distinct hydro-geomorphic unit.

It should be noted that the soft margin is not synonymous with the ELF catchment boundary (Figure 9), which is often a larger area again and features an uneroded, residual surface unless the ELF has formed to the upper limit of its catchment.

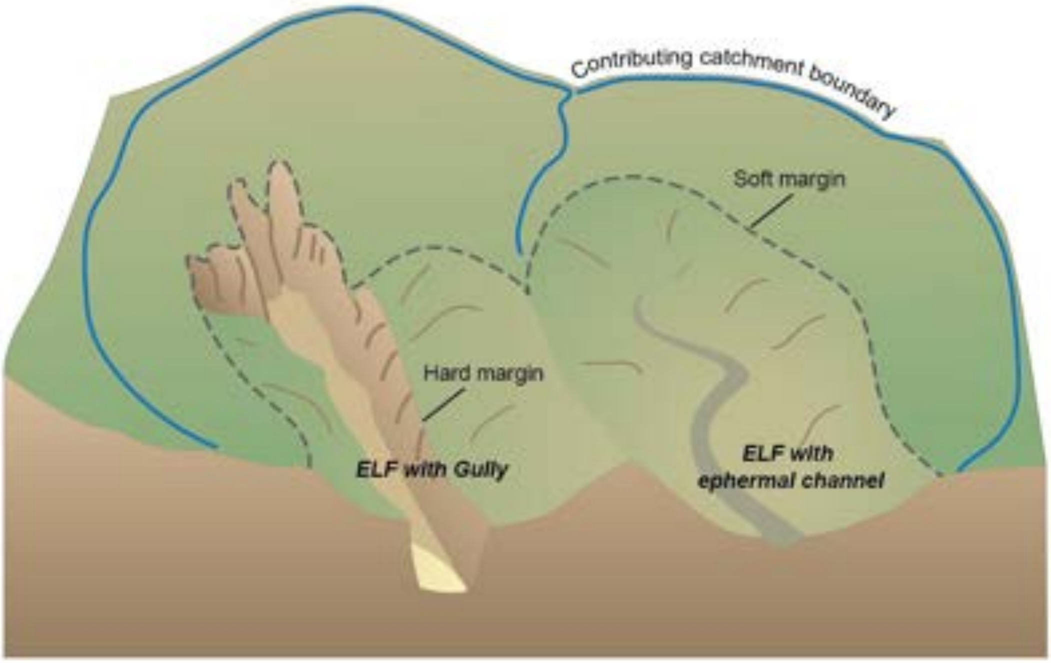

Figure 9: Conceptual model of two adjacent ELFs, one comprising a gully (left) and one without a gully (right). Also shown are the three distinct boundary features that are mapped to describe each gully; the 1) Hard Margin – denoting the erosion scarp of the gully; 2) the soft margin, denoted by the break in slope which defines a zone of topographic influence around an ELF; and (3) the catchment boundary – defining the surface flow contributing catchment area.

1.1.3 Types of gullies

Recent research undertaken by the authors (see Brooks et al., 2019) have highlighted the diversity of gully forms found throughout the GBR Lagoon, and how important it is to delineate the key gully forms in order to both model gully sediment yields and to aid in prioritisation for gully management. A multi-tiered classification has been developed that requires both remotely sensed data analysis as well as field assessment of soil materials and other finer resolution features not readily discernible from remotely sensed data. For the purposes of this study we have limited the classification to the highest level of the classification hierarchy, in which we differentiate gullies into the two fundamental types; alluvial and colluvial (*sensu* Brooks et al., 2009) according to their position in the landscape, and by extension the materials in which they are formed. Alluvial gullies as their name implies are formed within alluvial sediments which tend to have a relatively low (unincised) landscape surface slope (typically < 2 degrees), whereas colluvial (or hillslope) gullies are formed within colluvium and/or saprolite on moderately sloping hillslopes or toe-slopes. A third category is also mapped, which in effect is a subset of hillslope gullies we have termed rugged. These are gully features that have formed in steeper, more rugged and heavily dissected upper slopes within the landscape distinguished used the terrain ruggedness index (Riley et al.,1999). Given their position in the landscape, these are typically formed in coarser gravelly materials, and tend to have lower sediment yields than the typical hillslope gullies.

Gullies can be further differentiated beyond these three basic classes based on their soil materials and their resultant forms, as outlined in the gully classification framework (Brooks et al., 2019). However, for the purposes of this project we have limited the classification to the highest order classes, in the knowledge that they can be further differentiated at a later date with the benefit of ground survey data or other remotely sensed data overlays.

1.1.4 Gully Activity

Throughout this report reference is made to gully activity, both at the overall gully scale and at the pixel scale within a gully. While all gullies are, by definition, active erosion features, it is worth outlining in more detail what is meant by gully activity. The first point to make is that we are confining the temporal scale to what are typically referred to as engineering or management timescales (e.g. 10^0 – 10^2 years at most) (Schumm and Lichty, 1965). It is accepted that at geomorphic and geological timescales (i.e. timescales > 10^2 years) most of the landforms we are mapping are eroding at varying rates which are often imperceptible on management timeframes. In this study we are particularly interested in erosion processes that are likely to have been accelerated by anthropogenic landuse changes over the last ~150 years which have increased the erosion rates above what would be considered to be the natural background rates given the prevailing climatic, tectonic and longer term land-use conditions that prevailed throughout the Holocene (i.e. ~ last 10,000 years).

A detailed definition of pixel-scale activity is outlined in section 2.6.1, but at the gully scale it is assumed that multiple pixels would be active. Field indicators of active gullies include some or all of the following characteristics:

- Evidence of mass failure at the gully head or walls (i.e. block collapse or slumping)
- Bare ground with rills, flutes and micro-pedestals (< $1m^2$)
- Macro-pedestals (remnants of the prior land surface >$1m^2$)
- Recently undermined trees
- Trees with exposed roots
- Tunnel erosion
- Areas with iron, calcrete or dolomite concretions that have formed as the surface deflates via rainsplash erosion of the exposed dispersive and/or slaking subsoils

1.2 Background on mapping gullies

Accurate mapping of gullies is an essential precondition to the environmental management of such features, particularly given the capacity for rapid landscape change and sediment loss associated with gully erosion. With the advent of lidar and other high-resolution topographic datasets, a range of methods have been developed and promoted to identify and map gully-like features on the landscape.

The simplest, yet most subjective, means of mapping gullies involves manual identification, typically from optical imagery. Gilad et al. (2012) and Tindall et al., (2014) use visual assessment to manually assign gully presence in low resolution cells based on higher resolution aerial and satellite imagery. Such approaches rely on the operator's interpretation of (a) the definition of a gully, and (b) features within the imagery or DEM datasets. In developing a Google Earth-derived inventory, Saha et al. (2020) required field validation of all identified datapoints. Delineation and manual digitisation of gully boundaries from high resolution aerial imagery and DEMs (e.g. Betts et al. 2003; Martinez-Casasnovas, 2003), is a common site scale approach, but is limited in the subjectivity of the optimal boundary location and is time dependent. Yet, such datasets can serve as valuable “ground truthing” and are frequently employed in the validation process of automated mapping methods (Karami et al. 2015; Yang et al. 2017; Korzeniowska et al. 2018). Multitemporal imagery and DEMs provide the opportunity to estimate gully change, growth rates and volume estimates using DEM of Difference (DoD) analysis (Martinez-Casasnovas et al., 2003; 2004; Marzolff and Poesen, 2009; DeLong et al., 2012), but this is usually only possible over small spatial areas due to limitations in data availability.

James et al. (2007) assess the ability of lidar data to map gullies, establishing that high-resolution products derived from lidar provide the most accurate tools for mapping gully networks. A range of semi-automated and objective approaches using lidar have been developed, making use of topographic derivatives. Yang et al. (2017) introduce a relatively simple objective approach to map gullies in Loess Pleateau of China, using a multi-directional hillshading method by combining hillshade rasters from different azimuths to delineate the boundary of gullies. Costel Codru and Niascsu (2020) adopted the same hillshade technique, integrating it with profile curvature.

Baruch and Filin (2011) highlight the issues of mapping gullies at a fixed scale given the diversity of form and texture characteristics, arguing a multi-resolution approach is the only solution for accurate gully extraction and surface texture noise attenuation. Walker et al. (2020) followed a similar approach, using a multi-resolution method after Gallant and Dowling (2003) to map gully morphological components based on slope, curvature and topographic position. Components are then aggregated and rule sets based on representativeness applied for gully selection. Similarly, Castillo et al. (2014) introduce normalized topographic variables and hydrological factors to create a scale-invariant approach, followed by filtering to remove mapped elements and define gullies. Evans and Lindsay (2010) also consider topographic position to automate extraction of gully boundaries, using the difference from mean elevation, coupled with high positive plan curvature. These methods demonstrate capacity to extract gully edges, but are limited in their attempts to scrutinise the erosive activity of the features being mapped.

d’Oleire-Oltmanns et al. (2014) employ object-based image analysis (OBIA) to automatically map gullies using only optical imagery; multispectral QuickBird-2 satellite imagery and NDVI to identify areas of homogeneity, while Liu et al. (2017) develop a hierarchical OBIA method using both high spatial and spectral topographic and optical imagery to map individual gullies and gully networks. Karami et al. (2015) compare the value of OBIA over pixel based image classification of multi-spectral satellite imagery, finding the integration of texture and shape in OBIA provided significantly higher accuracy in mapping gullies and reducing noise.

Previously, Knight et al. (2007) used a comparative method of object-oriented image analysis (OOA) to semi-automate mapping of alluvial gullies over extensive areas, using a combination medium resolution ASTER imagery, airborne lidar and aerial photography, but with only limited quantitative validation and moderate accuracy. Shruthi et al. (2011) also use OOA to identify gullies from high resolution satellite imagery using a combination of topographic, spectral, geometric data, finding faster results and higher accuracies in detecting gully edges than manual digitisation. Random Forests models from OOA have shown promising results in identifying gullies from lidar-derived DEMs (Eustace et al. 2011) and ASTER imagery (Shruthi et al. 2014). Shruthi et al. (2014) determined the applicability of this method largely transferable to other imagery data.

In contrast, Saha et al. (2020) consider 16 topographical, hydrological and environmental factors across 120 identified gullies to examine machine learning techniques. While assessing only a relatively small point-based dataset, a Random Forests machine learning model had high predictive capabilities in gully erosion susceptibility mapping. Shahabi et al. (2019) integrate OBIA and machine learning analyses to detect gullies from moderate resolution data, using Sentinel 2A imagery and ALOS-derived topographic attributes in an ensemble stacking of Random Forests, Artificial Neural Network and Support Vector Machine models.

While this review is not intended to be comprehensive, it highlights the range of approaches used to map gullies over the last two decades, with considerable research efforts into a variety of techniques, further highlighting the ongoing challenge to create a broadly applicable and accurate method for mapping gullies. Most studies tend to focus on relatively small areas (<10 km^2) or individual gully systems, which may not be transferable to all environments, landscapes or regional scales. To the best of our knowledge, there is no gully mapping method that is both (a) derived at high resolution and (b) executed over extensive areas.

In Australia, the National Erosion Gully Density mapping is a nationwide 250 m dataset based on geostatistical modelling of biophysical variables to extrapolate measured gully density from aerial photographs. Gilad et al. (2012) and Tindall et al., (2014) undertook a semi-quantitative approach to map gully presence/absence (P/A) in the Burdekin catchment (130,000 km^2), using a combination of visual observation of satellite and aerial imagery and predictive modelling to map gullies across a large spatial area at 1 km and 5 km resolutions. The 1 km resolution mapping was achieved entirely through visual interpretation of a 100m x 100m cell grid of evident gullying, using the NCST (2009) definition to assist in identification.

At the time of writing this report, the predictive mapping component of this work has been superseded by visual observation and P/A mapping at a 100 m resolution. A 1 km resolution gully density map has replaced the 5 km mapping; generated by counting the number of 100 m presence cells within each 1 km cell. A single average or median figure for gully dimension derived from sample field surveys of width and depth is then applied at the sub-catchment scale to convert the 1 ha scale gully presence data to an areal extent and a volume (*sensu* Wilkinson et al., 2019). Despite the broad gully definition used and low resolution of the data, the mapping is currently being extended to other GBR catchments through a mapping program by DNRME (Queensland Government) and is being used to prioritise remediation investment by the Reef Trust (see Wilkinson et al. 2019) and the Great Barrier Reef Foundation (see Alluvium, 2019).

1.3 Issues in mapping gullies

Given the above review of gully mapping, it is clear that one of the largest shortcomings of all methods, is the inability to estimate the activity of the feature mapped. The majority of methods (e.g. Evans and Lindsay, 2010; Castillo et al., 2014; Korzeniowska et al., 2018; Liu, et al., 2017; Passalacqua et al., 2010; Patten et al., 2018; Vendrusculo, 2014; Walker et al., 2020, have shown that they are able to map depressions in the landscape and at many different scales. However, the goal of gully mapping and identifying likely sources of sediment is not just the mapping of ELFs but the actual prediction of whether these mapped ELFs are in fact gullies according to the accepted definition of a “gully” (see section 1.1). More importantly, for management prioritisation there is a need to be able to determine whether they are actively contributing sediment, and where these active gullies sit within the landscape. Therefore, what is needed is a method by which gullies can be mapped and identified as eroded landscape features which are likely contributing an excess source of sediment through active erosion. The initial mapping of the ELF is only the first step in a much more comprehensive set of procedures.

The methods reviewed above tend to be effective at mapping a single type of gully in similar terrain, but they do not demonstrate flexibility in mapping different gully types or forms (see Brooks et al., 2019, Figure 10), across highly diverse terrains. Yet this is what is required if all active gullies are to be mapped across large areas, in the diverse landscape comprising the catchments of the GBR.

In addressing the task before us in this project to develop a robust and objective method for mapping gullies across large areas (10^3 – 10^5 km^2) at high resolution (i.e. 1 m scale), we had to resolve the following issues:

1) Ensure we had a clear conceptual model of what a gully is (and is not) that can be practically applied to differentiate gullies from other gully like landscape features using 1 m scale lidar DEMs;
2) Building on existing methods develop approaches for mapping a considerable diversity of gully types/forms in diverse landscapes;
3) Where possible, adapt existing terrain analysis methods to enable the relative activity of mapped gullies to be assessed.
4) Develop methods for filtering the population of mapped ELFs (which is what all existing methods map) to leave only the active gullies
5) Develop an objective method for deriving gully volume at the regional scale (i.e. which can be applied objectively and in an automated manner across the whole gully population.
6) Derive approaches for extracting a broad range of metrics from the mapped gullies (e.g. width, depth, slope, catchment area, roughness, bare ground etc.) that can aid in the classification of gully types, and then the determination of sediment yields.

Trial mapping was carried out in a test area (see section 2.1.3) to investigate the viability of gully mapping methods from the following author: James et al., (2007); Evans and Lindsay, (2010), Passalacqua et al., (2010), Castillo et al., (2014), Vendrusculo, (2014), Yang et al., (2017) Liu, et al., (2017) Korzeniowska et al., (2018), Patten et al., (2018) and Walker et al., (2020). While most of the identified methods could map individual gullies (or more accurately ELFs) well over small areas and typically over similar terrain, no single method provided a valid solution to broad mapping of ELFs and gullies over varying terrain at the landscape scale. Hence, we have drawn upon and adapted aspects of many of the reviewed methods, along with existing tools in ArcGIS Desktop to produce a suite of methods that enable to meet the overall project objectives.

It is worth stressing again, due to the fact that the existing P/A dataset that covers the area we are working in, that the gully conceptual model we have used here differs significantly from that used in the P/A mapping method being implemented by the Queensland Government mapping program (after Tindall et al., 2014). As outlined in section 1.1 the refined gully conceptual model differs significantly form NCST (2009), given that we believe it is important to distinguish small, ephemeral stream channels from gullies, for the reason that their evolution and sediment yield is governed by different processes.

1.4 Project Objectives

Airborne lidar provides the best ability to accurately map gullies at a landscape scale at a suitable resolution for management planning (James et al. 2007). Given the large volume of lidar data now becoming available, the primary objective of this project was to develop and apply largely semi-automated tools to enable gullies to be objectively mapped from lidar-derived DEMs. In addition, extracting key attributes of the gullies to enable grouping into classes of similar gully types to aid prioritisation, management and catchment modelling. With these tools available to map gullies at the appropriate resolution for management, the P/A mapping data will become valuable in helping to focus investment of new airborne lidar data.

This project builds on NESP Project 4.9 (Brooks et al., 2019) which developed a gully classification prioritising gully rehabilitation effort and communicating to non-experts the diversity of gullies that exist in GBR catchments and across Queensland. The gully classification framework developed through NESP Project 4.9 has now gained broad acceptance amongst agencies and organisations responsible for GBR catchment water quality management. A new version of the classification is currently under development with the Queensland Water Modelling Network, however, the current project incorporates the latest thinking on how gullies should be defined, and what attributes of gullies are most likely to indicate their erosion potential. High-resolution mapping of areas of high-density gully erosion, grouped into key gully types and according to potential sediment yield, will enable standardisation and more objective management guidance.

The specific objectives of the project were to:

- Derive practical means of mapping gullies that are in keeping with the definition of a gully in Brooks et al., (2019), and subsequent refinements
- Review existing mapping methods and utilise the most appropriate existing methods, and/or develop new approaches, for mapping the considerable diversity of gully types/forms in the diversity of landscapes likely to be encountered in the GBR catchments
- Develop methods for filtering active gullies from non-active gully like landscape features
- Develop an objective method for deriving gully volume at the regional scale (i.e. which can be applied objectively and in an automated manner across the whole gully population
- Derive approaches for extracting a broad range of metrics from the mapped gullies (e.g. width, depth, slope, catchment area, roughness, bare ground etc.) that can aid in the classification of gully types, and then the determination of sediment yields.

Figure 10: A small sample of the large diversity of gully forms found throughout Queensland, representing variation in boundary conditions, processes and erosion rates and highlighting the issues in developing a method to adequately map all forms. These differences lead to substantial changes in sediment yield and trajectories, demonstrating the shortcomings of assuming that there is a single "unit" gully erosion rate that can be applied to all gullies or a standard rehabilitation strategy.

1.4.1 Approach

The following sections of this report outline and describe a semi-automated method by which gullies can be identified and assessed in terms of probable excess sediment contributions to receiving water bodies and eventually the GBR. The approach draws on aspects of a variety of established methods used in mapping gullies or other landscape features (e.g. Evans and Lindsay, 2010; Passalacqua et al., 2010; Castillo et al., 2014; Vendrusculo, 2014; Liu, et al., 2017; Yang et al., 2017; Zahra et al., 2017Korzeniowska et al., 2018; Patton et al., 2018). This report outlines a set of procedures using readily available tools in ArcGIS Desktop 10.2.1 and ArcGIS Pro 2.1 that enable us to fulfill the following mapping objectives:

- autonomously map eroded landforms as potential gullies based on topographic position and indicative erosional morphologies,
- Map the major landscape settings to classify gullies according to gully type (alluvial and hillslope),
- differentiate major stream channels from potential gullies,
- extract a range of attributes from potential gullies (after mapping their boundaries) that differentiate gullies based on an index of erosion activity,
- estimate gully volumes and a reconstruction of the original uneroded land surface to provide lifetime yield estimates for all each gully,
- produce gully maps and a gully database within three lidar blocks in three GBR catchments (Normanby, Burdekin/Bowen; Fitzroy).

2.0 MAPPING METHOD

2.1 Data

2.1.1 Lidar Acquisition

The methods developed in this project were applied to DEMs derived from lidar data. Airborne lidar data and orthophotography were acquired for the three study areas in 2018 and 2019 as part of Australian Government Reef Trust program to improve investment prioritisation in the management of erosion and fine sediment losses to the reef through the establishment of a new baseline of extent of gully and streambank erosion. CSIRO undertook and oversaw the program, contracting the aerial imaging and mapping company Aerometrex to acquire, process and provide the data. Three documents pertaining to the acquisition, processing, and quality assessment are included in Appendix 2 - 4.

The data provider supplied classified lidar point cloud data, orthophotography imagery, and DEMs (0.5 m cell size) derived from point cloud data. To produce DEMs the points within the cloud must be classified into ground and non-ground points. CSIRO performed quality control analyses of the provided point cloud data and the ground/non-ground classification. The lidar acquisition achieved average point densities in the range of 20 to 30 ground points per square metre. The DEMs supplied by the data provider, via CSIRO, were used in this project. Investigating the optimisation of ground/non-ground classification of the point cloud data for the refinement of the derive ground surface within gullies was not undertaken as part of this project. This is the subject of ongoing research.

2.1.2 Field Validation

Two datasets were used for validation of the mapped gully polygons: i) a dataset of 22 hand digitised gullies that was part of an earlier project involving hand digitising of gully margins based on a 1 m DEM derived from lidar collected in 2015 (Brooks et al., 2016) (Figure 26); ii) a dataset of RTK GPS surveys of gully margins at 10 locations in the Mount Wickham area. Field surveys of the gully soft margins was conducted at ten locations by GPS survey of the identifiable margin that indicated the initiation of erosional processes, such as surface scalding and/or changes in ground vegetation. Points were generated at 5 m increments along the surveyed boundaries (with lengths between 0.75 km and 2.6 km) and the deviation in distance between the mapping methods measured perpendicular to the surveyed line.

2.1.3 Study areas

Study areas within the three GBR focal catchments (Normanby, Burdekin/Bowen, and Fitzroy) were selected to represent disparate landscapes, ensuring the gully mapping methodology was as versatile as possible rather than limited to a single landscape setting. The study areas were selected based on preliminary mapping in the Burdekin/Bowen (Brooks and Spencer, 2018) and Normanby (Brooks et al. 2013; 2016), while in the Fitzroy, lidar acquisition was based on areas of high gully density according to P/A mapping. The extent of lidar acquisition was decided by a committee chaired by CSIRO.

In the Burdekin/Bowen catchment two existing lidar blocks at Strathalbyn Station (323 km^2 acquired in 2016) and a block at Mt Wickham Station (323 km^2 acquired in 2017), provided initial datasets to develop mapping protocols and investigate existing methods for mapping gullies (see section 1.3). In 2018, these sites were augmented by a new Reef Trust-funded acquisition in the Bowen, Broken and Bogie catchments (BBB) in 2018, with a total lidar extent of 3,481 km^2 (Figure 11 and Table 3).

Two further study areas were analysed in the Fitzroy catchment and Laura sub-catchment of the Normanby Catchment (Figure 11), 1,220 km^2 and 570 km^2, respectively. The extent of the study areas, along with other key characteristics of the regions, is shown in Table 3.

Table 3: Overview statistics of the lidar blocks and the regions where the lidar gully mapping was developed.

Region	Lidar area (km^2)	Percent catchment covered	Average rainfall (mm)	Dominant land use type	Proportion alluvial vs hillslopes	Dominant Vegetation
BBB	3,480	29.7%	750	Grazing native vegetation to modified pasture	1:2	Eucalypt to other acacia dominated open forest
Fitzroy	1,220	0.86%	640	Grazing modified pasture	1:2.85	Acacia dominated open forest
Laura (Normanby)	570	2.3%	830	Grazing native vegetation	1:1	Eucalypt Woodland to open forest

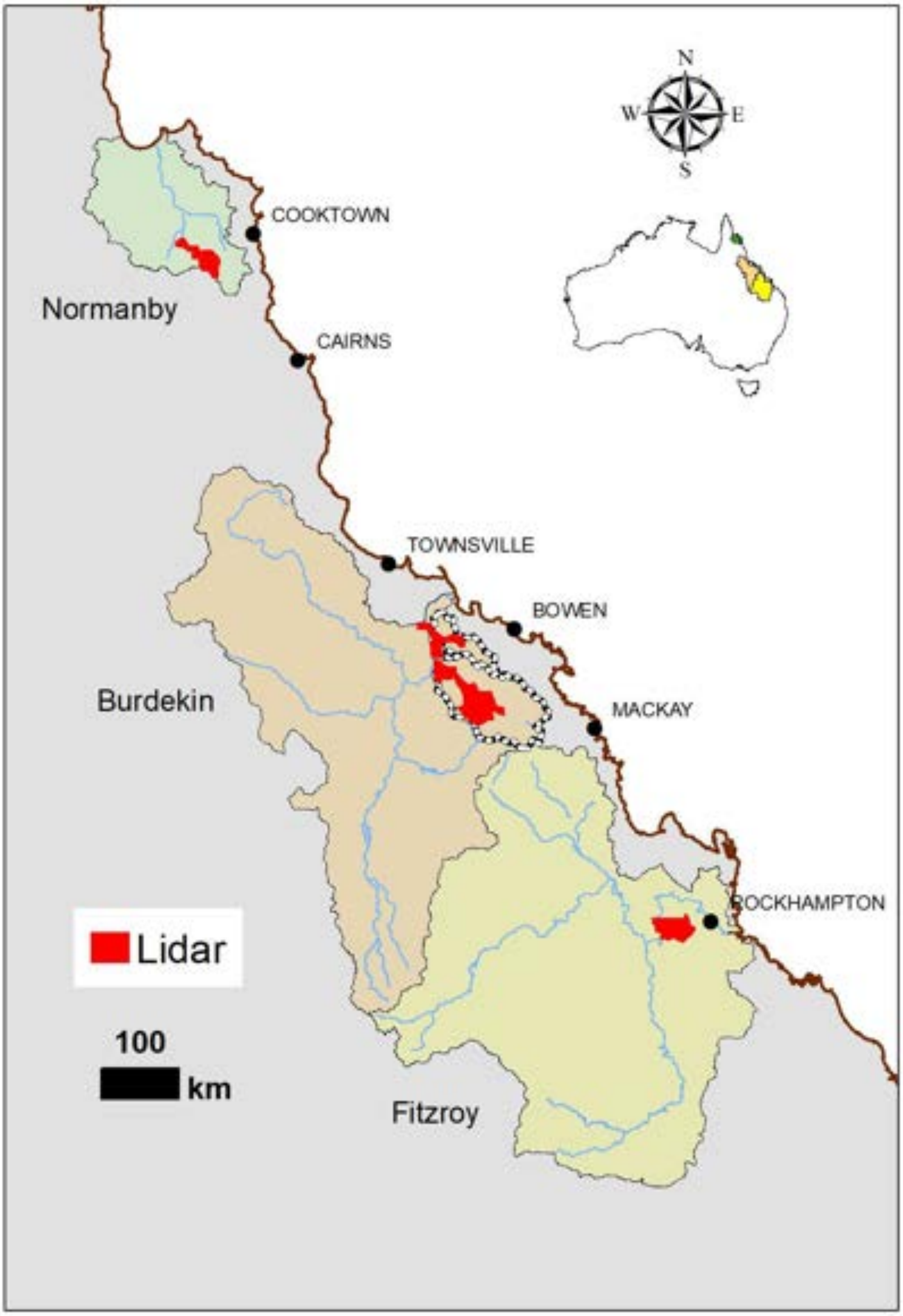

Figure 11: Location map of the three regions where gully mapping was performed. Each major catchment and waterway is shown with the lidar footprint where mapping was undertaken shown in red. The broken line represents the catchment boundaries for the BBB sub-catchments.

2.2 Overall workflow and pre-ELF geoprocessing methods

Due to limitations in existing mapping methods (see section 1.3), the method developed in this study utilizes different mapping procedures in different landscapes for the optimal identification of ELF boundaries. Once ELFs were mapped we then filtered out the non-gullied ELFs to produce a map of potential gullies that is consistent with the conceptual model of a gully.

Here we present our method to map and identify gullies and estimate a conservative lifetime total volume eroded. This method uses six separate procedures to map ELFs, which are then filtered to produce a final layer of probable gullies. The suite of mapping procedures (Figure 12) is outlined in further detail in subsequent sections.

The flow of mapping follows six steps

1. Mask channels, roads, dams (section 2.2.2).
2. Map landscape setting: Divide the landscape into steep landscape classes (i.e. colluvial or rugged hillslopes) and flat/ very low angle slopes (i.e. alluvial or peneplain country) (section 2.2.3).
3. Map soft margin boundaries:
    a. Using a Median DoD method for steep landscapes (section 2.3.1)
    b. Using concavity and multi-directional hillshading in flat landscapes (section 2.3.2)
4. Disaggregate soft margins into individual ELFs using the internal hydrology to produce a map of soft margins (section 2.3.3)
    a. Soft margins were delineated as continuous spatial units that define a zone of immediate influence surrounding a gully, and is not synonymous with gully catchment area
5. Filter ELFs to gullies based on evidence of erosion activity (section 2.5) according to the following criteria:
    a. Bare soil, roughness and PAE proportions used to drive rulesets for each gully type
    b. Hard margin mapping: The hard margin typically represents the visible scarps, which have contiguous cells of high roughness but may be discontinuous features within the soft margin (section 2.5.4).
6. Calculate metrics (section 2.6). Alongside calculating common metrics of morphology and vegetation, potentially active eroding areas are identified (section 2.6.1) and total volume eroded over the lifetime of the gully is estimated (section 2.6.2).

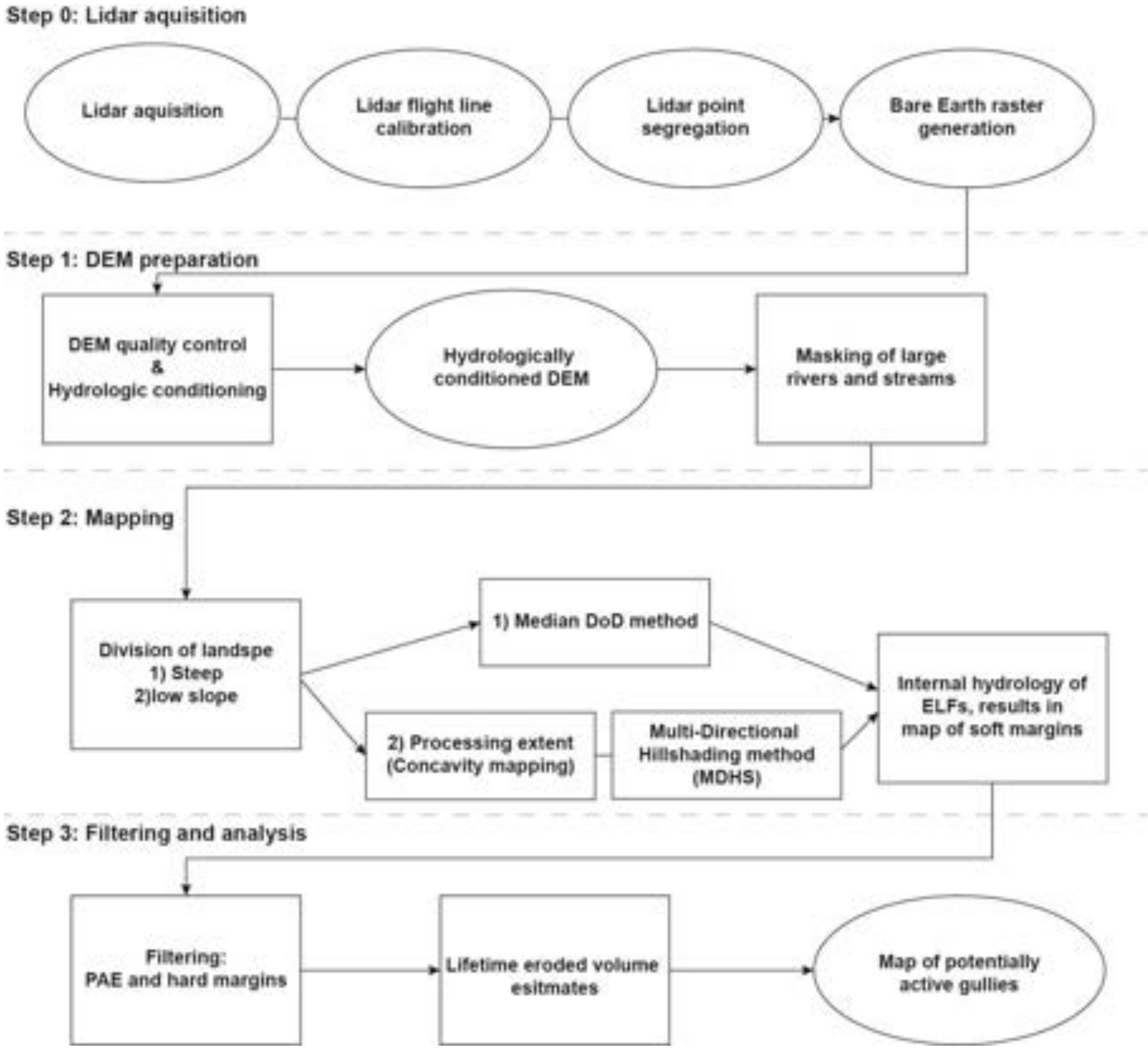

Figure 12: General workflow for mapping gullies. After lidar acquisition (Step 0) the analysis begins at Step 1, starting with a non-hydrologically conditioned raster DEM, moving through each of the subsequent geoprocessing methods until a final map of potentially active gullies has been produced.

2.2.1 DEM Preparation

The mapping and filtering methods developed for this project are dependent on data derived from D8 modelling of hydrology across the DEMs. Human infrastructure (buildings, bridges, roads, etc.) captured in the lidar data disrupt surface hydrology models derived from DEMs making them unrepresentative of the actual ground surface. Large infrastructure, such as bridges and buildings, are removed during ground/non-ground classification of point cloud data. Small low bridges are sometimes erroneously included in the DEM as ground surface. Features below the ground surface, such as, pipes and culverts under road and rail embankments which allow for the passage of water are not captured by lidar and are therefore not represented in DEM derive surface hydrology models. Unfiltered bridges, elevated roadways and railway lines appear as dam like artefacts which disrupt surface hydrology models. Many GIS programs have algorithms to modify a DEM by raising the elevation values of pixels upstream of any artefacts in the surface model that act as impediments to the modelled down slope flow. The pixel elevation values are raised to the level so that flow lines are continuous. The modified DEM is often referred to as a ‘filled DEM’. Subtraction of the filled

DEM from the original DEM was used to identify artefacts in the DEM that are disruptions to the derivation of a continuous surface hydrology model. Lines were manually digitised across these dam artefacts to mimic underground pipes or culverts or flow paths that would have existed prior to the building of an actual dam. The DEM pixel elevation along these digitised lines were then lowered to create flow pathways that breach the dam artefacts, this process of modifying the DEM is often referred to as burning in flow paths. The DEM produced following the burning of flows paths is hydrologically conditioned for the subsequent mapping and filtering methods. Figure 13 shows examples of artefacts that require the filling, subtracting, and burning steps described above to modify a DEM to hydrologically condition it for gully mapping.

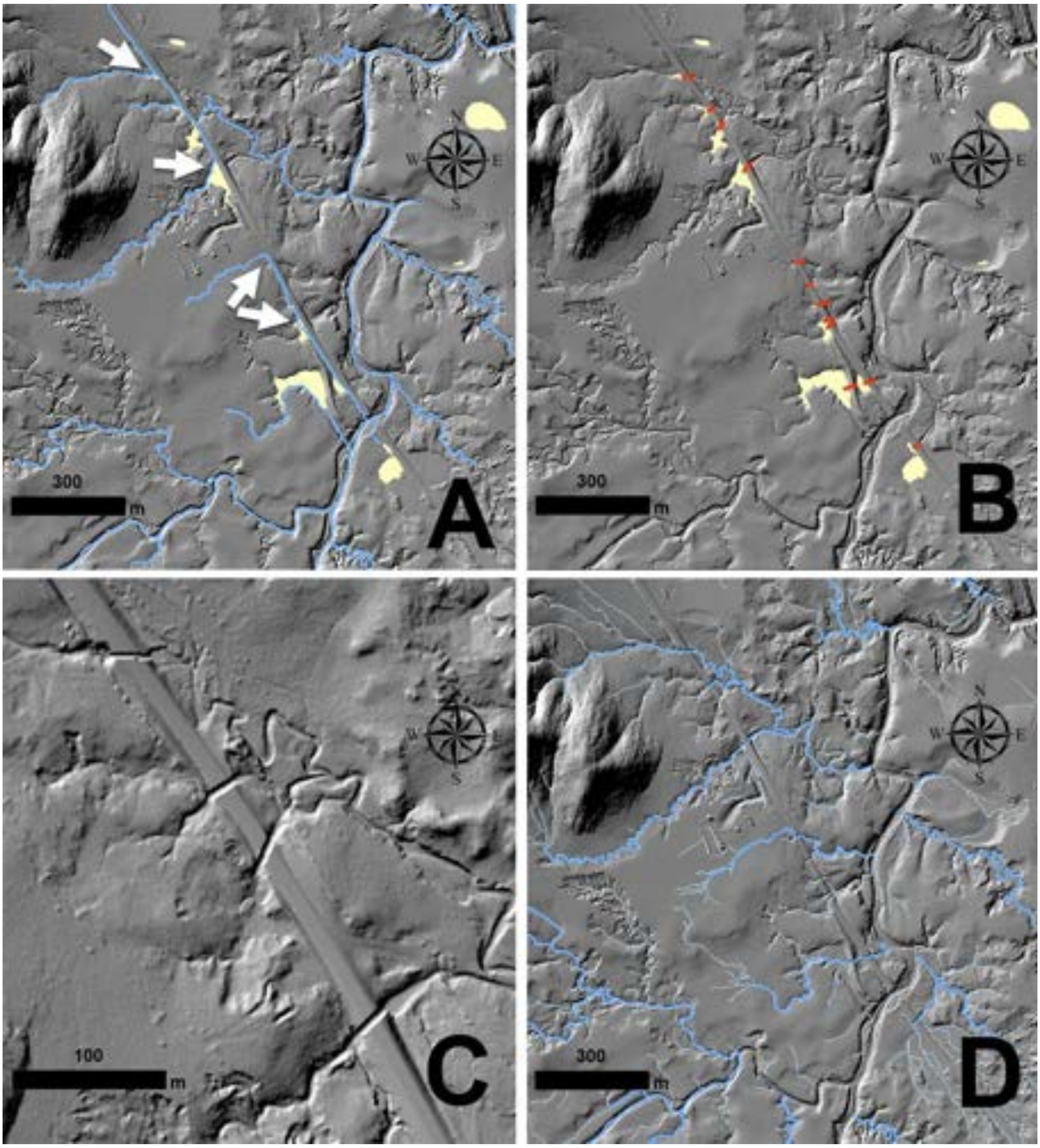

Figure 13: (A) illustrates erroneous flow paths (see arrows) caused by the presence of a road embankment. Note the flow paths (blue) run parallel to the road rather than through pipes and culverts under the roadway. The yellow areas are where the subtraction of the elevation of the original DEM and the filled DEM exceeds 0.5 m and represent natural and artificial disruptions to flow paths. The hand digitised red lines drawn across the road in (B) are 'burned' into the DEM to breach the embankment. (C) shows examples of breaches created across the road embankment. (D) shows the flow paths (blue) derived from the hydrologically conditioned DEM. The flow paths cross the road embankment, mimicking the existence of pipes and culverts under the road.

2.2.2 Masking of channels and other features

Two workflows were developed for mapping features within the DEM; internally draining features, as shown in Figure 14, and stream channels, as shown in Figure 15.

Internally drained features on the landscape such as farm dams, paleo-channels and swales, as well as embankments and drainage ditches beside roads and railways are surfaces that introduce error in the gully mapping method. The change in elevations associated with ditches and embankments presents a similar signature to gullies and channels at a similar scale. We have found the best solution to removing this source of error from the mapping method is to mask out these features across the landscape. Not only does this exclude these areas, but it also aids in the division of the landscape, and further mapping. Methods utilised here to mask roads and railways and associated engineering include: (1) obtaining cadastral boundaries if available, (2) identifying surfaces with very low variation in slope followed by buffering an appropriate distance, and (3) hand digitising a boundary.

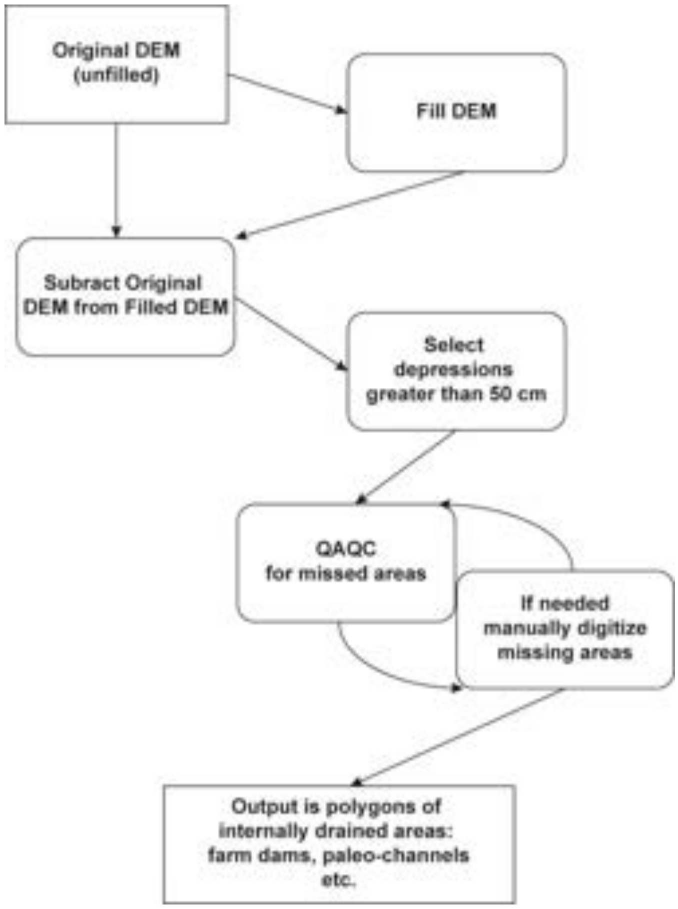

Figure 14: Flow of method to identify polygons of internally drained features such as farm dams and paleo-channels.

Figure 14 illustrates the method used to identify these internally drained features. By filling the DEM (using Fill tool in ArcGIS) and then differencing the Original DEM from the Filled DEM shows area where flow is impeded by impoundment. Selecting for depressions greater than 50 cm in depth and masking these areas from the analysis produces a cleaner and more accurate map of ELFs. Once these depressions are mapped, we then identify and mask out river and stream channels and combine the two data sets as masks for later use in the mapping method.

The masking of river channels initially follows a similar Height Above the Nearest Drainage procedure (*sensu* Nobre et al. 2011) and is shown in Figure 15. A buffer is produced around each flow line to mask out rivers and stream channels. This procedure is iterative, and the user must work through all flow lines that appear to have a bed, floodplain and fluvial features. Additionally, due to variations in the river bank heights, the confluence of tributaries and anomalously wide or narrow sections, it is necessary to manually edit parts of the channel mask that extend up tributaries or do not encompass the entirety of the river bed and banks (based on subjective identification of Top of Bank). The masks for channels and internally drained features are combined into a single mask layer. This layer is used in subsequent steps to aid in the division of landscape units and developing the processing boundary necessary to map ELFs by providing a suitable background measure of the landscape setting, uninterrupted by such incised features.

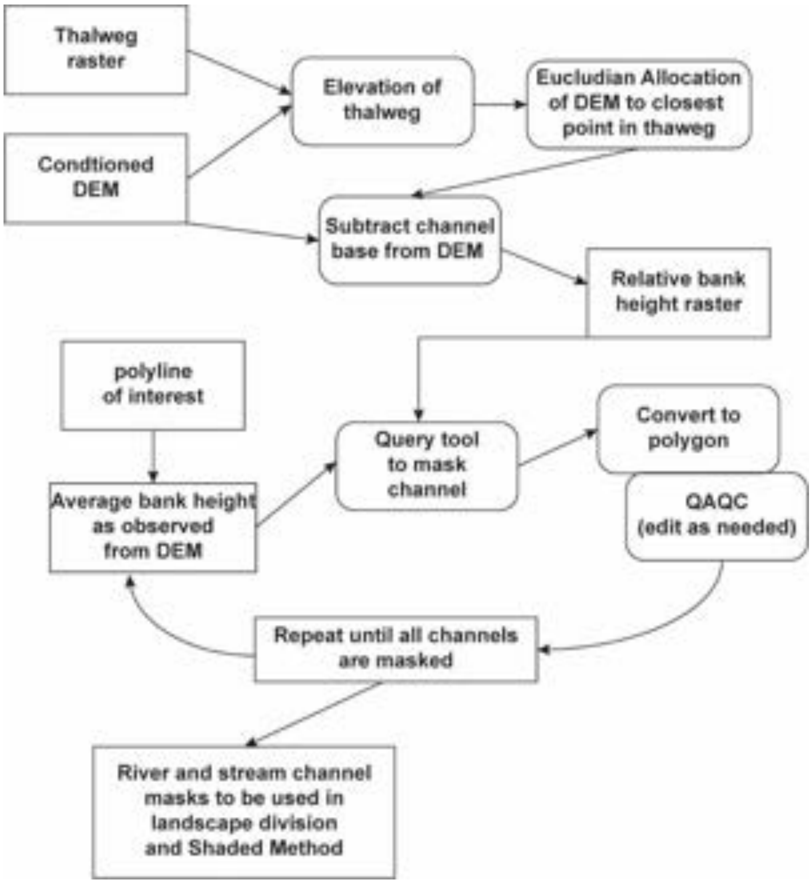

Figure 15: Flow diagram of the method to mask out river and stream channels.

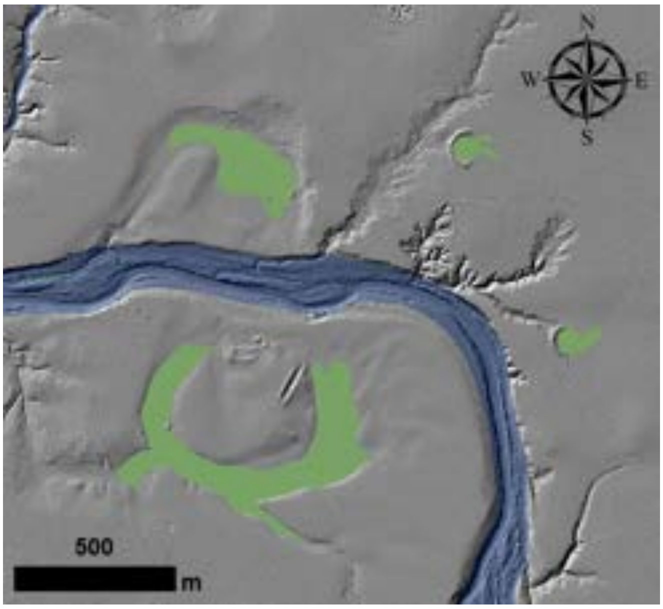

Figure 16: An example of the combined channel masks (blue) and depressions (green) These areas will be excluded from the gully mapping analysis.

2.2.3 Landscape setting

Following the conditioning of the DEM raster, landscape setting classes were mapped in order to inform generalised gully types and determine the mapping procedures followed in section 2.3. Landscape settings were mapped as Alluvial/Low Slopes, Colluvial hillslopes and Rugged hillslopes. In broad terms these landscape classes represent alluvial sediment storages, colluvial hillslopes and residual hillslopes. Initial investigations were undertaken using readily available 1:100 000 surface geology data (DNRME, 2018) to extract alluvial and colluvial settings, with bedrock assumed as rugged or areas of relatively shallow soils. While these data sufficiently delineated alluvium relatively well, the division of hillslope landscapes was not satisfactory for our analysis.

The mapping procedure used in this study and illustrated in Figure 17 borrowed from principles of digital terrain and landform mapping techniques. However, the landform mapping techniques tend to operate on finer spatial elements than is practicable for the purpose of this exercise, classifying segregated components of landforms (ie; toe, mid, scarp) rather than the generalised setting (MacMillan et al., 2000; 2003; Jasiewicz, 2013). Other techniques to map such settings, such as mapping valley floors by Gilbert et al. (2016) or hypsographic technique to map alluvial units by Pasternack (2017), perform well at a site scale but due to their methodologies were not feasible across the large spatial areas undertaken in this study.

In order to map landscape settings, the conditioned DEM was resampled by factors of three, coarsening the resolution through 3 m, 9 m and 27 m in order to distinguish an optimal level of smoothing and remove the noise of localised terrain features. After initial testing at the Mt Wickham Station lidar block, 9 m was determined to be an ideal resolution to generalise the landscapes into the above classes. Terrain attributes (Table 4) were generated and investigated for value as contributing components in mapping each landscape type.

Areas were mapped by integrating slope percent, Terrain Ruggedness Index (TRI - Riley et al. 1999), Multi Resolution Valley Bottom Flatness (MrVBF) (Gallant and Dowling, 2003) and normalised elevation at the 9 m scale. The combination of these components provided the most useful delineation of landscape into each type. Finally, grids of each landscape type were converted into polygons with a minimum area threshold of 10,000 m^2. As a result of our analysis of each of the components in Table 4 it was determined that by dividing the landscape into cells that were either less than or greater than 2 degrees slope we could reliably split the landscape into two distinct classes: Low slope (likely alluvial in our region) or steep (likely hillslopes or rugged terrain). Hillslopes were then divided into colluvial and rugged classes based on log-transformed geomorphometric TRI at a 9 m resolution. Rugged landscape zones were defined as areas >1.0 threshold (unitless number) and >10 ha. A subset of rugged settings included cliffs and very steep bedrock slopes which were associated with a threshold of > 2.1 and were excluded from subsequent analyses as they lack sediment to form gullies yet interrupt many of the mapping procedures used in this study.

In mapping the hillslopes, each cell meeting or exceeding the criteria was selected and the final raster converted to a polygon. Anomalies and small holes along edges and within the polygon area, which are generally very few, were manually edited. The alluvial landscape class was defined in the DEM as areas excluded by the mapped hillslope polygon.

Once landscape settings have been mapped, prior to mapping ELFs, the DEM within each setting was divided into sub-catchments to improve processing time and quality control. The settings for each tool used to map ELFs are kept consistent for each landscape setting within a sub-catchment. Figure 18 illustrates the division of the landscape produced, with examples of the final three mapped landscape classes.

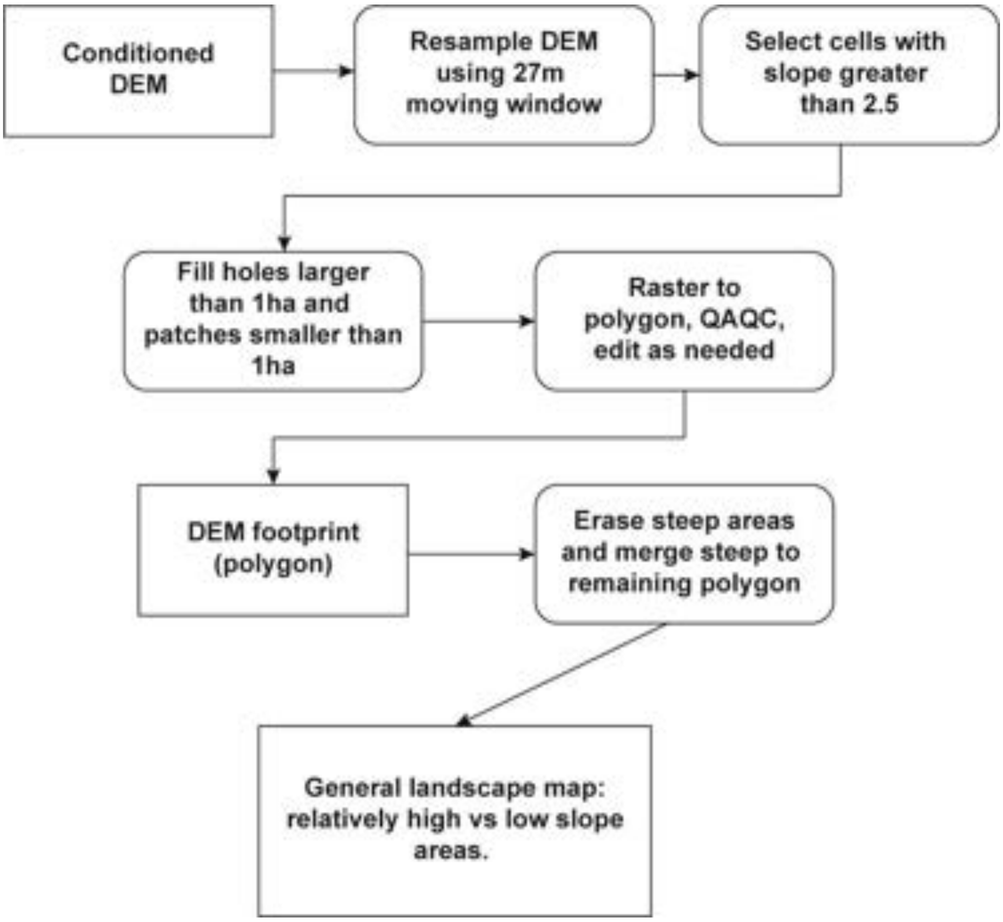

Figure 17: Methods used to differentiate between steep and low slope areas across the DEM. The produces a landscape class map that then dictates which ELF mapping procedure will be employed.

Table 4: Terrain attributes considered for mapping landscape setting.

Attribute	Units	Description
Slope	°	Steepness of the surface
Aspect	°	Direction a slope faces
Slope position	-	Scalable topographic exposure by subtracting an average raster from the original elevation raster
Ruggedness	-	Surface texture, topographic heterogeneity based on deviation in local elevation
Curvature	-	Maximum rate of change of the slope
Profile curvature	-	Rate of change parallel to the slope
Plan curvature	-	Rate of change perpendicular to the slope
Compound Topographic index	-	Steady state wetness index as a function of both slope and upstream contributing area
Stream Power index	-	Measure of the erosive power of flowing water across landscape
MrVBF	-	Measure of flatness and lowness
Normalised elevation	m	Elevation above drainage

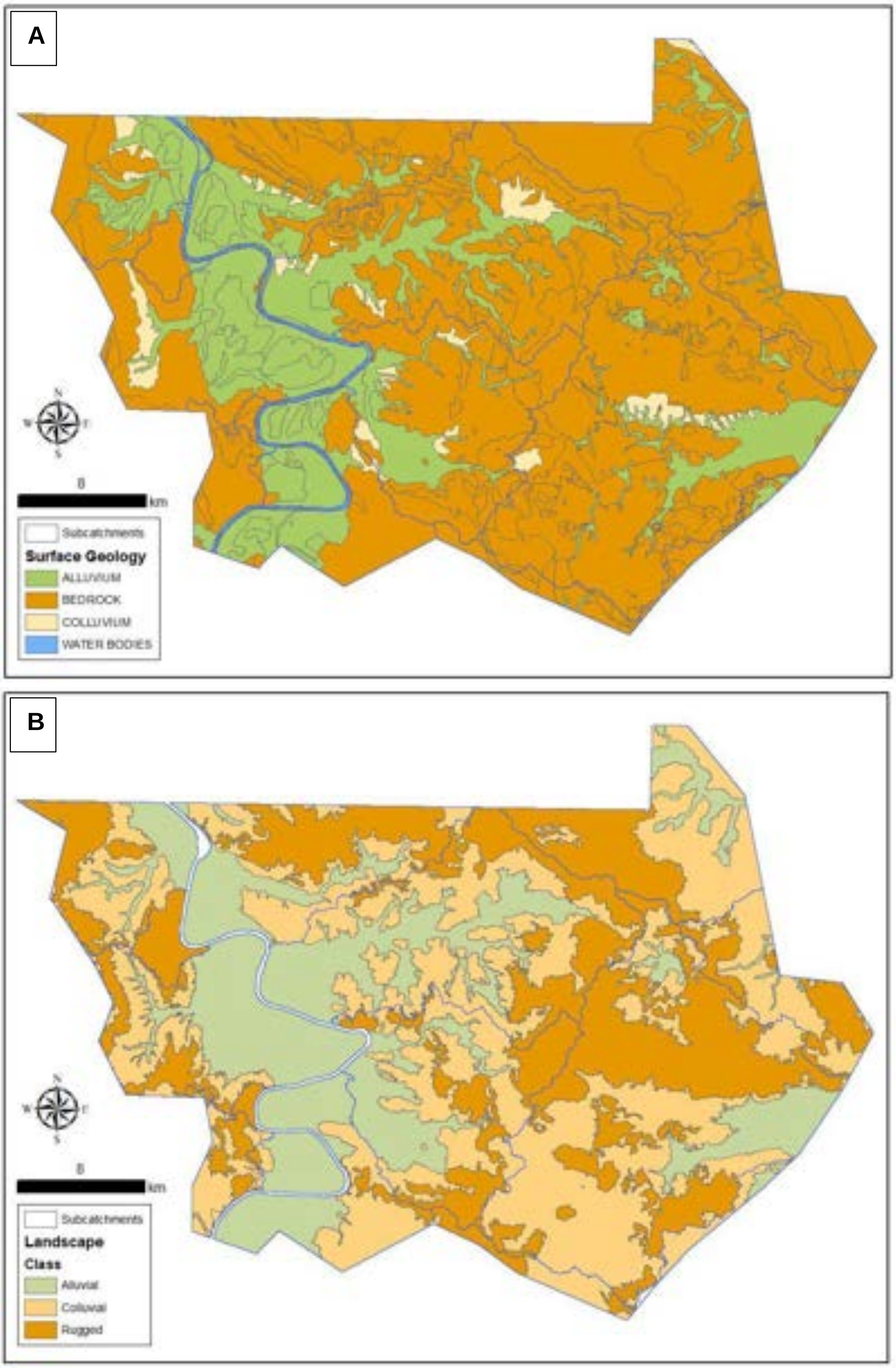

Figure 18: Map of the Fitzroy lidar block showing landscape settings derived from (a) highest resolution geological mapping available, and (b) the mapping method described in this study.

2.3 ELF Boundary Mapping

The purpose of the workflows in this section is to obtain polygons of ELFs for the three different land types and then isolate only those upstream of channel initiation points. This section does not address further segregation of ELFs into hard versus soft margin zones. Instead of showing detailed examples in this section, the following section provides a thorough example of each of the three ELF mapping workflows. ELFs within each landscape class are mapped with a different set of tools as the background terrain within different landscapes inhibits the performance of a single tool across all landscapes (see section 1.3). Creating different tools to map ELF boundaries within each landscape overcomes this issue and optimises the mapping within each landscape setting. For high slope landscapes mapped as colluvial and rugged hillslopes we employ the Median DoD method (section 2.4.1). Mapping ELFs in the low slope or alluvial landscapes requires a two-step procedure of concavity and application of the multi-directional hillshading (MDHS) method (after Yang et al., 2017), described in detail in section 2.4.2.

2.3.1 Mapping soft margins in hillslope settings

In higher slope (>2° slope) areas mapped as colluvial and rugged hillslopes we employ the Median DoD method which identifies abrupt changes in elevation assuming such changes equate to steep slopes on the walls of gullies. The necessity of this tool is driven by the background terrain slope which negates the use of slope in mapping the soft margin. Further, attempts to use MDHS used to map alluvial gullies was unsuccessful in many hillslope settings as the hills cast shadows from different aspects and delineate erroneous boundaries. Figure 19 demonstrates the workflow for this procedure and is illustrated conceptually in Figure 20.

To perform this procedure, we used the median focal statistic function available in ArcGIS Pro 2.6 as this function is not available in ArcGIS Desktop 10.6.1. Some prior knowledge of the landscape is required and perform several iterative attempts at determining the window size and the difference threshold. Initially, a manual measurement of approximate average ELF width within each sub-catchment was determined by identifying and measuring the width of a subset of ELFs within the DEM. A circular window (so as to minimize edges distortion) which is double the average width of ELFs is passed over the landscape, calculating the median value of elevation across the window (kernel) size. The kernel radius needs to be locally defined; in all of the mapped sub-catchments we found that a kernel radius between 21 and 35 m was sufficient.

The step utilises the same procedure as the difference from mean elevation (DFME) gully mapping procedure developed by Evans and Lindsay (2010), except using median elevation instead of mean elevation. Using mean elevation to average all values in the focal window caused over mapping of boundaries, with adjacent cells higher on a bank or hillslope creating a larger mean value. Significant inaccuracy and underestimation was found by Evans and Lindsay (2010) when mapping relatively narrow gullies.

By contrast, the median focal statistic smooths the landscape; muting rapid changes in topography by selecting the middle value within the range of the focal window. This layer is then differenced from the original DEM and from this DoD areas of pronounced topographic transitions are identified and selected using a threshold of 0.1 m (Figure 20). Small perturbations in the landscape may be smoothed over, while the transitions in elevation across drainage lines exceed elevation difference thresholds. In areas of cliffs and escarpments, the DoD may exceed thresholds and be erroneously mapped as an ELF (A to A' in Figure 20). But such features that are not hydrologically linked will be removed in subsequent step (section 2.3.3).

As with every semi-automated method, iteration is key, and some hand editing may be required to include areas which are below the limit of detection. Edits should be made using multiple lines of evidence, and when possible validated in the field. In general, an open editing session in this stage will take approximately one hour to edit ELFs across a 100 km^2 area. Method development at the Mt Wickham lidar block suggested that ELFs in alluvial/low-slope settings are too wide for this method. Therefore, this method (Median DoD) functions well in hillslope or rugged terrain but does not perform well in flat alluvial landscapes.

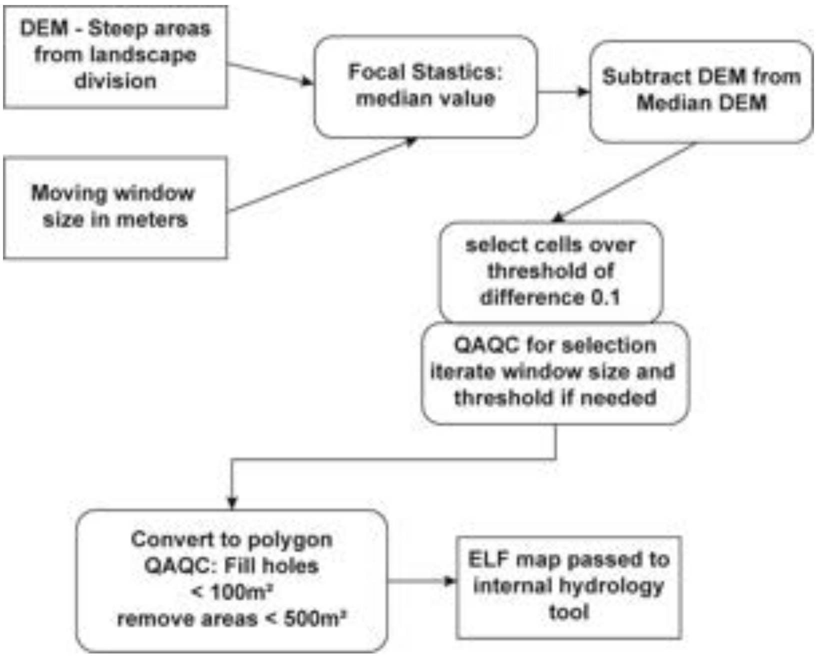

Figure 19: Flow diagram for the mapping of soft margins in steep landscapes using the Median DoD method.

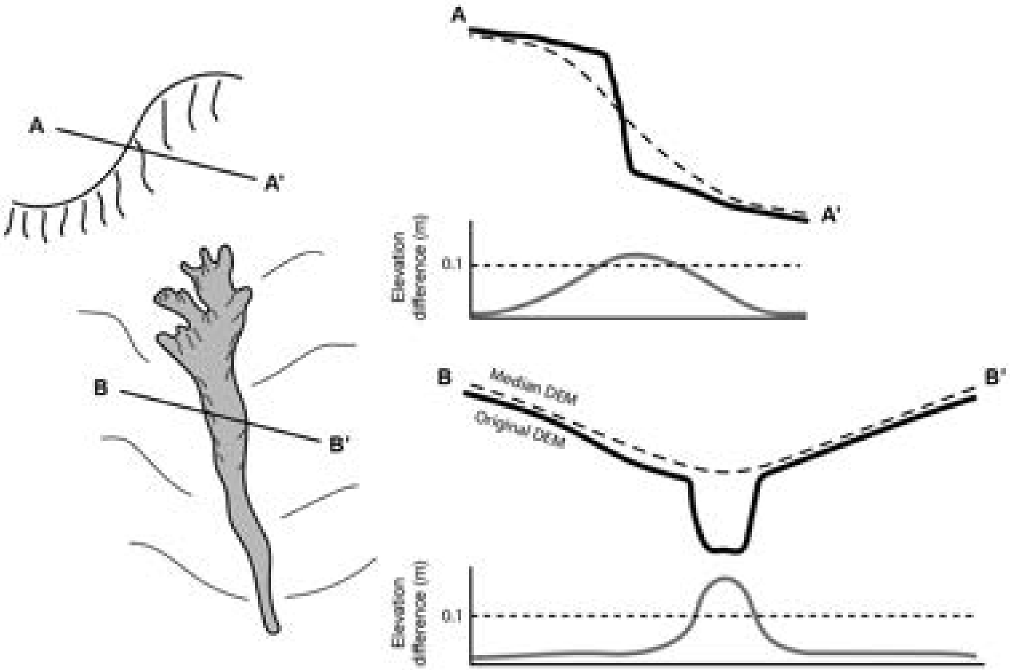

Figure 20: Conceptual diagram of the Median DoD method described in the text. Grey line is the elevation change transect in the DoD.

2.3.2 Mapping soft margins in alluvial settings

As river channels have been masked from the DEM in section 2.2.2, mapping soft margins in the alluvial or low slope landscape settings involved a two-step procedure to first define the processing extent and then, second, delineate margins using MDHS. The workflow for this procedure is shown in Figure 21 and illustrated conceptually in Figure 22. While MDHS reliably identifies the boundaries of individual gullies, using this approach alone across the entire landscape erroneously includes additional features that cast shadows. By first defining the processing extent within alluvial settings, the noise of such features is filtered by creating a generalised boundary around ELFs using thresholds of relative concavity and convexity.

Concavity and convexity were determined using the Landform tool in the Surface Texture toolbox of the Geomorphometry & Gradient Metrics Toolset (Evans et al. 2014). The tool operates a moving window (kernel) across the DEM, with an iterative procedure required to determine the kernel size depending on the general form and sharpness of depressions in the landscape. Optimal kernel sizes of 11, 15, 21 or 31 m radius were used in different sub-catchments. From the output of this tool, cells >= 0.05 are selected which are adjacent to but outside the soft margin, while concavity within the moving window was defined by values <= -0.05; selecting cells within the ELF (Figure 23A). These thresholds define areas of relative concavity and convexity, respectively which combine to define the processing extent (Figure 23B).

As some areas of the soft margin may not be selected in this step (Figure 23B), a dilation morphological filter (after Haralick et al., 1987) reclassified all pixels adjacent to the boundary, expanding the processing extent by two cells. This step served to smooth many of the boundaries, followed by a step to fill remaining parts by converting the raster processing extent to polygons and deleting internal parts. This produced a cleaned processing extent (Figure

23C) which was then used in MDHS to refine the outline of the ELF margin (Step 2 in Figure 21).

For MDHS, the DEM is clipped to the processing extent within each sub-catchment and, using the hillshade tool in ArcGIS Spatial Analyst, the sun angle is initially set at 15 degrees and passed through the six azimuths (0, 60, 120, 180, 240, 300 degrees). The output rasters of the hillshades are then mosaiced and <= 55 (i.e., lowest greyscale intensity value) are selected. These values are generally a function of slope and aspect for any given cell, but in this case, they are viewed as the amount of shadow generated by the moving sun. At each azimuth, the boundary of an ELF is shadowed perpendicular to the direction of light. By merging the six hillshades, the boundary of a given ELF is accurately extracted.

In certain instances when a feature has low or diffuse walls, or a broad floor, the centre of the ELF may not be shadowed. As per the processing extent above, the centre of these ELFs are filled to create a clean boundary (Figure 23D). The advantage of this method over other is that it creates a closed polygon feature of most of the gully, including downstream extents that often have a more diffuse margin. The final output is a single layer of alluvial ELF margins across the extent of the sub-catchment. The delineation of individual ELFs requires disaggregation of units from this layer using the internal hydrological analysis described in section 2.3.3.

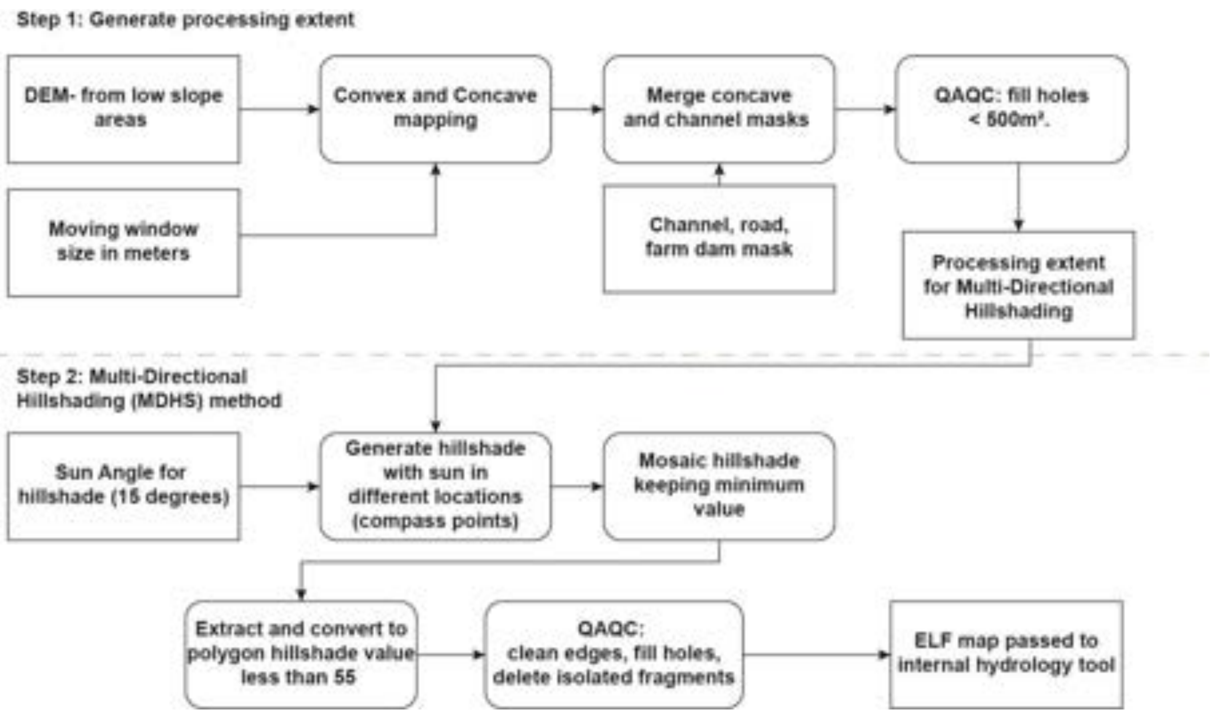

Figure 21: Flow diagram of MDHS. Step 1 further refines the processing area from the initial low slope or alluvial landscape unit. Step 2 utilizes MDHS developed by Yang et al 2017. Once ELFs are produced they are then passed to the internal hydrology tool for further refinement.

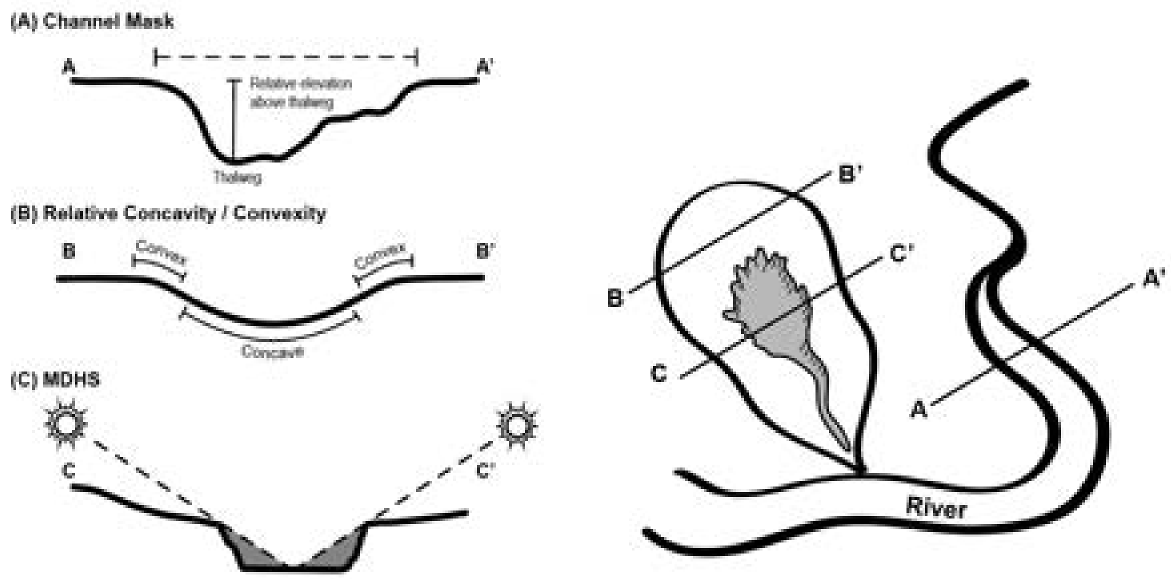

Figure 22: Conceptual model of masking the river channel (A to A') used in the development of the landscape division mask, the refinement of the low slope area to only include areas of concavity (B to B') and finally MDHS which maps ELFs by casting shadows across the landscape from different angles.

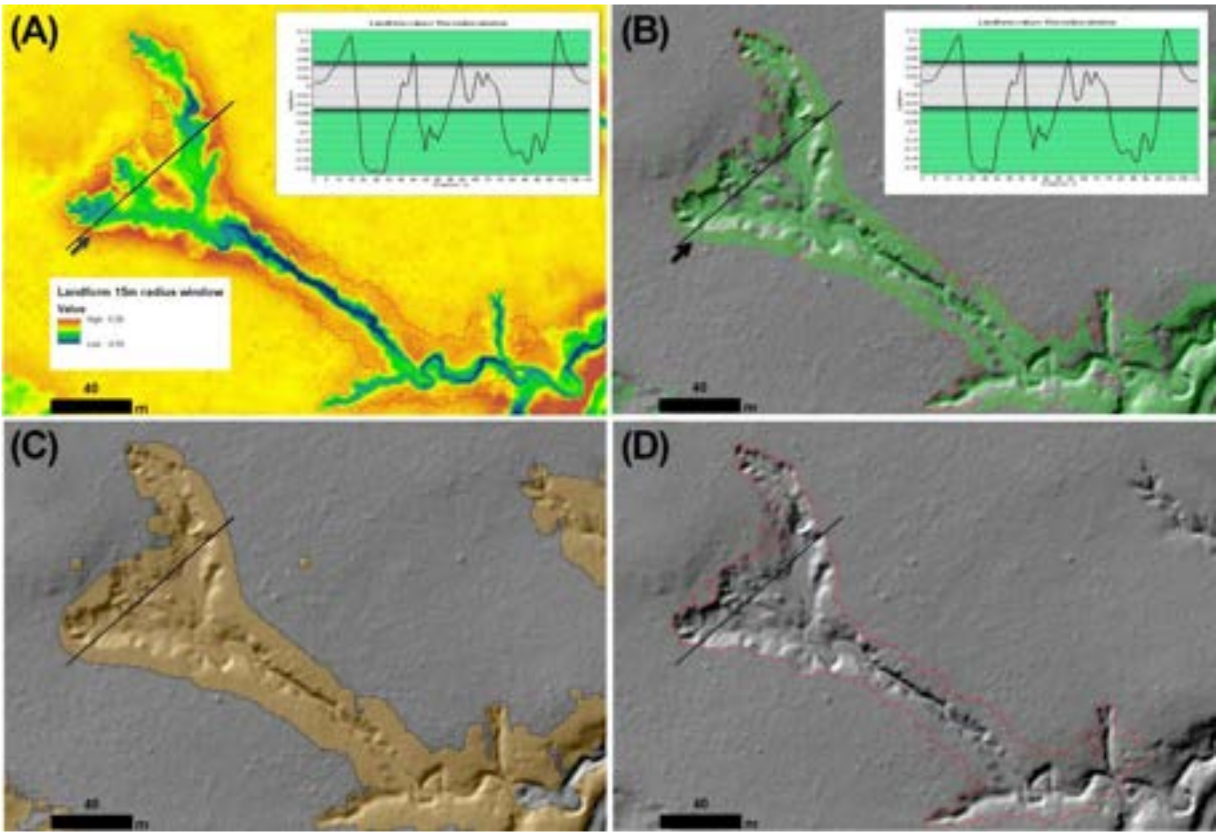

Figure 23: An example of the landform tool for determining the processing extent in alluvial settings. (A) Output of the landform tool with a cross section over the ELF headwall. Inset are the values with thresholds marking values <= -0.05 and >= 0.05. (B) Selection of convex and concave cells that exceed threshold values. Note some gaps in the selected area. (C) Final processing extent following filling and cleaning of the extent (D) Final ELF margin following the refinement of the boundary using MDHS within the processing extent. Note the downstream extent has been masked by the premade stream channel mask.

2.3.3 Disaggregate soft margins into individual ELFs

For the purposes of gully mapping in this project a minimum contributing catchment area of 500 m^2 was selected for gully/ELF initiation. Unless there was a high density of small units within an area, 500m^2 has been decided as the minimum feature area for mapping by our team for reasons a) an isolated gully smaller that 500m^2 would be too small to warrant a management plan given there are a plethora of larger active gullies and b) mapping ELFs smaller that 500m^2 would produce tens of thousands of polygons, most of which would be filtered out anyway (as outlined in the methods below).

Once soft margins have been delineated, the features within the margin may have a set of ELFs nested within it. In some part this is related to area thresholds considered appropriate for an individual ELF, which in this study is in the order of 10^2 - 10^4 m^2, with a minimum area threshold of 500 m^2. The mapping of soft margins above does not set any area threshold on the unit mapped and often adjoining features were mapped as a single unit. As such, the soft margins must be disaggregated to produce individual ELFs. This is achieved through a watershed analysis of the internal hydrology of the ELFs.

Flow accumulation of a DEM clipped within the soft margin is undertaken and flow lines initiating at 500 m^2 are generated to calculate internal Strahler order (Strahler, 1957, Figure 24). A critical step in mapping gullies from other ELFs is to distinguish between gullies and stream channels (see section 1.1). Once a drainage feature accumulates enough flow, processes are initiated that form a permanent channel (at least over 10^1 - 10^2 timescales) more typical of a stream or ephemeral channel. Two tools available to map the boundary between gullies and stream channels are catchment area or Strahler order. While both have limitations, selecting catchment area would definitively intersect a flow line once that area threshold is reached, regardless of the local context. Strahler order has other limitations, given that it is a function of drainage density. Nonetheless, here we have used Strahler order to identify the boundary of stream channels to produce features that have a consistent and complete hydrological relationship within their surrounding landform.

However, this is not done in parallel for all ELF (landscape) types. As with the boundary mapping, the disaggregation procedure is different for alluvial and hillslope (colluvial and rugged) ELFs due to the nature, form and physical differences between them. However, with this procedure the method employed is the same across all ELFs, but different decision boundaries are selected for each type. Decision boundaries were based on extensive visual observations of the available imagery and DEM, coupled with field investigations. Typically, we observed that the transition between gully and stream, while not consistent, occurred roughly over two Strahler orders. At this point ephemeral channels were apparent in most alluvial systems. In hillslopes, the transition tended to occur with a smaller contributing catchment area compared to alluvial/low slopes. Hillslope ELFs tend to be narrower and have less flow accumulation due to being higher in the catchment and having smaller contributing areas. As such, to remain conservative in our approach we have mapped ELFs at two levels of hydrological analysis, differentiated by Strahler order. For simplicity, herein we refer to these two levels as ELFs (i.e. single ELFs) and ELF Systems (two or more ELFs).

For hillslope gullies, the decision boundary for ELFs was Strahler 2, whereby all Strahler 2 flow lines and above were selected and described as channels. Thus, hillslope ELFs consisted solely of Strahler 1 flow lines mapped within the soft margin. ELF Systems were then classed as Strahler 1 and 2, with Strahler 3 flow lines described as channels.

Alluvial ELFs, which tend to be wider and larger in area and thus have a higher density of flow lines, required a higher Strahler order to define them. These ELFs consisted of Strahler 1 and 2 meeting a Strahler 3 or higher; Strahler 3 and above were classed as channels. As for alluvial ELF systems, Strahler order 4 were selected as channels.

Using these decision boundaries, a channel mask is made by buffering the flow line by 2.5 m. At the intersection between flow lines and the channel mask, initiation points for delineating ELF units are snapped to the flow line (Figure 25B). The purpose of this buffering is to move the initiation point away from the channel bed and localise the ELF polygon along the contributing branch. This prevents mapping erroneous units due to flow lines running downstream parallel to the channel flowline (Figure 25A). At these intersections, using the watershed toolbox in ArcGIS the contributing area above the initiation points are mapped (Figure 24). These small "watersheds" are now mapped as ELFs, producing hydrologically consistent units within the soft margin. In some instances, an initiation point may not snap exactly to the required flow line and an ELF is missed. In those circumstances, either the step was reiterated with a buffer of 1.5 m, or it was mapped during the next step mapping ELF systems. The same procedure is then repeated using the higher order Strahler line and producing buffered channel masks to map ELF systems. Examples of this procedure are shown for both hillslope and alluvial ELFs in section 2.4.

Lastly, a combination of the two ELF soft margins representing ELFs and ELF systems will be passed to the filtering procedure. During the filtering a decision is made whether to keep the individual units or combine all the units into the system. This based on the proportion of bare soil, roughness and the presence or absence of a hard margin.

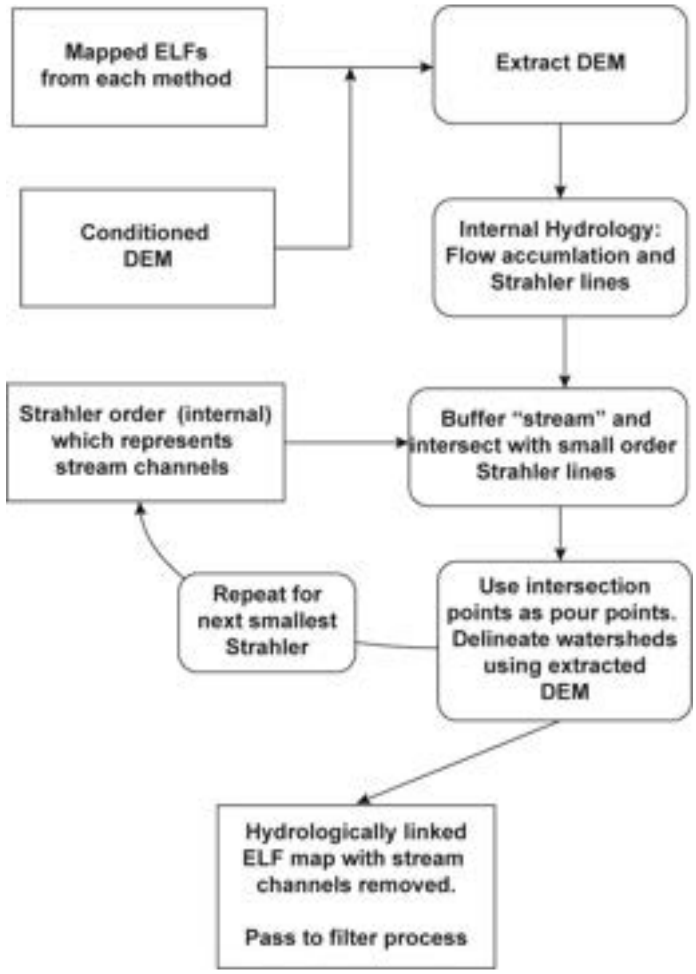

Figure 24: Internal hydrology and final selection of ELF shaded margins to be passed to filtering procedure.

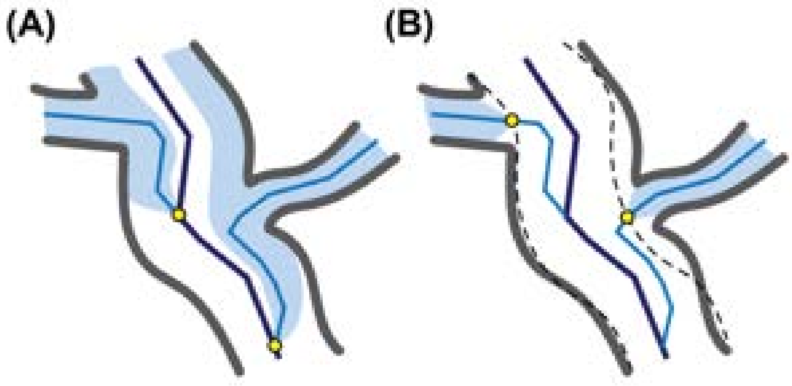

Figure 25: (A) Snapping initiation points (yellow points) at the intersection of flow lines maps erroneous units as flow accumulation within the channel connects pixels to the ELFs. (B) Once the stream channel flow line is buffered to create a channel mask (broken line) and the initiation points snapped at the intersection with the mask, ELF polygons are focused in the contributing branch.

2.3.4 Quality assessment of soft margin (ELF) mapping

Comparison of our results with ground-truthing showed a high degree of similarity between the methods (Figure 27), with a median root mean square error (RMSE) of 3.29 m, although the semi-automated mapping displays a better delineation of soft edges (low-angled slopes) than was detectable in the field. Note this validation was not attempting to follow the more obvious headscarp (or hard margin) of the gully (Figure 27A) as per Yang et al. (2017). At Mt Wickham, three gullies demonstrated overall agreement between the defined margins. Over 75% of the margins at all sites were within a 5 m distance of each other (limit of GPS detection) and > 99% of the data displayed < 10 m deviation (Figure 27B).

Additional quality assessment was undertaken by comparing 22 hand digitised gully boundaries with the mapping output. This validation yielded a similar median RMSE of 3.66 m. The results highlight a high degree of precision between mapping methods, but the method presented in this report is performed at a significantly quicker rate than is possible with other methods and can be executed across large landscape areas. A limitation of this method is that very shallow erosional features such as scalds are not readily included.

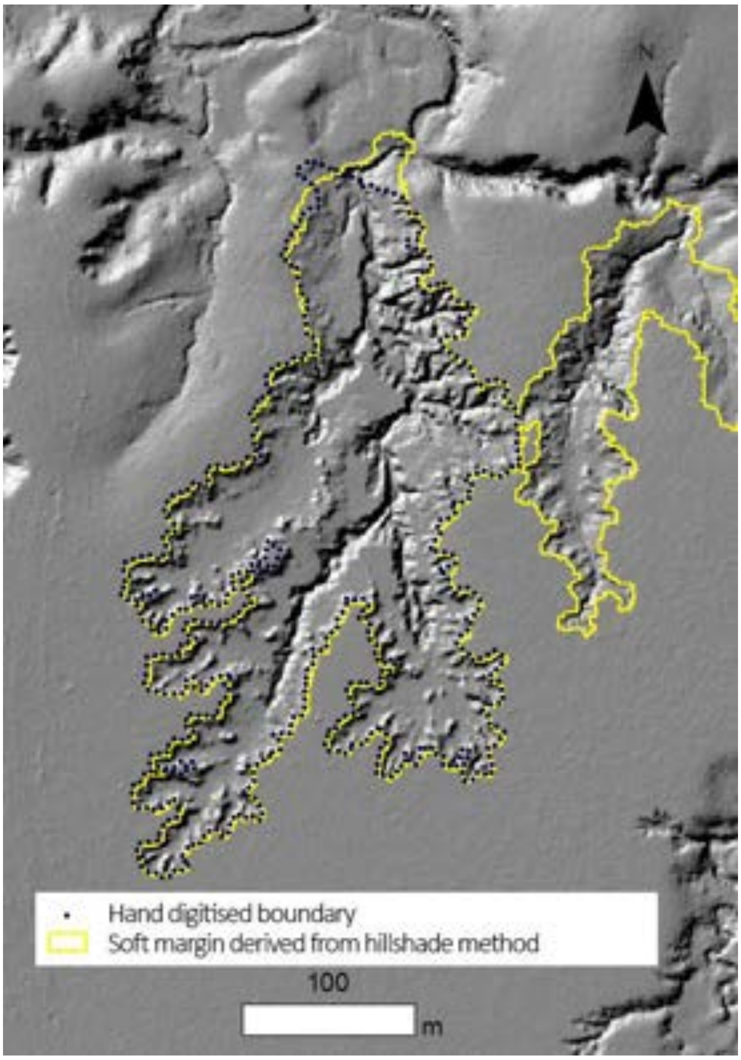

Figure 26: Comparison of soft margin mapping with hand digitised mapping boundaries.

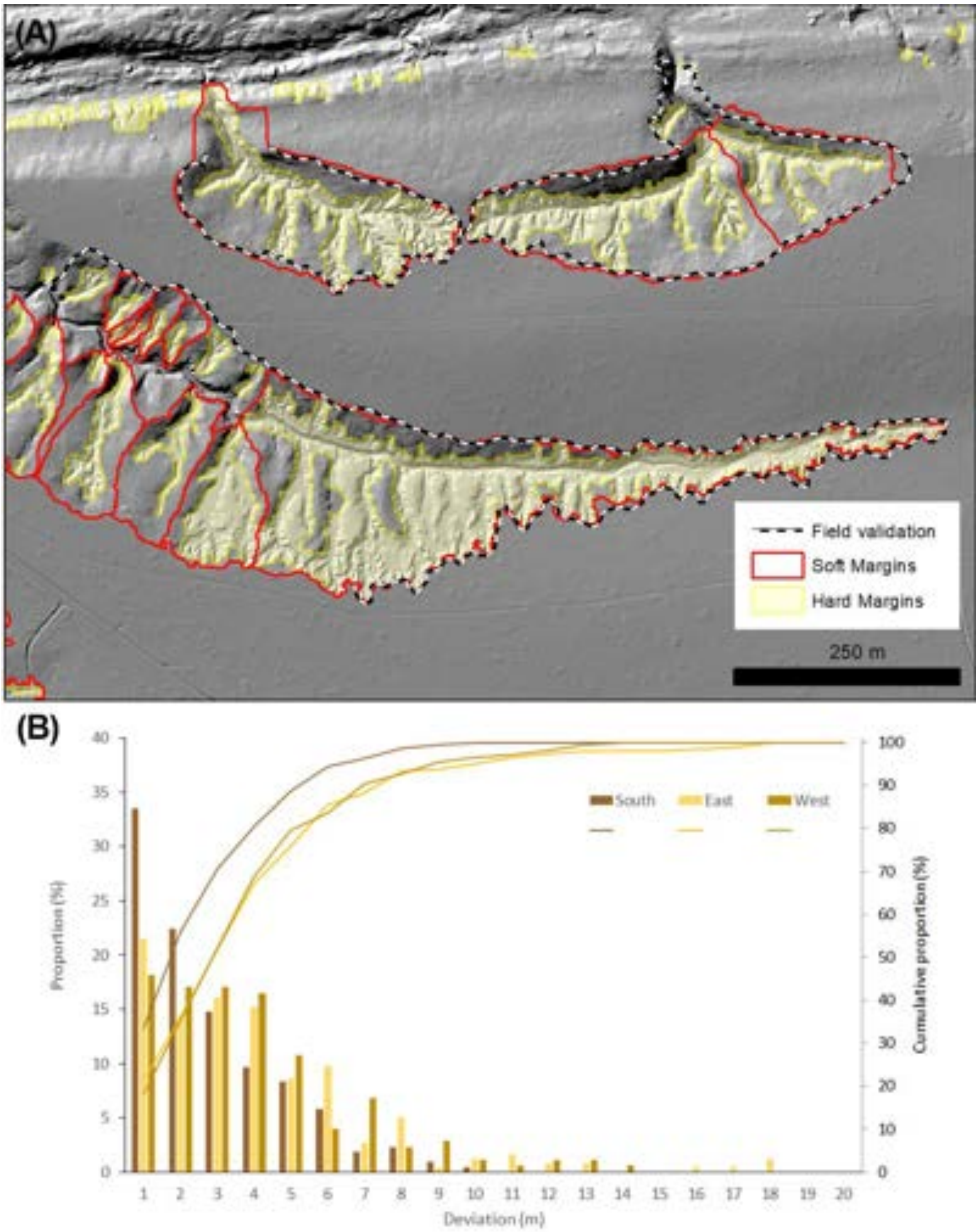

Figure 27: Example comparison of field validation of soft margins from semi-automated gully mapping at Mt Wickham Station. (A) Spatial comparison of mapped margins; and (B) the proportion of deviated distance between the semi-automated margin and field mapped boundary.

2.4 ELF Mapping Examples

The following two sections provide simple examples to illustrate the method of mapping in each of the two different landscape types. In each example, channel masking and landscape division has already occurred. This exercise is simply to illustrate to the reader the mapping and illustrate potential pitfalls that occur during the mapping procedure. This is not intended to be a tutorial of the method rather a report on what has been done.

2.4.1 Example mapping in hillslope settings

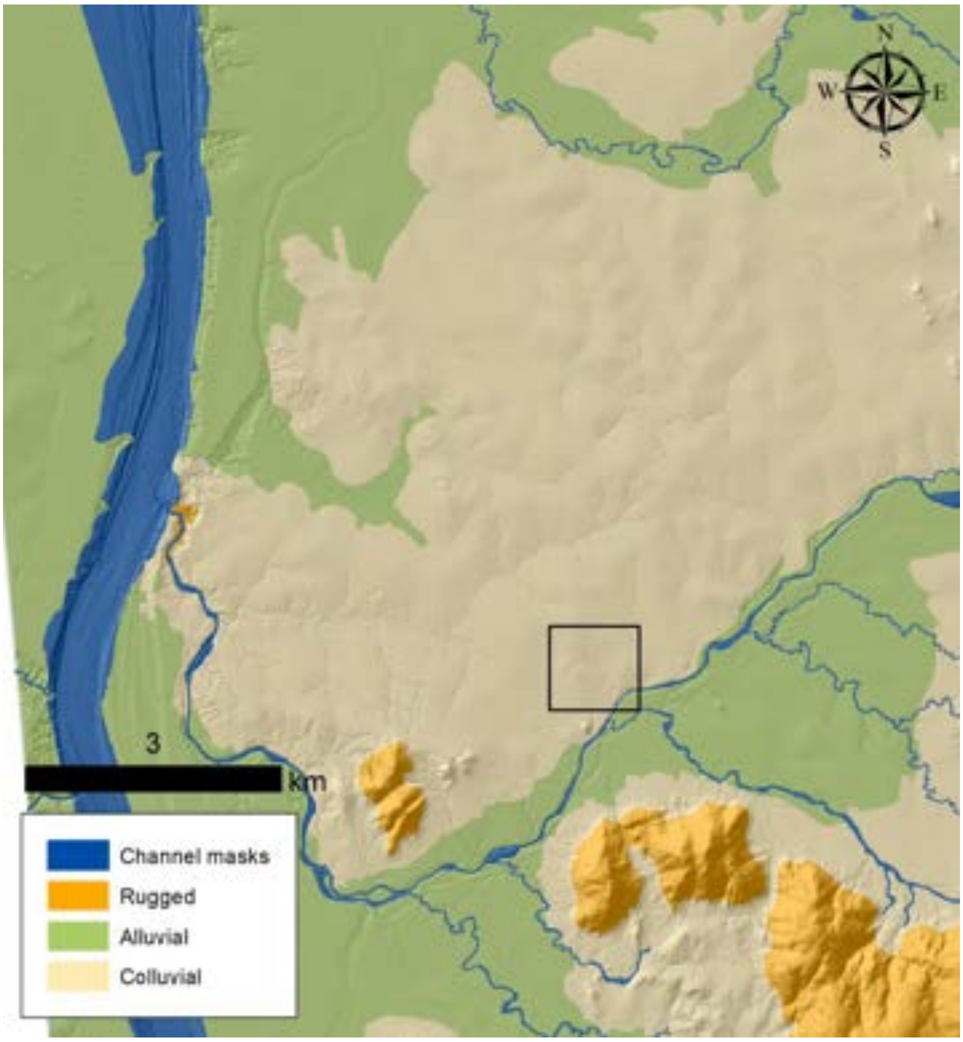

Figure 28: Example of mapping the landscape setting and stream channel masks. The inset box highlights the location of the example hillslope ELF map below.

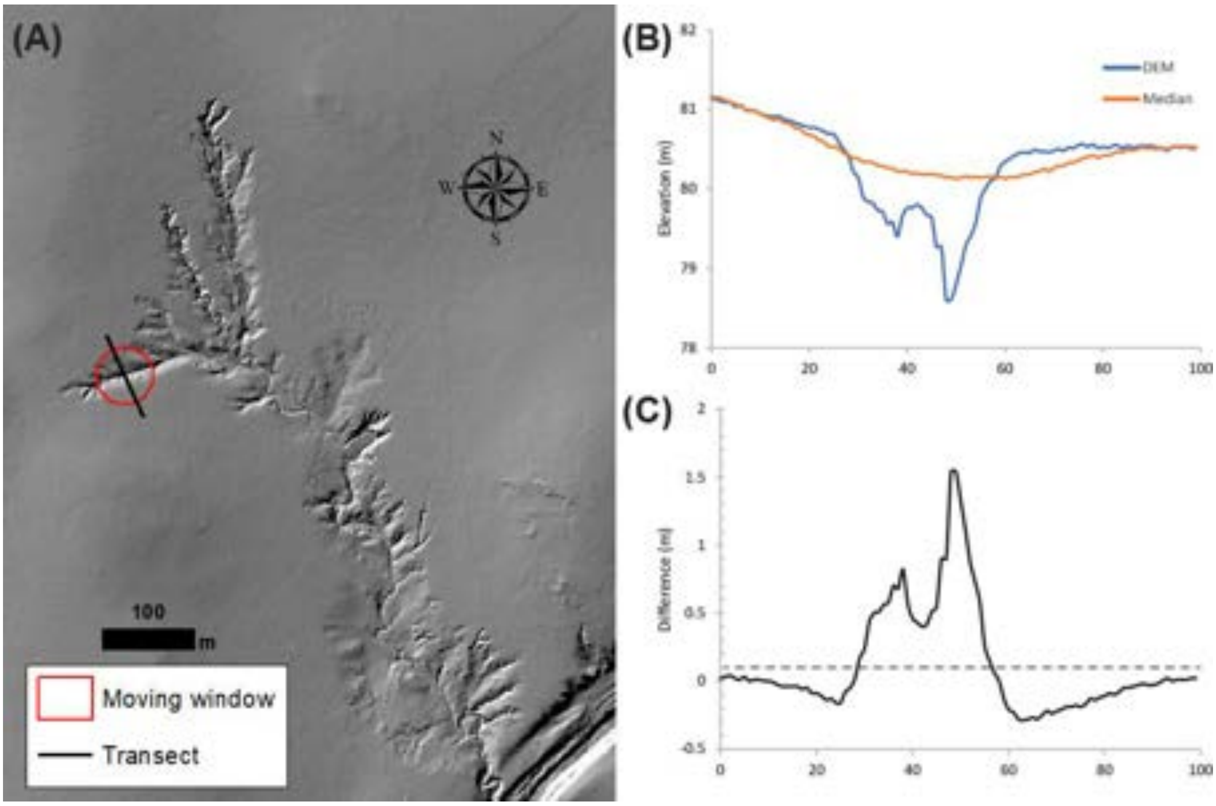

Figure 29: ELF boundary mapping procedure in an example hillslope ELF. (A) A moving window using a 31 m kernel radius is passed over the conditioned 1 m DEM. (B) Transect of the conditioned DEM and the Median DEM; and (C) Median DoD values, highlighting the 0.1 m threshold used to delineate the boundary.

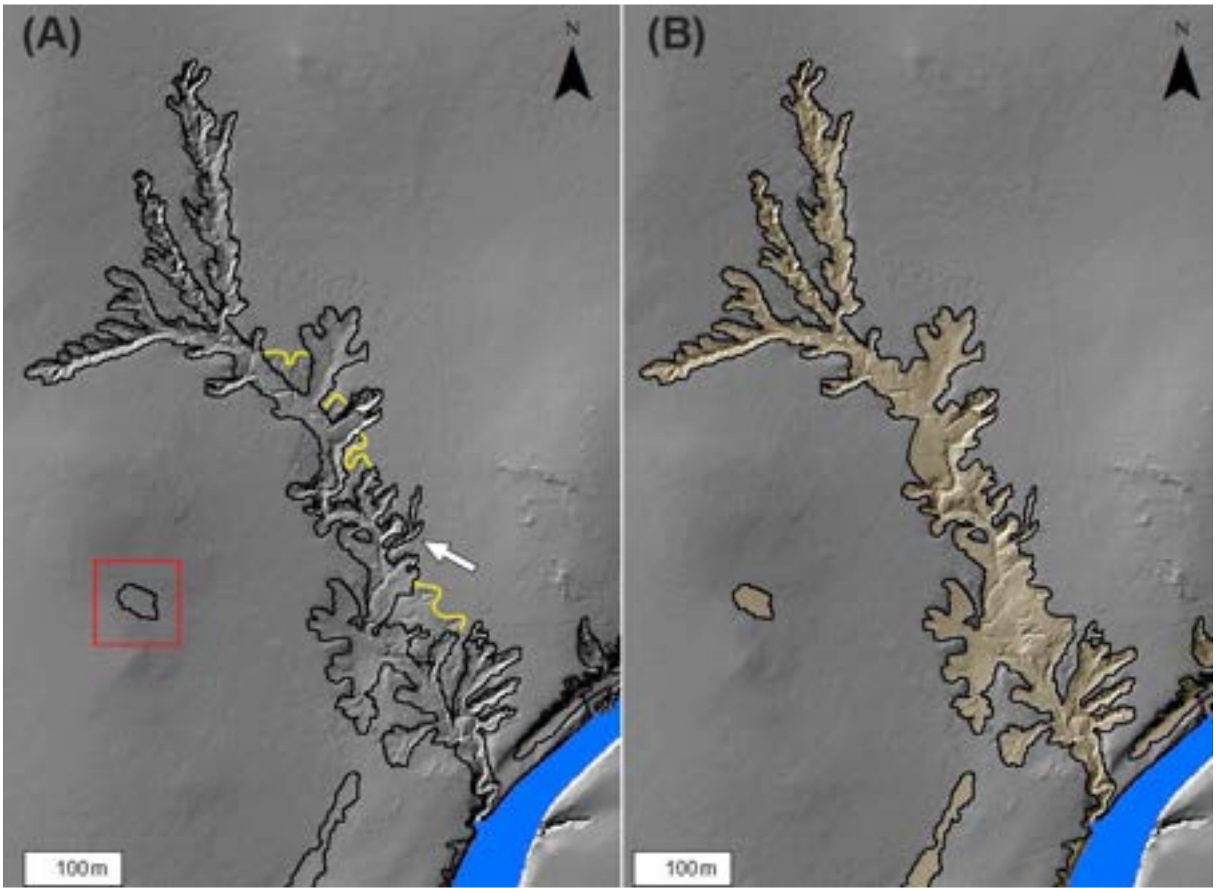

Figure 30: (A) Output soft margin from Median DoD. Yellow lines highlight shallow scarps associated with the gully that were below the 0.1 m threshold. The white arrow indicates a disconnected lobe, likely tunnelling that should be included even though it is not hydrologically connected on the DEM surface. Note a small depression (highlighted in red) that has been erroneously mapped. (B) Manual digitisation is required to include these features.

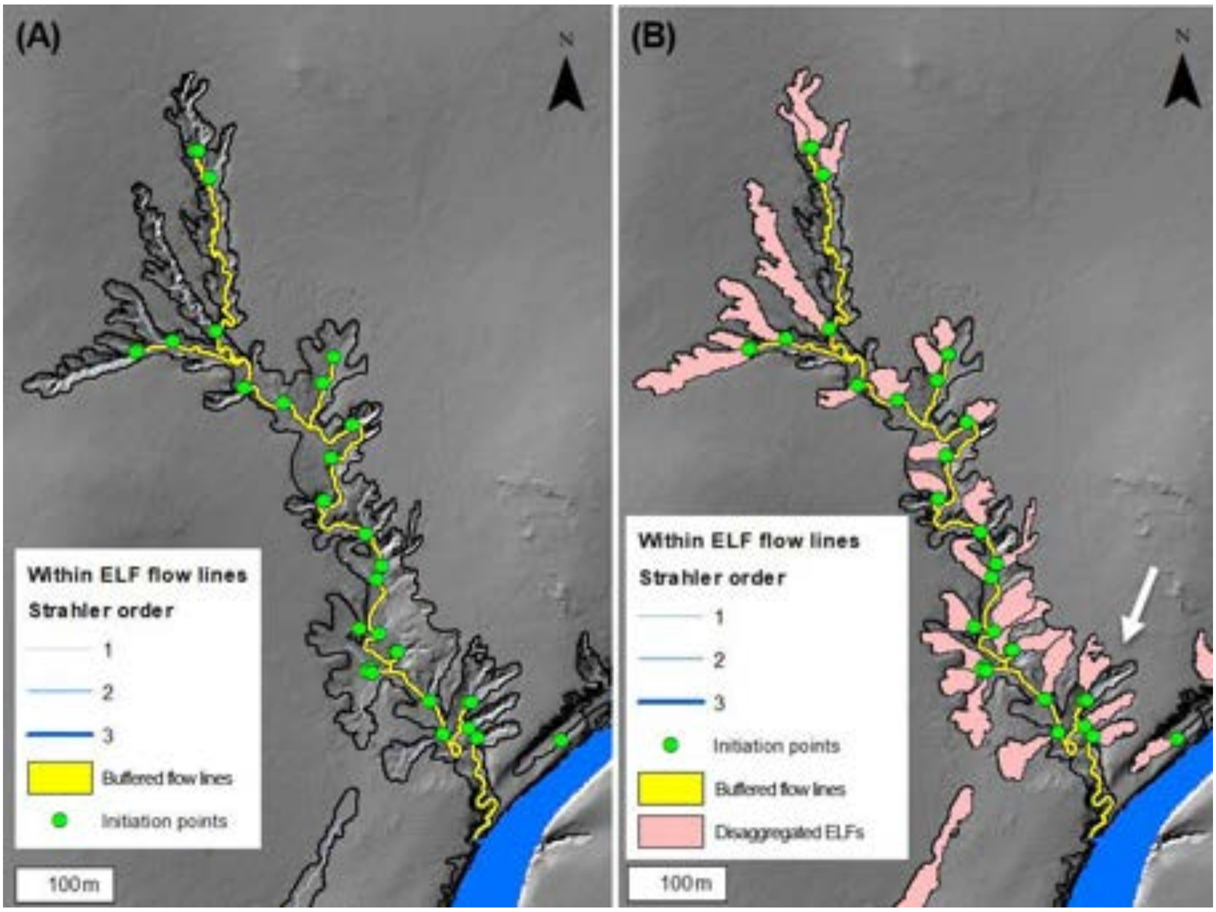

Figure 31: The hydrology within the soft margin is used to disaggregate the feature into functional ELF units (A) Buffer of Strahler Order 3 flow lines is intersected with lower order flow lines to produce initiation points. (B) Areas upstream of the initiation points are extracted to produce individual ELFs. Adjacent areas within the soft margin, which may feature lateral erosion, are not considered as potential gullies, as such features are considered streambank erosion. Other lobes, such as that marked by the white arrow, fall below the 500 m^2 area threshold.

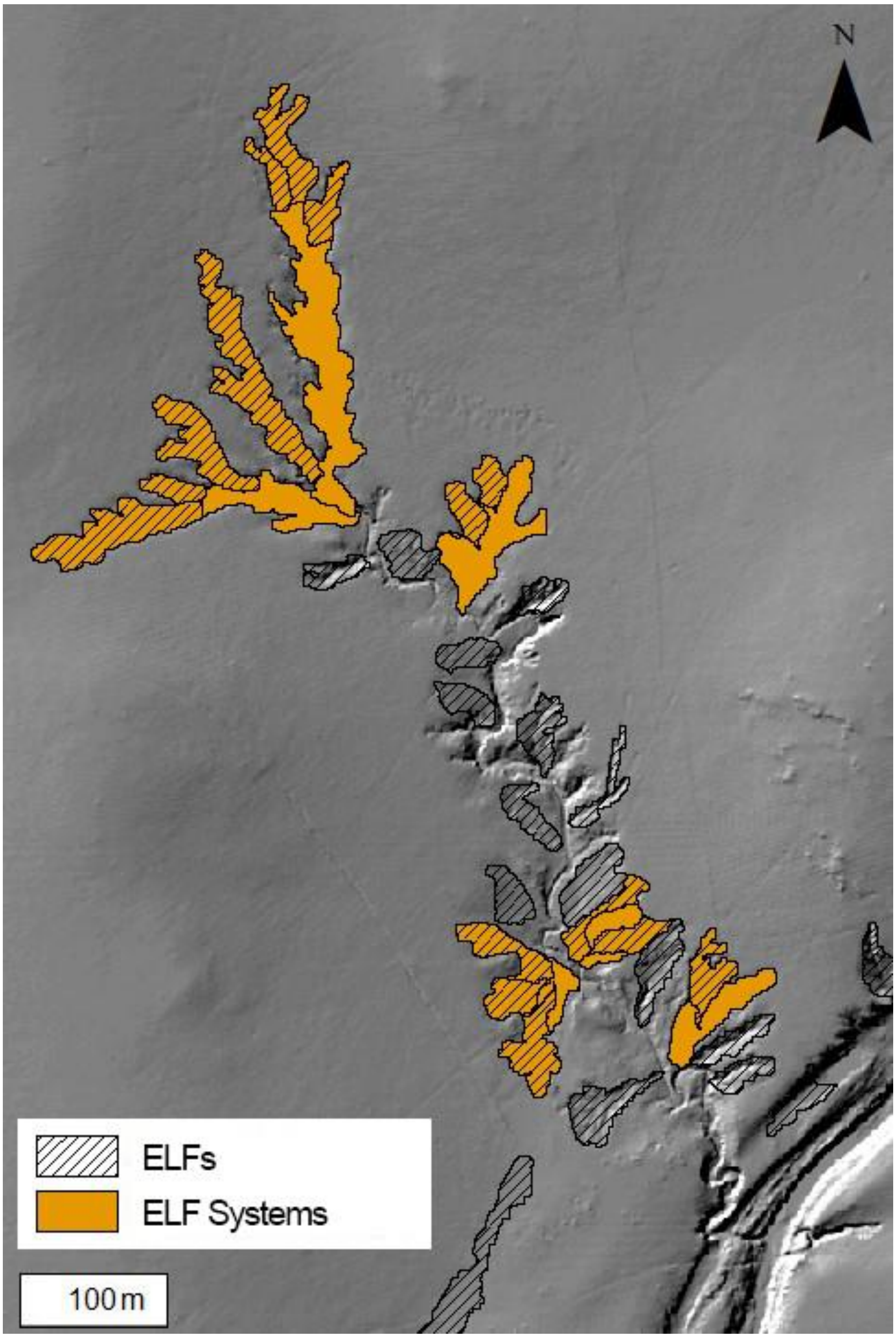

Figure 32: The importance of the internal hydrology in determining ELF boundaries is highlighted in the mapping of ELFs and ELF Systems; determined by respectively buffering second and third order streams in the disaggregation procedure. As both layers integrate important differences, both are assessed separately in the filtering stage.

2.4.2 Example mapping in alluvial settings

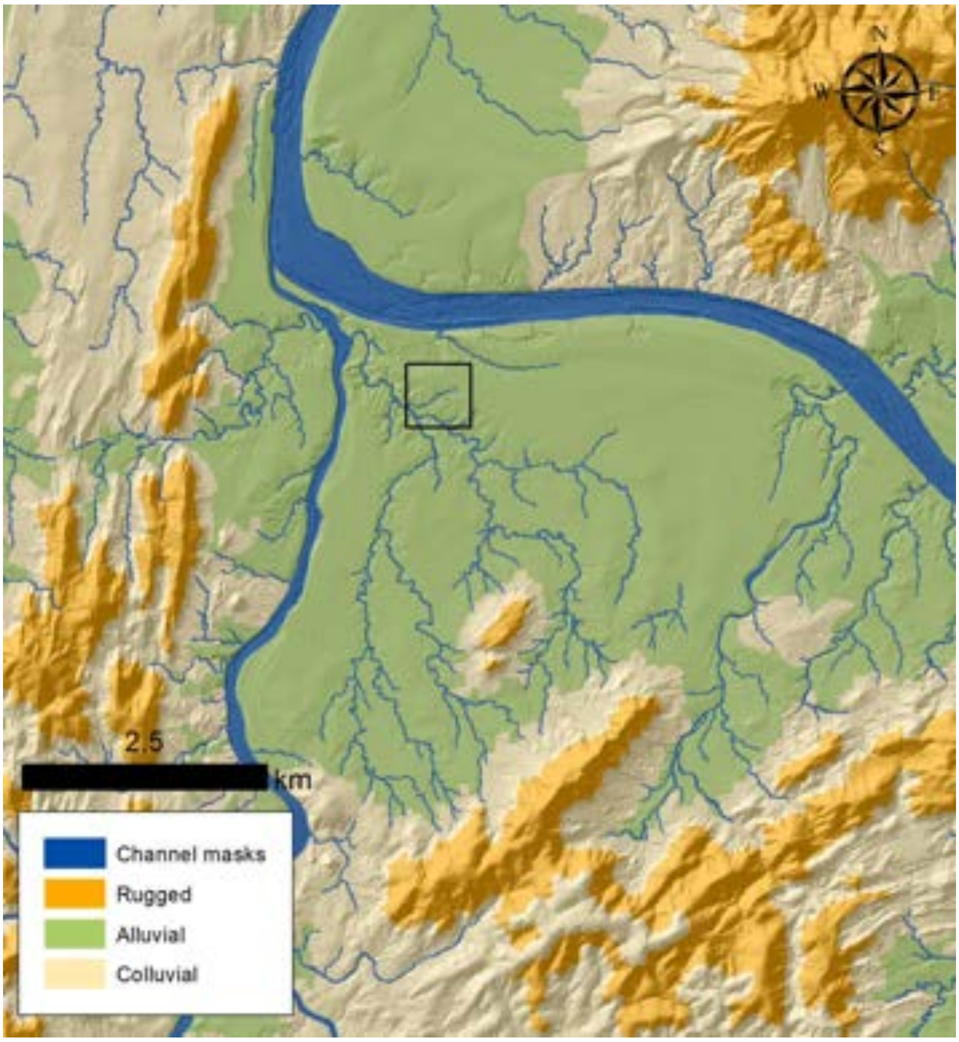

Figure 33: Example area of landscape setting classes and channel masks in the BBB study area. The inset box highlights an alluvial gully mapped in the following section. Mapping of the gully has been field validated.

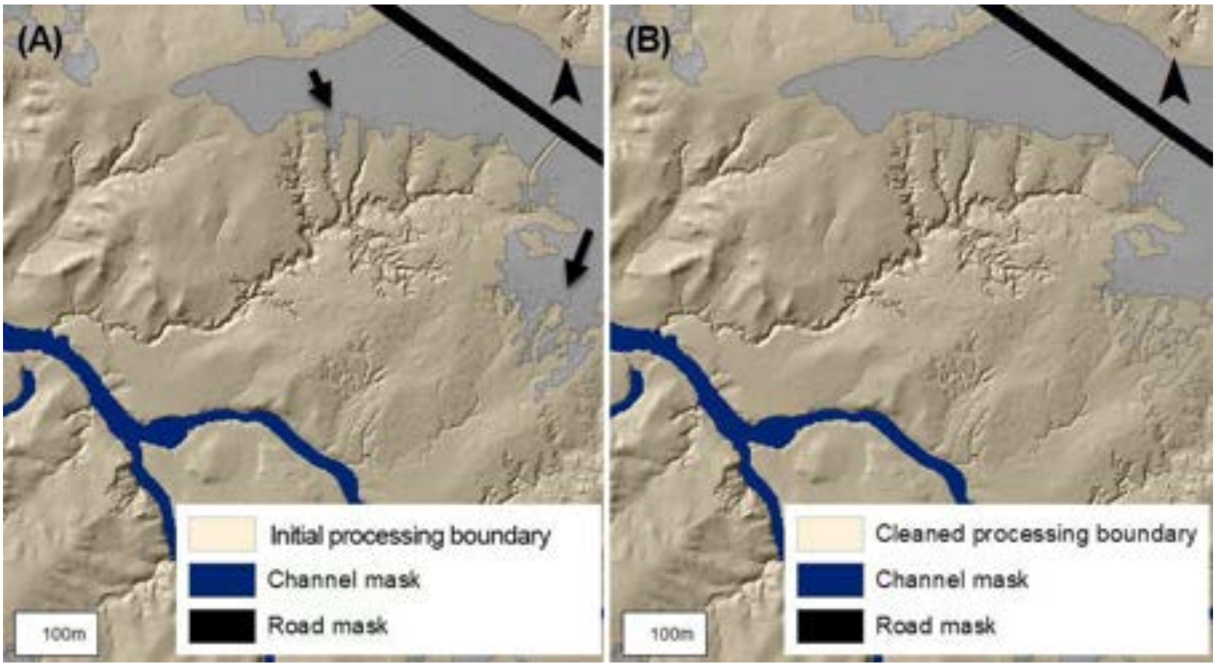

Figure 34: (A) Processing extent derived from concavity and convexity using the landform tool and a 21 m kernel radius. Arrows indicate areas requiring boundary cleaning. (B) Final processing extent after cleaning and smoothing of the boundary.

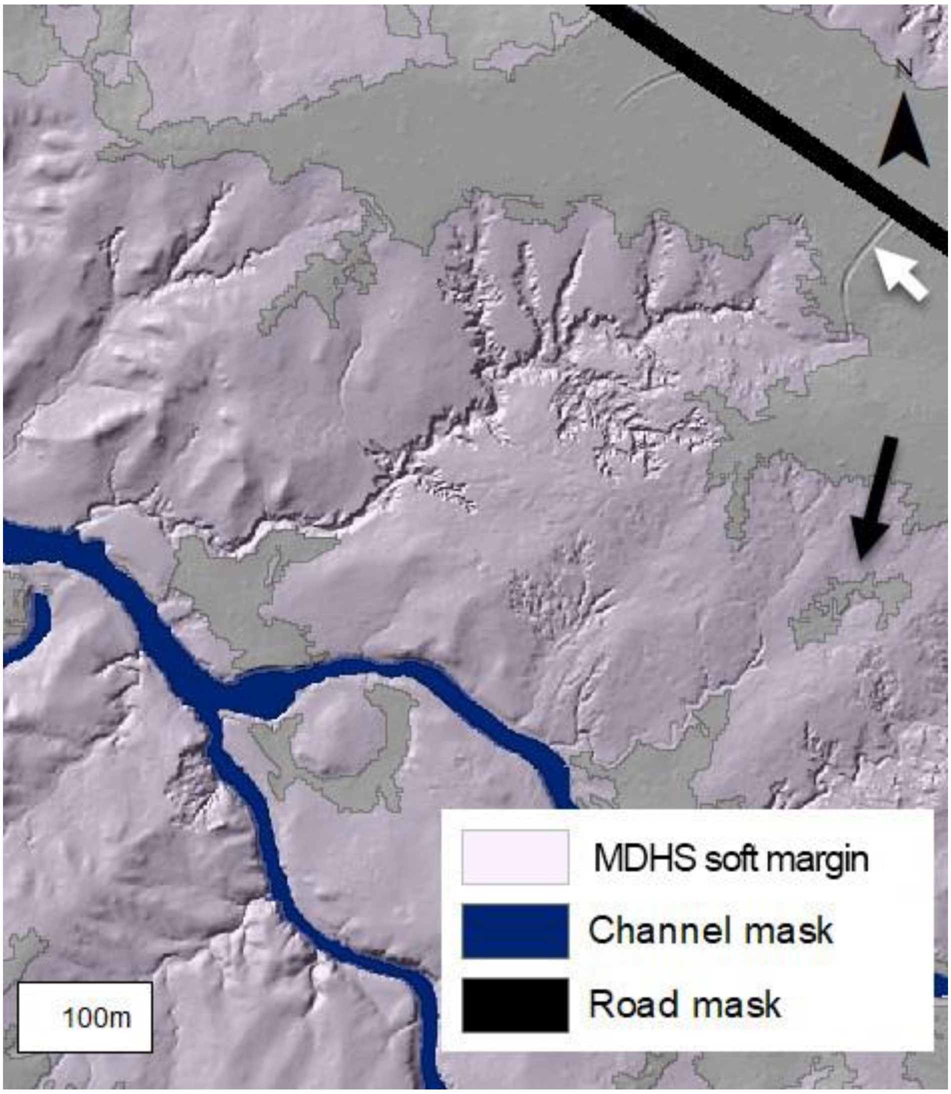

Figure 35: MDHS is operated within the processing extent to refine the soft margin. In this step, all ELFs with adjoining boundaries are mapped as a single unit. The road drain marked by the white arrow has been filtered out using morphological filters in the QAQC cleaning step. Some flat, open areas within the soft margin (e.g., the black arrow) will be filled in the cleaning step.

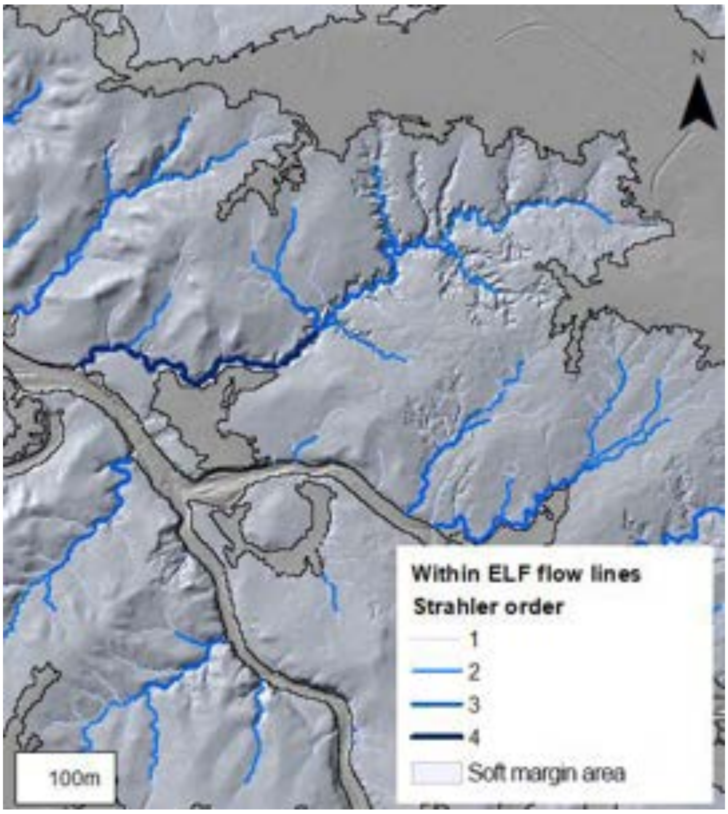

Figure 36: The internal hydrology of the soft margin is calculated using a flow accumulation threshold of 500m^2.

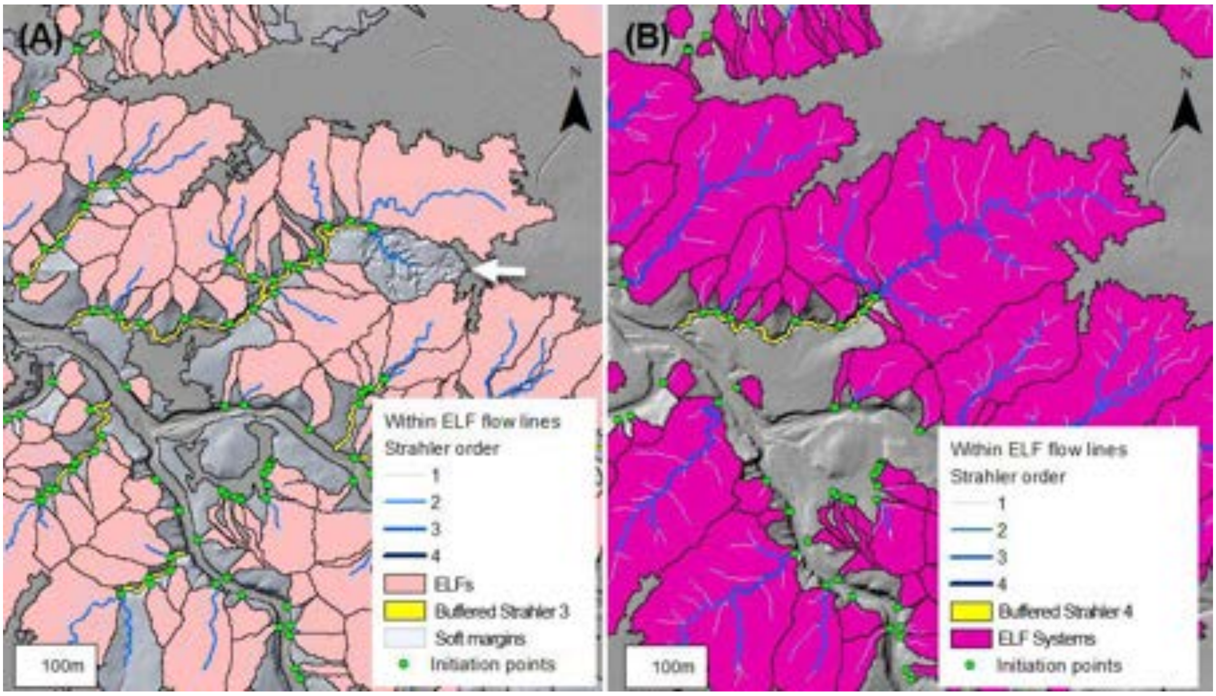

Figure 37: (A) Initiation points for ELFs are generated by buffering third order and above flow lines, and intersecting these with first and second order flow lines. ELFs are then derived through a watershed analysis of cells upstream of initiation points (within the soft margin). The white arrow indicates a missing polygon as the initiation point had not correctly snapped to the flow line. This can be iterated or hand-edited to adjust the point or mapped as part of the ELF System (B) The same procedure is used to map ELF Systems, except deriving initiation points by buffering only fourth order flow lines.

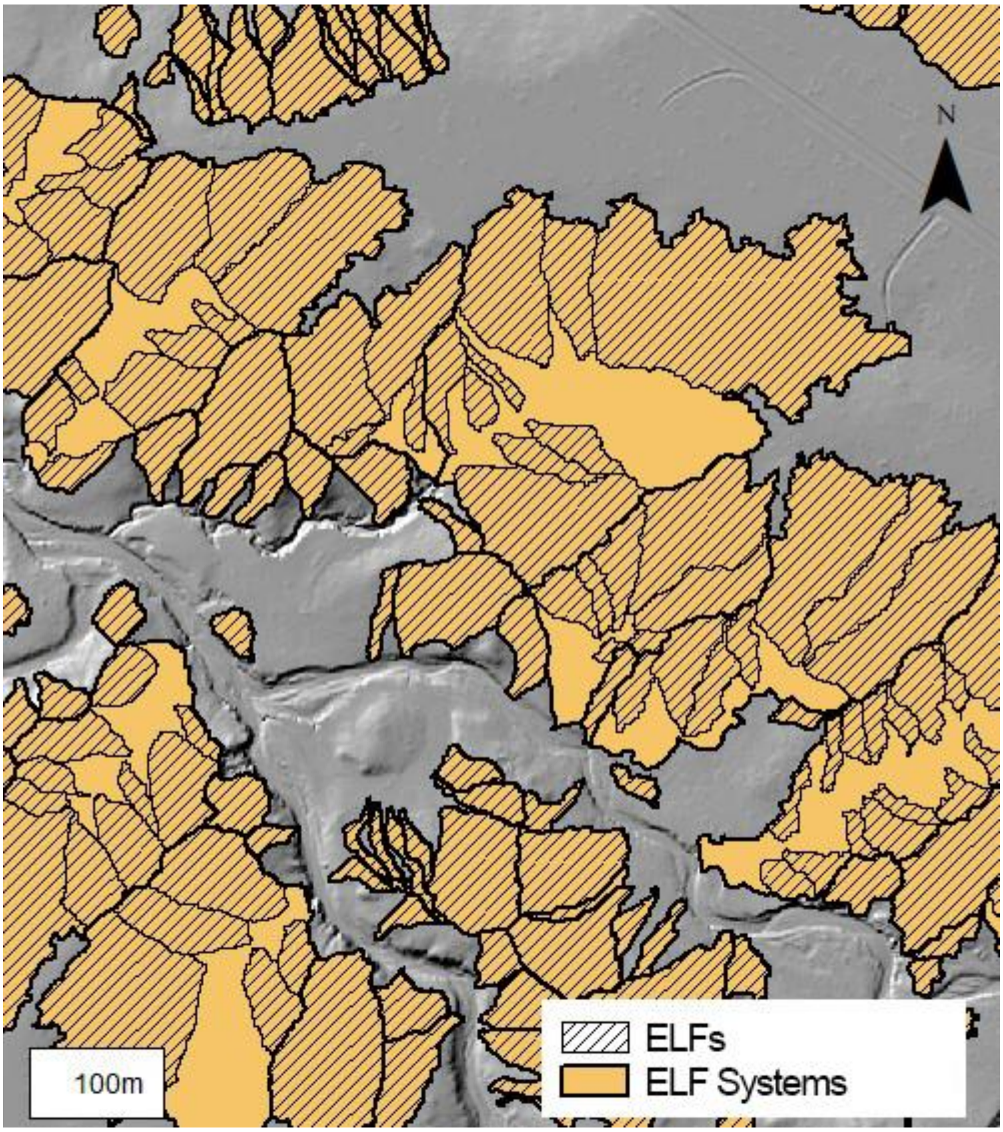

Figure 38: Alluvial ELFs and ELF systems tend to have a large amount of overlap, with systems generally including a greater downstream component and aggregating a group of ELFs. While both are mapped by the analysis, it is somewhat subjective as to which is the most appropriate scale.

2.5 Filtering mapped ELFs for actively eroding gullies

2.5.1 Conceptualization and indicators of active gullying

Following the mapping of ELFs, a rigorous filtering method was applied to distinguish between gullies and other ELFs, such as swales, depressions and low order drainage lines (Figure 9). As gullies are in principle distinguishable from residual landscape elements by high erosion activity, the filtering procedure relied on readily identifiable characteristics of active erosion from remotely sensed imagery. Characteristics of a gully defined in Section 1.1.2 relevant to this procedure include:

i. has a dominant proportion of a hard margin
ii. erodes unconsolidated materials and saprolite, dominantly bare soil materials;
iii. moderately steep bed gradient (~ 30^{o}; ~ 60 %),
iv. active head or walls on average > 0.5 m deep

In addition to these characteristics, the rapid nature of erosion within gullies, including block failure, rilling, tunneling, and deflation, generally produces high surface roughness (Figure 39). That quality has here been considered critical for the delineation of the hard margin, following the method of Korzeniowska et al. (2018). For mapping purposes, these criteria were interpreted to obtain spatially definable indices in accordance with the resolution of available data that could be processed across all ELFs systematically without operator judgement and decision-making. While the threshold values varied for each gully type (based on landscape unit), these spatially definable criteria were assessed within each ELF:

- Surface roughness: above a threshold for area (m^2)
- Baresoil: total area (m^2) and proportion of ELF
- Baresoil area within hard margins (m^2)
- Slope (%): maximum and mean threshold exceedances along flowlines
- Slope (%): maximum and mean threshold exceedance within hard margins
- Slope range along the perimeter of ELFs (for headcut detection)

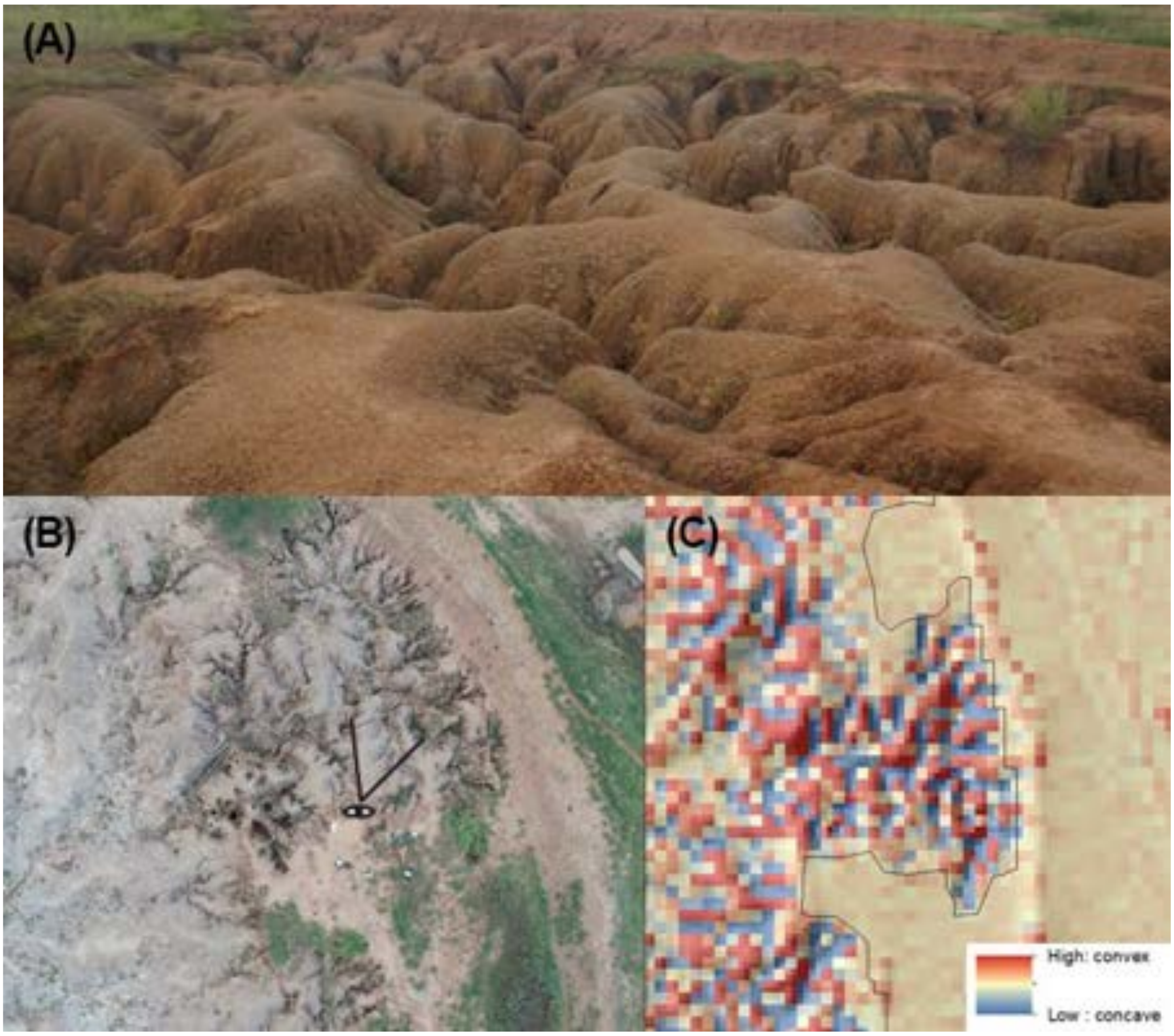

Figure 39: (a) The actively eroding head wall of a gully, with fluting, rilling, steep scarps and mass failures. (b) aerial photo of the gully, with photo point marked; and (c) The same location showing curvature of the gully, highlighting the complex pattern of concave and convex forms compared to the relatively neutral surrounding area. For gully analyses in this report, surface roughness has been calculated as the standard deviation of curvature.

2.5.2 Data sources and computed variables

Firstly, ELFs were defined into each category depending on which landscape setting class the majority of their area was located in (if they were along the boundary of two landscape classes). This formed the basis for gully type outlined in section 1.1.3. Variables used to analyze ELFs for active gully zones and to differentiate types of gullies were computed from four candidate data sources. The first was the 1-m resolution DEM derived from the lidar data. The second was commercial PlanetScope Analytic data surface reflectance data in 3.7-m resolution raster format (here after referred to as PS). The third was 0.1-m resolution RGB aerial imagery acquired alongside the lidar data. Finally, the lidar data included not only a DEM but also a canopy height model. This section explains how these data sources were considered and the workflows by which individual land surface variables were computed from them.

Surface roughness was calculated using the method of Korzeniowska et al. (2018) as the logarithm-transformed standard deviation of curvature. The method provides a relatively simple and unsupervised classification of the land surface. This index of surface roughness was used to define hard margin boundaries, which are generally interpreted as actively eroding portion of a gully, within the ELF (soft margin). In some features, the hard margin and soft margin are share the same boundary while in others the hard margin is discontinuous within an individual ELF. Total curvature was computed using a 2-m resolution DEM using the ArcGIS Curvature tool, following the method of Zevenbergen and Thorne (1987). Curvature values varied between -1 – 1 with a positive or negative curvature value indicating a concave or convex surface, respectively (Figure 39c). A value close to zero indicates a more planar surface. Roughness was calculated as the standard deviation of total curvature using a 5 × 5 kernel neighborhood, as per Korzeniowska et al. (2018). As the data was heavily right-skewed with most values approximating zero, a logarithmic function was used to normalize the distribution of the data, allowing greater ease of interpretation. The final output is a 2-m resolution raster of surface roughness with unitless values between -3 – 3.

Percent slope was generated using the spatial analyst Slope tool in ArcGIS. Values were extracted along flowpaths previously generated within the ELFs and separately from the hard margin area. Maximum slope percent and one standard deviation above the mean of slope were then calculated for both flowlines and hard margins within each ELF.

Baresoil was determined using PlanetScope Analytic data (Planet Team, 2017) and aerial imagery collected concurrently with the lidar acquisition. Available PS imagery, generated within a one-month period of the lidar acquisition date at each site, was selected and downloaded from the Planet Explorer. Planet provides 4-band multi-spectral ortho scene data for analytic and visual applications. The provided product is orthorectified, radiometrically calibrated into top-of-atmosphere radiance data and then atmospherically corrected to surface reflectance, resampled to 3 m (Planet Team, 2020). This data was specifically selected for <10% cloud cover and >90% coverage in a given flight. Additional data from neighbouring days were selected to fill in any gaps for complete coverage. Following data acquisition, scenes were mosaiced in GIS to provide a continuous coverage dataset of the project area.

Bare soil was derived from the PS imagery using the modified secondary soil-adjusted vegetation index (MSAVI2). MSAVI2 was selected as the most appropriate vegetation index for the region for its capacity to separate vegetation signatures in areas where vegetation cover is low, or features a high degree of exposed soil surface, and has the benefit over other soil-adjusted vegetation indices in that it does not require the calculation of a soil-brightness correction factor (L). MSAVI2 was developed iteratively by Qi et al. (1994) to determine the per-pixel difference of the red band reflectance value against the near infrared band, using equation (1).

$$MSAVI2 = \frac{2\times NIR + \sqrt{(2\times NIR + 1)^2 - 8\times (NIR - RED)}}{2} \qquad (1)$$

This yields an output of vegetation greenness with values ranging from -1 to +1. A threshold of 0.35 was derived to identify bare soils from the output following empirical investigations of detailed gully site values across the basin. This data was preferable to the lidar canopy height model (CHM) in more appropriately defining areas of bare soil. Due to the limit of detection in the vertical resolution of the lidar data (~0.25 m), the CHM is unable to distinguish between bare soil and grassland with sparse coverage or grass height shorter than 0.45 m. As such, relying on the CHM data would result in a substantial overprediction of bare soil as anything below this limit would be classed as baresoil.

In addition, 0.1-m horizontal resolution RGB aerial imagery (ECW) was acquired alongside the lidar data and utilised for a separate analysis of baresoil. A supervised classification was performed, identifying up to four soil spectral types in each catchment. Up to 10 regions of interest (ROIs) were selected for each class, in each catchment, with the spectral range of each band (between 0 – 255) used to define the soil class. A supervised analysis was then performed to select pixels within each class across the catchment. One issue faced in using RGB imagery was shadowing below scarps and erosion faces in gullies. These areas, although generally limited, had very dark pixels outside the spectral range of the identified soil classes. As such, these areas, while they may be bare of soil, could not be included in baresoil calculations. Another issue in both the Bowen and Fitzroy catchment lidar blocks, the spectral range of one soil class overlapped with vegetation data. As such, this soil class was excluded from the analysis to prevent an overprediction of baresoil.

As the 0.1-m resolution of the dataset imposed challenges in processing, following classification, the 0.1-m pixels were aggregated to 1 m to make the data more amenable for further analysis. The coarsening of the resolution maintained the relevance of the processes being investigated while aligning the resolution with other datasets. This was achieved using the Aggregate tool with a sum statistic, with any pixel then defined by >33% bare classed as baresoil (Figure 40B). Morphological image filters (Haralick et al., 1987), using the ArcGIS Shrink and Expand tools, were used to remove single baresoil pixels by geometrically transforming the boundary of selected zones in a binary raster. Zones below value set for the erosion filter (Shrink) are erased. This procedure allowed us remove noise of baresoil patches < 2 m in area and focus the analysis on larger patches of baresoil related to erosion processes. Each soil class was then mosaiced together to form a single baresoil layer.

For both PS and ECW baresoil, the area and percent coverage was calculated for both the ELF and hard margin areas. In all further analyses, both baresoil indices were used in order to account for the limitations (spatial and spectral resolution) within each. As the resolution of each raster was different and derived from different sources, all rasters were aligned to the conditioned 1-m lidar DEM and tools utilised a snap raster function to ensure pixel alignment between datasets. A final resampling of binary rasters to 1 m resolutions was performed as necessary for ease of further analysis.

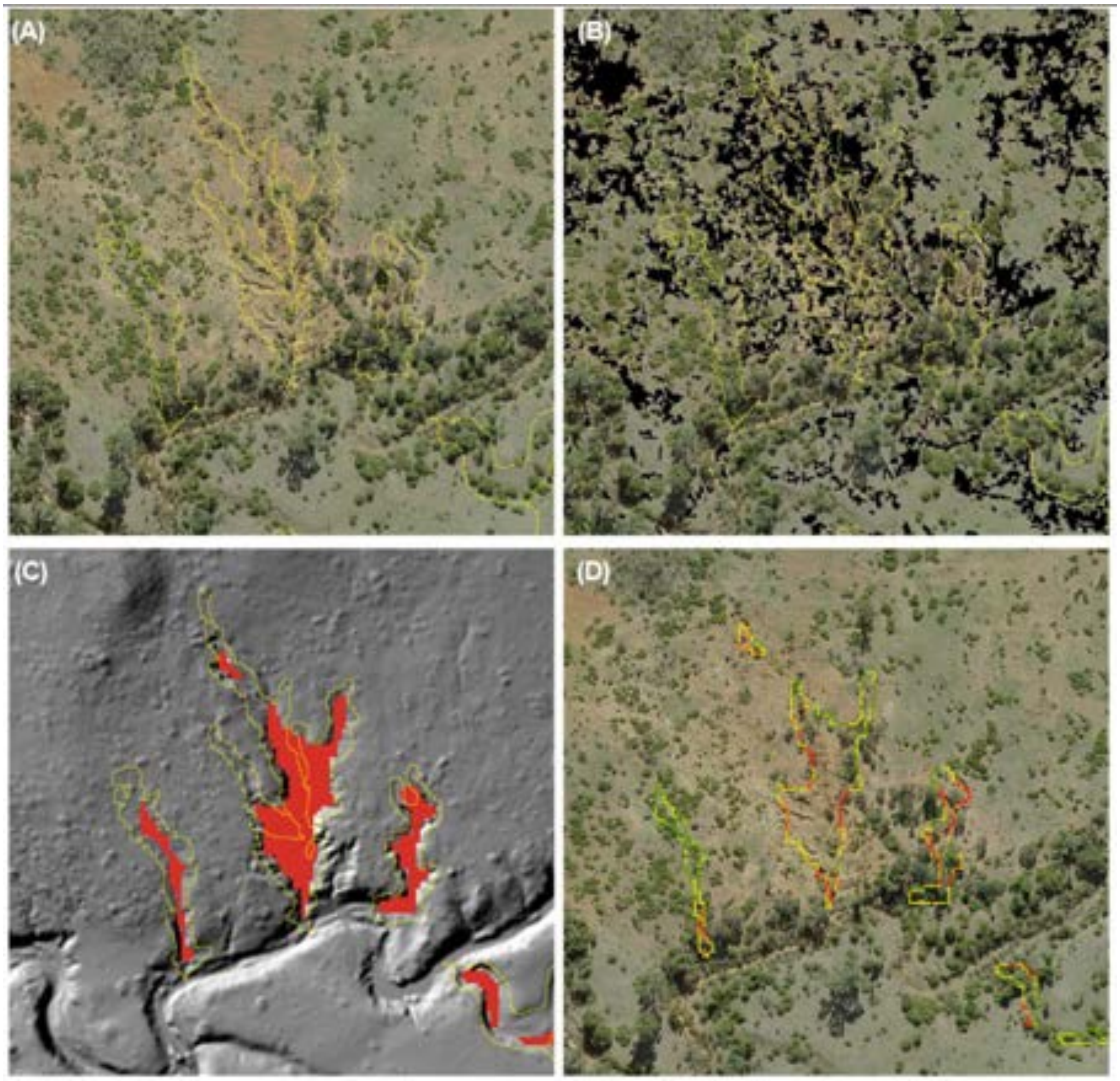

Figure 40: Example of ELFs attributes used for filtering to Gullies. (A) ELF soft margins delineated using Median DoD method, noting in the aerial imagery the centre ELF appears to be active, with scarps and rilling; (B) Baresoil shown in black was derived from a supervised analysis of the 0.1 m aerial imagery; (C) Hillshade overlay with hard margins (red) derived from surface roughness; and (D) Slope range along the hard margins from detecting head and sidewall scarps (red).

2.5.3 Filtering workflow

Given the differences in surface characteristics and gully types between landscape settings, a different set of filtering criteria and thresholds were applied in each landscape setting. For example, different criteria is required to identify larger, open gully forms in alluvial settings compared to the generally linear forms in most hillslope settings and as rugged landscapes were both steep and had high roughness, identifying actual gullies from stable drainage lines was a different challenge to identifying gullies on lower slopes. All ELFs went through a rigorous four-step procedure of filtering against these criteria to be considered actively eroding and therefore gullies (Figure 41). Thresholds were determined empirically and adjusted on the basis of operator- and field identified gullies and non-gullied ELFs. Figure 41 demonstrates the decision tree used for colluvial gullies, demonstrating the filtering procedure through each step with the conditions applied during this step.

As a first pass filter, any ELF greater than four hectares was assessed by the operator to determine whether it was a gully or a small stream. This was undertaken by visually assessing the lidar and aerial imagery data, considering vegetation cover, any apparent signs of erosion, planform morphology and terrain. ELFs with gully-like erosion features (i.e., scalding, rilling and headcut erosion) remained in the dataset, while others that clearly reflected small streams (i.e. vegetated, sinuous flowlines, in-channel bars) were removed. The small streams that were removed represented <1% of the dataset.

Following this manual step, an initial roughness threshold of 1.0 (unitless number) was set to define areas of high roughness across all gully types. This value was defined as an interim approximation of the hard margin following Korzeniowska et al. (2018) and repeat assessments in the Mt Wickham trial area. A morphological erosion filter as used in the baresoil analysis is preferred to remove any neighborhood effects in the calculation of roughness, shifting the boundary by the search radius width and producing tighter margins. However, for the initial analyses of hard margin this step was not undertaken; remaining conservative in the filtering steps and include the highest range of potentially active ELFs in the final gully selection. Within this high roughness area, any ELF with < 100 m^2 of both rough area or bare soil were removed and not considered potential gullies (Figure 41). A different set of metrics was used at this step for ELF systems, as they are larger in area and may contain several ELFs. As such, proportions of the above-mentioned metrics were preferred. In alluvial systems, 20% high roughness or 10% baresoil of the total area was required, while hillslopes (both colluvial and rugged) required either 20% high roughness or 1% baresoil (within roughness) to proceed. The discrepancy between these alluvial and hillslope systems is primarily due to the much more linear nature of hillslope systems analysed. Where baresoil is present, detection was generally more fragmented or occurred as narrow lines.

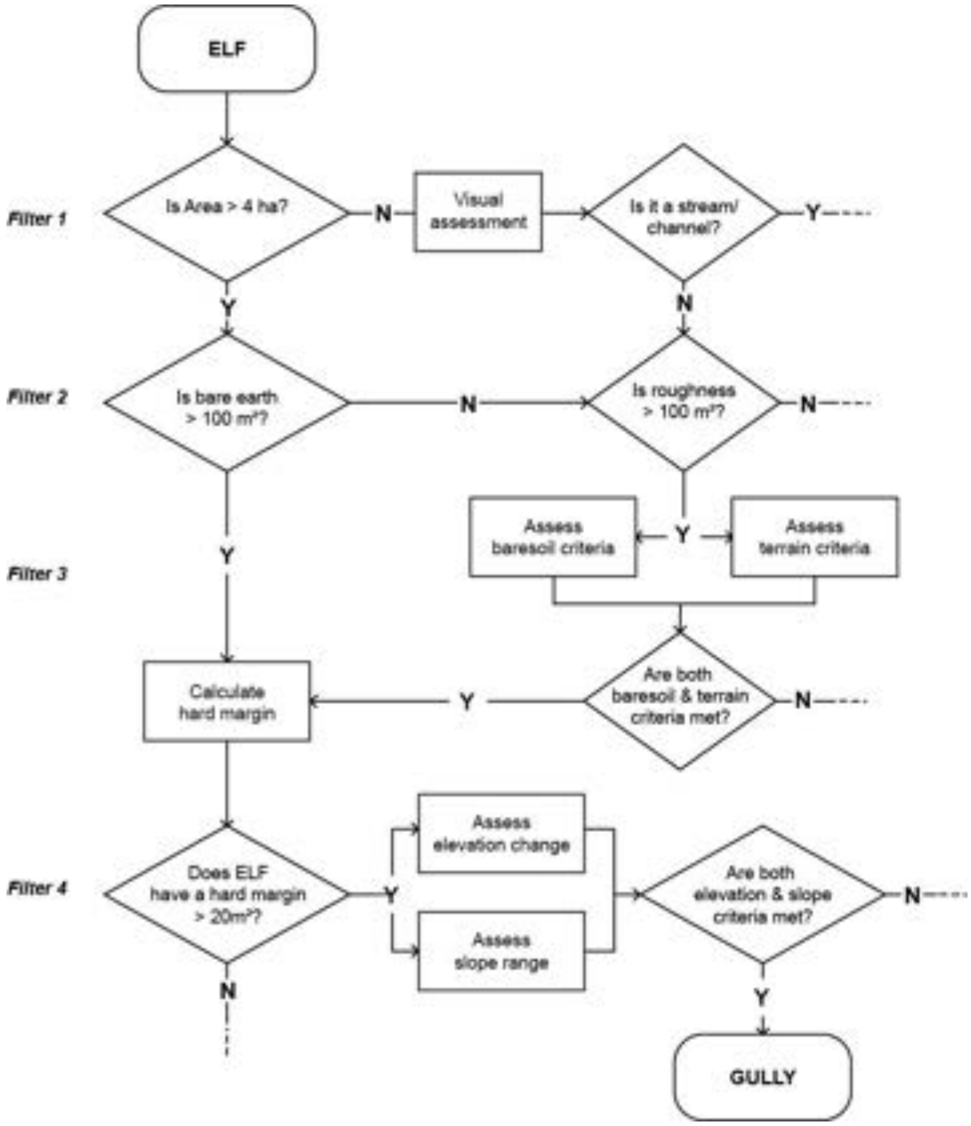

Figure 41: Flow chart of procedure used to filter ELFs and identify potentially active gullies. The assessment criteria in filter 3 and filter 4 varied for each gully type at both scales of analysis.

A third filtering step integrated baresoil and terrain components using AND/OR logical operators to rigorously assess the attributes of ELFs for spatially identifiable gully-like features. This step attempted to objectively apply minimum criteria comparative to the decisions an operator would make during visual assessment. An ELF had to achieve at least one baresoil condition, from either PS or ECW, and one terrain condition, being either a roughness component or slope component. The attributes and thresholds used within each setting are presented in Table 5. While these conditions were kept relatively constrained, ELFs that featured a high proportion or area of baresoil were maintained within the dataset for further investigation, on the assumption that a high proportion of baresoil is likely the result of erosion, despite lacking a significant roughness signature.

Table 5: Filtering variables and thresholds used for filtering ELFs within each landscape class during filter step 3.

	Alluvial	Alluvial Systems	Colluvial	Colluvial Systems	Rugged	Rugged Systems
ECW (m^2)			20			
ECW (m^2) – within Rough	25				50	50
ECW (%) – within Rough	2	10		3		3
PS (m^2)	75		5	150	10	
PS (%) – within rough		10				2
Slope (Channel) Max			25	25		
Slope (Rough) Max	40	40				
Roughness max	1.2	1.2				1.3
Roughness mean			1.2	1.2		

2.5.4 Hard margin mapping and filtering

A final filtering step integrated the results of the hard margin area and slope. To be considered a gully, ELFs are required to have a minimum area threshold of hard margin. Using roughness values extracted from within the ELF soft margins that remained in the dataset, a binary threshold was applied to the data following the histogram thresholding method by Otsu (1979). The Otsu method provides a relatively simple and straight-forward unsupervised approach to threshold selection by separating pixels of a grayscale image based on the intensity of pixels. The algorithm maximises the inter-class variability while minimising the intra-class variance, defined as the weighted sum of variances of the desired classes. This was performed in ArcGIS Pro 2.4 using the binary thresholding raster function. An erosion morphological filter was then performed to remove the effects of the kernel size in the neighborhood analysis step of calculating roughness, reclassifying a 2-pixel corridor along the hard margin boundaries as background and producing a more accurate map gully map. This generated a final hard margin layer which was then converted to polygons.

Once the hard margin layers were generated, the perimeter of the hard margin was extracted to investigate headscarps. While gullies have been characterized as requiring a headscarp with slopes of 30°, ~60%, such a simple slope threshold is impractical to identify headscarps. In steep, rugged terrain the natural profile of the hillslope can easily exceed such threshold. Likewise, due to the spatial resolution, actual headscarps can feature lower slopes with the elevation change spread across several meters.

A surrogate was derived from the range of slope over a 3 x 3 m area along the hard margin perimeter (Figure 42). Along the perimeter, if a sharp change in slope occurs, the slope range is high. In areas where the natural profile is steep yet continuous, the slope range remains relatively low (Figure 42B). A range of >30% change was classified as a high range and the sum of these values taken across the ELF. Figure 40d highlights the spatial distribution of slope range over several ELFs, in which the scarps on two are clearly divisible in red, while the leftmost ELF does not exceed required threshold along its perimeter. While total values varied for each gully type, gullies were required to feature a hard margin area, an elevation change in the hard margin > 0.5 m and a high slope range along their hard margin perimeter. This was again performed using logical operators.

A final manual, quality assurance check was undertaken after this filtering procedure to identify any infrastructure or manmade features, such as roads, dam walls, berms and contour ripping, which were manually deleted from the data. Overall, these manmade features represented <2% of the data. In each landscape setting, gullies and gully systems were then amalgamated into a single dataset for each gully type. For hillslope gullies (colluvial and rugged), where systems shared a boundary with individual ELFs, these were dissolved into a single unit. For alluvial ELF Systems, which comprised Strahler Order 4 and below, subordinate ELFs could be contained within their boundary. As such, an assessment was first conducted of whether erosion zones (assumed as the baresoil and hard margins areas) were > 80% located within subordinate ELFs or adjacent to these features within the Systems. If the erosion zones were dominantly constrained to the subordinate ELFs, the ELFs were preserved and the System disregarded. If erosion zones within the Systems were not dominantly constrained by the ELFs, the Systems were preserved and the ELFs dissolved. Figure 43 and Figure 44 highlight the distribution of ELFs in the Fitzroy block with each filtering step, at a broad regional scale and finer resolution example, respectively.

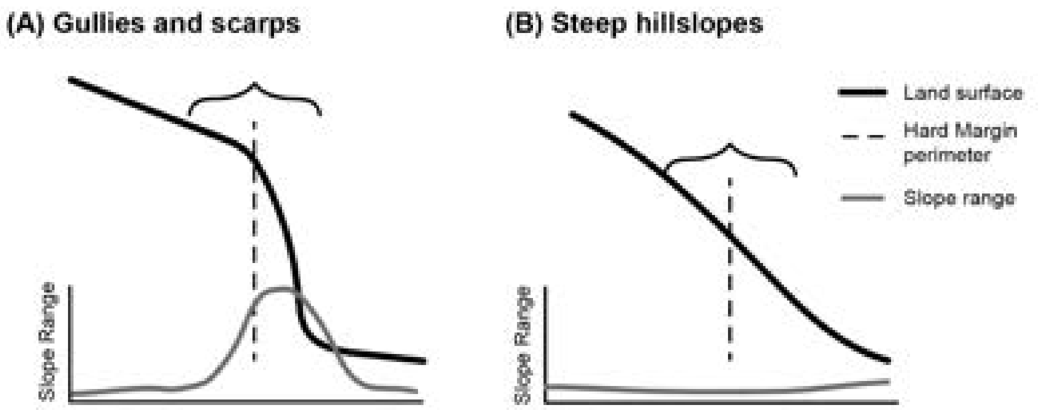

Figure 42: Conceptual idea how gully head walls, scarps and head cuts may be identified from the DEM.

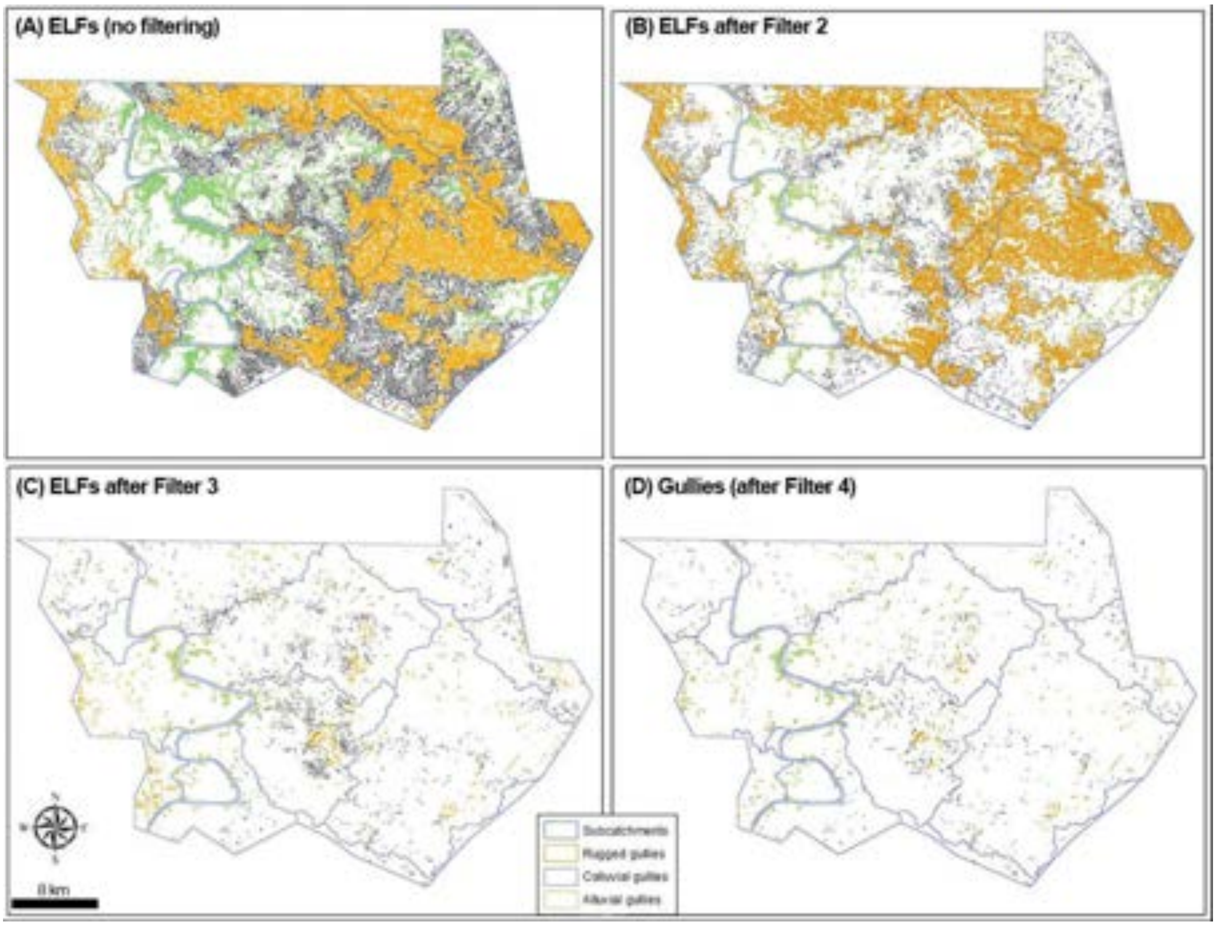

Figure 43: Example of the sequential filtering procedure from the Fitzroy lidar block showing the number of ELFs removed in each of the filtering steps until the final layer (bottom right) in which only ELFs with active gullies remain.

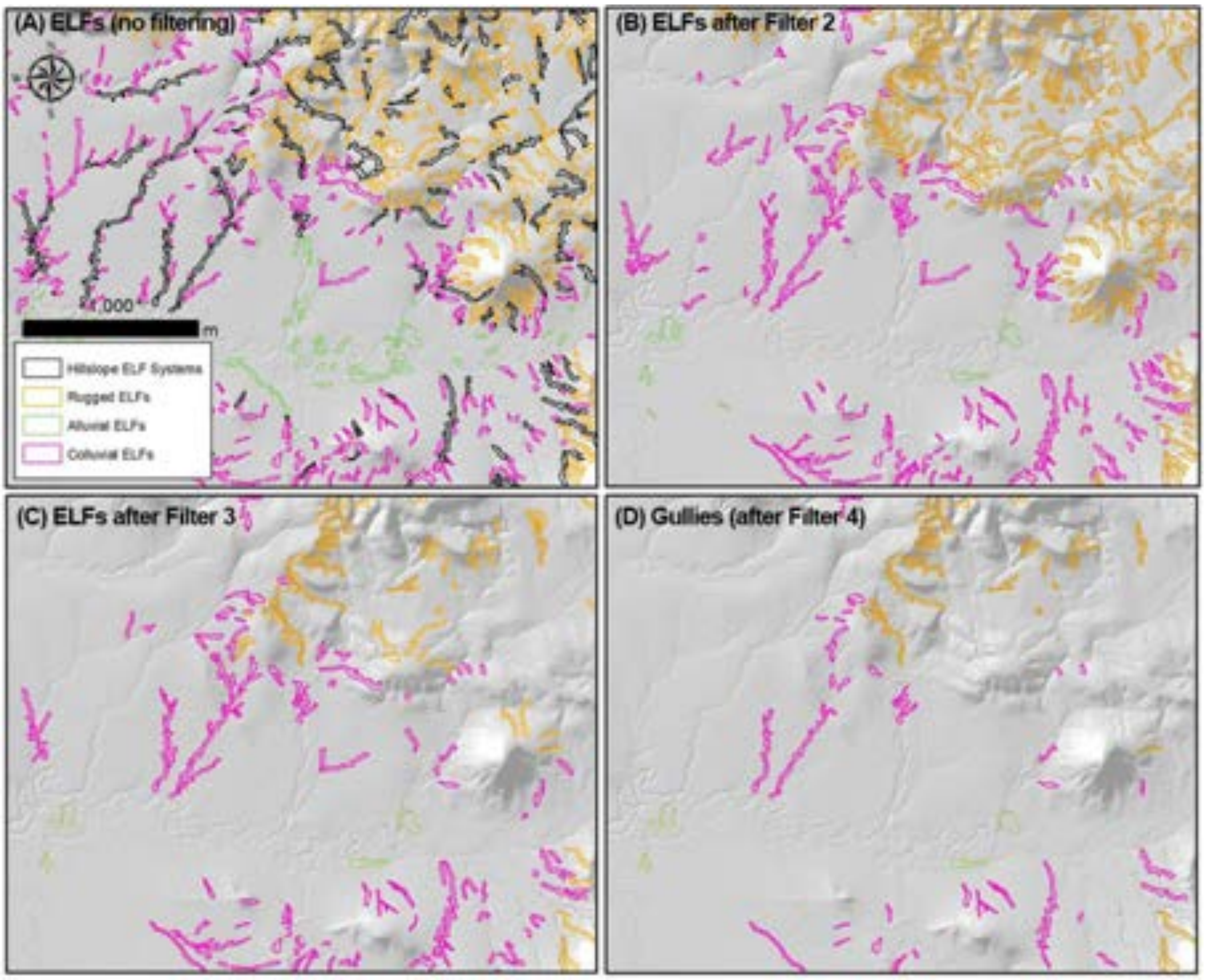

Figure 44: Higher resolution example of the sequential filtering procedure from the Fitzroy lidar block showing the number of ELFs removed in each of the filtering steps until the final layer (bottom right) in which on ELFs with active gullies remain.

2.5.5 Quality assessment of active gully mapping

The filtering procedure (Figure 43 and Figure 44) was validated on selected areas of the Fitzroy and Laura blocks of lidar. A sample area of 93.2 km^2 was chosen within the Fitzroy lidar area (Figure 45) and 81 km^2 was chosen within the Laura River lidar area (Figure 47). Within the sample area the underlying lidar data and high-resolution imagery of all erosional landscape feature polygons were individually inspected and scrutinised, and then the polygon was assigned a “gully” or “non-gully” status. This layer was then compared to the “gully” or “non-gully” status created by the gully filtering procedure. Performance statistics for each validation sample area are presented in Table 6. The total agreement (positive/positive and negative/negative) within the Fitzroy sample area between the two polygon layers was 90% (Table 6), and the confusion matrix of the total area of “Gully” status is shown in Figure 45. The total agreement (positive/positive and negative/negative) within the Laura sample area between the two polygon layers was 82%, and the confusion matrix of the total area of “Gully” status is shown in Figure 48. The F1 statistic for each sample area was 0.61 in the Fitzroy and 0.73 in the Laura (Table 6).

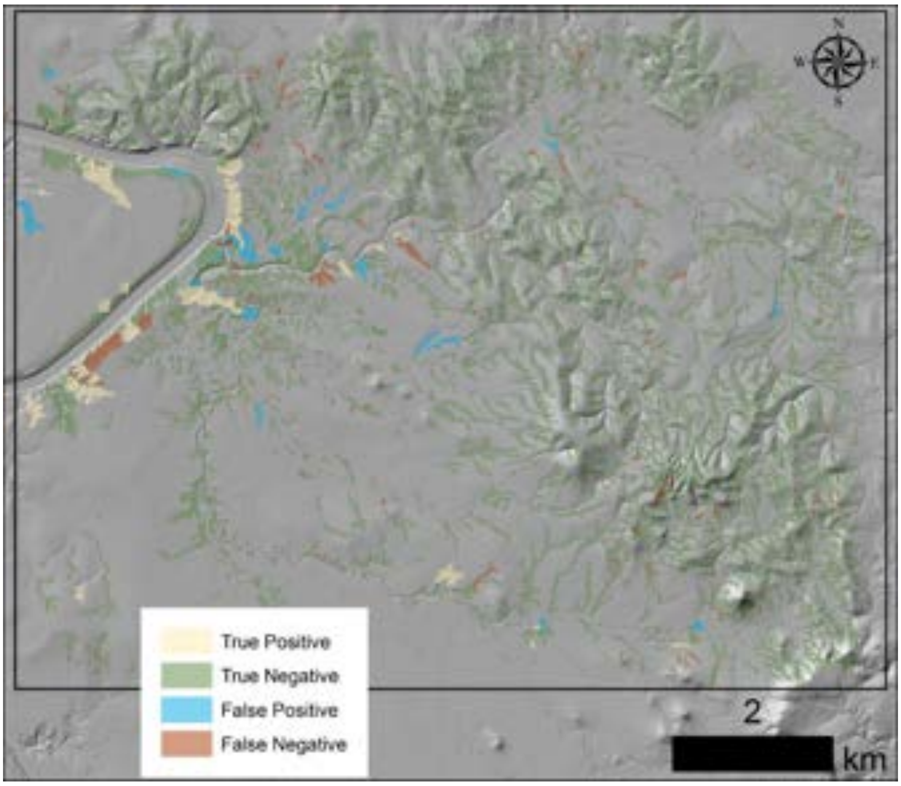

Figure 45: Fitzroy study area gully polygon filtering evaluation sample block (93.2 km2) with the occurrence of gully status agreement/disagreement.

		Filtered Gullies					
		Positive			**Negative**		
Erosional Landscape Features Assessed as Gullies	**Positive**	895,183 44.4%			237,144 11.7%		
		Alluvial 694,536 77.6%	Colluvial 162,183 18.1%	Rugged 38,464 4.3%	Alluvial 0	Colluvial 0	Rugged 0
	Negative	885964 43.9%			9484601		
		Alluvial 369,143 41.7%	Colluvial 322,835 36.4%	Rugged 193,986 21.9%	Alluvial 0	Colluvial 0	Rugged 0

Figure 46: Confusion matrix of positive and negative results from the filtering validation on the Fitzroy block. The percentages shown are the proportion of the sum of positive-positive, positive-negative, and negative-positive, that is, the negative-negative are excluded.

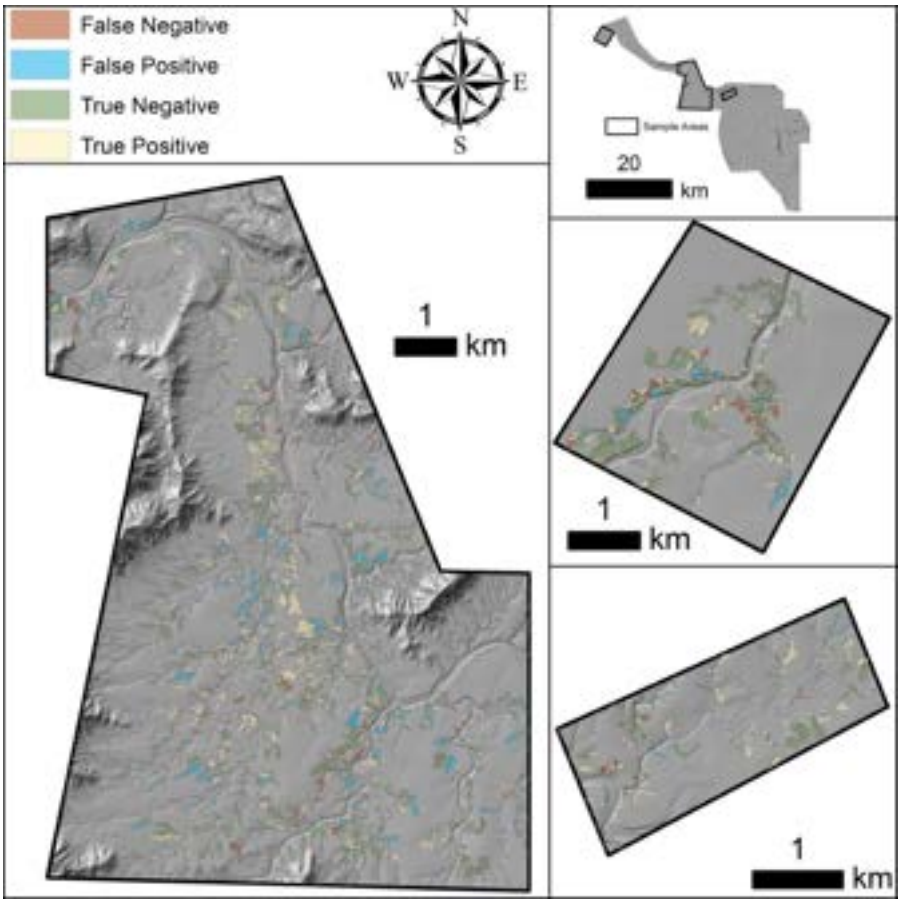

Figure 47: Gully polygon filtering evaluation sample blocks (81 km2) with the occurrence of gully status agreement/disagreement.

<table>
<tr><th colspan="2" rowspan="2"></th><th colspan="6">Filtered Gullies</th></tr>
<tr><th colspan="3">Positive</th><th colspan="3">Negative</th></tr>
<tr><td rowspan="4">Erosional Landscape Features Assessed as Gullies</td><td rowspan="2">Positive</td><td colspan="3">2,889,446
57.1%</td><td colspan="3">886,722
17.5%</td></tr>
<tr><td>Alluvial
2,873,945
99.5%</td><td>Colluvial
13,838
0.5%</td><td>Rugged
1,663
0.1%</td><td>Alluvial
0</td><td>Colluvial
0</td><td>Rugged
0</td></tr>
<tr><td rowspan="2">Negative</td><td colspan="3">1,285,544
25.4%</td><td colspan="3">6,981,288</td></tr>
<tr><td>Alluvial
1,200,537
93.4%</td><td>Colluvial
60,151
4.7%</td><td>Rugged
24,856
1.9%</td><td>Alluvial
0</td><td>Colluvial
0</td><td>Rugged
0</td></tr>
</table>

Figure 48: Confusion matrix of positive and negative results from the filtering validation on the Laura block. The percentages shown are the proportion of the sum of positive-positive, positive-negative, and negative-positive, that is, the negative-negative are excluded.

Table 6: Summary performance statistics of active gully filtering in each lidar block.

	Fitzroy	Laura	Total
Accuracy	0.90	0.82	**0.86**
Precision	0.50	0.69	**0.64**
F1	0.61	0.73	**0.70**
Cohen's kappa	0.56	0.59	**0.61**

2.6 Gully Metrics

A total of 88 attributes were derived for each gully. Primary metrics helped characterise gully morphology, degree of erosion activity and the extent of vegetation cover. A range of secondary metrics were also derived to further enable estimates of the intensity required for remediation treatment, although quantifying such estimates was not further considered in this study. A description of each of the 88 attributes defined for the mapped gullies (soft margins) is presented in Appendix 3. Most of the morphological metrics are well known functions drawn from the geomorphic literature.

In this section we outline in some detail several metrics developed for this project which we have used in the derivation of sediment yields for the gullies, and subsequently for determining rehabilitation requirements. The following outlines the creation and testing of the Potential Active Erosion (PAE) index and a method of estimating total volume of eroded sediment within a gully.

2.6.1 Potential active erosion

Following the mapping of the gully boundaries, there is a need to determine what proportion of the gully is eroding as opposed those sections that on a trajectory of stabilization. Ideally, multi-temporal lidar datasets can provide DEMs of difference to rigorously detect areas and volumes of landscape change. However, once a single lidar DEM has been created there is a time lag before subsequent datasets become available. To make the most of the existing dataset, on top of the delineation gullies to provide a baseline dataset, the areas of likely erosion can also be mapped.

It is a principle index in establishing mapped units as gullies as well as informing prioritisation of rehabilitation efforts and intensity of treatment required. The index of potential active erosion (PAE) highlights areas that are rapidly eroding at rates of > 0.07 m a^{-1}. The index uses a measure of surface roughness derived using the same workflow as the hard margin mapping, adapted from the method of Korzeniowska et al. (2018) and Patton et al. (2018). This uses a log-transformed standard deviation of terrain curvature, but at a finer resolution. Most erosion activity indicators translate to the morphology of gullies exhibiting high values of surface roughness (Figure 49), including fluting, rilling, block collapse, slumping and exposed tree roots. As erosion activity decreases, slopes relax to more diffuse forms with lower roughness.

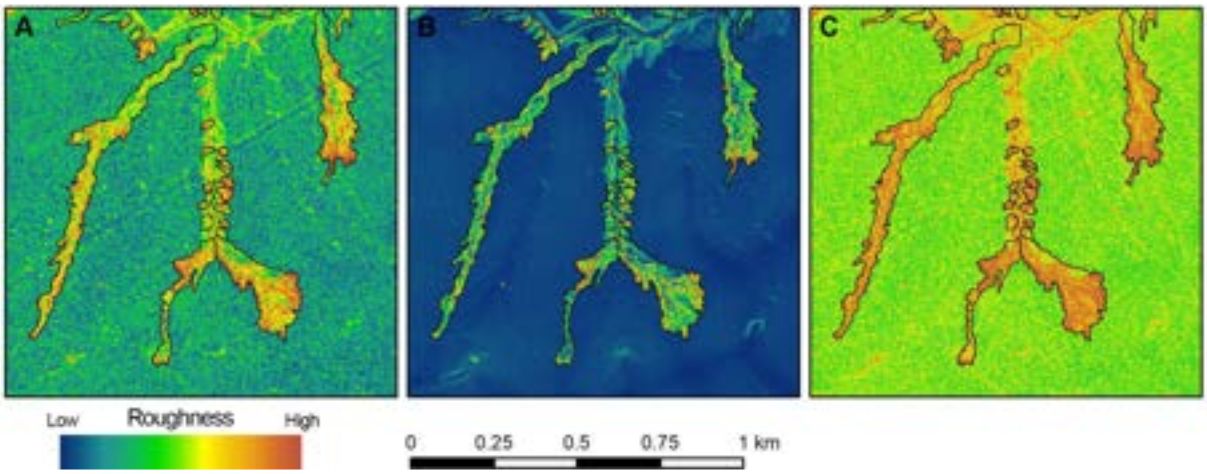

Figure 49: Example gullies demonstrating high surface roughness compared to residual landscape using (A) standard deviation of curvature (Korzeniowska et al. 2018), (B) Terrain Ruggedness Index (Riley et al. 1999) and (C) residual topography (Cavalli et al. 2008).

Four sites were selected in the Bowen River and Normanby River basins of Queensland, Australia (Figure 50). Each site has experienced considerable land degradation and gullying since European settlement (Stout et al., 2020), and has the availability of multi-temporal lidar-derived digital elevation models (DEMs). All sites had a minimum of five years between lidar missions to accommodate for the limit of detection within the data and readily detect erosion (Table 7). The sites represent a diversity of different gully types (amphitheatre, dendritic, linear; *sensu* Brooks et al., 2019) and landscapes (alluvial and colluvial) to assess the performance of the index in different settings. Site details are provided in Table 7.

Observed erosion was determined at each site by generating a difference raster (DoD) between the lidar DEMs to determine erosional and depositional characteristics. A 0.3 m limit of detection was applied to filter active erosion, based on compounding the accuracy limit of each lidar dataset, and data divided into training and test datasets (75:25 accordingly). This limit of detection was visually assessed in the residual zones (areas of assumed no change) at each site. Additionally, erosion and deposition data were further adjusted to produce a binary raster of erosion presence or absence within each gully. 'Active erosion' is considered as evident by moderate to high erosion and considered in this study as rates of > 0.07 m a-1. for both multi-temporal lidar change detection and operator perception in the field.

In addition, field validation was conducted at 550 observation sites across 21 gullies at five validation locations (Figure 50A). Observation sites were randomly generated in a GIS within digitised gullies and then located in the field. At each site, evidence of erosion was qualitatively assessed within a 2 m radius based on observations of ground cover, topsoil, nodules, gravels and the surface terrain. Each site was ascribed an activity class as shown in Table 8. While diffuse, low-level but extensive down-wearing across gullies may be a significant erosional process and contributor to sediment outputs, this type of erosion is within the limit of lidar detection and cannot be accurately accounted for using standard lidar change detection. As such, this erosion process was not further considered as 'active' erosion. Field code 2 represents transfer zones in the floor of gullies. These sites are somewhat ambiguous in whether they are erosional or depositional. Although in many instances transfer zones are likely in a state of flux between the two, they have been labelled as low erosion activity as they are not a major source of sediment within a gully. We anticipate the majority of erosion to be focused around the head and side walls of a gully.

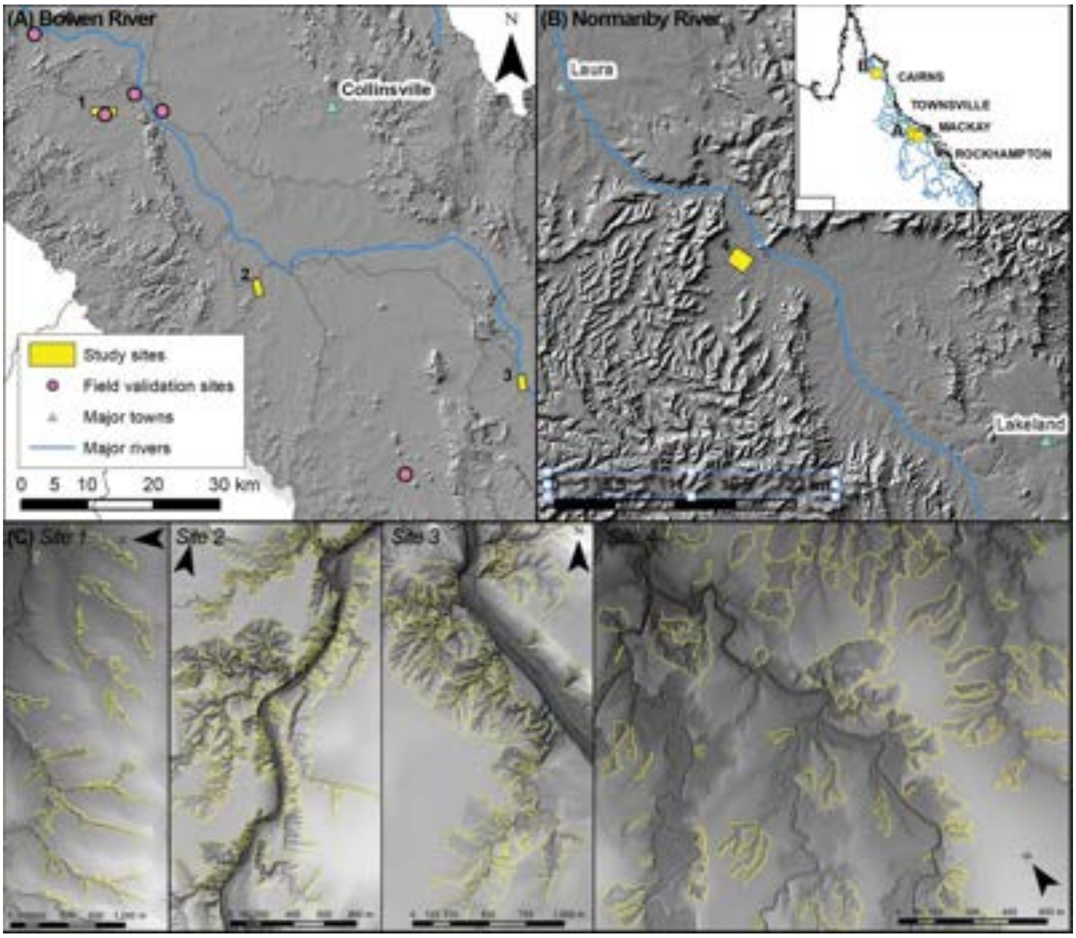

Figure 50: Regional maps of study locations within (A) the Bowen River basin and (B) the Normanby River basin, with inset map identifying site locations in north-eastern Australia. (C) Site specific hillshade renders with digitised gully boundaries (yellow) at the four study sites, highlighting the different gullied landscapes assessed in this study.

Table 7: Site description for PAE analysis.

	Site 1	Site 2	Site 3	Site 4
Catchment	Bowen River	Bowen River	Bowen River	Normanby River
Area (ha)	465	302	285	327
Landscape setting	Gentle hills, colluvial	Alluvial	Alluvial	Alluvial
Dominant surface geology	Moderately porphyritic granodiorite	Carbonaceous and micaceous labile sedimentary	Carbonaceous and micaceous labile sedimentary	Amalgamated fine to coarse-grained arenite
Dominant soil material	-	-	-	-
Elevation (mASL)	125	135	190	125
Climate (Stern 2000)	Grassland hot winter drought	Grassland hot winter drought	Subtropical dry winter	Tropical Savanna
Lidar flight missions	2010 - 2018	2010 - 2018	2013 - 2018	2009 - 2019

Table 8: Field evaluation codes for degree of erosion activity.

Field code	Erosion activity	Description of local characteristics	Binary "active" class	n
0	Inactive	Well vegetated / ground cover (algal crust) / bedrock	0	162
1	Low	Relatively flat / residual surface w/ bare ground and some deflation (nodules)	0	92
2	Low	Gully floor, transfer zone	0	44
3	Moderate	Sloping/vertical, bare ground w/ deflation, fluting, rilling, etc	1	126
4	High	As above with mass failure / tunnelling / incision	1	125

Terrain roughness was measured as the local standard deviation of curvature in a 3 m kernel window, assessed from total, plan and profile curvatures. As roughness was highly skewed, with most values approximating zero, the data was log-transformed for ease of interpretation. Planform, profile and total curvatures were calculated within a 9-cell (3 x 3 m) neighbourhood using the ArcGIS curvature tool following the method of Moore et al. (1991) and Zevenbergen and Thorne (1987). All three types of curvature were evaluated to generate roughness indices following current literature as the log-normalised standard deviation of curvature (Korzeniowska et al. 2018; Patton et al. 2018). As standard deviation values in a 3 m cell kernel size were strongly right skewed, values were transformed using a base-10 logarithm function to normalise the distribution for ease of interpretation.

Predicting the presence of erosion activity was restricted to within digitised gully boundaries by assessing only the cells within those boundaries (Figure 50C) and evaluated against observed binary data. An initial visual comparison was utilised to identify whether separability of the data into eroding and background (non-eroding) pixels from a DEM of Difference (DoD) using multi-temporal lidar data could be made (Figure 51). At most sites, roughness histograms had a bimodal distribution and displayed clear separability between background and eroding values at the pixel scale (Figure 51). As the proportion of background (non-erosional) cells accounted for 90-95% of total cells, these data were randomly subsampled to the proportion of presence (erosional) cells. This was done in order to limit overestimates of model performance biased by the overwhelming proportion of background cells in both predicted and observed data. If total absence data were included, predictive indices exceeded 99% accuracy. The distributions of roughness values in both the total and subset background cells were evaluated to verify representativeness of the subset data.

We investigated two methods of identifying a threshold boundary for defining PAE from surrounding areas. One method investigated a logistic regression function provided a supervised binary classification approach using the Classification Learner in MATLAB R2020a (MATLAB and Statistics and Machine Learning Toolbox Release, 2020). Another utilised the Otsu (1979) multilevel histogram threshold using the *multithresh* function in MATLAB. An effectiveness ratio was used to assess threshold values in separating the data, with higher values indicating greater separability. Several performance measures appropriate for predictive classification modelling were computed to evaluate roughness indices at each site, including confusion matrices, receiver operating characteristic (ROC) curves, area under the curve (AUC) and Cohen's Kappa (Cohen, 1960; Swets, 1988; Congalton, 1991; Stehman, 1997; Sithole and Vosselman, 2004).

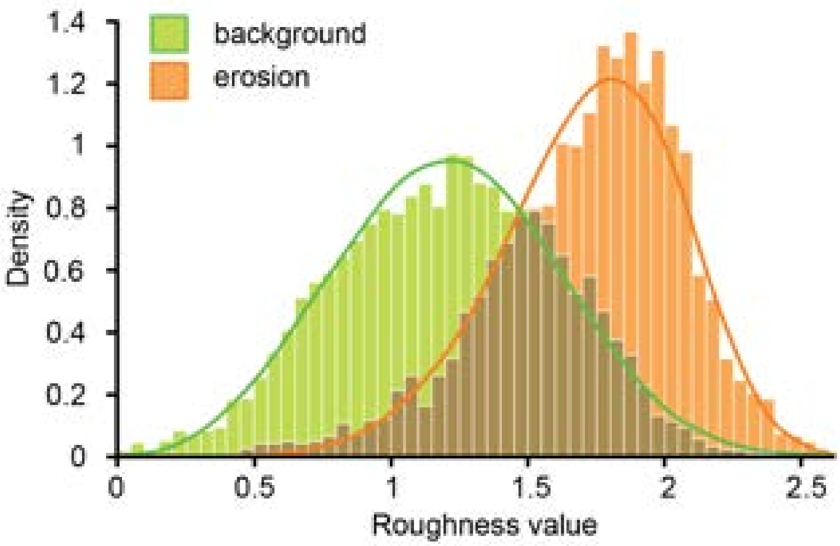

Figure 51: Example of bimodal distribution of roughness (total curvature) values at a sampling site, with pixels classed as either erosion or background (non-eroding). The inflection point at 1.47 separates erosion and background values with approximately 76% of the data unique to each class.

Threshold values of roughness varied between each site, but approximated valued between 1.4 - 1.6 using logistic regression and 1.54 – 1.84 with the Otsu method (Table 9). We assessed the PAE prediction against measured erosion rates from the DoD data at the pixel scale. Visual assessments were made between the DoD data and the PAE mapped areas, which generally identified the same areas of the gully as actively eroding (Figure 52). While at the pixel scale there is some variability in those selected, overall, the PAE provides an appropriate estimate of areas within a gully that have eroded.

The Otsu method detected a consistently higher threshold value than the logistic regression at each site. Between both methods, the accuracy statistics indicate that despite the differences in absolute threshold value, both performed well (Table 9). The PAE assessment predicted approximately 140,000 eroding pixels of which 83% were validated by the DoD assessment. Across the sample sites, the performance of the PAE had an accuracy of 86% and precision of 83% using logistic regression (Table 9). The Otsu method had accuracies >90% across all sites, but precision was lower at an average of 36%. Approximately 10% of eroding pixels were not identified by PAE index. AUC values for the logistic regression were > 0.9 at all sites, while Cohen's Kappa values against measured DoD data show only moderate agreement of approximately 0.28 across sites all sites, while F1 statistics ranged from 0.2 – 0.4.

Table 9: Performance statistics of PAE threshold selection against measured DEM of Difference data.

	Site 1	Site 2	Site 3	Site 4
n (eroding)	40,220	15,691	14,095	6,447
n (total)	535,615	1,039,690	1,048,575	587,915
Logistic Regression				
Threshold value	1.4312	1.6	1.6104	1.3815
Accuracy	0.824	0.886	0.851	0.87
Precision	0.801	0.859	0.823	0.854
F1	0.831	0.882	0.857	0.873
Positive predictive value	0.801	0.866	0.823	0.854
False discovery rate	0.199	0.134	0.177	0.146
Area under the curve (AUC)	0.90	0.95	0.91	0.94
TPR	0.79	0.86	0.81	0.85
FPR	0.14	0.09	0.11	0.11
Otsu Threshold				
Threshold value	1.5474	1.8431	1.7191	1.5494
Effectiveness metric	0.8675	0.8528	0.8677	0.875
Cohen's kappa	0.3571	0.2979	0.1926	0.2555
Accuracy	0.9174	0.9782	0.9572	0.9799
Recall	0.4402	0.2964	0.1390	0.2214
Precision	0.3684	0.3227	0.4205	0.3307
F1	0.4011	0.3089	0.2089	0.2652

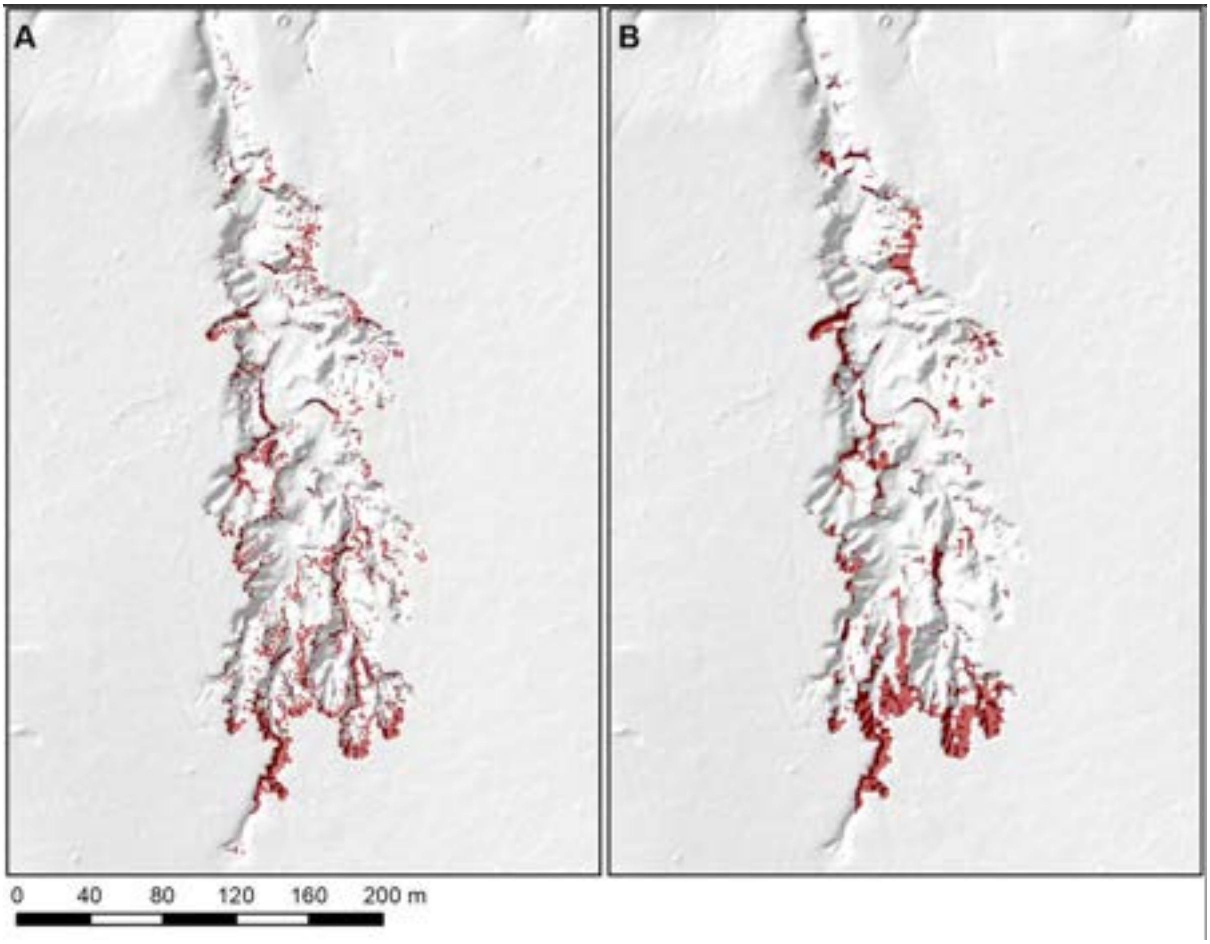

Figure 52: Spatial comparison between (a) measured and (b) predicted erosion, highlighting the general spatial agreement in areas of erosion activity within an example gully. We would not anticipate both measured and predicted mapping to be equal, given one is mapping the elevation difference (erosion) between two intervals, while the other is mapping the resulting form of that process. The key is the correlation between the two and relative extent of erosion within the gully.

A comparison of field data with the PAE indicates it is appropriate for estimating highly active surfaces, with 0.914 correlation with the validation dataset. An overall accuracy of 79.9% and a Cohen's Kappa of 0.597 was achieved, indicating strong agreement between the predicted sites of erosion and erosion intensity identified in the field. The roughness index demonstrates a strong correlation with high active erosion sites identified in the field, with an overall >90% agreement between the two datasets (Field Code 4 in Figure 53). These observation sites exhibited mass failure, tunnelling and rilling and other features indicative of highly active erosion.

Greater uncertainty was apparent with the moderate erosion class (Field Code 3), with 68% of correlation between identified sites. While 40 sites were not identified as eroding, these sites generally featured more diffuse signs of erosion within the gully complex, such as along toe slopes or interfluves on the gully floor. Areas of low erosion (Field code 0-1) had an 83% agreement between field measured and predicted values. The transfer zones (Field code 2) appear to display a relative balance in the predicted potential erosion of these points, as per the expectation established above.

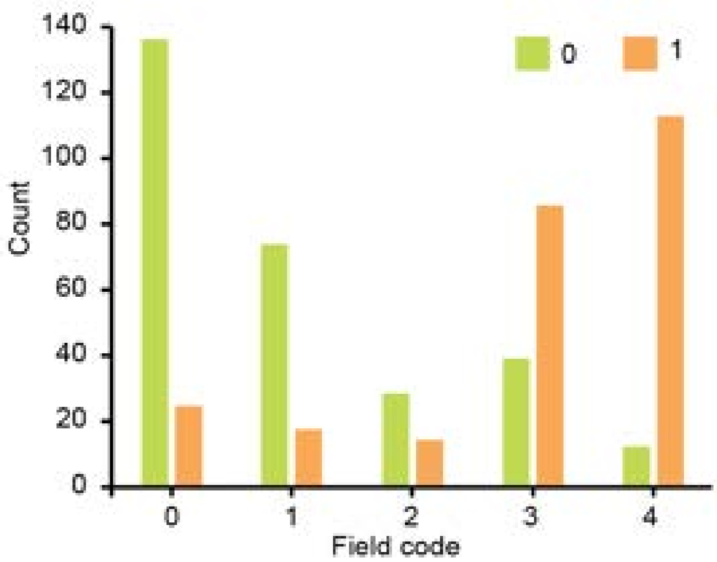

Figure 53: Field observation sites by erosion activity categories, with binary potential erosion activity metric within each class. 1 = eroding, 0 = not eroding.

Given the high correlation with both field observation points and lidar derived erosion data, the PAE provides a useful index in determining the both the location and degree of erosion within a gully. A further assessment was conducted at the gully scale, quantifying all pixels within the soft margins across 408 gullies to determine the predictability in classifying the proportion of erosion and actively degrading land to help inform the erosion rate models. The regression models shown in Figure 54 highlight that PAE at the gully scale perform as useful predictive variables for erosion, with the PAE having > 0.7 R^2 values when compared with measured erosion from a DoD analysis. Site 4 in the Normanby catchment has an R^2 value of 0.62, but this improved to > 0.8 when six outliers highlighted in Figure 54 were excluded. The correlation at the gully scale suggests the PAE is useful in comparing the relative erosion activity between a set of gullies and, as such, is a useful tool in identifying and selecting individual gullies for remediation and prioritisation in a given locality.

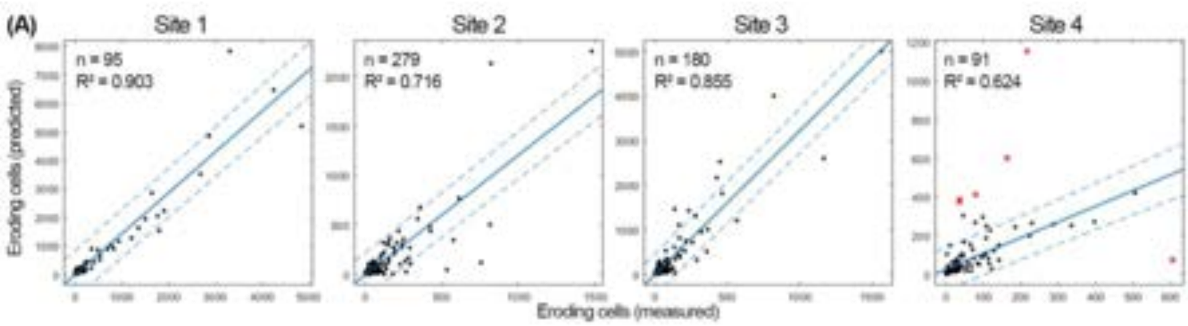

Figure 54: Comparison of the PAE index with measured DoD data at the gully-scale. (A) The number of 'eroding' cells per gully; and (B) estimated gully sediment yield assumed from local deviation in elevation.

2.6.2 Estimating lifetime eroded volumes using the Prior Land Surface (PLS) reconstruction change detection method

Once potentially active gullies are mapped across the landscape an additional analysis that can be added to the data set is the estimated total lifetime volume of sediment eroded from each gully. Conceptually, if a prior surface was projected at every cross section along the margins of the gully, a prior surface could be produced, and when subtracted from the existing land surface a total volume eroded over the lifetime of the gully can then be calculated (Figure 55). This calculated volume can be used to develop hotspot maps of high yielding gullies, or if an initiation date could be estimated from historic aerial imagery or local knowledge the average annual yield could be calculated.

While in the field, we observed that the prior surface (the land surface prior to gullying) could be visually projected from one side of the gully to the other. This idea of projecting a prior surface across a gully is not new, prior work by (Gomez et al, 2014 , Evans and Lindsay, 2010), have performed a similar exercise. However, in each method, the procedure is manual and requires input from each gully to identify the tie points that the prior surface must pull down too (Evans and Lindsay, 2010) or they project a flat surface across the eroded area with no consideration for any prior swale in the landscape (Gomez et al, 2010).

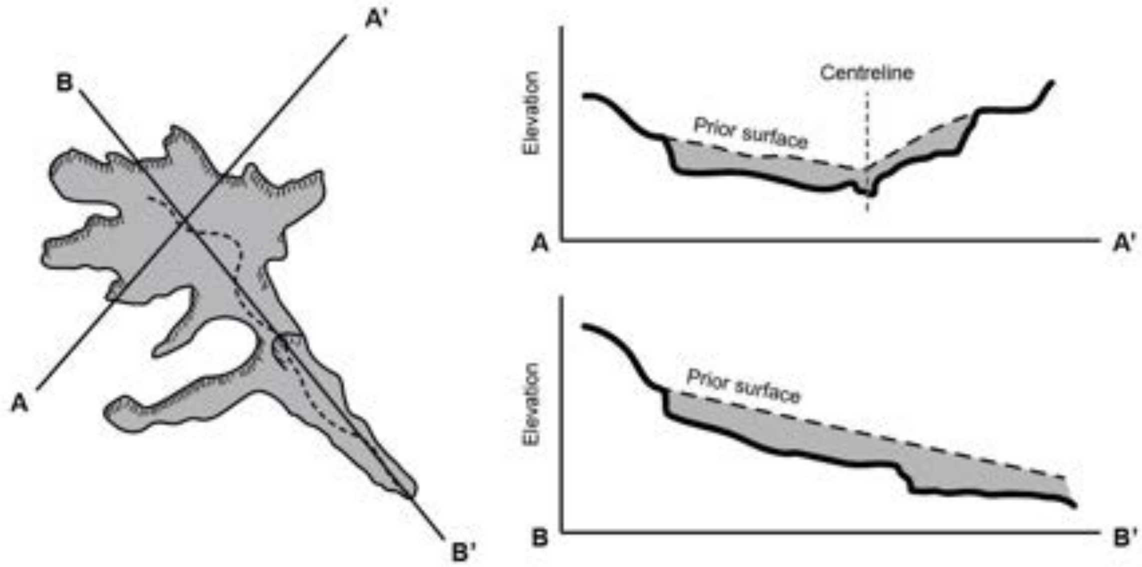

Figure 55: A conceptual diagram illustrating the idea that if a surface were projected across the gully cross section (A to A'), and was then propagated along the length of the gully (B to B1) a prior surface of the gully could be reconstructed, and an estimated volume of eroded sediment calculated.

Method:

Building on the methods of Gomez et al (2014) and Evans and Lindsay (2010) we developed an automated tool which constructs a prior land surface and differences the prior land surface from the existing surface as represented by the DEM to estimate the total volume of sediment that has been eroded from the gully over its lifetime. This method is designed to be a conservative estimate and more accurate than simply multiplying the length and width and average depth of the gully. The Prior Land Surface (PLS) work flow is illustrated in Figure 56, and is run as a standalone toolbox run in ArcGIS or Python 2.7. The necessary inputs for the tool are:

1) A hydrologically conditioned DEM
2) A polygon shapefile representing the outline of the potentially active gullies of interest
3) A polyline shapefile representing the longest flow path along, or partially along the length of the gully.
4) Optional: surveyed points which represent remnants of the prior surface.

The tool converts all shapefiles to points, and extracts the elevation of each point from the DEM. The gully margin points are then used to produce a flat "lid" of the gully. As the prior surface was very unlikely to have been flat and instead was likely a gentle swale, the flow lines are used to force a swale in the new "gully lid". Simply using the flat lid to represent the prior surface would result in an overestimate of the sediments eroded. Using the flow line of each gully, the depth between the "flat lid" and the existing surface is calculated. This depth is then decrease by 20 percent, representing 80 percent of "lid depth", and assigned to points along the flow line. A new lid with a forced swale is then generated to represent the prior surface.

To assess the suitability of simply lowering the flat lid by 20 percent, a sensitivity analysis was performed to see if lowering the prior surface elevation by some amount along the flow path would produce a realistic surface. The elevation reduction of 20 percent (or 80 percent of the lid depth) was found to minimize the proportion of land protruding above the lid but maximize the influence of a swale in the prior land surface. From this sensitivity analysis we opted to use the elevation representing 80 percent of the flat lid depth. Figure 57 (top panel) conceptualizes the forcing of a swale, and the bottom panel illustrates from the sensitivity test that by pulling the flat lid down by 20 or 30 percent we minimize the proportion of existing surface protruding above the lid.

Once the final gully lid with a forced swale is generated a low pass filter is used to smooth the lid, and then using the Fill tool the lid is hydrologically conditioned producing an estimated prior land surface. Lastly the prior land surface is subtracted from the existing DEM. From this difference layer zonal statistics for each gully are generated resulting in the total volume of sediment eroded, the maximum eroded depth and the average eroded depth. These values are output as a table.

Figure 56: Flow diagram illustrating the steps used to develop the prior land surface and the final estimate of total volume of sediments eroded from each gully.

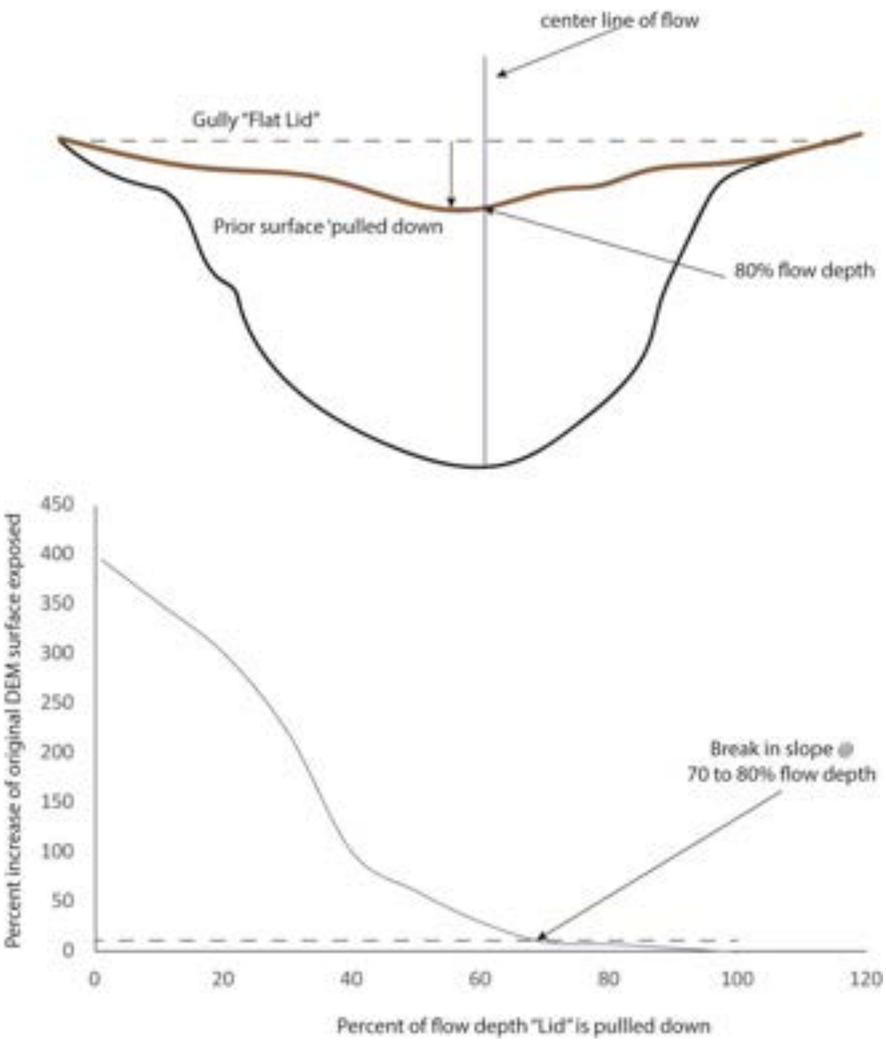

Figure 57: Illustration showing the "pull down depth, and the data from the sensitivity test showing that pull down depths between 70 and 80 percent of flow depth minimizes the amount of original surface exposed.

As an example of the prior surface method, we illustrate this method on a group of gullies on Strathmore Station near the Bowen River Hotel. Figure 58 illustrates the DEM of Difference between the prior land surface and the current DEM. Figure 59 is an example of the reconstructed or prior land surface using the method described above. As you can see, G5 (Figure 59) has a slight swale evident, and all gullies maintain the generalized topography from the valley.

The Prior Land Surface method was applied to all mapped gullies across the three study regions, and total lifetime volumes, average eroded depth, and maximum eroded depth were calculated. While it was not within the scope of this project to estimate initiation dates of the gullies, if a dataset were developed for gully initiation dates, spatially explicit bulk density, and particle size distributions, we would be able to estimate long-term average annual erosion rates at the individual gully scale.

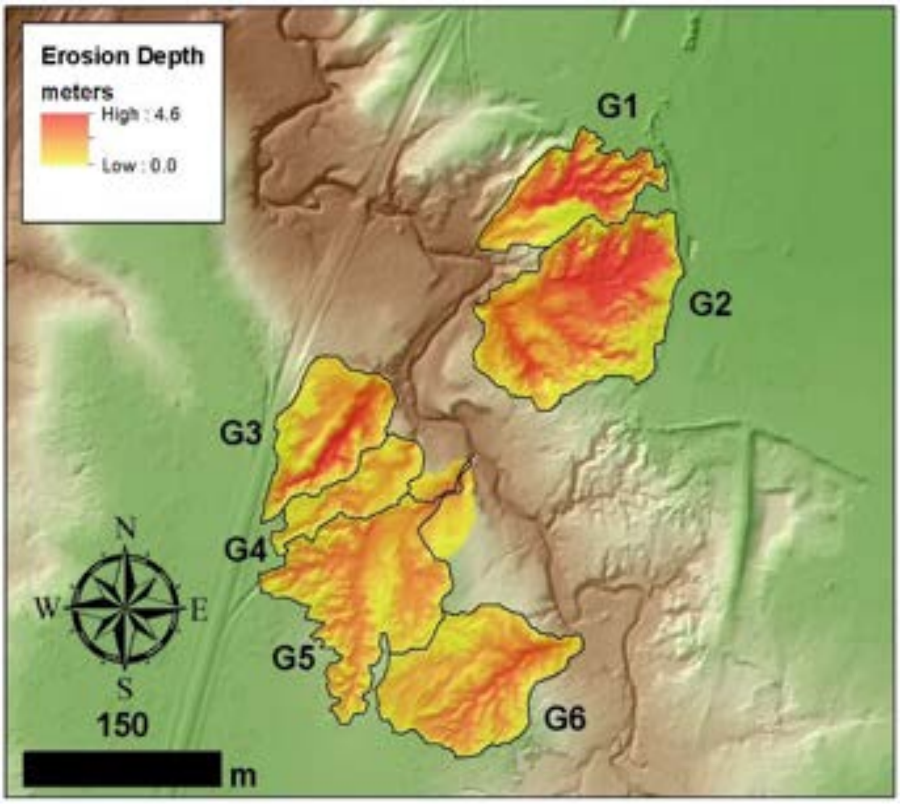

Figure 58: Illustration of the erosion depth estimated by the Prior Surface Estimate tool.

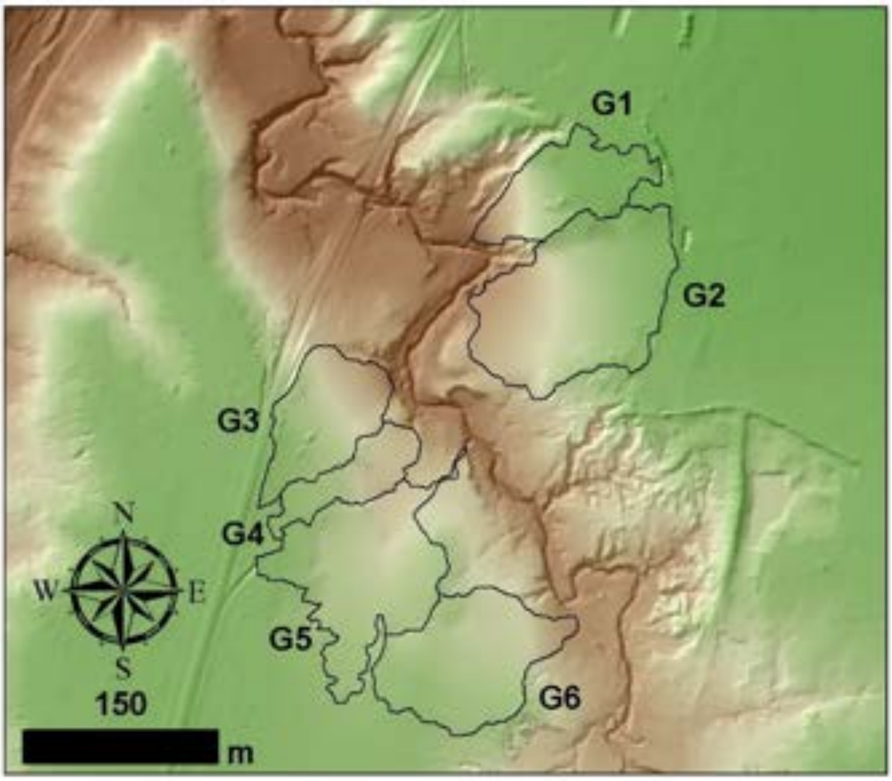

Figure 59: Illustration of the prior land surface. Note the eroded gully to the south of G2 which has not had a prior land surface reconstruction.

3.0 SUMMARY RESULTS

3.1 Summary statistics for each region

The following figures summarise the distribution of gully numbers and area in the three study areas. It should be recognised that the land area mapped in each catchment differs significantly in terms of total area and the proportion of the catchment area that has been mapped. Hence these data should be regarded as a sample only, albeit focused in areas thought to have some of the highest density of gullying in the respective catchments.

Figure 60 shows the relative proportions of landscape types and gullies in each case study area. The total area analysed was 5,288 km^2, with both the BBB and Fitzroy dominated by colluvial landscapes, albeit with a relative balance across the three landscape types, and the Laura dominated by alluvial landscapes. Across the BBB, Fitzroy and Laura case study areas, 25,916 gullies were mapped. Of these, 22,311 were mapped in the BBB area, 1,785 in the Fitzroy and 1,820 in the Laura area. In total, 47% of gullies mapped were colluvial, while 47% were alluvial. In the Laura area, alluvial gullies comprised 79.8% of the 1,820 gullies mapped (Figure 60B). In all three catchments, rugged gullies were disproportionately low compared to their land area.

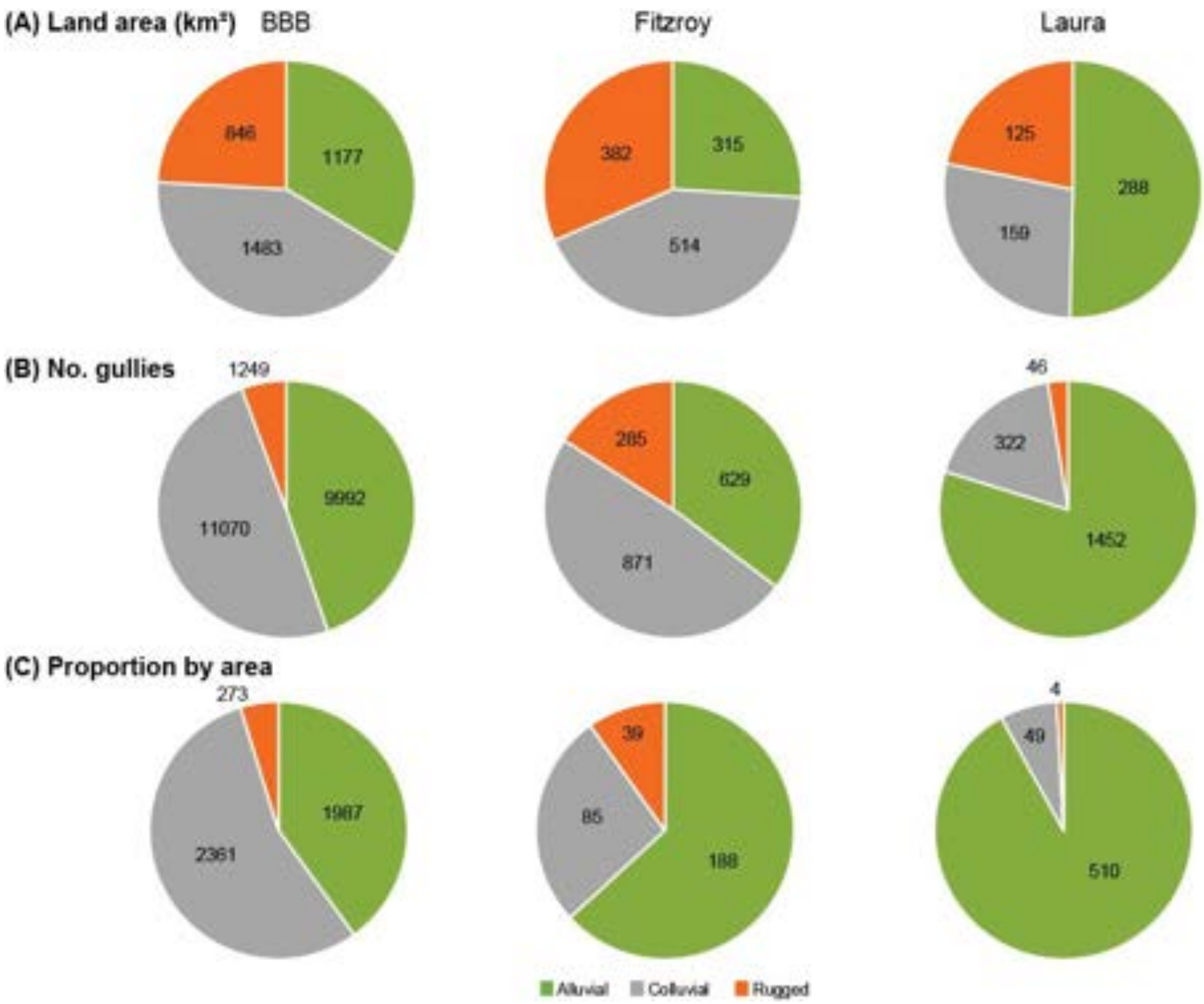

Figure 60: (A) The relative proportion of each landscape type in each catchment lidar block and (B) the amount of gullies mapped in each landscape unit, (C) the proportion of each landscape area affected by gullying.

While these proportions are relatively consistent with gully type by area in the BBB, these proportions are quite different in the Fitzroy and Laura (Figure 60C). Figure 61 show the total area of each gully type by both soft margin and hard margin in each gully. As the hard margin tends to more closely align with area of actively contributing sediment within a gully, it likely provides the most appropriate measure of gully area. But the proportions of gully area by both measures are relatively consistent across all three study areas. In the Fitzroy, alluvial gullies comprise 63% of gullies Alluvial gullies make up 92% of the area of gullies mapped in the Laura study area.

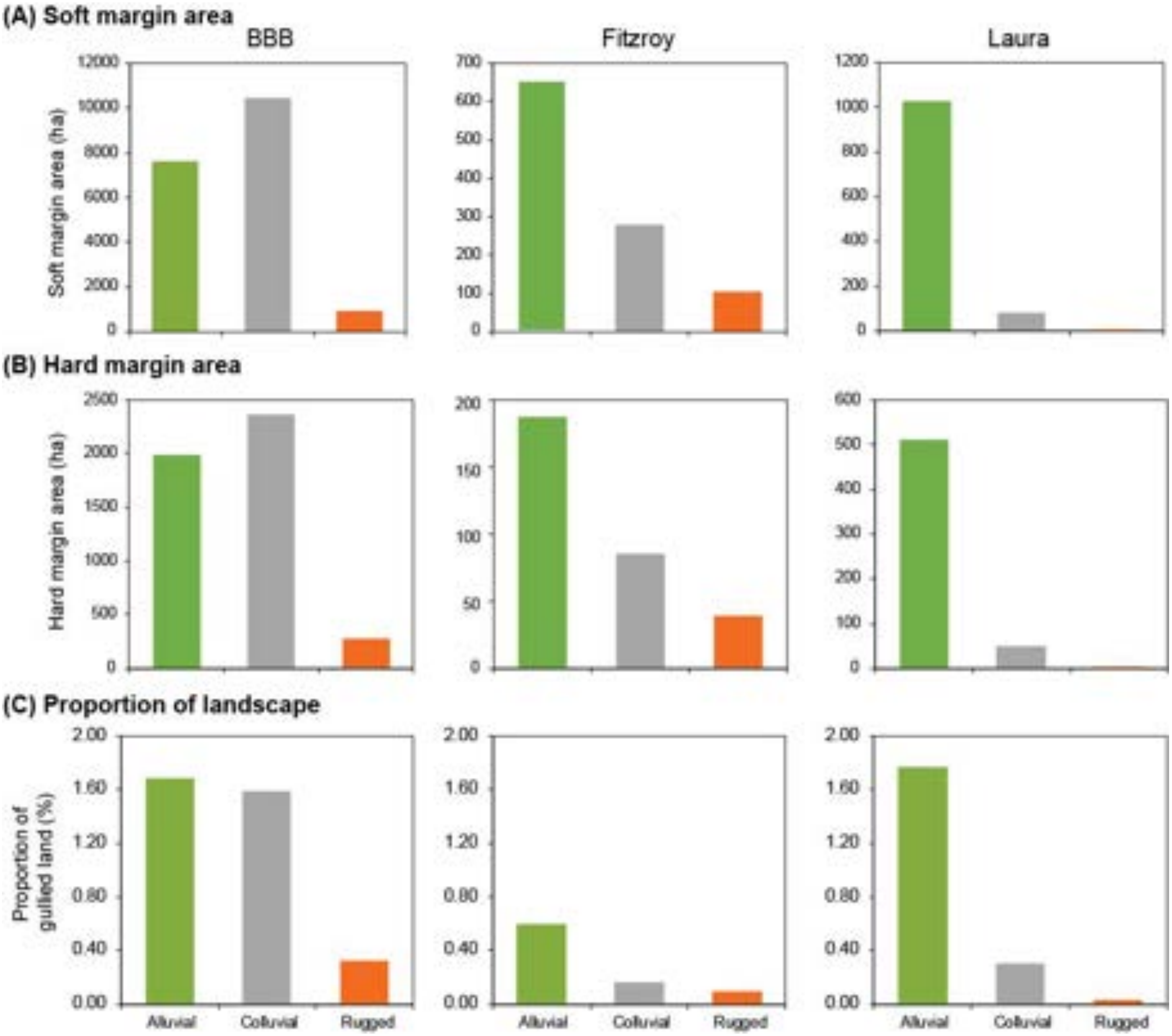

Figure 61: The proportion of gully types in each catchment by area, for both the hard and soft margins, and as a proportion.

Across the three study areas, an approximate total of 5,500 ha (by hard margin) of gullied land was mapped, while the soft margin mapping comprised 21,000 ha. In the BBB, colluvial gullies have the largest area at 2,400 ha, while alluvial and rugged gullies make up 2,000 and 300 ha, respectively (Figure 61B). In the 1,200 km^2 of Fitzroy study area there was 310 ha of gullied land, 190 ha of which was alluvial, 85 ha from colluvial and 40 ha from rugged gullies. In the Laura area, 500 ha of alluvial gullies is by far the largest contributor to erosion processes, with 50 ha of gullies in colluvial areas and 4 ha of rugged gullies.

From these data it can be seen that there is considerable variation in the relative proportion of the land area affected by gullying in the different catchments, and the relative proportion of gully type (i.e. gully landscape unit) varies considerable between catchments (Figure 61C). In the BBB, 1.32% of the land is affected by gullying, with alluvial and colluvial areas both seeing 1.69% and 1.59% respectively. A similar degree of gullying (1.77%) occurs in the alluvial landscapes of the Laura area. The Fitzroy area appeared to display a much lower proportion of gullying at a total of 0.26%, with the highest value across landscapes types in the alluvial areas at 0.6% (Figure 61C).

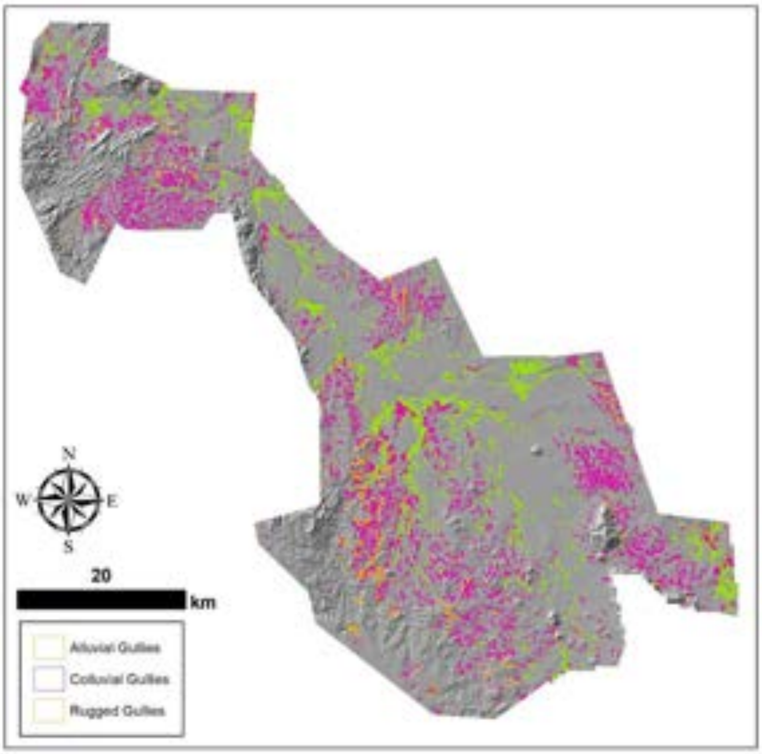

Figure 62: Map of the distribution of gully types in the BBB (southern) lidar block.

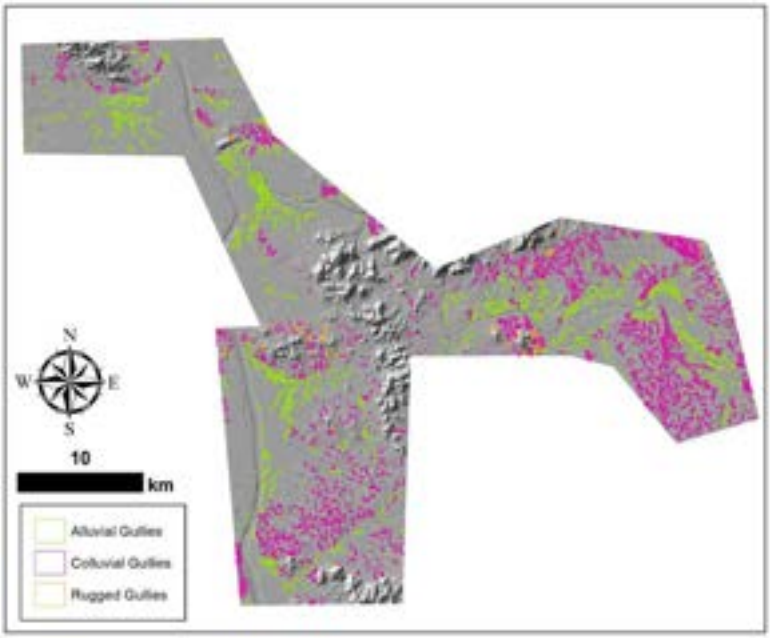

Figure 63: Map of the distribution of gully types in the BBB (northern) lidar block.

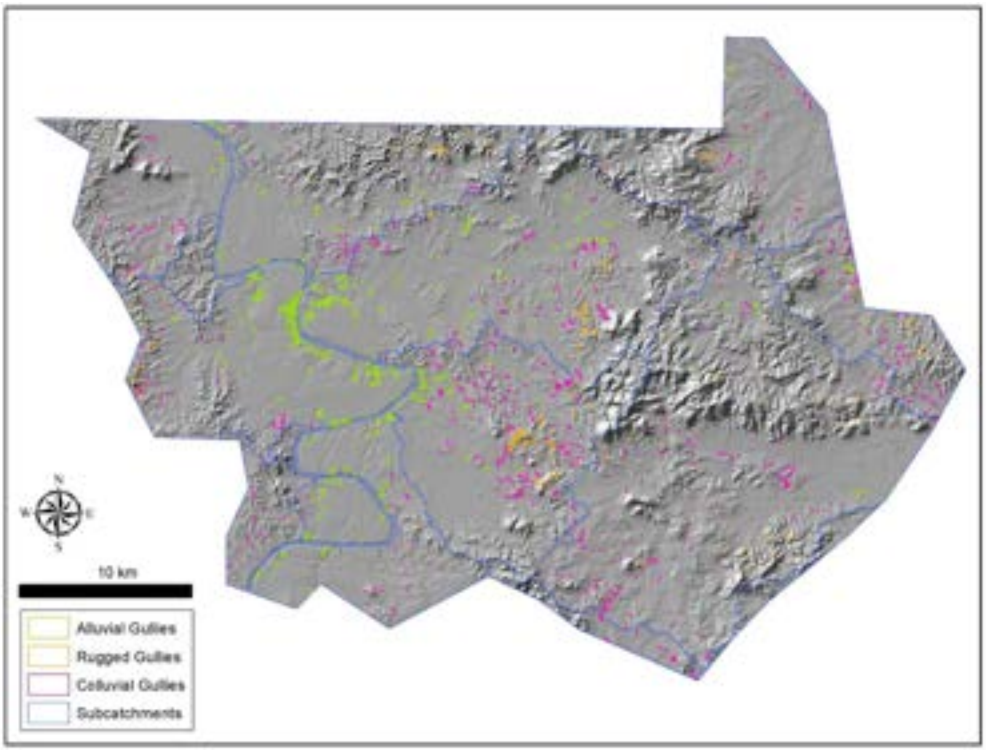

Figure 64: Map of the distribution of gully types in the Fitzroy lidar block.

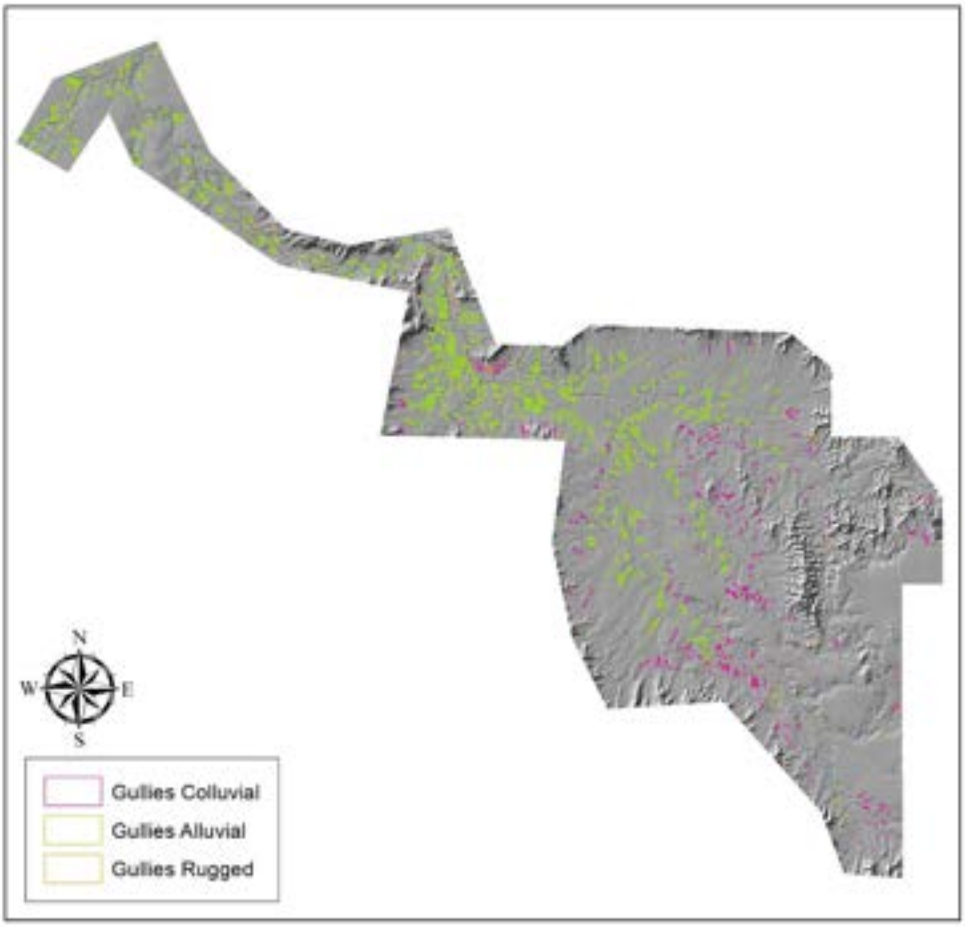

Figure 65: Map of the distribution of gully types in the Laura (Normanby) lidar block.

The potential active erosion (PAE) area provides a proxy of gully activity and erosion intensity, identifying areas within a gully that are likely contributing the largest amount of sediment. The area of PAE within each catchment is shown in Figure 66. While BBB represents 66% of the total mapped area, the 830 ha of PAE mapped in this region represents 88% of all mapped PAE. Of this, 415 ha, or 50%, occurs in alluvial gullies (Figure 67A) which suggests the alluvial gullies in this area have a greater area of active erosion than hillslope gullies. Colluvial gullies comprise 350 ha of the PAE area, which equates to 43% of the total PAE area. Heat maps of the BBB gullies by PAE area are shown in Figure 68 - Figure 69, which show clear spatial trends in the distribution of erosion activity. Taken as a surrogate for erosion activity, these maps suggest some areas of the landscape in both blocks tend to have much higher concentrations of active erosion than others.

While the Fitzroy study area was 23% of the mapped area, it comparatively only amounts to 48 ha or 5% of the PAE area (Figure 66). As per the analysis in the BBB, PAE appears to be more concentrated in alluvial gullies than in colluvial or rugged gullies, with 26 ha representing 55% of the PAE area (Figure 67b). The PAE area mapped in colluvial and rugged terrain were both found to be approximately 10 ha each. The distribution of gullies by PAE area (Figure 70) shows that only several gullies feature high concentrations of erosion activity, with the majority of mapped gullies having < 250 m^2 of PAE area.

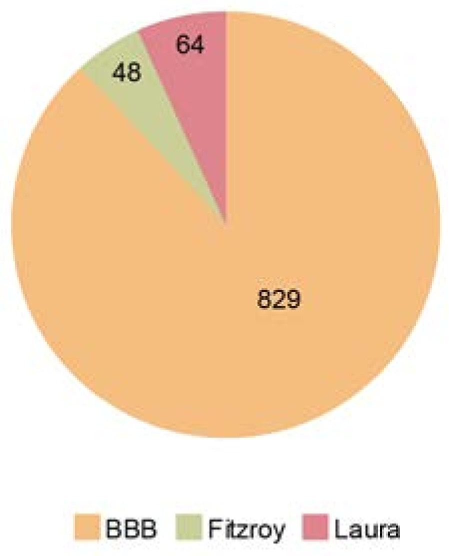

Figure 66: Total sum of PAE area (ha) per lidar block, as a surrogate for gully erosion intensity. Note these are absolute values and have not been corrected for the different lidar block areas in each catchment.

Of the 64 ha of PAE area identified in the Laura study area, 92% is concentrated in the alluvial gullies. This proportion is consistent with the gully area analysis for the Laura study area in Figure 60C. The spatial distribution of gullies by PAE area is shown in Figure 71. While there does not appear to be consistent trends in the heat map, a larger concentration of gullies and active gullies is evident in the centre of the study area and another pocket of high PAE area gullies in the north-west corner of the block. There appears to be a broad range of erosion activity across all gullies, with a number of gullies having > 1,000 m^2 of PAE area across the block.

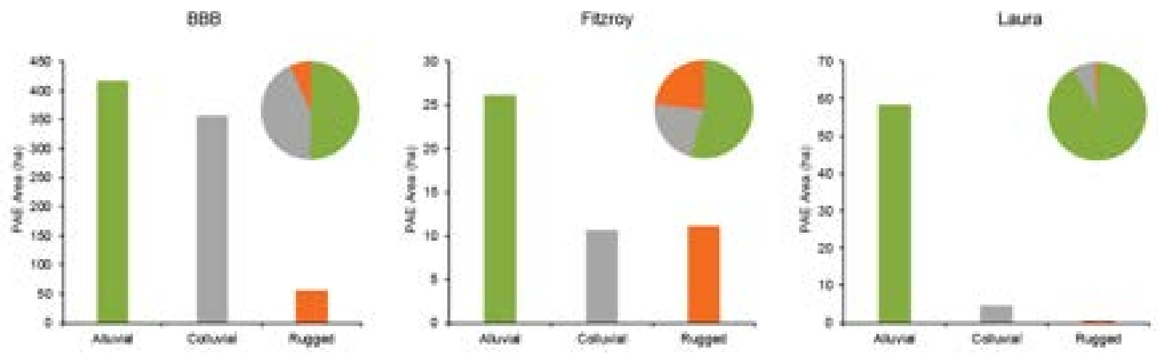

Figure 67: PAE area per landscape class, as a surrogate for gully erosion intensity.

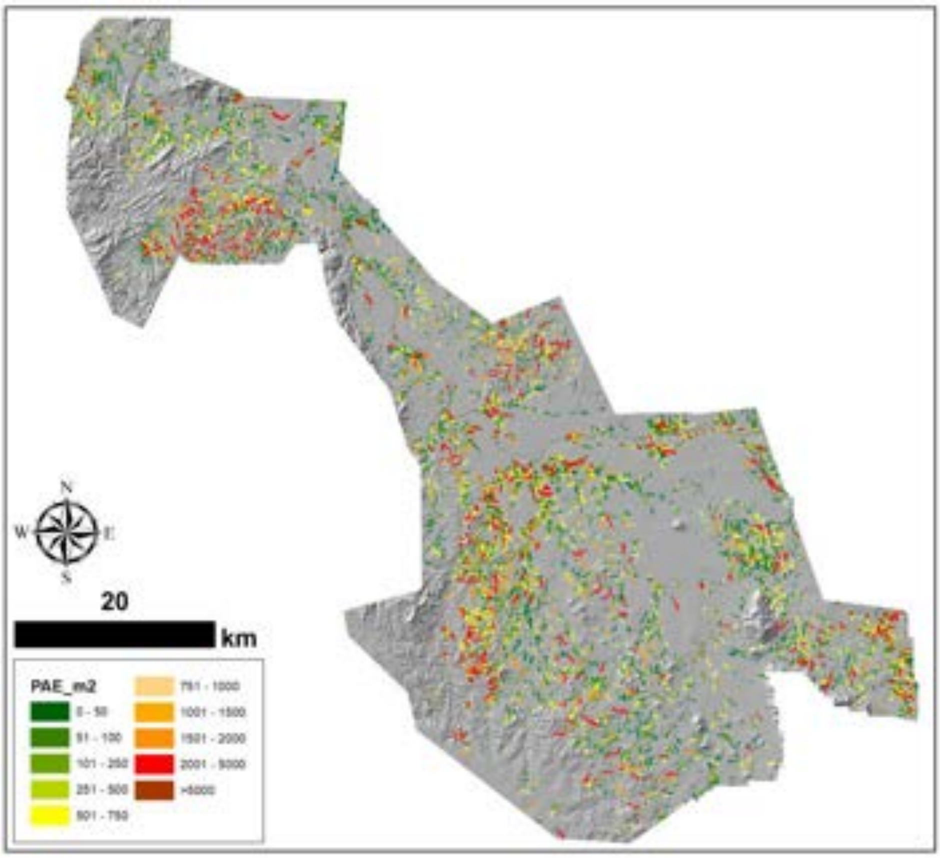

Figure 68: The distribution of gullies by their area of potential active erosion (PAE) in the BBB southern Block.

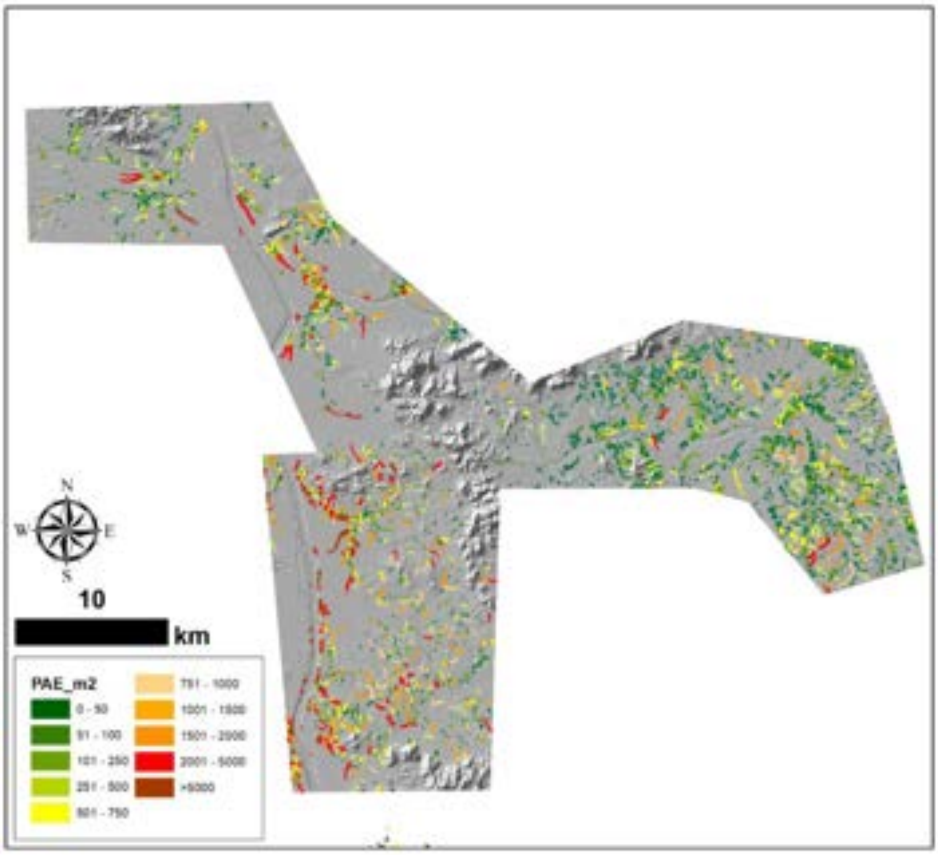

Figure 69: The distribution of gullies by their area of potential active erosion (PAE) in the BBB northern Block.

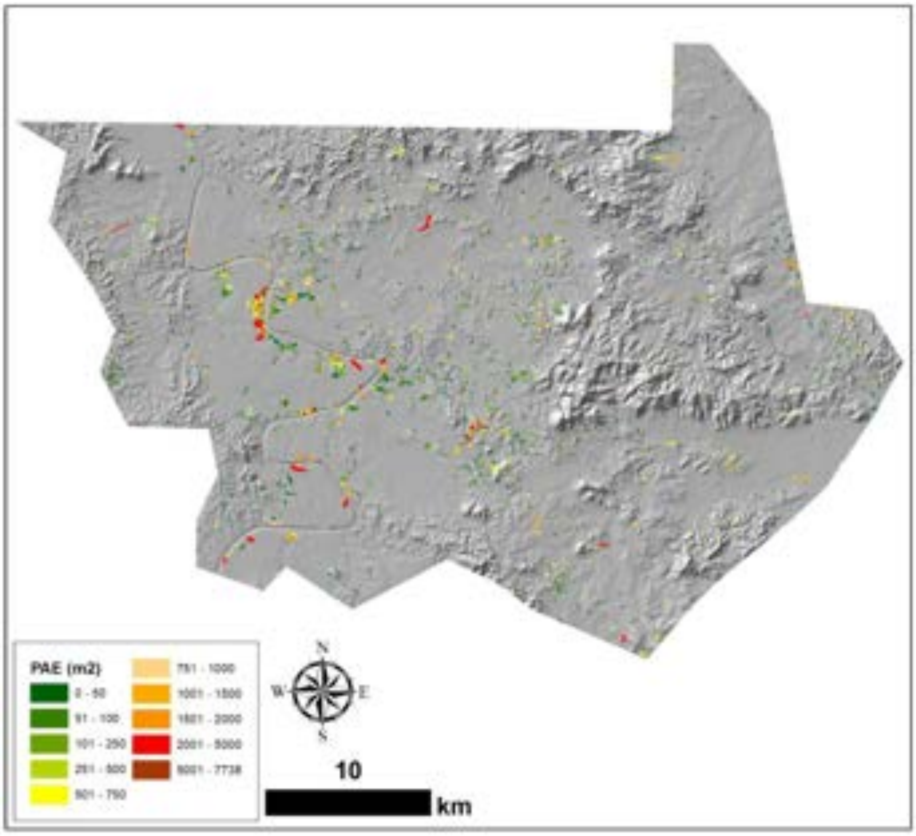

Figure 70: The distribution of gullies by their area of potential active erosion (PAE) in the Fitzroy Block.

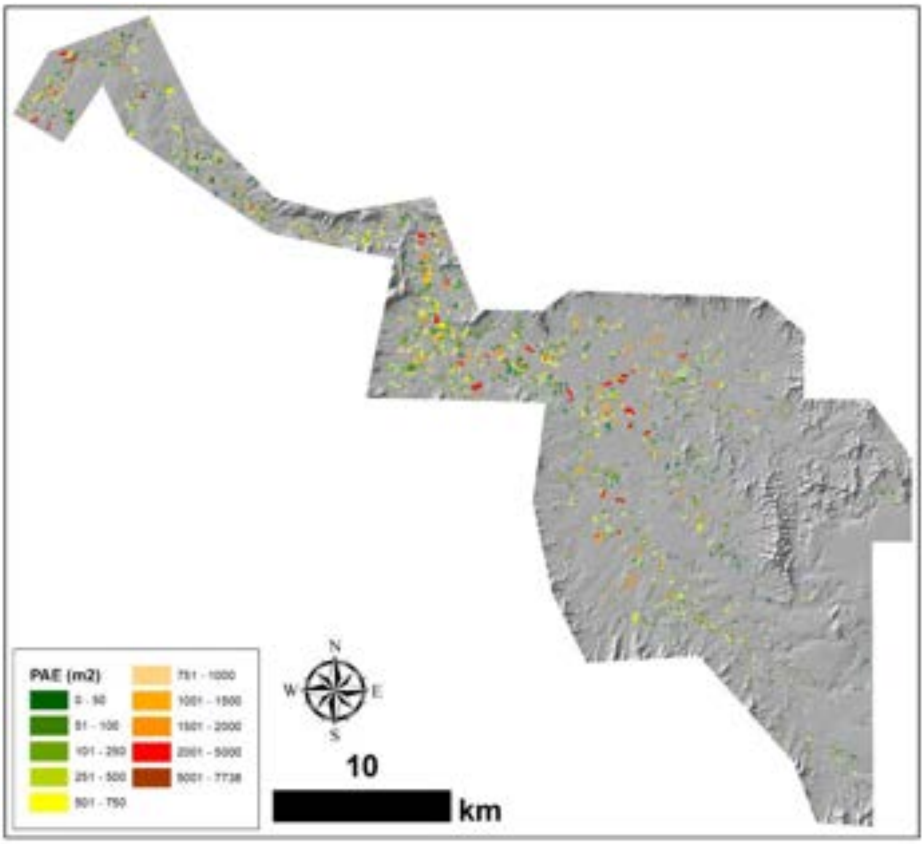

Figure 71: The distribution of gullies by their area of potential active erosion (PAE) in the Laura Block.

3.2 Gully dimensions and volume estimates

Further to the PAE metric, used to identify potential active erosion in the mapped gullies, four other metrics (gully length, gully width, average eroded depth, and maximum eroded depth) are used to quantify the size and dimensions of each individual gully. These four metrics, combined with the volume of eroded sediment derived from the Prior Land Surface (PLS) method are useful in the not only describing the potential magnitude of the sediment flux from each gully, but are also useful in identifying individual gullies or groups of gullies which would be likely candidates for rehabilitation. Values of length and width were calculated from each gully outline, by extracting the longest straight line to represent the length of the gully, and the width was calculated by extracting the width of the minimum bounding geometry box for each gully. Average eroded depth and maximum eroded depth were extracted using zonal statistics from the DoD derived during the PLS method.

3.2.1 Gully dimensions

Box and whisker plots were plotted to compare the median value of each metric and to identify outliers in the data sets (Figure 72). In a cross comparison of the four dimension metrics and the volume of eroded sediment estimates (Figure 73) generally, alluvial gullies are typically much larger than colluvial and rugged hillslope gullies with greater variability in dimensions, particularly gully widths and over all have produced more sediment. In the BBB, median length and width were approximately 100 and 20 m respectively, but with a considerable spread across all landscape types. Hillslope gullies tended to be longer than alluvial gullies, up to 750 m and an interquartile range of approximately 350 m, while most alluvial gullies were less than 500 m long and a third quartile length of < 250 m. The average depth and maximum depth of gullies in the BBB exhibit a similar pattern, with the alluvial gullies showing a larger spread in the range of depths and having relatively more outliers (points which are numerically different to the distribution of gully dimensions).

Similar trends in gully length and width are observed across the other two study areas (Fitzroy and Laura), with some differences in absolute values, but generally there no difference in the distributions of gully width, length, average eroded depth, and maximum eroded depth. Alluvial gullies in the Fitzroy and Laura areas exhibit a wider range in gully widths relative to colluvial and rugged gullies. These alluvial gullies have a median value of 26 and 38 m respectively, with an interquartile range of 41 and 28 m and outliers up to 200 m wide. Comparatively, colluvial gullies in the Fitzroy and Laura study areas show respective widths of 15 and 10 m and a range of < 10 m (Figure 72). Interestingly this difference between alluvial and colluvial gullies is not as readily apparent in the BBB. This is likely due to the presence of numerous small alluvial bank gullies (small gullies occurring on river banks with areas not much larger than 500 m^2). Additionally, many of the mapped alluvial gullies are actually sub-sets of larger alluvial gully complexes.

Comparing the distribution of average eroded depths and maximum eroded depths of gullies between gully type at each site illustrates the variability in the erosion patterns occurring in each gully (Figure 72C-D). In the BBB, the median of the average eroded depth and the median maximum eroded depth is relatively consistent between alluvial, colluvial, and rugged gullies ranging between values of 0.50-0.64 m and 1.9-2.6 m respectively. The distributions are near normal, but the alluvial gullies tend to have larger outliers with the largest outlier of 5 m for average depth and 15.5 m for maximum eroded depth (Figure 72). All of the distributions tend to have several outlier values which are points that are numerically different to the distribution of gully dimensions.

A similar trend in the distributions of average eroded depth and maximum eroded depth is observed in the Laura and Fitzroy datasets. The median average eroded depth in the Fitzroy has a larger range between gully type (0.21-0.62 m) relative to the range between the different gully types in the Laura (0.41-0.61 m). However, the range of the median values for maximum eroded depth between gully types is similar (Fitzroy = 1.3-2.4 m, Laura = 1.3-2.3 m). The maximum eroded depth of alluvial gullies in the Fitzroy are strongly right skewed indicating that while the majority of alluvial gullies have a median max eroded depth around 2m, there are many gullies which have eroded to depth up to 4.8m. This right skew in the data indicates that using a median value and the interquartile range to describe the morphology and dimensions of gullies may underestimate the influence of a smaller number of gullies, which may be producing large volumes of sediments.

The dimensions and eroded depths of all gully types and the regions exhibit a similar median value, and a similar spread (interquartile range) in the data for each gully type (Figure 72). While these values are useful to quantitatively describe the gullies, what is even more useful is the identification of gullies which are outliers in the datasets. We posit that these outliers are extremely large gullies, relative to the population of mapped gullies, and would be locations where gully and landscape rehabilitation practices should be implemented. These gullies can be identified from shapefile of mapped gullies associated with this report by extracting gully dimensions which are larger than the upper value of the upper whisker value.

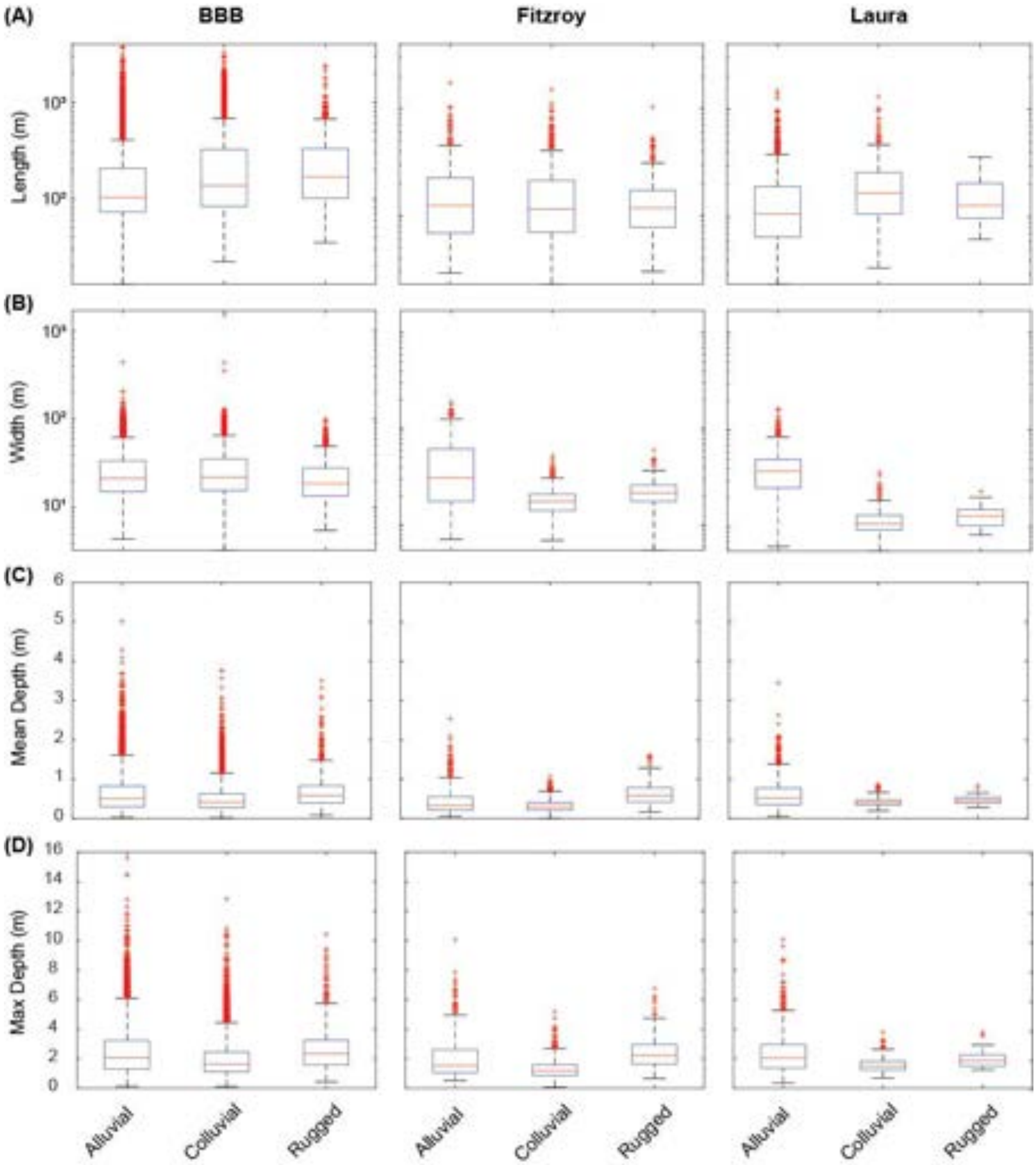

Figure 72: Box plots of gully dimensions for each region and gully type; (A) length; (B) average width; (C) average depth and (D) maximum depth.

3.2.2 Volume Estimates

Overall, alluvial gullies (Figure 73) have produced the majority of sediment in all three regions mapped. In the BBB the colluvial gullies have produced nearly 2 orders of magnitude more than the colluvial gullies in the Fitzroy and Laura regions. This is due to the large number of colluvial gullies present in the BBB region. Table 10 reports the total volumes eroded for each region and gully type as well as the average depth of all the gullies, and the average maximum depth for all gullies.

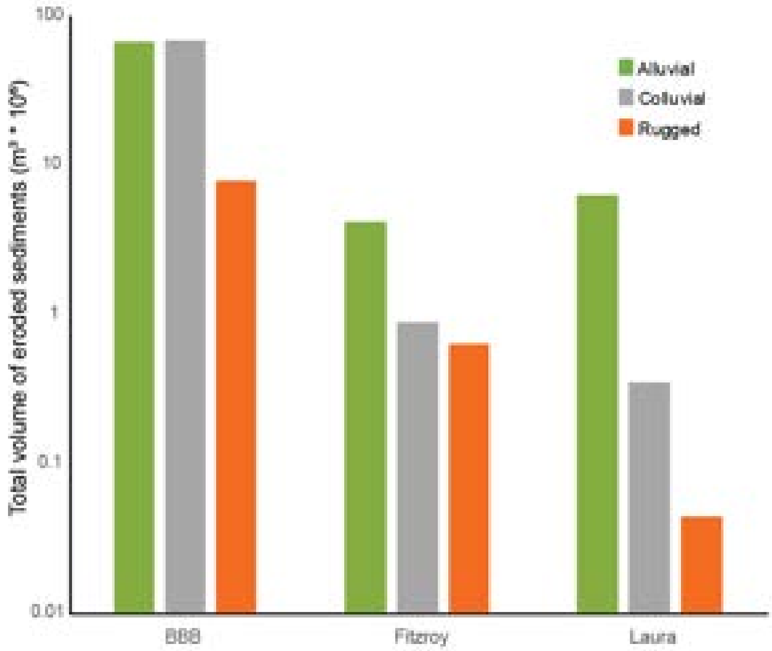

Figure 73: Total volume of sediments eroded from each region split by gully type. Note log scale used due to large differences between the catchment blocks.

Table 10: Summary table of total lifetime Volumes eroded, average eroded depths, and maximum eroded depths by gully land unit type. Eroded depths are the median value for all gullies within each gully type.

BBB			
Gully Type	***Total Volume Eroded (m^3)***	***Median of Average Eroded Depths (m)***	***Median of Maximum Eroded Depths (m)***
Alluvial	67×10^6	0.64	2.5
Colluvial	69×10^6	0.50	1.9
Rugged	7.8×10^6	0.68	2.6
All Types	144×10^6	0.60	2.4
Fitzroy River			
Gully Type	***Total Volume Eroded (m^3)***	***Median of Average Eroded Depths (m)***	***Median of Maximum Eroded Depths (m)***
Alluvial	4.2×10^6	0.45	2.0
Colluvial	0.9×10^6	0.21	1.3
Rugged	0.6×10^6	0.62	2.4
All Types	5.7×10^6	0.46	1.9
Normanby – Laura Block			
Gully Type	***Total Volume Eroded (m^3)***	***Median of Average Eroded Depths (m)***	***Median of Maximum Eroded Depths (m)***
Alluvial	6.4×10^6	0.61	2.3
Colluvial	0.35×10^6	0.41	1.6
Rugged	0.04×10^6	0.47	1.9
All Types	6.7×10^6	0.50	1.9

Using the DoD from the PLS method we estimate that roughly 156 million cubic meters of sediment has been eroded from the mapped gullies in all three study regions. Cumulatively the BBB region contributed 144 million cubic meters of sediment. Of the 22,311 gullies mapped in this region (Figure 74),

- 30 percent of the sediment was produced by 2 percent of the gullies (502 gullies)
- 50 percent of the sediment was produced by 6 percent of the gullies (1290 gullies)

In the Fitzroy (Figure 74) the cumulative contribution was 5.6 million cubic meters and from the 1,785 mapped gullies.

- 30 percent of the sediment was produced by 1.5 percent of the gullies (26 gullies)
- 50 percent of the sediment was produced by 4 percent of the gullies (74 gullies)

In the Laura (Figure 74) the cumulative contribution was 6.7 million cubic meters and from the 1,857 mapped gullies.

- 30 percent of the sediment was produced by 3.5 percent of the gullies (65 gullies)
- 50 percent of the sediment was produced by 10 percent of the gullies (179 gullies)

This large contribution of sediments from a small number of gullies indicates that if gully rehabilitation were to take place in these regions that managers could target this small number of high yielding gullies which may result in a more effective use of both time and money.

3.2.3 Annualized sediment yields

Although the PLS method only produces a total volume eroded estimate (over the lifetime of the gully), if a gully initiation date were to be estimated or derived, the volumes, combined with sediment particle distributions and bulk density measurements, an annualized sediment yield estimate could be calculated (tonnes per year). Table 9 reports a range of potential sediment yields (tonnes per year) assuming a range of potential initiation dates, ranging from gullying starting 120 years ago, 100 years ago, 80 years ago, and 50 years ago. These estimates are the average lifetime sediment yield since initiation and should not be used without further investigation into the actual timeframe when gullying initiated in each of the study regions. In order identify gully initiation time frames multiple lines of evidence will likely be needed (i.e. historical air photos to develop a time series of erosion rates, historical documentation, local knowledge). From this very simple application of assumed start dates of gullying we would predict that, as a whole, the three mapped regions are yielding between 2.1 million to 5.2 million metric tonnes of sediment each year. This estimate includes the entire particle size distribution of the sediment and does not fractionate for clay sized particles. Further research and investigation are needed to develop spatially explicit maps of sediment particle size distributions, bulk density, gully initiation dates, and sediment delivery ratios. Once these maps are developed, then we will be able to better estimate the annual fine sediment contribution of each individual gully to the Great Barrier Reef.

Table 11: Using the estimate total volume of sediment from the PLS method, a range of potential start dates and a bulk density of 1.65 kg*m-3 were used to estimate a likely range of annualized sediment yield (tonnes per year).

		Range of potential initiation dates			
		120 years ago	*100 years ago*	*80 years ago*	*50 years ago*
	Volume eroded m^3	**Average annual tonnes of sediment eroded relative to estimated initiation date (tonnes per year)**			
BBB	*144×10^8*	*2.0×10^6*	*2.4×10^6*	*3.0×10^6*	*4.8×10^6*
Fitzroy	*5.6×10^6*	*7.7×10^4*	*9.2×10^4*	*1.2×10^5*	*1.8×10^5*
Laura	*6.7×10^6*	*9.2×10^4*	*1.1×10^5*	*1.4×10^5*	*2.2×10^5*
Total	*1.56×10^8*	*2.1×10^6*	*2.6×10^6*	*3.2×10^6*	*5.2×10^6*

Note: Bulk Density assumed to be 1.65 kgm^{-3}*

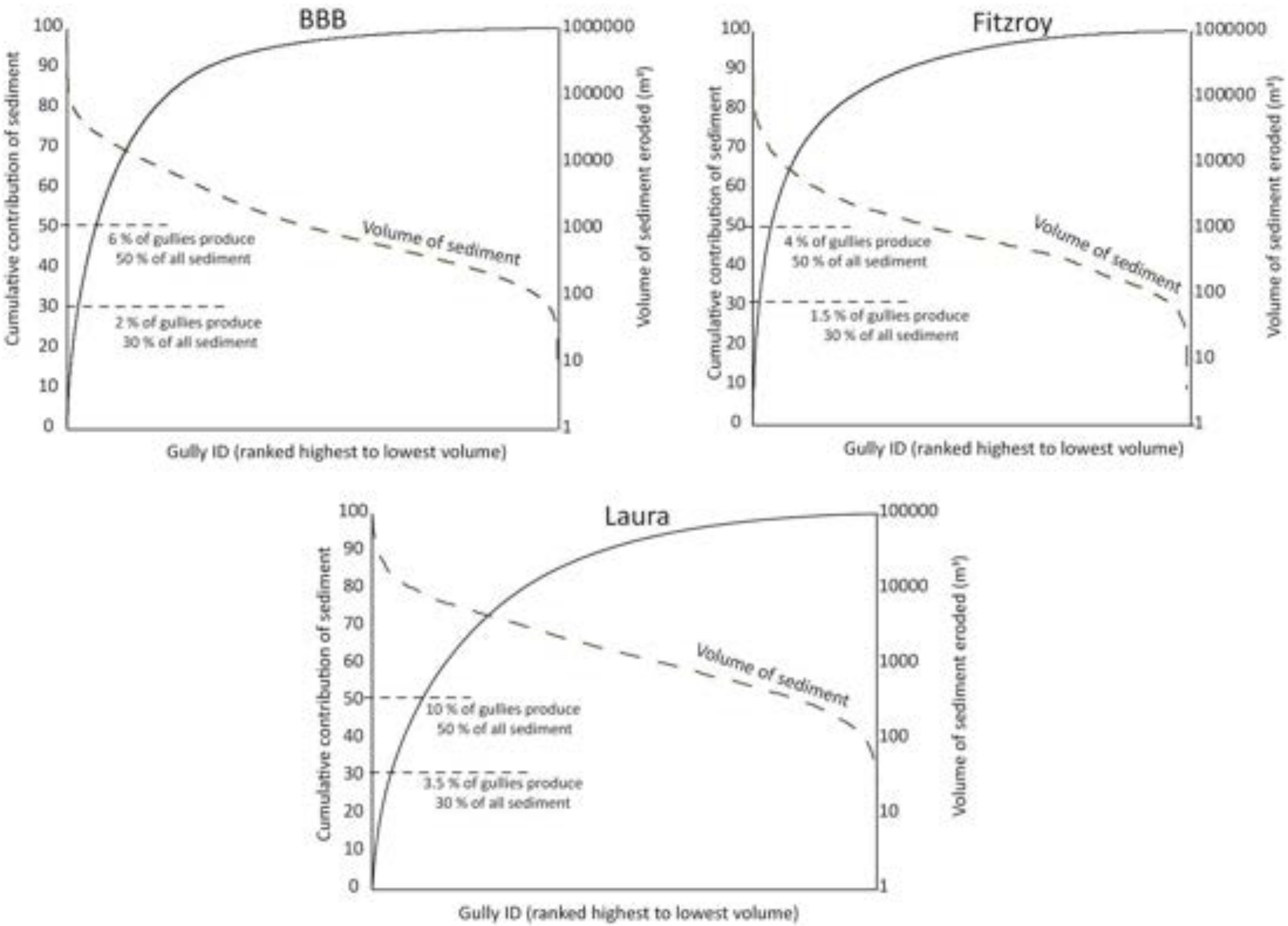

Figure 74: Cumulative proportional lifetime sediment yield curves for ranked gullies in the three catchments. The solid line represents the cumulative proportion of lifetime sediment yield (left axis) delivered by the mapped population of gullies in each lidar block when ranked according to sediment yield - across the X axis (highest on left). N= 22311 for BBB; 1785 for Fitzroy and 1820 for Laura. The dashed line is the eroded volume per gully (show on right axis).

3.3 Contributing catchment area

Much of the discussion to this point has been with regard to the characteristics of ELFs and gullies, but as was made clear in the conceptual model in Figure 9, an important characteristic of a gully is the hydrologic catchment boundary, or watershed. As part of the mapping process we have delineated the contributing catchment area for each mapped gully, provided we could delineate the complete catchment area within the lidar block. So, for the purposes of this analysis we have excluded all gullies that had their catchment boundary truncated by the limit of the lidar data. In some cases, the soft and hard margin may actually define the catchment, but more often, the catchment area is larger than the area of the soft margin. A Catchment Ratio has been quantified as the catchment area over the gully area.

Figure 75 - Figure 76 provide an example of a subset of gullies, including topographic and imagery data highlighting the hard margin and bare soil characteristics of each, in particular, the contributing catchment of each gully is highlighted in Figure 76. The data in Table 12 shows the areas of the different mapped components of the gullies, including the catchment area and the derived gully area/gully catchment area ratio. From this small sample, it is apparent that there is a significant range in the relative area of the active gully to the gully catchment area. In this example the largest alluvial gully (gully 1) has very little catchment area beyond the hard margin, which in this case is almost the same as the soft margin. The very low catchment ratio (1.2) indicates that there is very little additional runoff from outside the active part of the gully that is driving the erosion of the gully. Assuming the gully is still active, the ongoing erosion is being driven by direct rainfall on the gully itself and/or backwater within the gully from floods in the adjoining river. Both these hydrological drivers appear to be a common phenomenon within alluvial gullies (see Shellberg et al., 2013).

The summary data also shows that some gullies (e.g. gully 7 and 8) can have quite large catchment area/gully area ratios which could be an important consideration for management of the gully when coupled with other attributes. For example, in a gully that is active but has little or no catchment area, the only treatment that will have any benefit on gully sediment yields will be direct remediation of the active part of the gully. Whilst grazing exclusion will be a critical part of the management of that gully, it is unlikely that on its own this will have a measurable impact on catchment water yields and therefore the hydrological drivers of the erosion in that gully. Conversely, if the catchment/gully area ratio is high (e.g. > 20), and it can be shown that the catchment is highly degraded, it may be that catchment area hydrology can be influenced to such an extent that it may have a measurable influence on gully rainfall/runoff relationships, and hence a measurable influence on gully sediment and nutrient yields.

Another scenario may be a relatively small in area (compared to the catchment), such as gully 8 (Figure 76), has a rapid headcut retreat rate. The retreat rate data combined with the catchment area ratio data might indicate that this is a relatively young gully that requires immediate early intervention to prevent a small gully from becoming a large gully.

When we look at the overall gully population data, it is readily apparent that the three broad gully classes have very distinct patterns in their catchment ratios. From the data in Figure 77 and Table 13 (focusing on soft margin data) it is evident that the trend with alluvial gullies is strongly skewed towards low catchment area/gully area ratios; while colluvial gullies much less so, and rugged gullies less again. The summary statistics in Table 13, in which the proportion of the gully population have a ratio of 2 or less (i.e. gully catchment area is less than double the gully area), highlight these distinct differences in these populations. These data also serve to highlight some interesting differences between catchments. The alluvial gullies with a catchment ratio < 2 (based on soft margin area) represent between 48% and 67% of the population; whereas for colluvial gullies it is between 0.6% and 32.2%, and for rugged gullies it is between 2 and 20%. In relative terms the differences between the three gully classes are even more stark, with there being no colluvial or rugged gullies in the Fitzroy and Laura that have catchment ratio (based on hard margin area) < 2, whereas alluvial gullies have between 8 and 24% of the population that are in this category. In the BBB with a much larger gully population, colluvial and rugged are 7 and 3% respectively of the population, while alluvial gullies are 26%.

It is also interesting to note that in all three catchments, when the population is broken into the smaller subset of gullies that are contributing 50% of the lifetime gully sediment yield (see section 3.2.2), a large proportion of the gullies that are contributing the bulk of the sediment have relatively low catchment area/gully margins (9-43% hard; and 35-51% soft). This tends to support evidence from section 3.2.2 that alluvial gullies are dominating the sediment yields for the small cohort of gullies that are disproportionately delivering sediment to the stream network and the GBR. This smaller cohort of gullies is not going to respond to any great extent to catchment hydrological changes associated with passive management activities.

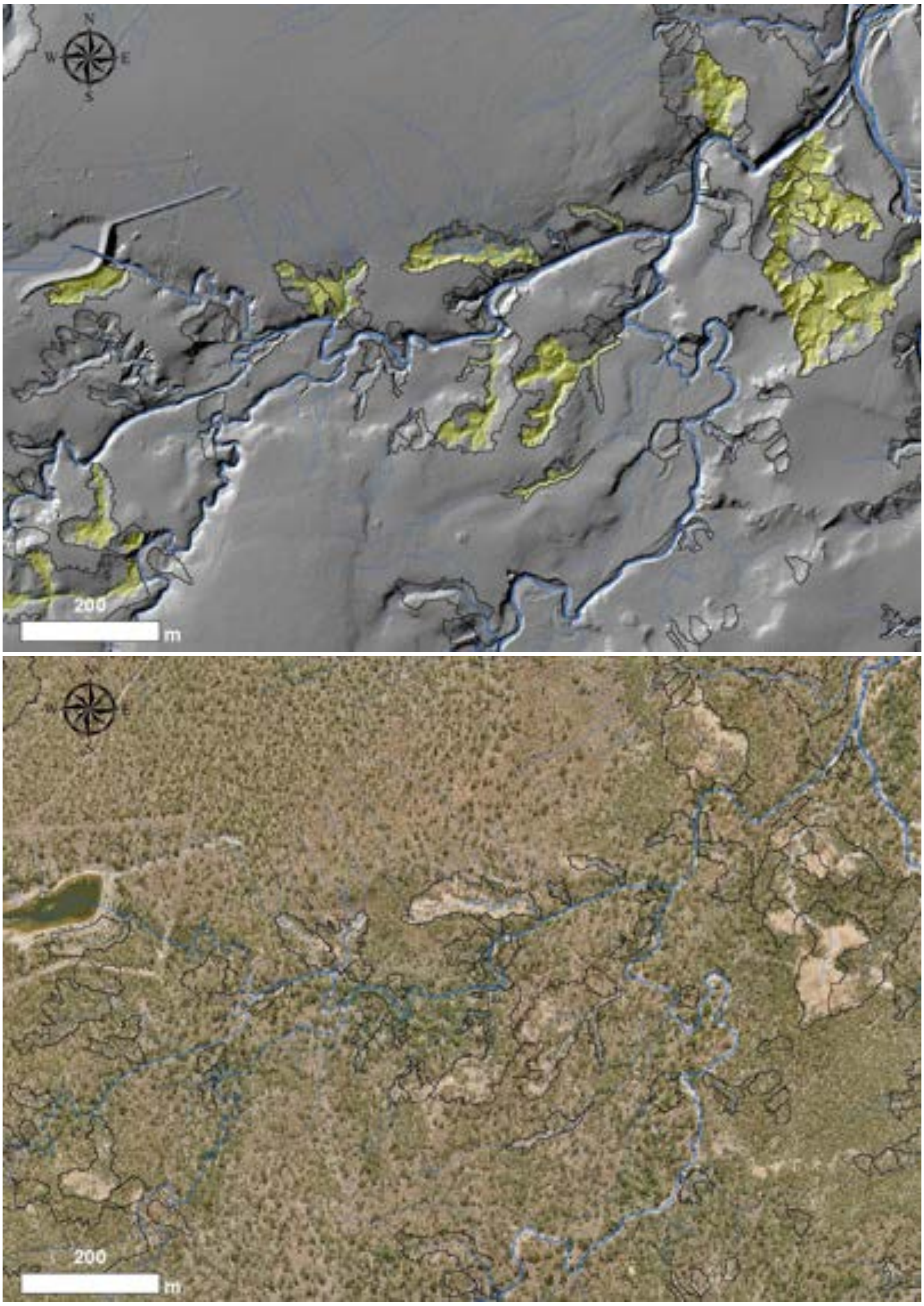

Figure 75: Example of ELFs mapped (black outline) in the Laura catchment shown on the bare ground hillshade DEM (top) and orthophoto image with flow lines (bottom), (Earls Creek is at the top right of the picture). Active alluvial gullies are indicated with the yellow shading.

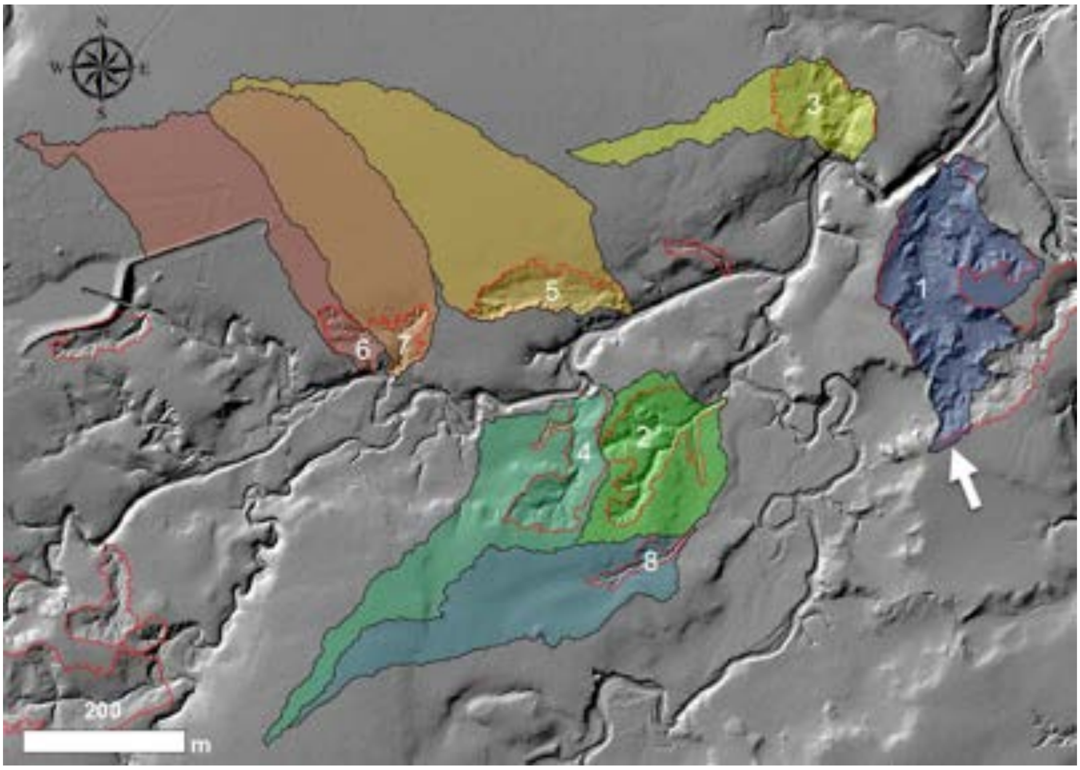

Figure 76: Selected ELFs have had contributing catchments generated. White arrow indicates the most visually impressive gully has almost reached the upper extent of its contributing catchment. Areas of hard margin, soft margin, contributing catchment and catchment ratio are presented in Table 12.

Table 12: Statistics of the areas for the three key delineated geomorphic boundaries for example alluvial gullies.

ID	Hard margin (ha)	Soft margin (ha)	Proportion hard margin (%)	Contributing catchment (ha)	Catchment ratio	Catchment ratio (hard margin)
1	2.44	3.31	74	3.8	1.2	1.6
2	0.64	1.17	55	2.7	2.3	4.2
3	0.52	1.08	48	2.1	1.9	4.0
4	0.38	1.00	38	4.2	4.2	11.1
5	0.42	0.85	49	5.7	6.8	13.6
6	0.19	0.34	56	3.8	11.3	20.0
7	0.24	0.34	71	4.2	12.4	17.5
8	0.12	0.20	60	3.7	18.9	30.8

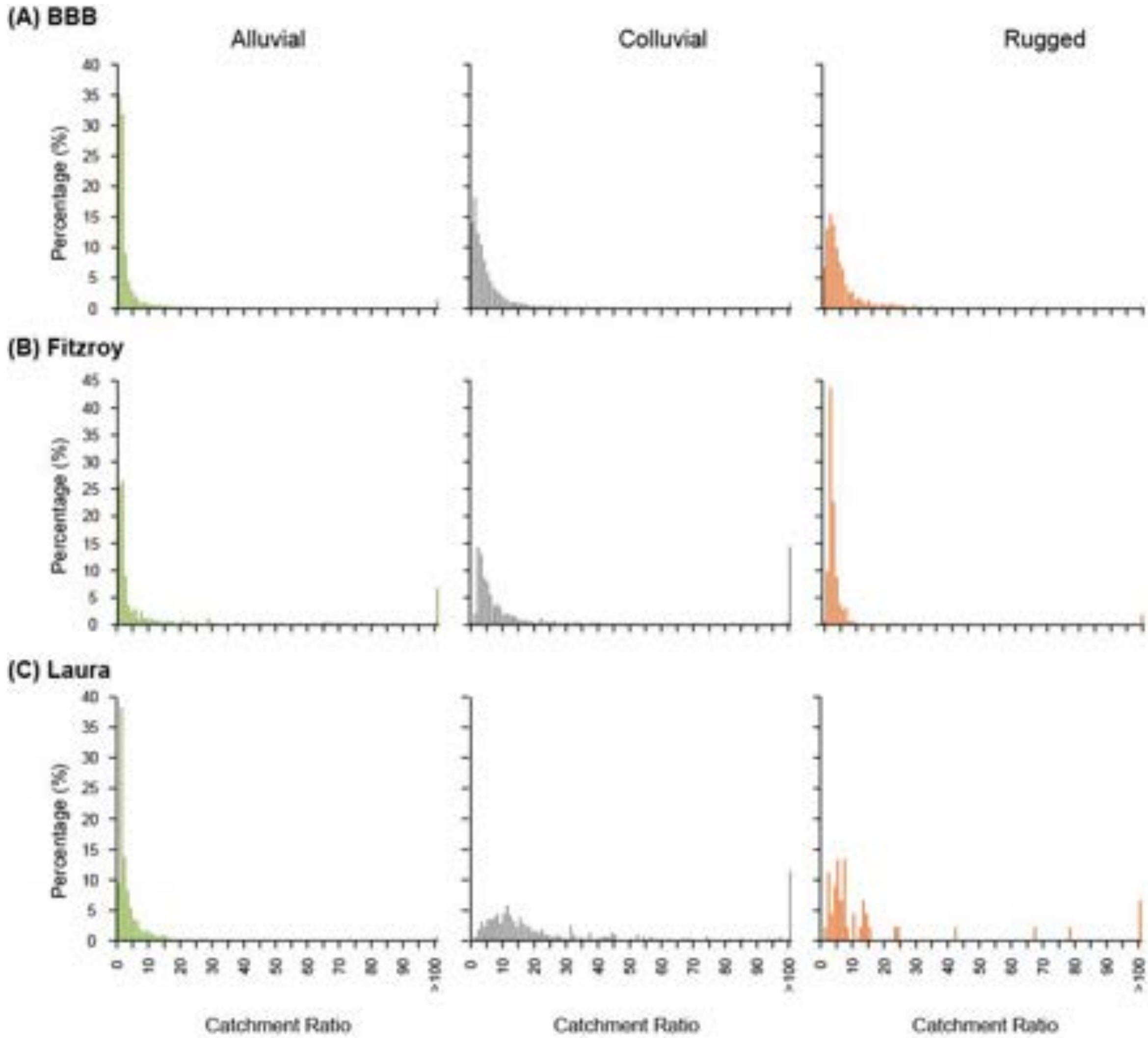

Figure 77: Contributing catchment area at the gully outlet to gully area ratios (soft margin) in the three study catchments broken down by gully type, plotted as percentage of the population in unit ratio categories. A ratio of 2 means the catchment area is the same size as the gully area.

Table 13: Percentage of contributing catchment to gully area ratio that is <2, i.e. catchment is less than double the area of the gully, using both hard and soft areas.

		Alluvial	Colluvial	Rugged	Top50% by Vol
BBB	Soft	66.8	32.2	19.8	35.0
	Hard	25.9	6.8	3.2	8.8
Fitzroy	Soft	52.1	2.4	10.6	51.1
	Hard	8.2	0	0	43.2
Laura	Soft	47.9	0.6	2.2	45.3
	Hard	24.2	0.0	0.0	17.9

3.4 Comparison with current gully P/A Mapping

3.4.1 Comparison methodology

As mentioned in section 1.2 and 1.3, P/A mapping (after Tindall et al., 2014) has involved overlaying a 100 m (1ha) grid on an assortment of aerial and satellite imagery, and manually assigning a binary presence of gully erosion within each 1 ha grid cell.

The P/A mapping and the lidar-based mapping were compared to assess the degree of agreement between the methods. The scales of the two methods (P/A mapping at 100 m and lidar-based mapping at 1 m) are two orders of magnitude apart and the two datasets are in different projections. To accommodate these differences the comparison was undertaken as a vector analysis between the P/A mapping 100 m grid and the lidar-based mapping vector polygons of gullies. The lidar-based gully polygons were clipped with the P/A mapping 100 m grid. Any 100 m grid square that contained any amount of lidar-based gully polygon was assigned the value of “presence of lidar-based mapped gully”. This process generates a 100m grid that has assigned to each grid square a presence/absence value for the P/A mapping and for the lidar-based mapping. For each study area the agreement/disagreement between the two methods is presented as a confusion matrix. The confusion matrix contains the count of grid squares in the four possible states of presence/absence. One, a grid square that has a value of gully present for lidar-based mapping and present for P/A mapping (positive-positive). Two, a grid square that has a value of gully present for lidar-based mapping and absent for P/A mapping (positive-negative). Three, a grid square that has a value of gully absent for lidar-based mapping and present for P/A mapping (negative-positive). Four, a grid square that has a value of gully absent for lidar-based mapping and absent for P/A mapping (negative-negative).

3.4.2 Fitzroy study area

The spatial distribution within the Fitzroy study area of gully presence/absence values of the 100 m grid of the P/A mapping and lidar-based mapping is shown in Figure 78. As shown in the confusion matrix (Figure 79), the presence/absence values correlate across 91% of grid squares (positive-positive and negative-negative values). However, of all grid squares with gully present values for either mapping methods, there is only 12.5% agreement between the datasets. The count of grid squares with lidar-based mapping positive and P/A mapping negative is 4,689 (36.8%), while the count of grid squares with lidar-based mapping positive and P/A mapping negative is 6,455 (50.7%). In the confusion matrix (Figure 79), the proportion of alluvial, colluvial, and rugged gullies are shown for the states; lidar-based mapping positive – P/A mapping positive and lidar-based mapping positive – P/A mapping negative.

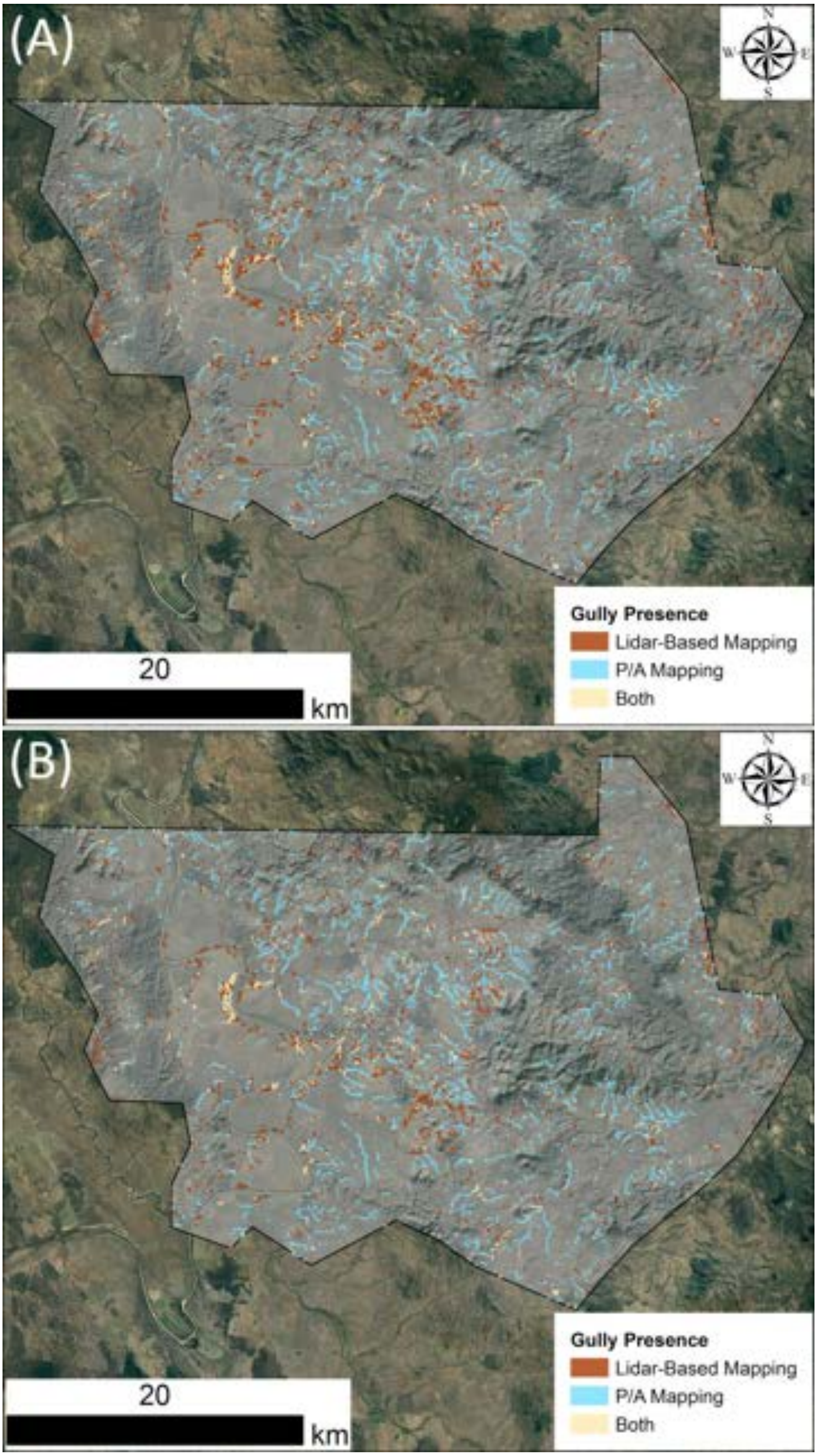

Figure 78: A comparison of mapping methods across the Fitzroy study area, using (a) soft margins; and (b) hard margins. Blue represents grid squares identified as gully present exclusively by P/A mapping, brown grid squares exclusively by lidar-based mapping.

<table>
<tr><td colspan="2"></td><td colspan="2">P/A Mapping</td></tr>
<tr><td colspan="2"></td><td>Positive</td><td>Negative</td></tr>
<tr><td rowspan="2">Lidar-Based Mapping
(Soft Margins)</td><td>Positive</td><td>1,589 grid squares
(12.5%)
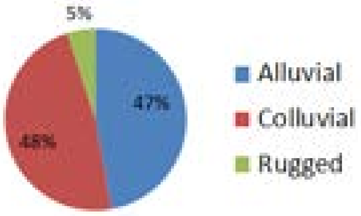
</td><td>4,689 grid squares
(36.8%)
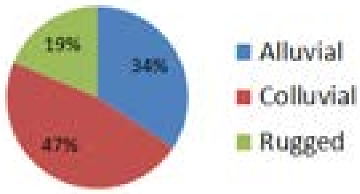
</td></tr>
<tr><td>Negative</td><td>6,455 grid squares
(50.7%)</td><td>110,414 grid squares</td></tr>
</table>

Figure 79: Confusion matrix of mapping methods between the P/A mapping and lidar-based mapping (soft margins) across the Fitzroy study area. The pie charts show the breakdown of alluvial, colluvial, and rugged gullies for the lidar-based mapping.

<table>
<tr><td colspan="2"></td><td colspan="2">P/A Mapping</td></tr>
<tr><td colspan="2"></td><td>Positive</td><td>Negative</td></tr>
<tr><td rowspan="2">Lidar-Based Mapping
(Hard Margins)</td><td>Positive</td><td>1,445 grid squares
(12.7%)</td><td>3,335 grid squares
(29.3%)</td></tr>
<tr><td>Negative</td><td>6,599 grid squares
(58.0%)</td><td>111,768 grid squares</td></tr>
</table>

Figure 80: Confusion matrix of mapping methods between the P/A mapping and lidar-based mapping (hard margins) across the Fitzroy study area. Note that as negative-negative values comprise >80% of the data, this value has not been included in the displayed percentages.

3.4.3 BBB study area

The spatial distribution within the BBB study area of gully presence/absence values of the 100 m grid of the P/A mapping and lidar-based mapping is shown in Figure 81 (south lidar block, Bowen River) and Figure 82 (north lidar block, Bogie and Strathalbyn). As shown in the confusion matrix (Figure 83), the presence/absence values correlate across 88% of grid squares (positive-positive and negative-negative values). However, of all grid squares with gully present values for either mapping methods, there is only 36% agreement between the datasets. The count of grid squares with lidar-based mapping positive and P/A mapping negative is 23,459 (34%), while the count of grid squares with lidar-based mapping positive and P/A mapping negative is 20,202 (30%).

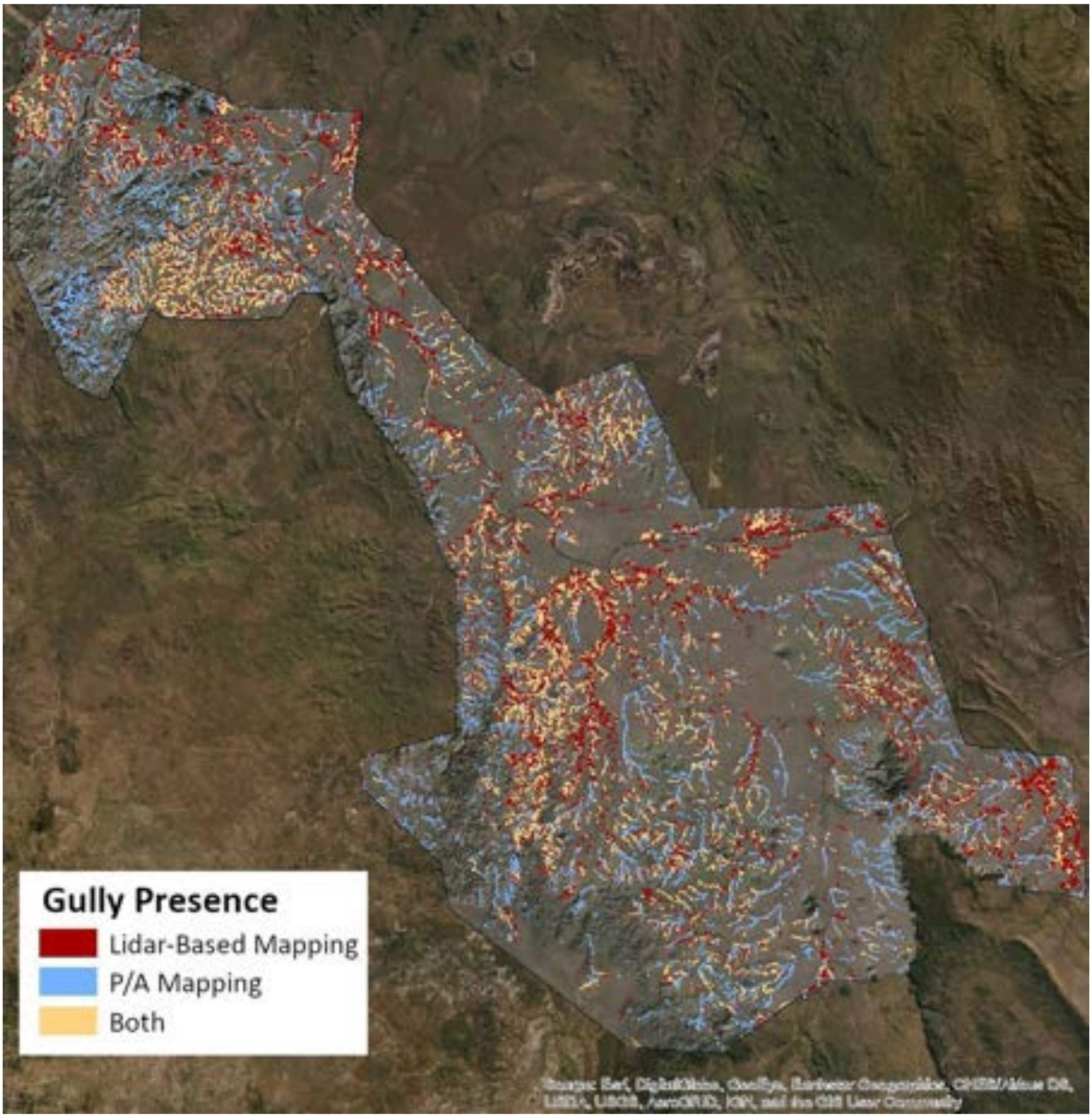

Figure 81: A comparison of mapping methods across the south lidar block. Blue represents grid squares identified as gully present exclusively by P/A mapping, brown grid squares exclusively by lidar-based mapping.

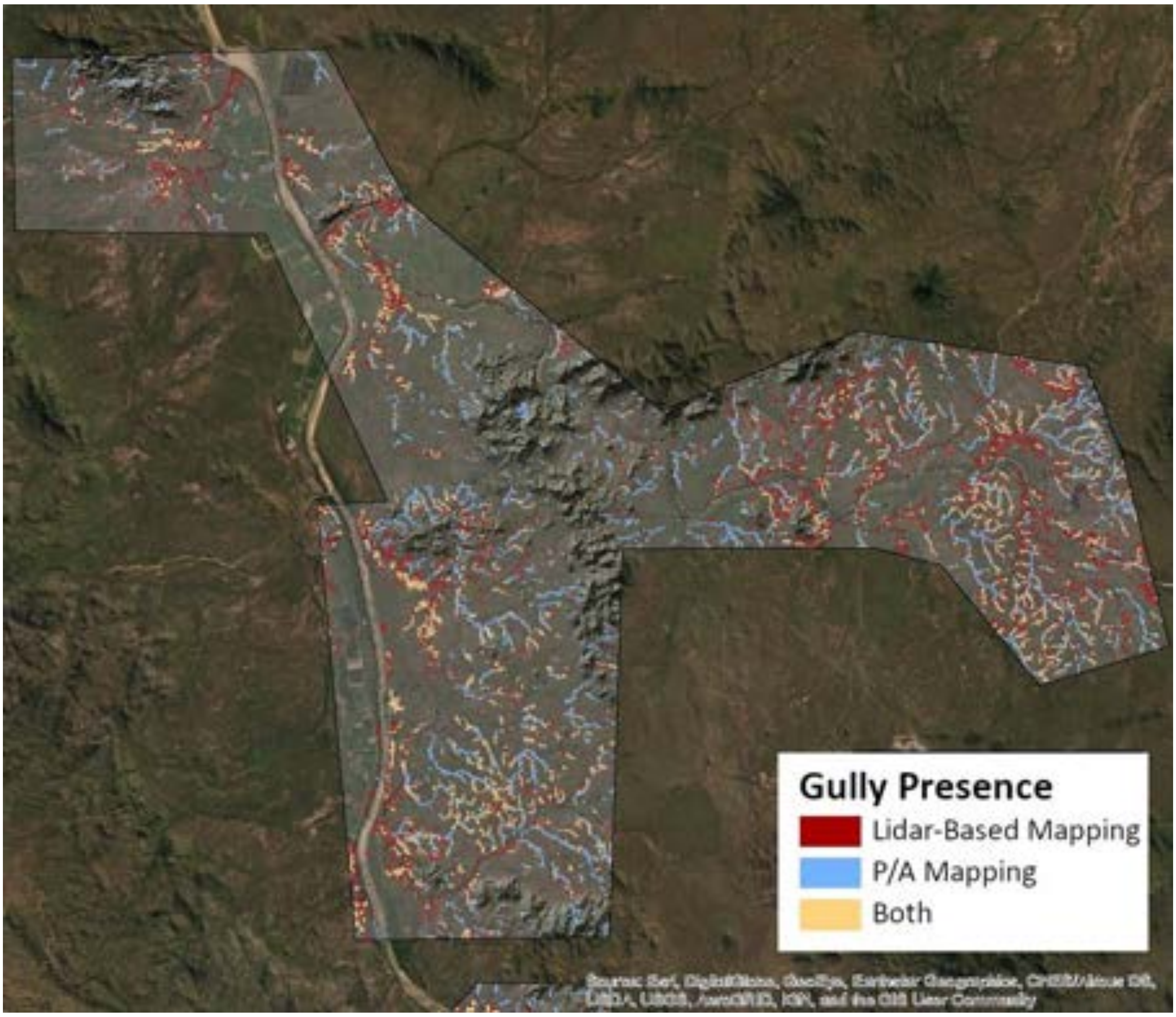

Figure 82: A comparison of mapping methods across the north lidar block. Blue represents grid squares identified as gully present exclusively by P/A mapping, brown grid squares exclusively by lidar-based mapping.

		P/A Mapping	
		Positive	Negative
Lidar-Based Mapping	Positive	24,756 (36%)	23,459 (34%)
	Negative	20,202 (30%)	303,318

Figure 83: Confusion matrix of mapping methods between the P/A mapping and lidar-based mapping across the BBB study area. Note that as negative-negative values comprise >80% of the data, this value has not been included in the displayed percentages.

Both study areas have a high degree of agreement of gully presence and absence (positive-positive and negative-negative values), 88% for the BBB study area and 91% for the Fitzroy study area. But this high degree of agreement is predominantly the result of the large proportion of grid squares assigned a value of gully absence (negative-negative) by both mapping methods. When considering only the grid squares that are assigned a gully present value by either mapping method (critical region of interest (ROI) grid squares), the degree of dis-agreement is high. The percentage of the ROI grid squares with values of the lidar-based mapping positive and P/A mapping negative range between 29% and 34%. The percentage of the ROI grid squares with values of the lidar-based mapping negative and P/A mapping positive range between 30% and 58%. This pattern of high agreement overall and high dis-agreement in the ROI grid squares indicates that both mapping methods are identifying the parts of the landscape where gullying occurs, but there is some disconnect between the mapping methods when identifying gullies within these parts of the landscape. This disconnection is the result of the different definitions of what a gully is that are used by the two mapping methods.

Figure 84 shown two locations within the Fitzroy study area that illustrate the disconnection between mapping methods resulting from the use of differing gully definitions. The images display the 100m grid squares that are lidar-based mapping positive and P/A mapping negative (red), lidar-based mapping negative and P/A mapping positive (blue), lidar-based mapping positive and P/A mapping positive (yellow) and the lidar-based mapping gully polygon outlines (black). Figure 84A shows the P/A mapping delineating the small stream channels and, in the lower right, the lidar-based mapping delineating a gully. Figure 84B has a range of grid squares that are assigned a gully present value by both mapping methods (positive-positive). But the configuration of these grid squares indicates that the positive-positive case can result from the P/A mapping of small stream channels just being in the same grid square as the lidar-based mapping gully polygon. That is, the two methods are not mapping the same thing, but that small stream channels and gullies are usually adjacent and connected within the landscape.

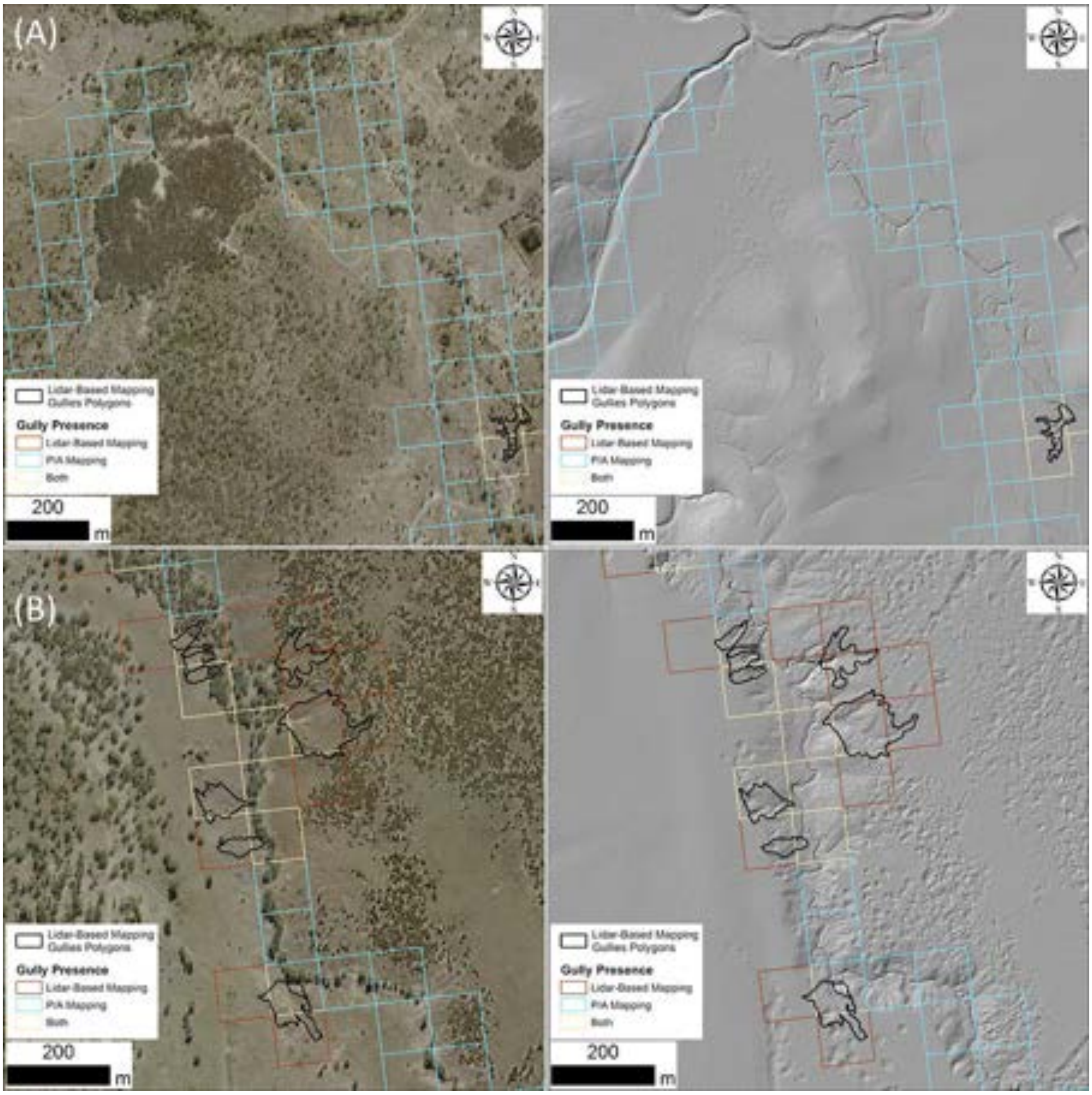

Figure 84: Examples of the P/A mapping and lidar-based mapping in the Fitzroy study area

Figure 85 shows examples of the mapping comparison within the BBB study area. Another consequence of the differing definitions of what is a gully is that large alluvial gullies, producing a significant proportion of the fine sediment pollution, are not being mapped by the P/A mapping method. Along the banks of the relatively large rivers featured in Figure 85 are numerous red grid squares, that is, grid squares that contain lidar-based mapping gully polygons and are not identified as a gully value by the P/A mapping.

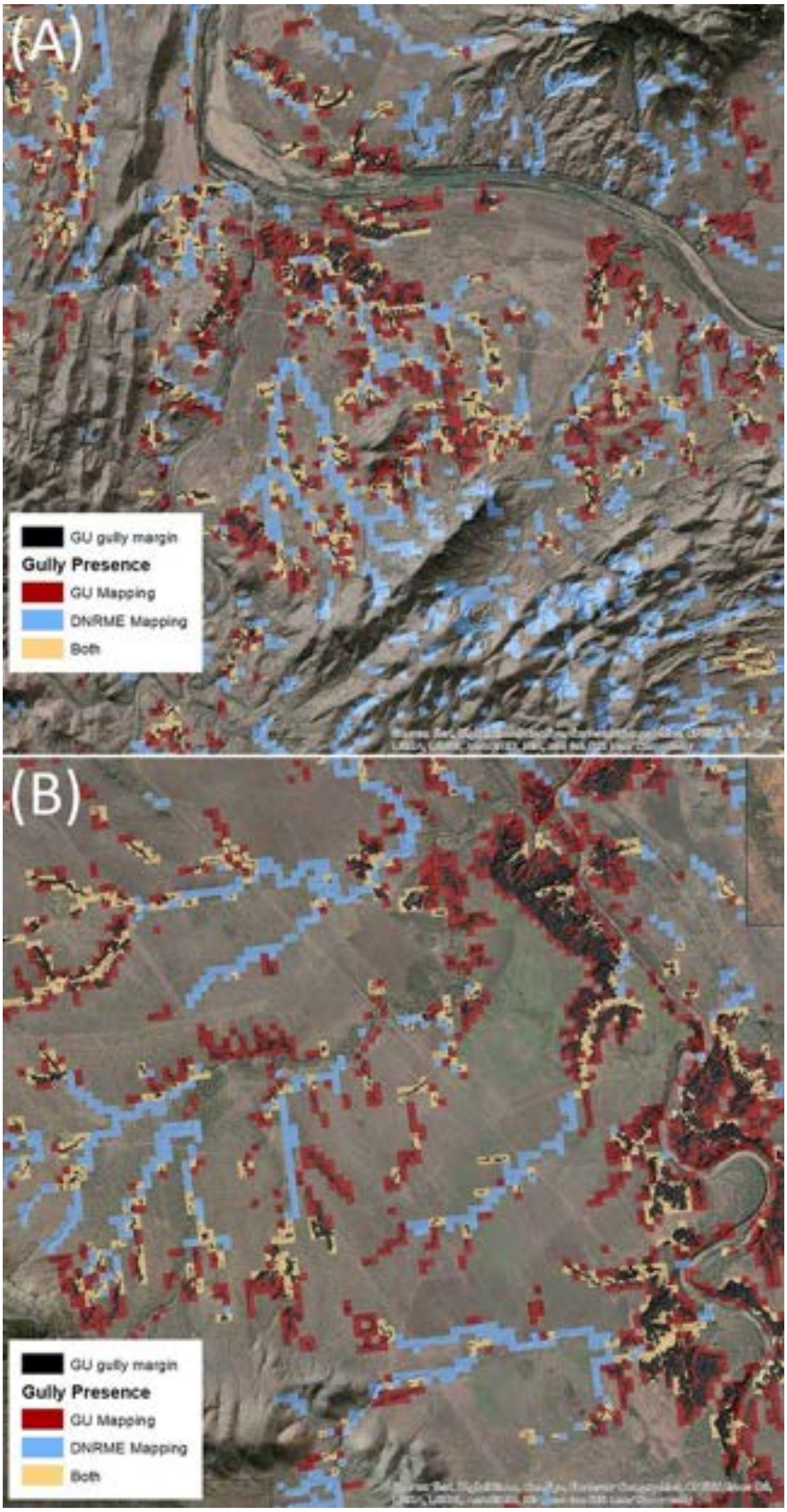

Figure 85: A comparison of mapping methods around (A) the Mt Wickham area and (B) Exmoor Station area, both within the BBB. Note in particular that rugged and steep terrain in (A) is predominantly P/A mapping gully present exclusively, while in (B) the P/A mapping appears to be mapping stream channels while significant areas of alluvial gullying along the banks are only mapped by the lidar-based mapping.

Small streams are geomorphically and hydrologically distinct from gullies. Channel and bank erosion of small streams does occur, but deposition also occurs within stream. In general, the ratio of deposition to erosion is skewed toward erosion in a gully to a much greater degree than a stream. A consequence of the geomorphological and hydrological distinctiveness of stream and gullies is that if either is actively eroding the techniques and methods that could be implemented to rehabilitate or remediated are also distinct. At the scale of evaluating a gully or a section of stream channel for remediation works, understanding the proximity and connectivity of one to the other is important. To know how and when to address stream channel erosion and/or gully erosion, gullies and stream channels need to be mapped and understood as separate parts of the landscape that may or may not have a complicate positive or negative feedback interaction.

The differing definition of what is a gully between the two mapping methods and the consequences for the mapping of gullies clearly indicates the importance and necessity of a rigorous definition of the terms: gullies, streams, drainage lines, ephemeral streams, rivers and water courses. The mapping of gullies and the datasets produced become a foundation for a range of undertakings, such as, sediment budget modelling and the prioritisation of cost-effective gully rehabilitation. These undertakings in turn are components of the interventions that can be implemented to protect the future of the GBR. To effectively map gullies, and therefore improve the undertakings that lead to improvements in GBR water quality, there must be a considered and qualified definition of what is a gully.

4.0 CONCLUSION

GBR Gully Mapping

The suite of methods outlined here provides a repeatable method by which gullies have been mapped across 5,300 square kilometres of lidar and has produced the largest and most complete inventory of gullies in a subset of the GBR catchment. The methods developed map eroded landforms (ELFs) and within these features identify actively eroding gullies across a large spatial area utilizing high resolution lidar and multiple lines of evidence. This gully activity map can now be used by managers and researchers to pin-point locations in all three GBR catchments that are likely contributing excess sediment to the reef and target these areas for remediation. As more lidar data becomes available it will now be feasible to carry out similar mapping at high resolution across large areas.

In its current state, application of the method requires an operator with a strong geomorphic background and first-hand knowledge of the sites being mapped. Nevertheless, the approach provides a significant improvement when compared with the existing coarse resolution P/A approach. It is acknowledged the P/A approach is being applied across the entirety of the GBR catchment area, so it has a different objective to the gully mapping and characterisation outlined here.

In addition to the higher resolution of mapping product presented here, a key difference with the existing P/A dataset is that we have applied an improved conceptual model to define the gullies that are the target for mapping. The existing P/A method incorporates low order ephemeral channels, many of which do not possess the fundamental characteristics of a gully. Many small ephemeral channels are unlikely to be dominantly erosional landscape features, and as such if assumptions about lifetime gully growth rates are applied to them on the assumption they are gullies, then modelled sediment yields will be artificially inflated in some parts of the landscape, and artificially reduced in others. The net result of this will be misleading prioritisation mapping.

Comparison between the P/A gully mapping and the lidar mapping showed a very poor spatial correlation between the two approaches. For the purposes of comparison, the lidar mapping was converted to a common one-hectare grid resolution in order to minimise the resolution effect. Comparative analysis showed that there was only a true positive result in 12.5% and 36% of pixels in the Fitzroy and BBB respectively (NB it was not possible to compare both methods in the Laura as the P/A mapping has not been completed here yet). Much of this variation is a result of the different conceptual model that was used to underpin the P/A mapping. The net result of the mapping in the Fitzroy in particular, is that an area that was thought to be a gully hotspot, with gully management resources applied accordingly, is in fact not a gully hotspot. Indeed, across the ~1,200km^2 lidar block in the Fitzroy, there are only a small number of gullies that would be regarded as a management priority.

Need to Characterise gully types

Regardless of whether the mapping is being used for model parameterisation or management prioritisation, the lumping of the small ephemeral channels with gullies is not tenable because they are governed by different processes and require different management strategies. These are two fundamentally different landscape features, and land managers need to be able to distinguish between them in their management prioritisation. Gullies and small channels require fundamentally different management approaches and pose different risks to local waterways and the GBR.

In addition to separating small channels from gullies, evidence presented in this study highlights fundamental differences between alluvial and colluvial gullies. Sediment yields, gully dimensions, and other parameters such as gully catchment ratios, are fundamentally different between these basic gully classes. Hence it is crucial that for both prioritisation and modelling purposes, at the very least gullies are classified into these two fundamental gully types. Applying average gully dimensions regardless of the gully type will lead to spatial distortions in modelled sediment yields. Indeed, the highly skewed gully dimension population statistics would suggest that applying the mean dimensions when extrapolating from a field sample to the population will lead to further spatial distortions in modelled sediment yields. Until higher resolution mapping becomes available everywhere, it may be more appropriate to apply a probability density function to the gully dimensions, based on lidar mapped data, and produce a more realistic estimate of the data uncertainty.

Complementary Approach to P/A mapping

Given that it is unlikely that sufficient resources will be available to collect lidar data across the entire GBR in the near future, the P/A mapping data will be useful for assisting in identifying hotspot areas of high-density gully erosion where lidar data can be acquired and higher resolution mapping undertaken along the lines outlined in this report. Thus, a refined gully mapping programme can be developed to complement the P/A mapping and be extended across the entire GBR for prioritisation, management and modelling purposes.

Mapping techniques appropriate to gully type and landscape setting

While a number of appropriate and accurate mapping techniques for extracting gully boundaries have been developed, the integration of these techniques provides a solid foundation for regional mapping. Here we utilise the existing mapping techniques of Evans and Lindsay (2010), Yang et al. (2017) and Korzeniowska et al. (2018) to create a comprehensive dataset of gullies across different landscape settings. The combination of these mapping approaches applied in different ways in different parts of the landscape provides the basis for mapping erosional landforms (ELFs), which is in effect the first step in the process of mapping and characterising gullies Virtually all existing landform mapping processes get to that point and go no further.

The approach taken in this study not only integrates these existing methods but creates individually mapped units based on consistent hydrological and morphological components, and filters such units based on multiple lines of evidence for erosion activity. In doing so, these developments provide a foundational basis for management and prioritisation by determining (a) eroding area and (b) volume and yield estimates for individual units. Only through this next step can gullies be truly prioritised for management or estimated for modelling.

To provide useful data on the relative importance of individual gullies in terms of their sediment yield and management priority, requires that much more is known about the mapped features. Hence, in this project considerable effort was directed towards the development of the methods that enable us to understand the relative erosion potential of each gully, and to filter non eroding “gully like” erosional landforms from the first pass of the mapping. The steps outlined in this report provide a first attempt at quantifying gully variables and thresholds, translating conceptual characteristics of gullies into objective, measurable criteria. Validation of the filtering against subjective operator decisions shows an accuracy of 86% with moderate to substantial agreement between objective and subjective approaches, with an F1 statistic of 0.7 and Cohen's Kappa of 0.61. Despite these results, it is important from a management perspective that gullies are not excluded from mapping, while being overly inclusive of ELFs erroneously inflates the issue and can result in gross overestimates in modelled data. It is anticipated that further refinement of the variables used to filter gullies from ELFs will be made as additional gully data becomes available, including field-validated gully classification data. Establishing such criteria and thresholds will dramatically improve our ability to map and further understand gully networks.

Potential Active Erosion (PAE) Index

The PAE metric developed for this project, uses field knowledge of the morphology of actively eroding gullies and uses a topographic roughness index as a proxy for gully erosion activity, with considerable success. This a significant development, because previously we were completely dependent on repeat lidar DEMs flown some years apart to derive erosion rates from DoD analyses. While lidar data is increasingly available, it will be a considerable time (at a minimum of 10-15 years) before adequate DoD data is available to quantify erosion The PAE index allows an initial estimate to be made from DEM representing a single point in time. Comparison of the index with DoD data indicates a high correlation with erosion activity at the gully scale which will enable further estimates of contemporary sediment yield and relative comparison to at least local gullies for prioritisation.

Prior Land Surface (PLS) reconstruction method

An alternative and complementary approach to the PAE, as a means of estimating relative lifetime gully erosion rates, is the PLS method. This approach, which is run using an automated script across the entire mapped gully dataset, provides an objective, but conservative, method for estimating the total lifetime gully erosion volume. Having calculated gully volume, a range of additional gully dimensional metrics can also be automatically calculated. Using the method, we have been able to calculate the lifetime volume of erosion across these lidar blocks and have determined that it amounts to around 28% of the volume of Sydney Harbour. Another way of thinking about this, is that if these gullies were feeding into the Sydney Harbour estuary, over the last ~130 years they would have delivered enough sediment to fill in the upper reaches of the Harbour down to about the Harbour Bridge.

REFERENCES

Alluvium (2019). Effective and Efficient Pathways for Investment in Improved Water Quality in the Great Barrier Reef: Final Report. A report for the Great Barrier Reef Foundation, Brisbane. https://www.barrierreef.org/uploads/Alluvium-2019-Effective-and-Efficient-Pathways-for-Investment-in-Improved-Water-Quality-in-the-GBR-Web-1.pdf

Anon (2018) Reef 2050 Water Quality Improvement Plan, 2017 – 2022, Queensland Government

Baruch, A., Filin, S., (2011) Detection of gullies in roughly textured terrain using airborne laser scanning data. ISPRS J. Photogramm. Remote Sensing, 66:564–578. https://doi.org/10.1016/j.isprsjprs.2011.03.001.

Bartley, R., Waters, D., Turner, R., Kroon, F., Garzon-Garcia, A., Kuhnert, P., Lewis, S., Smith, R., Bainbridge, Z., Olley, J. and Brooks, A., (2017). 2017 Scientific Consensus Statement: land use impacts on the Great Barrier Reef water quality and ecosystem condition, Chapter 2: sources of sediment, nutrients, pesticides and other pollutants to the Great Barrier Reef.

Betts, H.D., Trustrum, N.A. and Rose, R.C.D. (2003), Geomorphic changes in a complex gully system measured from sequential digital elevation models, and implications for management. *Earth Surface Processes and Landforms*. 28: 1043-1058. https://doi.org/10.1002/esp.500

Brooks, A. P., Shellberg, J. G., Knight, J., & Spencer, J. (2009). Alluvial gully erosion: an example from the Mitchell fluvial megafan, Queensland, Australia. *Earth Surface Processes and Landforms: 34*(14), 1951-1969.

Brooks, A.P., Spencer, J., Olley, J., Pietsch, T., Borombovits, D., Curwen, G., Shellberg, J., Howley, C., Gleeson, A., Simon, A., Bankhead, N., Klimetz, D., Eslami-Endargoli, L., Bourgeault, A., (2013) An Empirically-based Sediment Budget for the Normanby Basin: Sediment Sources, Sinks, and Drivers on the Cape York Savannah. Griffith University, 506pp. https://www.researchgate.net/publication/258337838

Brooks, A.P., Curwen, G., Spencer, J., (2016). A Framework for Prioritising Gully Management in the Normanby Basin Cape York. A report to South Cape York Catchments for the Cape York Water Quality Improvement Plan by the Australian Rivers Institute, Griffith University, 28 pp

Brooks, A.P. and Spencer J. (2018). LDC Landscape Remediation Characterisation and Prioritisation Project, Stage 1 Prioritisation Report. Griffith University 50 pp.

Brooks, A.P., Stout, J.C., Daley, J.S., Curwen, G, Spencer, J., Hasan, S., Thwaites, R, Smart J.C.R., Pietsch, T., Dale, G., Lucas., R. (2020). Gully Rehabilitation Prioritisation in the Bowen and Bogie Catchments; Full Report Report to the Landholders Driving Change Project. Precision Erosion & Sediment Management Research Group, Griffith University, pp. 230.

Brooks AP, Thwaites RN, Spencer J, Pietsch T and Daley, JS (2019). A Gully Classification Scheme to Underpin Great Barrier Reef Water Quality Management: 1st Edition. *NESP Project 4.9 Final Report*. The National Environmental Science Programme, Townsville http://www.nesptropical.edu.au .

Castillo, C., Taguas, E.V., Zarco-Tejada, P., James, M.R., Gómez, J.A., (2014) The normalized topographic method: an automated procedure for gully mapping using GIS. *Earth Surface Processes and Landforms*. 39, 2002–2015

Castillo, C, and Gómez, JA 2016. A century of gully erosion research: Urgency, complexity and study approaches. *Earth-Science Reviews* **160**: 300-319.

Cohen, J., (1960) A coefficient of agreement for nominal scales. *Educational and psychological measurement*. 20: 37–46. https://doi.org/10.1177/001316446002000104.

Congalton, R.G., (1991) A review of assessing the accuracy of classification of remotely sensed data. *Remote sensing of Environment*. 37: 35–46. https://doi.org/10.1016/0034-4257(91)90048-B.

Costel Codru, I., Niacsu, L. (2020) Using GIS techniques for automatic mapping of gullies in the Moldavian Plateau, Romania, *proceedings from the 22nd EGU General Assembly, held online 4-8 May, 2020*, id.19925

DeLong, S.B., Prentice, C.S., Hilley, G.E. and Ebert, Y. (2012), Multitemporal ALSM change detection, sediment delivery, and process mapping at an active earthflow. *Earth Surface Processes and Landforms*, 37: 262-272. https://doi.org/10.1002/esp.2234

DNRME, Department of Natural Resources and Mines (2018) *Detailed Geology Release, June, 2018,* Queensland Government

d'Oleire-Oltmanns, S., Eisank, C., Drăgut, L., & Blaschke, T. (2013). An object-based workflow to extract landforms at multiple scales from two distinct data types. *IEEE Geoscience and Remote Sensing Letters*, *10*(4), 947-951.

Eustace, A., Matthew, P., Christian, W. (2009) *Give me the dirt: detection of gully extent and volume using high-resolution LiDAR*, in S. Jones, K. Reinke (Eds.), Innovations in Remote Sensing and Photogrammetry, Springer-Verlag, Berlin Heidelberg (2009), pp. 255-269

Evans, M., & Lindsay, J. (2010). High resolution quantification of gully erosion in upland peatlands at the landscape scale. *Earth Surface Processes and Landforms*, *35*(8), 876-886.

Evans JS, Oakleaf J, Cushman SA (2014) An ArcGIS Toolbox for Surface Gradient and Geomorphometric Modelling, version 2.0-0. URL: https://github.com/jeffreyevans/GradientMetrics Accessed: 2020-01-15.

Haralick, R.M., Sternberg, S.R., Zhuang, X., (1987) Image analysis using mathematical Morphology. IEEE Transactions on Pattern Analysis and Machine Intelligence, 9:532–550. https://doi.org/10.1109/TPAMI.1987.4767941.

Gallant, J. C., & Dowling, T. I. (2003). A multiresolution index of valley bottom flatness for mapping depositional areas. *Water resources research*, *39*(12).

Gilad, U., Denham, R., Tindall, D. (2012) Gullies, Google Earth and the Great Barrier Reef: a remote sensing methodology for mapping gullies over extensive areas, *proceedings from*

International Archives of the Photogrammetry, Remote Sensing and Spatial Information Sciences, Volume XXXIX-B8, 2012 XXII ISPRS Congress, 25 August – 01 September 2012, Melbourne, Australia, pp. 469 - 473

Gilbert, J.T., Macfarlane, W.W., Wheaton, J.M. (2016) The Valley Bottom Extraction Tool (V-BET): A GIS tool for delineating valley bottoms across entire drainage networks, Computers & Geosciences, 97: 1-14, https://doi.org/10.1016/j.cageo.2016.07.014.

Gómez-Gutiérrez, Á., Schnabel, S., Berenguer-Sempere, F., Lavado-Contador, F., & Rubio-Delgado, J. (2014). Using 3D photo-reconstruction methods to estimate gully headcut erosion. *Catena*, *120*, 91-101.

Graf WL. 1983. The arroyo problem – palaeohydrology and palaeohydraulics in the short term. In Background to Palaeohydrology: A Perspective, Gregory KJ (ed.). John Wiley & Sons: Chichester; 279–302.

James, L. A., Watson, D. G., & Hansen, W. F. (2007). Using LiDAR data to map gullies and headwater streams under forest canopy: South Carolina, USA. *Catena*, 71(1), 132-144.

Jasiewicz, J., Stepinski, T.F. (2013) Geomorphons — a pattern recognition approach to classification and mapping of landforms, *Geomorphology*, 182: 147-156, https://doi.org/10.1016/j.geomorph.2012.11.005.

Karami, A., Khoorani, A., Nuhegar, A., Shamsi, S.R.F., Moosavi, V. (2015) Gully Erosion Mapping Using Object-Based and Pixel-Based Image Classification Methods, *Evironmental & Engineering Geoscience,* 21 (2): 101–110. https://doi.org/10.2113/gseegeosci.21.2.101

Knight, J., Spencer, J., Brooks, A., Phinn, S (2007) Large-area, high-resolution remote sensing based mapping of alluvial gully erosion in Australia's tropical rivers, P*roceedings of the 5th Australian Stream Management Conference: Australian Rivers: Making a Difference*, Charles Sturt University, Thurgoona, New South Wales, pp. 199-204

Korzeniowska, K., Pfeifer, N., & Landtwing, S. (2018). Mapping gullies, dunes, lava fields, and landslides via surface roughness. *Geomorphology*, 301, 53-67

Liu, K., Ding, H., Tang, G., Zhu, A. X., Yang, X., Jiang, S., & Cao, J. (2017). An object-based approach for two-level gully feature mapping using high-resolution DEM and imagery: a case study on hilly loess plateau region, China. Chinese Geographical Science, 27(3), 415-430.

MacMillan, R., Pettapiece, W., Nolan, S., Goddard T. (2000) A generic procedure for automatically segmenting landforms into landform elements using DEMs, heuristic rules and fuzzy logic, *Fuzzy Sets and Systems*, 113: 81-109, https://doi.org/10.1016/S0165-0114(99)00014-7

MacMillan, R.A., Martin, T.C., Earle, T.J., McNabb, D.H. (2003) Automated analysis and classification of landforms using high-resolution digital elevation data: applications and issues, *Canadian Journal of Remote Sensing*, 29:5, 592-606, DOI: 10.5589/m03-031

Martínez-Casasnovas, J.A., Ramos, M.C., Poesen, J. (2003) Sediment production in large gullies of the Mediterranean area (NE Spain) from high-resolution digital elevation models and geographical information systems analysis, *Earth Surface Processes and Landforms,* 28(5): 443 – 456, https://doi.org/10.1002/esp.451

Martínez-Casasnovas, J.A., Ramos, M.C., Poesen, J. (2004) Assessment of sidewall erosion in large gullies using multi-temporal DEMs and logistic regression analysis, *Geomorphology*, 58(1–4): 305-321, https://doi.org/10.1016/j.geomorph.2003.08.005.

Marzolff, I., Poesen, J. (2009) The potential of 3D gully monitoring with GIS using high-resolution aerial photography and a digital photogrammetry system, *Geomorphology*, 111(1–2): 48-60, https://doi.org/10.1016/j.geomorph.2008.05.047.

Moore, I.D., Grayson, R.B., Landson, A.R. (1991) Digital Terrain Modelling: A Review of Hydrological, Geomorphological, and Biological Applications. *Hydrological Processes* 5: 3–30.

Nobre, A.D., Cuartas, L.A., Hodnett, M., Rennó, C.D., Rodrigues, G., Silveira, A., Waterloo, M., Saleska, S. (2011) Height Above the Nearest Drainage – a hydrologically relevant new terrain model, *Journal of Hydrology*, 404(1–2): 13-29, https://doi.org/10.1016/j.jhydrol.2011.03.051.

NCST (National Committee on Soil and Terrain) 2009. *Australian Soil and Land Survey Field Handbook*, 3rd edn. National Committee on Soil and Terrain, CSIRO. 246 pp.

d'Oleire-Oltmanns, S., Marzolff, I., Tiede, D., Blaschke, T., (2014) Detection of gully-affected areas by applying Object-Based Image Analysis (OBIA) in the region of Taroudannt, Morocco. *Remote Sensing*, 6:8287–8309. https://doi.org/10.3390/rs6098287.

Olley, JM, Brooks, AP, Spencer, JR, Borombovits, D (2013) Subsoil erosion dominates the supply of fine sediment to rivers draining into Princess Charlotte Bay, Australia, *Journal of Environmental Radioactivity*, 124: 121-129

Otsu, N., (1979) A threshold selection method from Gray-level histograms. IEEE Transactions on Systems, Man, and Cybernetics, 9(1): 62–66. https://doi.org/10.1109/TSMC.1979.4310076.

Pasternack, G. B. 2017. Lower Yuba River Corridor Inundation Zones. Prepared for Yuba County Water Agency. University of California, Davis, CA.

Patton, N. R., Lohse, K. A., Godsey, S. E., Crosby, B. T., & Seyfried, M. S. (2018). Predicting soil thickness on soil mantled hillslopes. *Nature communications*, 9(1), 3329.

Passalacqua, P., Do Trung, T., Foufoula‐Georgiou, E., Sapiro, G., & Dietrich, W. E. (2010). A geometric framework for channel network extraction from lidar: Nonlinear diffusion and geodesic paths. *Journal of Geophysical Research: Earth Surface*, 115(F1).

Planet Team (2017). Planet Application Program Interface: In Space for Life on Earth. San Francisco, CA.

Planet Team (2020) Planet Imagery Product Specification. San Francisco, CA.

Poesen, J., Nachtergaele, J., Verstraeten, G., & Valentin, C. (2003). Gully erosion and environmental change: importance and research needs. *Catena*, *50*(2-4), 91-133.

Riley, S.J., De Gloria, S.D., Elliot, R., 1999. A terrain ruggedness index that quantifies topographic heterogeneity. International Journal of Science, 5: 23–27.

Saha S., Roy J., Arabameri A., Blaschke T., Tien Bui D. (2020) Machine Learning-Based Gully Erosion Susceptibility Mapping: A Case Study of Eastern India. *Sensors*. 20(5):1313. https://doi.org/10.3390/s20051313

Schumm, S. A., & Lichty, R. W. (1965). Time, space, and causality in geomorphology. *American journal of science*, *263*(2), 110-119.

Shruthi, R.B.V., Kerle, N., Jetten, V., (2011) Object-based gully feature extraction using high spatial resolution imagery. Geomorphology 134:260–268. https://doi.org/10.1016/j.geomorph.2011.07.003.

Shellberg, J. G., Brooks, A. P., Spencer, J., & Ward, D. (2013). The hydrogeomorphic influences on alluvial gully erosion along the Mitchell River fluvial megafan. *Hydrological Processes*, *27*(7), 1086-1104.

Shruthi, R.B.V., Kerle, N., Jetten, V., Stein, A. (2014) Object-based gully system prediction from medium resolution imagery using Random Forests, Geomorphology, 216: 283-294, https://doi.org/10.1016/j.geomorph.2014.04.006.

Shahabi, H., Jarihani, B., Tavakkoli Piralilou, S., Chittleborough, D., Avand, M., & Ghorbanzadeh, O. (2019). A Semi-Automated Object-Based Gully Networks Detection Using Different Machine Learning Models: A Case Study of Bowen Catchment, Queensland, Australia. *Sensors*, *19*(22), 4893. https://doi.org/10.3390/s19224893

Sithole, G., Vosselman, G., (2004) Experimental comparison of filter algorithms for bare-Earth extraction from airborne laser scanning point clouds. *ISPRS journal of photogrammetry and remote sensing*. 59: 85–101. https://doi.org/10.1016/j.isprsjprs.2004.05.004.

Stehman, S.V., (1997) Selecting and interpreting measures of thematic classification accuracy. *Remote sensing of Environment*. 62: 77–89. https://doi.org/10.1016/S0034-4257(97)00083-7.

Strahler, A. N. (1957). Quantitative analysis of watershed geomorphology. *Eos, Transactions American Geophysical Union*, *38*(6), 913-920.

Swets, J.A., (1988) Measuring the accuracy of diagnostic systems. *Science* 240: 1285–1293. https://doi.org/10.1126/science.3287615.

Thwaites, R, Brooks, A, Spencer, J. and T Pietsch (in review) What Type of Gully is That? I. The Need for a Classification of Erosion Gullies, *Earth Surface Processes and Landforms*.

Tindall, D., Marchand, B., Gilad,U., Goodwin, N., Byer, S., Denham, R.(2014). Gully mapping and drivers in the grazing lands of the Burdekin catchment. RP66G Summary Report , Queensland Dept Science Information Technology Innovation and the Arts. Pp. 22.

Vanmaercke, M, Poesen, J, Van Mele, B, Demuzere, M, Bruynseels, A, Golosov, V and Fuseina, Y (2016). How fast do gully headcuts retreat? *EarthScience Reviews* **154**, 336-355.

Vendrusculo, L. G. (2014). Classical gully spatial identification and slope stability modeling using high-resolution elevation and data mining technique, PhD Thesis, Iowa University.

Walker, S.J., Wilkinson, S.N., van Dijk, A.I.J.M. Hairsine, P.B. (2020) A multi-resolution method to map and identify locations of future gully and channel incision, Geomorphology, 358, https://doi.org/10.1016/j.geomorph.2020.107115.

Wells, NA 2004. Gully. In Goudie A, (ed.) *Encyclopedia of Geomorphology*, 1484 Volume 2, IAG, Routledge; 503–506.

Wilkinson, S.N., Dougall, C., Kinsey-Henderson, A.E., Searle, R.D., Ellis, R.J., Bartley, R. (2014). Development of a time-stepping sediment budget model for assessing land use impacts in large river basins. *Science of the Total Environment*, *468*, 1210-1224.

Wilkinson S.N., Bartley, R., Hairsine, .P.B., Bui, E.N., Gregory, L., Henderson, A.E. (2015). Managing gully erosion as an efficient approach to improving water quality in the Great Barrier Reef lagoon. Report to the Department of the Environment. CSIRO Land and Water. https://publications.csiro.au/rpr/pub?pid=csiro:EP1410201.

Wilkinson S, Hairsine P, Brooks A, Bartley R, Hawdon A, Pietsch T, Shepherd R, Austin J. 2019. *Gully and Stream Bank Toolbox. A technical guide for the Reef Trust Gully and Stream Bank Erosion Control Program. 2nd Edition.* Commonwealth of Australia.

Yang, X., et al. (2017). "Gully boundary extraction based on multidirectional hillshading from high-resolution DEMs." Transactions in GIS 21(6): 1204-1216.

Zahra, T., et al. (2017). "Knickzone Extraction Tool (KET) – A new ArcGIS toolset for automatic extraction of knickzones from a DEM based on multi-scale stream gradients." *Open Geosciences* 9(1).

Zeverbergen, L.W., Thorne, C.R. (1987) Quantitative Analysis of Land Surface Topography. *Earth Surface Processes and Landforms* 12: 47–56.

APPENDIX 1. GULLY METRIC METADATA

Attribute	Description of attribute
FID	Feature ID from ArcGIS
Id	ID used by ArcGIS for analysis
ZONAL_ID	Unique value for extracting zonal statistics
Area_m2	Area of the soft margin (m^2)
GullyID	Prefix for landscape class plus gully number
GulNum	Unique number for each soft margin
Hard_m2	Area of the hard margin (m^2)
Hard_pct	Area of hard margin as % of soft margin
PAE_m2	Area of Potential Active Erosion margin (m^2)
PAE_pct	Area of Potential Active Erosion as % of soft margin
VegeData	A note that data on vegetation follows
Ht2m_plus	Area of vegetation >= 2m tall (m^2)
pct2mPlus	Area of vegetation >= 2m tall as % of soft margin
Soft_Geom	A note that data on geometry of soft margins follows
SoftLen_m	Length of soft margin as defined by minimum bounding rectangle (m)
SoftWith_m	Width of soft margin as defined by minimum bounding rectangle (m)
SftPerim_m	Perimeter of soft margin (m)
Soft_L_W	Ratio of soft margin Length divided by Width
S_Prm_Area	Ratio of soft margin Perimeter divided by Area
Hard_Geom	A note that data on geometry of hard margins follows
HardLen_m	Length of hard margin as defined by minimum bounding rectangle (m)
HardWith_m	Width of hard margin as defined by minimum bounding rectangle (m)
HrdPerim_m	Perimeter of hard margin (m)
Hard_L_W	Ratio of hard margin Length divided by Width
H_Prm_Area	Ratio of hard margin Perimeter divided by Area
Ht_Range	A note that data on elevation range within soft margins follows
Elev_Range	Maximum elevation minus minimum elevation within soft margin (m)
HtRng_PAE	A note that data on elevation range within potentially active erosion follows
PAE_Range	Maximum elevation minus minimum elevation within potentially active erosion (m)
FlowDist	A note that data on length of maximum flow path within soft margins follows
FlowDist_m	Maximum flow length minus minimum flow length within soft margin, using downstream operator (m)
Slope_FL	A note that data on gully slope derived from flow length follows
Slope_FLen	Gully Slope calc from (Ht Range div by Flow Length) div by Pi times 180
Slope_GL	A note that data on gully slope derived from geometric length follows
Slope_GLen	Slope using gully length from Minimum Bounding Geometry (Ht Range div by Length) div by Pi times 180
Connected	A note that data on gully connection to channel system follows
Conxt_Y_N	Yes or No for connected or disconnected

Attribute	Description of attribute
Disconnect	A note that data on the distance of disconnection follows
DisCnctDis	The distance each individual gully is disconnected from the channel system (m)
ErasedDis	The distance each individual gully is disconnected from the channel system minus the distance the flow path passes through other gullies (m)
Diff	Total disconnected distance minus erased distance. Is the distance of diffuse overland flow (m)
GulVol	A note that data on the excavated volume of material as calculated by the reconstructed lids method follows
GulVol_m3	Volume of eroded material (m^3) Derived from Prior Land Surface estimate
AveDepth	Average depth of eroded pixels from Prior Land Surface method
MaxDepth	Max eroded depth of eroded pixels from Prior Land Surface method
UpArea	A note that data on the area of catchment contributing to the gully outlet follows
Catmnt_ha	Area of contributing catchment as defined by the maximum flow accumulation value (m^2)
Cat_Ratio	A note that data on the ratio of gully soft margin to contributing catchment follows
CatmtRat	Ratio of gully soft margin divided by contributing catchment area
ContrbArea	A note that data on whether the area of catchment contributing to the gully outlet is completely within the extent of the Lidar follows
WthInLidr1	1 = contributing area is within Lidar extent. 0 = contributing area runs off Lidar
CircRatio	A note that data on the circularity ratio of gully soft margin follows
CircRato	Circularity Ratio (4*Pi*Gully Area) divided by perimeter squared
SA_Ratio	A note that data on the Berry 2002 method for surface/area ratio of gully soft margin follows.
SAR_SUM	Sum of 3D surface area values
SAR_Norm	Ratio of 3D surface area to 2D surface area
FiltMethd	A note that data on the success or failure to pass filtering criteria for presence of hard margins of PAE within soft margin follows.
HardFilt	1 = success. 0 = fail
PAE_Filt	1 = success. 0 = fail
HardCount	A count of the fragments of Hard-edge inside each soft margin
Hard_Count	Count
PAECount	A count of the fragments of PAE inside each soft margin
PAE_Count	Count
Planet3m	A note that data on the area of bare earth identified from Planet Scope 3m imagery within soft margin follows
PS_bare	Area of bare soil from Planet Scope (m^2)
PS_pct	Area of Planet Scope 3m bare earth divided by area of soft margin
ecw_Bare	A note that data on the area of bare earth identified orthophoto RGB imagery within soft margin follows
ecwBare_m2	Area of bare soil from ecw imagery (m^2)
ecwBarePct	Area of orthophoto bare earth divided by area of soft margin
Fencing	Length of fencing based on minimum bounding perimeter
FenceLen	Length (m)
Clust_10m	A note that data on the clustering of soft margin within 10m of each other follows
Clust10mID	Alphanumeric Identifier of gully clusters within 10m of each other

Attribute	**Description of attribute**
Clust_50m	A note that data on the clustering of soft margin within 50m of each other follows
Clust50mID	Alphanumeric Identifier of gully clusters within 50m of each other
Roughness	A note that data on the roughness within each soft margin follows
Sum_Rough	Sum of Roughness over any eroding pixels
Sum_RoughA	Sum of roughness normalized to area of soft margin
SoilClass	A note that data on soil type within each soft margin follows
Soil_Desc	A brief description of soil type
Soil_Intgr	Integer classification of soil type
LandClass	A note that data on landscape classification for each soft margin follows
Land_Desc	Landscape class is alluvial, colluvial or rugged
Land_Intgr	Alluvial = 1, colluvial = 2, rugged = 3

APPENDIX 2. THE LIDAR ACQUISITION SPECIFICATION DOCUMENT (GBR CATCHMENTS GULLY LIDAR 2019) THAT WAS PART OF THE CONTRACTING PROCESS;

Great Barrier Reef catchments Gully Lidar 2019

Contents

1 Project Brief

CSIRO has been contracted by the Department of Environment and Energy to acquire lidar and orthophotography to improve the Department's investment prioritisation in the management of erosion and fine sediment losses to the reef through the establishment of a new baseline of extent of gully and streambank erosion.

An initial acquisition was completed in 2018 and this 2019 acquisition is the first of the smaller second phase acquisitions.

2 General Project Requirements

This lidar acquisition project is providing consistent high quality baseline data in key areas of the Great Barrier Reef catchments for assessing the state of gully and streambank erosion and monitoring change over time.

This project has higher than usual accuracy and point density requirements to achieve the level of detail required for mapping and monitoring gully and streambank erosion features. **Eight outbound pulses per square metre** are required, and at **at least 50% swath overlaps** to ensure all areas are illuminated in two different directions and increase the likelihood of capturing gully sidewall positions and heights. The combination of pulse density and swath overlap should produce an effective 16 pulses per square metre.

Queensland Government agencies intend to capture data on ground concurrently with lidar data capture where possible, so advance notice of acquisition times and locations will be required.

3 Project Timeframe

Acquisition should commence as soon as possible after contracting. Delivery of data is required by 28 September 2019 and the final project report is required within two weeks of final data delivery. The contract is expected to be completed by late October 2019.

Additional acquisitions may be sought over the following three years, subject to the Department's needs, and will be commissioned separately.

4 Project Area

The acquisition areas are in the Normanby catchment west of Cooktown (about 900 km2) and the lower Burdekin catchment southwest of Bowen (about 300 km2), as shown in the attached specification (Attachment B). In the event that the full area cannot be covered within the nominated budget, or more area can be covered, the exact areas to be acquired will be agreed in negotiation with the selected Supplier.

The purpose of this acquisition is delineating and measuring gully and streambank erosion, so the terrain covered is generally low relief near drainage lines. The gully features commonly have near-vertical walls 1 to 3 m in height. Trees and low vegetation are common in these areas, including within the gullies.

Some higher relief areas are included which may impact on swath width and overlap. The higher areas are not the primary interest of the acquisition so the requirement for 50% swath overlap in the higher areas can be relaxed if required for efficient flight planning.

The acquisition area is generally over privately owned grazing land.

5 General LiDAR Specifications

	Description	Specifications
1	Coverage	See attached shapefile for draft priority list of acquisition areas.
2	Date of Capture	1. LiDAR: from June to August 2019 2. Orthophotography: with lidar, or within four weeks before or after lidar capture, to be delivered at the same time as the lidar data 3. Note that details of acquisition time and areas must be provided to CSIRO and to nominated contacts in Queensland Government in advance to facilitate collection of on-ground data concurrently with the lidar collection.
3	Delivery Dates	Expected contract execution: 31 May 2019 Data delivery: by 20 Septempber 2019
4	Fundamental Spatial Accuracy Requirements	Fundamental spatial accuracy of the survey must conform to the following standard, noting that FVA is tighter than the usual ICSM category 1 standard: a. Fundamental Vertical Accuracy (FVA) i. <= **+/- 20cm.** 95% confidence interval (1.96 x RMSE) b. Fundamental Horizontal Accuracy (FHA) i. <= +/- 80cm. 95% confidence interval (1.73 x RMSE)
5	Horizontal Datum	The Geocentric Datum of Australia 1994 (GDA94).
6	Map Projection	The coordinate system for all deliverables is the Map Grid of Australia (MGA), zone 55.
7	Vertical Datum	1. Orthometric: All deliverables specified below as *orthometric* will be referenced to the Australian Height Datum (AHD) – as determined by the published heights of local survey control marks within or adjacent to the project extent. 2. Ellipsoid: All deliverables specified below as *ellipsoidal* will be in terms of the GDA94 reference frame. The source of the ellipsoidal height control shall be explained in the 'Post-Survey Spatial Accuracy Report'.
8	Geoid Model	AUSGeoid09 shall be used to derive orthometric heights from ellipsoidal data.
9	Adjustment to local AHD	1. Adjustment to "local" AHD as defined above is required under the following circumstances: a. Where the FVA described above is exceeded when the Geoid derived orthometric heights are validated against local AHD, or b. Where a bias in the vertical validation resulting from anomalies in the Geoid model or other sources is identified across the whole project area. 2. Details of this adjustment are required as part of the 'Post-Survey Spatial Accuracy Report', including the coordinates of points with Geoid and AHD heights used to define the adjustments.

10	Survey Control	1. All survey control data used or derived from this contract must be supplied to ensure independent Quality Assurance (QA) of the survey operations, and for possible inclusion in the State's survey control infrastructure. It is therefore essential that all primary ground stations are permanently marked in accordance with the appropriate State system. 2. The primary ground control and check point surveys must be referenced to the local datum specified above comprising State survey control marks with "established" GDA94 coordinates and/or "accurate AHD" heights as defined in the relevant State Surveying regulation. 3. Survey to establish new primary control shall use techniques to achieve a minimum standard of: a. Horizontal: PU less than 30 mm at 1 sigma b. Vertical: PU less than 50 mm at 1 sigma As described in the ICSM Standards and Practices for Control Surveys (SP1) Version 2.1. *Elevation data must be validated and corrected for systematic errors to ensure accuracy specifications are met. Documentation must describe how this has been achieved. Refer to the Quality Assurance Section for specific deliverables in relation to this topic.*
11	Sensor Requirements	The sensor must be capable of: a. detecting multiple discrete returns, with a minimum of 4 potential returns for each outbound laser pulse. b. recording the intensity of each return. The ground footprint of the laser pulses should be less than 30 cm. All data is to be collected using a single sensor type to ensure consistent data.

12	Collection Requirements	1. The survey design must plan on: a. recording a minimum Nominal Post Spacing (NPS) of **eight (8)** outbound pulses per square metre b. an across/along track point spacing ratio not exceeding 2/3. 2. **Flight line overlap must be 50%** or greater, delivering 16 points per square metre coverage, to ensure that all ground points are acquired from two different directions and increase the likelihood of capturing gully edges effectively. In higher terrain areas where swaths become narrower an overlap of not less than 40% will be allowed, provided those areas are identified and agreed in advance of the acquisition. 3. Any data with gaps between the geometrically usable portions of the swaths will be rejected. 4. Data Voids (areas =>0.5 m^2), measured using 1st-returns only within a single swath are not acceptable, except: a. where caused by water bodies b. where caused by areas of low near infra-red (NIR) reflectivity such asphalt or composition roofing c. where appropriately filled-in by another swath *5.* The spatial distribution of geometrically usable points is expected to be uniform and free from clustering. 6. Environmental conditions for data capture. a. Cloud and fog free between the aircraft and the ground. b. Floodplain/wetland data must be captured during times of base-flow and outside of significant surface inundation due to natural events and /or regulated environmental flows. c. Coastal surveys (areas under tidal influence) should be flown within 2 hours either side of low tide to minimise the effect of standing water or wave action. d. Flights should not be undertaken during periods of heavy smoke haze. e. Approval for variations from these conditions may be sought where necessary

6 LiDAR Point Cloud Specifications

	Deliverables	Specifications
1	Unclassified Point Cloud	1. All returns, all collected points, fully calibrated and adjusted to specified vertical datum, by swath. 1 file per swath, 1 swath per file. 2. Fully compliant LAS v1.2 (or v1.3), point record format with all standard attributes including: a. Intensity values (native radiometric resolution). b. Return number. c. Georeferencing information in all LAS file headers. d. GPS times recorded as adjusted GPS time, at a precision sufficient to allow unique timestamps for each pulse. 3. LAS v1.3 deliverables with waveform data are to use external "auxiliary" files with the extension ".wdp" for the storage of waveform packet data. See the LAS v1.3 specification for additional information). 4. Data is to be provided in the following Vertical Datums: a. Ellipsoidal (GDA94). 5. File naming as per Appendix B.
2	Classified Point Cloud	1. All returns, all collected points, fully calibrated and adjusted to specified vertical datum, and classified as specified below. 2. Fully compliant LAS v1.2 (or v1.3), point record format with all standard attributes including: a. Intensity values (native radiometric resolution). b. Return number. c. Georeferencing information in all LAS file headers. d. GPS times recorded as adjusted GPS time, at a precision sufficient to allow unique timestamps for each pulse. e. ASPRS/LAS "Overlap" classification (Class=12) shall not be used. ALL points not identified as "Withheld" are to be classified. 3. LAS v1.3 deliverables with waveform data are to use external "auxiliary" files with the extension ".wdp" for the storage of waveform packet data. See the LAS v1.3 specification for additional information) 4. Data is to be provided in the following Vertical Datums: a. Orthometric (AHD) b. Ellipsoidal (GDA94). 4. Tiled delivery, as per Data Supply Specifications below. 5. File naming as per Appendix B.

<table>
<tr>
<td>3</td>
<td>LiDAR Point Cloud Classification Scheme</td>
<td>
1. All classified point cloud data must adhere to the following modified ASPRS classification scheme.
2. *The minimum number of point classes to be delivered according to this scheme is defined by the Classification Level specified below.*
<table>
<tr><th>Number</th><th>Point class</th><th>Description</th></tr>
<tr><td>0</td><td>Unclassified</td><td>Created, never classified</td></tr>
<tr><td>1</td><td>Default</td><td>Unclassified</td></tr>
<tr><td>2</td><td>Ground</td><td>Bare ground</td></tr>
<tr><td>3</td><td>Low vegetation</td><td>0 – 0.3m (essentially sensor ‘noise’)</td></tr>
<tr><td>4</td><td>Medium vegetation</td><td>0.3 – 2m</td></tr>
<tr><td>5</td><td>High vegetation</td><td>2m ></td></tr>
<tr><td>6</td><td>Buildings, structures</td><td>Buildings, houses, sheds, silos etc.</td></tr>
<tr><td>7</td><td>Low / high points</td><td>Spurious high/low point returns (unusable)</td></tr>
<tr><td>8</td><td>Model key points</td><td>Reserved for ‘model key points’ only</td></tr>
<tr><td>9</td><td>Water</td><td>Any point in water</td></tr>
<tr><td>10</td><td>Bridge</td><td>Any bridge or overpass</td></tr>
<tr><td>11</td><td>not used</td><td>Reserved for future definition</td></tr>
<tr><td>12</td><td>Overlap points</td><td>Flight line overlap points</td></tr>
<tr><td>13-31</td><td>not used</td><td>Reserved for future definition</td></tr>
</table>
3. Class 1 (default) are points which have been subjected to a classification process but emerged in an undefined state. Class 0 have never been subjected to a classification process. This definition is necessary to maintain compatibility with common LiDAR processing suites.
4. When a simple ground/non-ground classification has been applied, all non-ground points will be allocated to Class 1.
5. Class 8 “model key points” is actually a subset of class 2 and so is created as a separate product.
</td>
</tr>
</table>

4	LiDAR Point Cloud Classification Levels	Classification to Level 3 standard is required for this acquisition. The results of the Level 1 automated classification are also to be delivered to provide a better understanding of the gains achieved with the manual classification to Level 3 standard **Level 1. Automated Classification.** Fully or semi-automated, batch processing of the point cloud data into ground (2) and default (1) classes. Level 1 point clouds may be provided either by swath or by tiles. Classification Accuracy Required: 95% for Ground points (minimum), and other classes as specified. **Level 3. Ground Correction.** Significant and highly supervised (often manual or semi-automated) effort is generally required for this level to ensure that only actual ground points are assigned to class 2. Typically, this editing will both remove and add points to the ground, vegetation and water classes derived using the automated algorithms. Full manual line scan editing of batch output may be required in highly complex environments. This level of classification is required for this project because of difficulties experienced with ground point classification around gullies in previous acquisitions. The rapid changes in ground height at gully edges appear to cause some classification algorithms to reject too many ground points, thus missing the gully features that this lidar acquisition must capture. Classification Accuracy Required: 99% for ground points (minimum), and other classes as specified. It is understood that some human structures such as fences and cars may remain in the medium vegetation class and that culverts do not need to be identified; the key requirement is for high quality identification of ground points around complex terrain features associated with gullies. CSIRO will provide examples of gully features and their locations in each area to inform the manual classification effort. *Classification accuracy requirements may be relaxed to accommodate collections in areas where CSIRO agrees classification to be particularly difficult, but complex gully areas are the key target features and classification accuracy will not be relaxed for those features.*

5	Required Point Cloud Classification Level	1. The following point cloud classification levels are required:

Number	**Point class**	**Required classes**	
		L1	**L3**
0	Unclassified	☐	☐
1	Default	☒	☒
2	Ground	☒	☒
3	Low vegetation < 0.3m	☐	☒
4	Medium vegetation 0.3 – 2m	☐	☒
5	High vegetation > 2m	☐	☒
6	Buildings, structures	☐	☒
7	Low / high points	☐	☒
8	Model key points	☐	☐
9	Water	☐	☒
10	Bridge	☐	☒
11	not used	☐	☐
12	Overlap points	☐	☐
13-31	Other As specified	☐	☐

7 LiDAR Derivative Data Specifications

Deliverables		Specifications
1	Intensity Image	1. 1m grid intensity image 2. Mosaic generated using average laser intensity values from "first return" LiDAR points. 3. ECW format using 5:1 compression. 4. Tiled delivery, as per Data Supply Specifications below. 5. File naming as per Appendix B.
2	Digital Surface Model (DSM) (orthometric)	1. 1m grid Digital Surface Model (DSM) 2. The DSM should be generated from the "first return" LiDAR mass point data. This will include ground and non-ground points such as vegetation and buildings. 3. The DSM generation should employ a Point to TIN and TIN to Raster process with Natural Nearest Neighbour interpolation. 4. Void areas (i.e., areas outside the project boundary but within any tiling scheme) shall be coded using a unique "NODATA" value. 5. GeoTIFF format preferred, ESRI floating point GRID format acceptable. 6. Tiled delivery, as per Data Supply Specifications below. 7. File naming as per Appendix B.

3	Digital Elevation Model (DEM) (orthometric)	1. **0.5m** grid bare earth Digital Elevation Model (DEM) 2. The DEM should be generated from the LiDAR mass point data classified as “Ground” only, so that it defines the “bare earth” ground surface. 3. The DEM generation should employ a Point to TIN and TIN to Raster process with Natural Nearest Neighbour interpolation. 4. Hydro-flattening will be undertaken for natural and man-made water bodies and water courses as defined below: a. Non-tidal water bodies with a surface area greater (>) than 625m^2 b. Non-tidal water courses greater than 30m nominal width. This should not unnecessarily break a stream or river into multiple segments. At times it may reduce below 30m for short segments. Data producers should use their best professional judgment. c. Flat and level bank-to-bank with a gradient following the immediate terrain. d. Water courses should break at road crossings and bridges. e. Sinks must not be filled. f. The entire water surface edge must be at or immediately below the surrounding terrain. g. Tidal variations over the course of the collection or between different collections may result in discontinuities along shorelines. The provider must confirm with CSIRO <u>if and how</u> these shorelines and water bodies will be processed. h. Any additional data layers created for the purposes of hydro-flattening such a masks or breaklines must be provided as shapefiles. CSIRO must be provided with all necessary data to re-produce the DEM from the mass point data. i. The methodology used for hydro-flattening is at the discretion of the data producer. *Note: The “hydro-flattening” specifications defined above are not intended to satisfy detailed hydrological or hydraulic modelling. Detailed hydrological enforcement and conditioning specifications are under development for these purposes. For more information contact* elevation@ga.gov.au 5. Void areas (i.e., areas outside the project boundary but within any tiling scheme) shall be coded using a unique “NODATA” value 6. GeoTIFF format preferred, ESRI floating point GRID format acceptable. 7. Tiled delivery, as per Data Supply Specifications below. 8. File naming as per Appendix B.
4	Canopy Height Model (CHM)	1. Not required
5	Foliage Cover Model (FCM)	1. Not required

8 Data Supply Specifications

Deliverables		Specifications
1	File naming	See Appendix B for NEDF file naming conventions.
2	Coordinate Origins for Gridded Data.	The origin of all gridded data must be placed on a whole metre coordinate value that will align with the zero (0) origin of the MGA Zone.
3	Data Tiling	1. All standard data sets should be supplied as single files where possible and tiled to manageable file sizes if necessary as below: a. 1km x 1km tiles based on MGA coordinates with origins that align with the zero (0) origin of the MGA Zone. b. Larger tile sizes which maximise workflow efficiency will be considered. c. The origin of the tile must be placed on a whole metre coordinate value of the south west corner of each tile. e.g. 426000mE_7243000mN 2. A Tile Index is to be provided by the contractor in ESRI shape file format. The tile name as specified above must be included as an attribute in the Tile Index file. 3. File naming as per Appendix B.
4	GPS data for occupations of base-stations	□ GPS data for all base station occupations in excess of 6 hours is to be provided in RINEX V1.2 format (Receiver Independent Exchange Format). 2. GPS observation log sheets which include the following details: a. Survey mark id b. Occupation time & date c. Antenna height measurements d. Instrument /antenna types & serial numbers The GPS observation log sheets should be provided in pdf format or Excel spreadsheet if data is captured digitally. *Where appropriate, some jurisdictions may find it useful to also request GPS data for any static primary control surveys.*
6	Data Delivery Reports	1. A delivery report describing the contents of the data supplied with every data delivery (interim, staged, final). The delivery report must also contain reference to the metadata supplied within the delivery.
7	Metadata	1. For each supplied data product a complete metadata statement consistent with the ANZLIC Metadata Profile (Version 1.1) must be provided in XML format. The ANZMET Lite metadata tool will be used to validate all XML records. http://www.anzlic.gov.au/resources/metadata 2. Additional metadata to meet NEDF lidar metadata requirements will be provided. The list of additional NEDF metadata required is shown in Appendix C. The NEDF Lidar Metadata tool can be obtained on request from elevation@ga.gov.au. 3. Metadata must be provided with every delivery including interim, partial and final deliveries. 4. Delivery will not be considered complete until the metadata is satisfactorily supplied.

8	Delivery Media	1. Data should be delivered on External Hard Drive (USB) or through a suitable online delivery system. External hard drives will be retained by the CSIRO. 2. Data deliveries should be clearly labelled with name of Service Provider, date of supply and list of contents.
9	Report Formats	All reports are to be provided in PDF, Word (.doc) format, Excel spreadsheet (.xls) or appropriate digital format approved by CSIRO.

9 Project Planning and Reporting Specifications

Deliverables		Specifications
1	Project Plan	Project plan detailing work breakdown structure, agreed data capture plans, project milestones and delivery schedules, progress reporting schedules etc within 10 working days of commencement of the contract.
2	Pre-Survey Quality Assurance Plan	The Contractor shall prepare and submit to CSIRO a Quality Assurance Plan that conforms to an identified management system and generally complies with ISO 9001. The plan must address the organisation and management of the project, work procedures, environmental considerations, safety and risk control and test procedures. The Plan must also detail the procedures to be used in verifying that the deliverables meet the required specification including: - The procedures and methodologies to be used to verify that the deliverables meet the required specifications. - Details of proposed calibration checks and methodology to be used to establish both reference stations and ground test sites. The Project Plan and Quality Assurance Plan must be submitted and accepted prior to commencement of the survey.
3	Post-Survey Spatial Accuracy Report	A post-survey spatial accuracy report is to be supplied for each acquisition area (Normanby and Lower Burdekin). The absolute and relative accuracy of the data, both horizontal and vertical, and relative to known control, shall be verified prior to classification and subsequent product development. This validation is limited to the Fundamental Spatial Accuracy (defined below), measured in clear, open areas. A detailed report of this validation is a required deliverable. The report will include the following: - Flight trajectories as specified below. - Point density map at 1 m resolution demonstrating consistent density of returns - Details of system calibration checks. - Results of relative (flight run) matching and details of any adjustments made. - Source of primary ellipsoidal height control. - Details of ellipsoid to orthometric corrections applied including any final adjustment to local AHD supplemental to the standard Geoid correction. - Results of vertical and horizontal accuracy validation. - All survey control coordinates, site id and check point comparisons in both Excel spreadsheet and ESRI shape file formats. - Digital photographs of all survey and check sites, with the site id included in the filename. The bearing of the photo direction should also be included. - Other related information.
4	Flight Trajectories	All flight trajectories used for the capture of the delivered LiDAR data will be supplied in ESRI Shape files. The shape file table's must include the date of capture, local start time, local end time and which reference station was used for each trajectory.

5	Progress Reports	The contractor, as a minimum will report by email each two week period. The report should contain a summary of progress, delivery and implementation, and details of any problems encountered and remedial action taken. The report should also address the planned activities for the two weeks ahead, regardless of whether successful capture has been achieved. **Details of these activities must be sufficient to allow for planning by CSIRO and Qld Govt agencies of on-ground data collection concurrent with lidar collection.**
6	Project Report	The Project Report should comprise a technical discussion addressing how each of the contract specifications has been met, a statement of consistency with any specified standards, results of independent accuracy and validation tests, metadata statements and extra-ordinary issues that may have affected the nature or delivery of the project. All aspects of the project operations must be adequately reported.

10 Quality Assurance Specifications

Description		Specifications
1	Fundamental Spatial Accuracy Validation (FSA)	Vertical Accuracy Validation 1. The fundamental vertical accuracy of the point cloud dataset must be determined with check points located only in open, relatively flat terrain, where there is a very high probability that the sensor will have detected the ground surface. 2. The vertical accuracy of the point cloud dataset is to be tested using a TIN surface constructed from bare-earth LiDAR points compared against ground survey check points. 3. Check points are to be surveyed independently of any LiDAR GPS operations. 4. Check points must be established to adequately cover the full extent of the survey area, and be representative of the project area landscape. For the purpose of determining the number of check points required, the acquisition area should be considered as two separate survey areas, one comprising the Normanby polygons and the other the Burdekin polygons. 5. For each survey area a minimum of 20 check points (locations) are required, then 1 per 50km² where LiDAR coverage exceeds 400km². At least 3 check points are required within each polygon of the survey area. When 20 points are tested, the 95 percent confidence interval would generally allow 1 point to fail the threshold given in product specifications 6. The proposed check point survey design must be submitted with the Pre-Survey Quality Assurance Plan, and approved by CSIRO prior to implementation. Acceptance of the post-survey spatial accuracy report discussed above is dependent on the quality, number and distribution of these check points. 7. If additional independent validation is required, data should be assessed in accordance with ASPRS Accuracy Reporting Guidelines. Horizontal Accuracy Validation 8. The onus for reaching the required accuracy lies with the data supplier. Independent accuracy assessments may also be carried out by CSIRO. 9. Independent testing of horizontal accuracy for LiDAR products is not required as part of this base specification. Instead data producers are required to report on the expected horizontal accuracy of elevation products as determined from system and sensor calibration studies. 10. In the above circumstances a “compiled to meet” statement of horizontal accuracy at 95 percent confidence should be reported. 11. As an alternative, the producer may demonstrate compliance through analysis of distinct features which are identifiable in the elevation data (e.g fences) or intensity images with other data sources such as high resolution imagery with known horizontal accuracy. 12. If additional independent validation is required, data should be assessed in accordance with ASPRS Accuracy Reporting Guidelines.
2	Supplemental Vertical Accuracy Validation (SVA)	1. Not required

<table>
<tr><td>3</td><td>Classification Accuracy Validation</td><td>1. It is expected that due diligence in the classification process will produce datasets that meet the required classification accuracies according to the specified LiDAR Point Cloud Classification Levels and specified classes. It is expected that the data will meet the following tests within any 1km x 1km area:

<table>
<tr><th>Classification Level</th><th>Demonstrated erroneous classification values for specified classes</th></tr>
<tr><td>Level 0 - Unclassified</td><td>Unspecified</td></tr>
<tr><td>Level 1. Automated Classification</td><td><=5%</td></tr>
<tr><td>Level 2. Ground surface improvement</td><td><=2%</td></tr>
<tr><td>Level 3. Ground Correction</td><td><=1%</td></tr>
<tr><td>Level 4. Detailed Classification and correction</td><td><=1% for all specified classes</td></tr>
</table>

These requirements may be relaxed to accommodate collections in areas where the CSIRO agrees classification to be particularly difficult.
2. In most circumstances detailed visual inspections of individual classified scan line profiles and use of high quality reference imagery will be sufficient to independently demonstrate if classification standards have been achieved for the specified classes.
3. Classification accuracy tests should be presented in the form of an error matrix for each specified class reporting errors of omission and commission generated from randomly selected points.</td></tr>
<tr><td>4</td><td>Classification Consistency Validation</td><td>1. Point classification is to be consistent across the entire project.
2. Noticeable variations in the character, texture, or quality of the classification between tiles, swaths, lifts, or other non-natural divisions will be cause for rejection of the entire deliverable.</td></tr>
<tr><td>5</td><td>Spatial Distribution of Points Validation</td><td>1. In order to ensure uniform densities throughout the data set:
a. A regular square grid, with cell area equal to the design NPS*2 will be laid over the data.
b. At least 90% of the cells in the grid shall contain at least 1 LiDAR point.
c. Assessment to be made against single swath, first return data located within the geometrically usable centre portion (typically ~90%) of each swath.
d. Acceptable data voids identified previously in this specification are excluded.</td></tr>
<tr><td>6</td><td>Interpolation Consistency Validation</td><td>All products derived from the LiDAR mass point data as tiles will show no edge artefacts or mismatch. A quilted appearance in the overall project surfaces, whether caused by differences in processing quality or character between tiles, swaths, lifts, or other non-natural divisions, will be cause for rejection of the entire deliverable.</td></tr>
</table>

Appendix A – Project Area Map

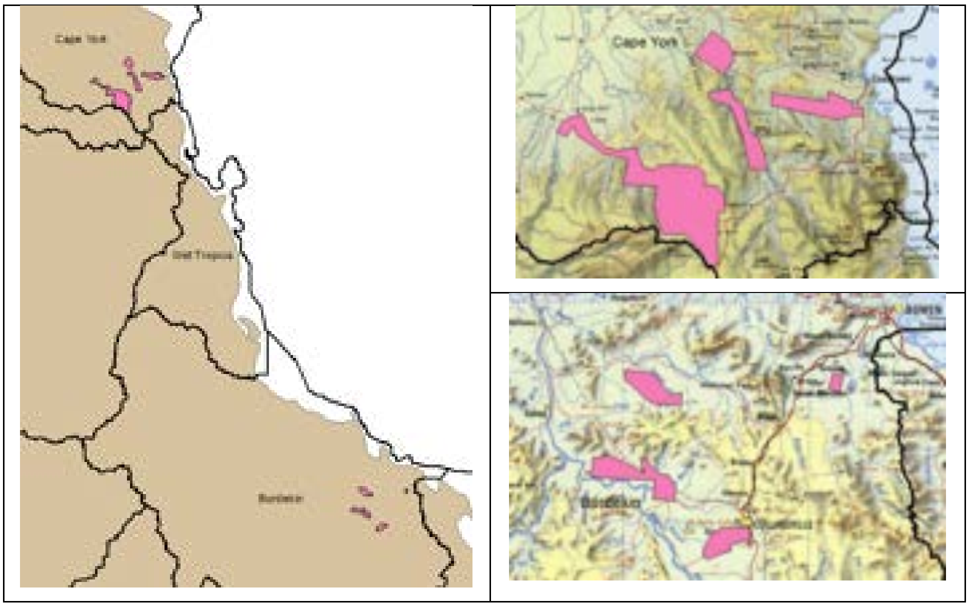

See supplied shapefile Capture2019_forQuoting.shp

Appendix B - File Naming Conventions

The following naming conventions have been developed to provide easy ingestion into the NEDF-Portal. The NEDF-Portal utilises the following file naming conventions for spatial and attribute searching, with the "_" used to separate each component of the file name. It is therefore a critical element of the process. There are a number software tools available for renaming existing data files. One used regularly in is the Bulk Rename Utility which can be downloaded from http://www.bulkrenameutility.co.uk/Main_Intro.php. Importantly, ESRI GRIDS cannot be renamed using this tool. Geoscience Australia can make an ESRI GRID renaming tool available by contacting elevation@ga.gov.au.

NEDF Data Naming Conventions

The NEDF Portal uses 2 types of spatial searching. For ESRI GRIDs it uses the dataset itself to undertake geoprocessing, and for rapid searching it uses the spatial extent of datasets by incorporating the extents into the name of the file. A single file image mosaic is named in a similar manner to a tiled dataset only with the added flexibility of defining tiles of any width and height in addition to traditional square tile. The Portal also uses "_" as a delimiter so it is crucial that you only use these where specified. Using this naming system allows files of any type to be spatially indexed and catalogued. For example, in addition to LiDAR tile and mosaic products, you can also catalogue project reports, pictures or any other reference information and retrieve them through the Portal.

The following file naming conventions have been developed to achieve national consistency, to improve dataset management, and to minimise data transfer and ingest costs for both producers and users.

Intensity imagery, or other forms of imagery provided

This image will generally cover the entire extent of the survey and uses the following filename convention in ECW or geoTIFF format as specified.

Naming Convention for LiDAR intensity or other forms of imagery:		
ProjectNameYYYY-INT-GSD_xxxyyyy_zz_wwww_hhhh.ecw		
ProjectName	*KempseyLidar*	A meaningful description of the total survey area of interest. Do not use "_" as part of the Project Name
YYYY	*2009*	Year of survey
INT/RGB	*-INT*	Intensity image file identifier. Use RGB for 3 band natural colour imagery or RGBI for 4 band infrared
GSD	*-002*	Ground sampling distance or resolution of image in metres.
xxxyyyy	*_4806558 (480,000mE) (6558,000mN)*	Easting and northing value (whole kilometre) of the south- west corner of the tile. A single "_" must be used to separate the remaining file name components.
zz	*_56*	MGA zone of the file
wwww	*_0020*	Width of the **dataset or tile** in whole kilometres
hhhh	*_0050*	Height of **dataset or tile** in whole kilometres
For example: KempseyLidar2009-INT-002_4806558_56_0020_0050.ecw		

LiDAR Unclassified Point Cloud in LAS Format
All LiDAR point cloud data are to be delivered fully compliant LAS v1.2 (or v1.3), Point Record Format

Naming Convention for LiDAR point clouds: *ProjectNameYYYY-UNC-DAT-SWT_xxxyyyy_zz_wwww_hhhh.las*		
ProjectName	*KempseyLidar*	A meaningful description of the total survey area of interest. Do not use "_" as part of the Project Name
YYYY	*2009*	Year of survey
UNC	*-UNC*	Unclassified point cloud. Fully calibrated and adjusted to specified datum
DAT	*-ELL*	Ellipsoidal heights (GDA94)
SWT	*-1..n*	Swath number (1 file per swath)
xxxyyyy	*_4806558 (480,000mE) (6558,000mN)*	Easting and northing value (whole kilometre) of the south- west corner of the tile. A single "_" must be used to separate the remaining file name components.
zz	*_56*	MGA zone of the file
wwww	*_0002*	Width of the tile in whole kilometres
hhhh	*_0002*	Height of the tile in whole kilometres
For example: KempseyLidar2009-RAW-ELL-001_4806558_56_0002_0002.las		

LiDAR Classified Point Cloud in LAS Format
All LiDAR point cloud data are to be delivered fully compliant LAS v1.2 (or v1.3), Point Record Format .

Naming Convention for LiDAR point clouds: *ProjectNameYYYY-CL-DAT_xxxyyyy_zz_wwww_hhhh.las*		
ProjectName	*KempseyLidar*	A meaningful description of the total survey area of interest. Do not use "_" as part of the Project Name
YYYY	*2009*	Year of survey
CL	*-C2*	classification level.
DAT	*-ELL or AHD*	Specified vertical datums. Ellipsoidal (ELL) or Orthometric (AHD)
xxxyyyy	*_4806558 (480,000mE) (6558,000mN)*	Easting and northing value (whole kilometre) of the south- west corner of the tile. A single "_" must be used to separate the remaining file name components.
zz	*_56*	MGA zone of the file
wwww	*_0002*	Width of the tile in whole kilometres
hhhh	*_0002*	Height of the tile in whole kilometres
For example: KempseyLidar2009-C3-AHD_4806558_56_0002_0002.las		

LiDAR Classified Point Cloud Model Key Points in LAS Format
Model Key points (MKP) are a generalised subset of the original mass points and represent the minimum number of points required to determine the shape of the ground. The filename convention is identical to that above with "-MKP" appended to the classification level:

Naming Convention: *ProjectNameYYYY-CL-MKP-DAT_xxxyyyy_zz_wwww_hhhh.las*		
ProjectName	*KempseyLidar*	A meaningful description of the total survey area of interest. Do not use "_" as part of the Project Name
YYYY	*2009*	Year of survey
CL-MKP	*-C2-MKP*	classification level and Model Key Point identifiers.
DAT	*-ELL or AHD*	Specified vertical datums. Ellipsoidal (ELL) or Orthometric (AHD)
xxxyyyy	*_4806558 (480,000mE) (6558,000mN)*	Easting and northing value (whole kilometre) of the south- west corner of the tile. A single "_" must be used to separate the remaining file name components.
zz	*_56*	MGA zone of the file
wwww	*_0002*	Width of the tile in whole kilometres
hhhh	*_0002*	Height of the tile in whole kilometres
For example: Kempsey2009-CL2-MKP-AHD_4806558_56_0002_0002.las		

ESRI GRID Format
ESRI GRID's have the following constraints which require specific naming conventions:

a. Names cannot be more than 13 characters
b. Names must start with a letter

Due to these constraints the following folder and filenaming convention for ESRI GRIDs must be used for both projected and geographic units. It is also important to note that each individual ESRI GRID must be stored within a standardised folder structure consistent with the following convention to provide appropriate project information to easily associate the ESRI GRID's with the other files from which they may have been derived.

Separate folder structures for GDA and MGA projections are required in addition to each Product Type specified (e.g. DEM, DSM). <u>All ESRI GRIDS must also have all necessary projection definitions populated.</u>

The following folder structure may be used as a guide for GDA and MGA datasets. The folder structure may change slightly to suit requirements, and should be confirmed with CSIRO at project commencement.

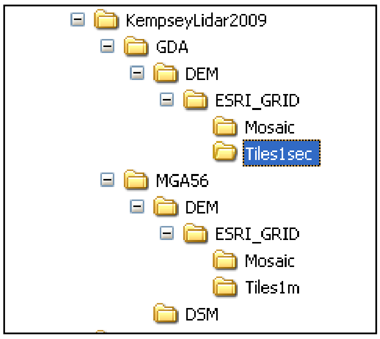

Naming Convention for tiled MGA ESRI GRIDS: *txxxyyyyssppp* *(in addition to folder structure above with MGA GRIDS stored in separate folders, with all projection information defined.)*		
t = surface type.	*e*	Surface type □ s – digital Surface model (DSM) □ e – digital Elevation model (DEM) □ f - canopy Foliage model (CFM) □ c - Canopy elevation model (CHM) □ h – Hydro digital elevation model (DEMH) □ b – Bathymetry □ m – Bathymetry and terrain elevations □ t – Derived terrain variables (add as necessary)
xxxyyyy	*6458595* (645,000mE) (8,595,000mN)	□ Easting and northing value (whole kilometre) of the south- west corner of the tile.
ss	*01*	Tile size (km) (square tile) □ 01 – one kilometre □ 02 – two kilometre □ 05 - five kilometre □ 10 – 10 kilometre □ _5 (represents half a kilometre)
ppp	*001*	Ground sampling distance (GSD) or pixel size □ 0_5 - half a metre □ 001 – one metres □ 002 – two metres etc
For Example: e645859501001		

<table>
<tr><td colspan="3">Naming Convention for Mosaic (MGA) ESRI GRIDS:
txxxxxxxyyppp
(in addition to folder structure above with MGA GRIDS stored in separate folders, will all projection information defined.)</td></tr>
<tr><td>t = surface type.</td><td>e</td><td>Surface type
- s – digital Surface model (DSM)
- e – digital Elevation model (DEM)
- f - canopy Foliage model (CFM)
- c - Canopy elevation model (CHM)
- h – Hydro digital elevation model (DEMH)
- b – Bathymetry
- m – Bathymetry and terrain elevations
- t – Derived terrain variables (add as necessary)</td></tr>
<tr><td>xxxxxxx</td><td>hunter</td><td>A meaningful description of the total survey area and or sensor, dataset version etc.</td></tr>
<tr><td>yy</td><td>07</td><td>Year of Survey</td></tr>
<tr><td>ppp</td><td>010</td><td>Ground sampling distance (GSD) or pixel size in metres (MGA)
MGA
- 0_5 - half a metre
- 001 – one metres
- 002 – two metres etc</td></tr>
<tr><td colspan="3">For Example: ehunter07010</td></tr>
</table>

Naming conventions for other files

The following naming conventions should be used for other file types and formats that may be specified as deliverables.

Naming Convention for all other MGA files: *ProjectNameYYYY-SSSS-PPPP-GSD_xxxyyyy_zz_wwww_hhhh.asc*		
ProjectName	*KempseyLidar*	A meaningful description of the total survey area of interest. Do not use "_" as part of the Project Name
YYYY	*2009*	Year of survey
SSSS-PPPP	*-DEM-GRID*	Surface type. □ DSM □ DEM □ HDEM □ CHM □ CFM □ Bathymetry (BAT) □ Mixed (MIX). Bathymetry and terrain elevations □ TTT (Other terrain variables e.g. slope (SLP). Add as necessary. Product type □ Mass points (MASS) □ Breaklines (BRK) □ TIN (TIN) □ GRID (GRID) □ Contours (CON) □ Cross Sections (CROSS) □ Imagery (BIL, TIF, IMG, ECW etc) □ Other Use additional field width and more characters if required.
GSD	*-010*	Ground sampling distance or resolution of product where appropriate. Where GSD is not required producers can extend the surface type and product description field.
xxxyyyy	*_4806558* *(480,000mE)* *(6558,000mN)*	Easting and northing value (whole kilometre) of the south- west corner of the tile. A single "_" must be used to separate the remaining file name components.
zz	*_56*	MGA zone of the file
wwww	*_0020*	Width of the **dataset or tile** in whole kilometres
hhhh	*_0050*	Height of **dataset or tile** in whole kilometres
ext		File extension according to format conventions □ LAS □ xyz ascii format for easting, northing, elevation, intensity □ asc – ESRI ascii GRID format □ shp □ dxf etc
For example: *KempseyLidar2009-DEM-GRID-010_4806558_56_0020_0050.asc*		

Naming Convention for all other GDA files: *ProjectNameYYYY-SSSS-PPPP-GSD_xxxxyyy_wwww_hhhh.ext*		
ProjectName	*SwanCoastLidar*	A meaningful description of the total survey area of interest. Do not use "_" as part of the Project Name
YYYY	*2009*	Year of survey
SSSS-PPPP	*-DEM-CON*	Surface type. - DSM - DEM - HDEM - CHM - CFM - Bathymetry (BAT) - Mixed (MIX). Bathymetry and terrain elevations - TTT (Other terrain variables e.g. slope (SLP). Add as necessary. Product type - Mass points (MASS) - Breaklines (BRK) - TIN (TIN) - GRID (GRID) - Contours (CON) - Cross Sections (CROSS) - Imagery (BIL, TIF, IMG, ECW etc) - Other Use additional field width and more characters if required.
GSD	*20cm*	Ground sampling distance or resolution of product where appropriate. Where GSD is not required producers can extend the surface type and product description field.
xxxxyyy	*1185324* *(118.5E, 32.4S)*	Lower left ***longitude and latitude*** *(to 1 decimal place)* A single "_" must be used to separate the remaining file name components.
wwww	_0015 (1.5deg)	Width of the **dataset or tile** in whole degrees *(including 1 decimal place)*
hhhh	_0028 (2.8deg)	Height of **dataset or tile** in whole degrees *(including 1 decimal place)*
ext	*shp*	File extension according to format conventions - LAS - xyz ascii format for easting, northing, elevation, intensity - asc – ESRI ascii GRID format - shp - dxf etc
For example:	*SwanCoastLidar2009-DEM-CON20cm_1185324_0015_0028.shp*	

Appendix C – NEDF Metadata Specifications

For each supplied data product a complete metadata statement consistent with the current ANZLIC standard (http://www.anzlic.gov.au/resources/metadata) is required. Additional metadata specific to LiDAR data is also required.

These metadata may be entered via the ANZMET Lite facility for the general description and via the NEDF Metadata entry tool for the LiDAR-specific data. The two tools are integrated to produce one comprehensive entry. The NEDF Metadata Tool is available by contacting elevation@ga.gov.au.

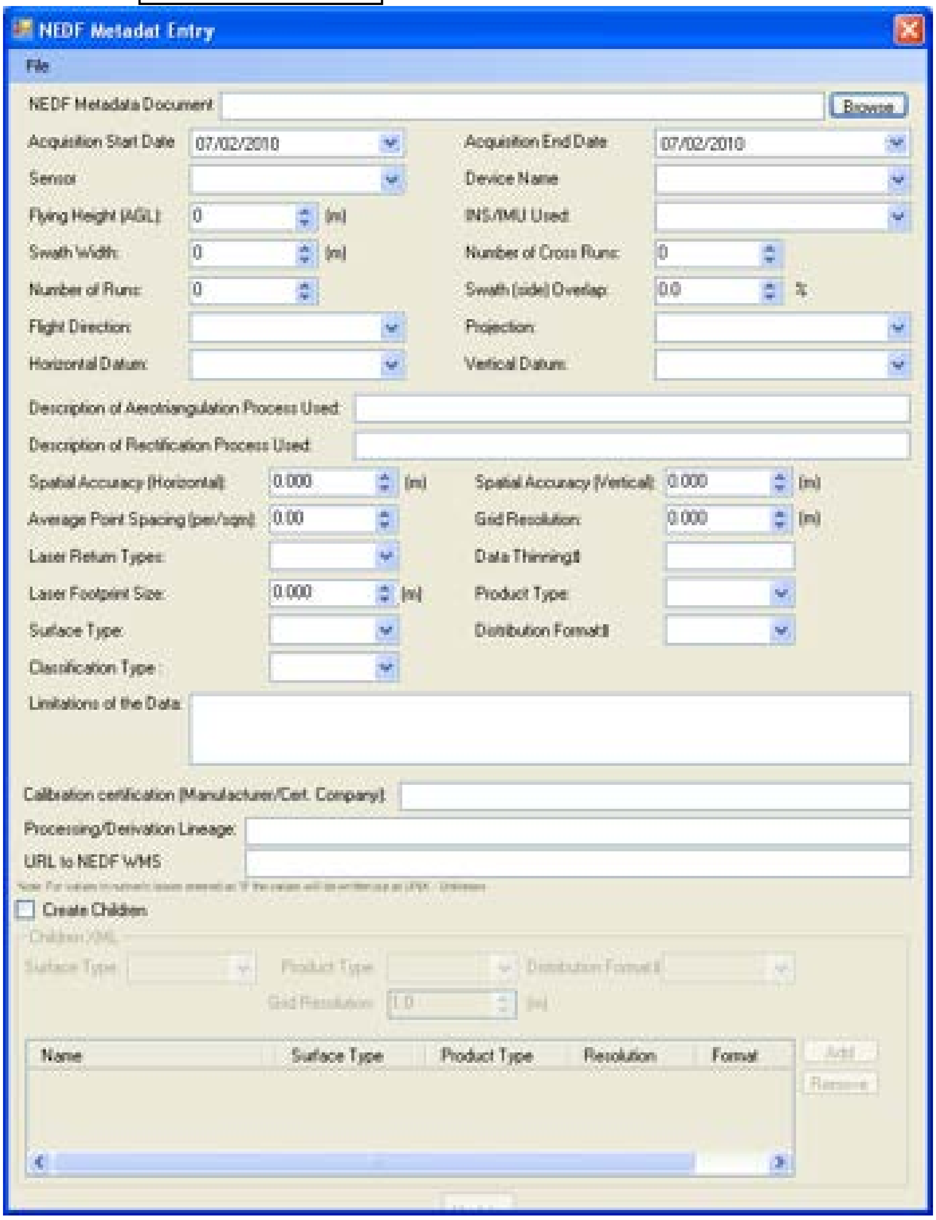

Figure 1 - NEDF Metadata Entry facility

APPENDIX 3. AN EXAMPLE OF THE METADATA SUPPLIED BY THE DATA PROVIDER DESCRIBING THE LIDAR ACQUISITION (AEROMETREX METADATA_REPORT_ BR01325_LAURA_CREEK);

aerometrex

Metadata - BR01325 Laura Ck

Generated: 2019-11-28 04:18:36GMT

Metadata Table - Full Area

	0
Area name	BR01325 Laura Ck
Company name	Aerometrex
Acquisition start date	11/08/2019
Acquisition end date	29/08/2019
Flight count	6
Sensor types	VQ-780i
Sensor calibration_dates	S2222940: 25/07/2019, H2223370: 06/09/2019
Camera types	RIEGL-CS6
Camera calibration dates	YC030345: 25/07/2019,YC030228: 06/09/2019
Horizontal datum	Geocentric Datum of Australia 1994 (GDA94)
Vertical datum	Australian Height Data (AHD)
Map projection	Map Grid of Australia (MGA) Zone 55
Number of runs	86
Run direction	N-S
Number of frames	7147
Cross runs - total	32
Average ppsm	All returns 44.15, last only 29.62
Average point spacings, along and across	All returns 0.15, last only 0.18
Swath agreement accuracy	<5cm
Laser return types	Type(1): 18449456458, Type(2): 7231564223, Type(3): 54361, Type(4): 1242, Type(5): 0, Type(6): 0, Type(7): 0
Laser footprint sizes	For VQ-780i, footprint at altitude 1250m is 0.225, and footprint at altitude 900m is 0.162, and footprint at altitude 1000m is 0.18
Max PDOP	4.01
Max down position error	0.023
GNSS processing methods	RTX
X shift	0.0m
Y shift	0.0m
Z_shift	-0.1499m
Z adjustment RMSE	0.0173

		0
CI95 interval	0.0339	
Ground control points given	29	
Ground control points used	19	
Ground control points excluded	0	
RGB GSD	0.1	
RGB Rectification process	High end commercial photogrammetric software and Aerometrex proprietary software has been utilised in the Ortho Rectification and Mosaicking process. This methodology assists Aerometrex to produce a seamless geo-referenced dataset.	
Rectification - horizontal accuracy	+/-0.30m @ 95% confidence (Sigma 2)	
Rectification - vertical accuracy	+/-0.80m @ 95% confidence (Sigma 2)	
RGB - AT process used	Bundle Adjustment	
RGB - Control points	N/A	
RGB - AT RMSE control points	N/A	
RGB - AT projection centres	N/A	
AT - RMSE	N/A	
Data - Limitations	As per project brief	
Data - Graphic Overview Conditions of Supply	As per project brief	
Data - Conditions of supply	As per project brief	

Metadata for Flight date: 2019-08-11

Generated: 2019-11-28 04:18:41GMT

Metadata Table - single flight

	0
Date of flight	2019-08-11
Start time	08:35:43
End time	13:02:11.732
Scanner type	VQ-780i
Scanner serial	S2222940
INS type IMU name	Applanix POS AV/LV/MV
IMU serial	9233
Camera type	RIEGL-CS6
Camera serial	YC030345
Columns	11608
Rows	8708
Resolution	100MP
Forward overlap	70%
Side overlap	35%
Captured GSD	0.1
Swath width	Not calculated
Number of runs	30
Number of frames	1781
Flying height	['1000m']
Laser frequency	['200lps']
Wavelength	1068nm
Laser power	['100%']
Scan rate	['200lps']
Calibration date	25/07/2019
Flying speed(kts)	['135kn']
Run direction	8 swaths in direction SW-NE, 7 swaths in direction N-S, 7 swaths in direction W -E, 7 swaths in direction NE-SW, 1 swaths in direction E-W
Min scan angle	24
Max scan angle	40
Density, all returns	13.91

	0
Density, last returns	7.98
Base station list	RTX
Solution type	RTX
Maximum PDOP	<3.0
Down position error max	0.023

aerometrex

Metadata for Flight date: 2019-08-21

Generated: 2019-11-28 04:18:39GMT

Metadata Table - single flight

	0
Date of flight	2019-08-21
Start time	10:22:51
End time	13:14:19.977
Scanner type	VQ-780i
Scanner serial	S2222940
INS type IMU name	Applanix POS AV/LV/MV
IMU serial	9233
Camera type	RIEGL-CS6
Camera serial	YC030345
Columns	11608
Rows	8708
Resolution	100MP
Forward overlap	70%
Side overlap	35%
Captured GSD	0.093
Swath width	Not calculated
Number of runs	19
Number of frames	1057
Flying height	['900m']
Laser frequency	['208lps']
Wavelength	1068nm
Laser power	['50%']
Scan rate	['208lps']
Calibration date	25/07/2019
Flying speed(kts)	['130knts']
Run direction	10 swaths in direction NE-SW, 8 swaths in direction N-S, 1 swaths in direction S-N
Min scan angle	34
Max scan angle	41
Density, all returns	16.05
Density, last returns	9.72
Base station list	RTX

	0
Solution type	RTX
Maximum PDOP	<3.0
Down position error max	0.023

Metadata for Flight date: 2019-08-22

Generated: 2019-11-28 04:18:40GMT

Metadata Table - single flight

	0
Date of flight	2019-08-22
Start time	07:37:18
End time	12:20:07.522
Scanner type	VQ-780i
Scanner serial	S2222940
INS type IMU name	Applanix POS AV/LV/MV
IMU serial	9233
Camera type	RIEGL-CS6
Camera serial	YC030345
Columns	11608
Rows	8708
Resolution	100MP
Forward overlap	70%
Side overlap	35%
Captured GSD	0.093
Swath width	Not calculated
Number of runs	28
Number of frames	2639
Flying height	['900m']
Laser frequency	['200lps']
Wavelength	1068nm
Laser power	['50%']
Scan rate	['200lps']
Calibration date	25/07/2019
Flying speed(kts)	['130kn']
Run direction	14 swaths in direction NE-SW, 13 swaths in direction N-S, 1 swaths in direction SW - NE
Min scan angle	33
Max scan angle	38
Density, all returns	12.93
Density, last returns	9.12

	0
Base station list	RTX
Solution type	RTX
Maximum PDOP	<3.0
Down position error max	0.023

Metadata for Flight date: 2019-08-22

Generated: 2019-11-28 04:18:42GMT

Metadata Table - single flight

	0
Date of flight	2019-08-22
Start time	13:40:02
End time	16:43:16.807
Scanner type	VQ-780i
Scanner serial	S2222940
INS type IMU name	Applanix POS AV/LV/MV
IMU serial	9233
Camera type	RIEGL-CS6
Camera serial	YC030345
Columns	11608
Rows	8708
Resolution	100MP
Forward overlap	70%
Side overlap	35%
Captured GSD	0.093
Swath width	Not calculated
Number of runs	16
Number of frames	1669
Flying height	['900m']
Laser frequency	['200lps']
Wavelength	1068nm
Laser power	['50%']
Scan rate	['200lps']
Calibration date	25/07/2019
Flying speed(kts)	['130kn']
Run direction	8 swaths in direction NE-SW, 7 swaths in direction N-S, 1 swaths in direction SW -NE
Min scan angle	35
Max scan angle	41
Density, all returns	12.44
Density, last returns	9.15
Base station list	RTX

	0
Solution type	RTX
Maximum PDOP	<3.0
Down position error max	0.023

aerometrex

Metadata for Flight date: 2019-08-24

Generated: 2019-11-28 04:18:43GMT

Metadata Table - single flight

	0
Date of flight	2019-08-24
Start time	10:55:04
End time	13:29:17.242
Scanner type	VQ-780i
Scanner serial	S2222940
INS type IMU name	Applanix POS AV/LV/MV
IMU serial	9233
Camera type	RIEGL-CS6
Camera serial	YC030345
Columns	11608
Rows	8708
Resolution	100MP
Forward overlap	70%
Side overlap	35%
Captured GSD	0.093
Swath width	Not calculated
Number of runs	13
Number of frames	906
Flying height	['900m']
Laser frequency	['200lps']
Wavelength	1068nm
Laser power	['50%']
Scan rate	['200lps']
Calibration date	25/07/2019
Flying speed(kts)	['130kn']
Run direction	6 swaths in direction N-S, 6 swaths in direction NE-SW , 1 swaths in direction SW-NE
Min scan angle	35
Max scan angle	7
Density, all returns	12.83
Density, last returns	9.47
Base station list	RTX

	0
Solution type	RTX
Maximum PDOP	1.64
Down position error max	0.023

aerometrex

Metadata for Flight date: 2019-08-29

Generated: 2019-11-28 04:18:39GMT

Metadata Table - single flight

	0
Date of flight	2019-08-29
Start time	09:40:02
End time	13:27:26.691
Scanner type	VQ-780i
Scanner serial	H2223370
INS type IMU name	Applanix POS AV/LV/MV
IMU serial	18012
Camera type	RIEGL-CS6
Camera serial	YC030228
Columns	11608
Rows	8708
Resolution	100MP
Forward overlap	70%
Side overlap	35%
Captured GSD	Frames not captured
Swath width	Not calculated
Number of runs	6
Number of frames	0
Flying height	['1250m']
Laser frequency	['180lps']
Wavelength	1068nm
Laser power	['100%']
Scan rate	['180lps']
Calibration date	06/09/2019
Flying speed(kts)	['135kn']
Run direction	4 swaths in direction N-S, 1 swaths in direction W -E, 1 swaths in direction E-W
Min scan angle	33
Max scan angle	36
Density, all returns	11.79
Density, last returns	6.61
Base station list	RTX

	0
Solution type	RTX
Maximum PDOP	<3.0
Down position error max	0.023

APPENDIX 4. AN EXAMPLE OF THE CSIRO METADATA ACCOMPANYING THE LIDAR AND DERIVED DEM DATA FOLLOWING CSIRO QA ANALYSES (REEF TRUST LIDAR 2018 QA PRODUCTS – FITZROY AREA).

Reef Trust lidar 2018 QA products – Fitzroy area

Dataset citation

Title: Reef Trust lidar collection 2018 QA products – Fitzroy Area

Description

Abstract:

Lidar data was collected for Reef Trust by Atlass Aerometrex during June and July 2018, with CSIRO as the project manager. The data was acquired at a target density of 16 points per square metre. Aerial imagery was collected during July 2018 in separate flights.

CSIRO conducted a quality assessment on the lidar data and derived the products comprising this dataset from the supplied raster and point data to support that assessment.

Geographic bounding box:

North bounding latitude: -23.27°
South bounding latitude: -23.63°
East bounding longitude: 150.35°
West bounding longitude: 149.80°

Data currency

Lidar data for the Fitzroy area was collected in June and July 2018. Derived products were produced over the period December 2018 to May 2019. Following the quality assessment some data was re-processed by Atlass Aerometrex and re-supplied in 2019.

Dataset status

Progress: Complete as at 30 September 2019

Maintenance and update frequency: None anticipated.

Reference system: Horizontal datum GDA94. Vertical datum AHD.

Access

Data format: Raster data in GeoTIFF format at 0.5 m and 1.0 m resolution. Counts are integer data and elevations are floating point.

Access constraints: (To be confirmed with Reef Trust – Creative Commons is suggested)

Data quality

Lineage:

Lidar data was collected by Atlass Aerometrex during June and July 2018. (The business name changed from Atlass to Atlass Aerometrex during the project and subsequently to Aerometrex). Delivered data comprised:

- lidar point data
    - unclassified points by swathe
    - classified points in 1×1 km tiles, with both ellipsoidal and AHD heights
    - model key points (MKP) classified points in 1×1 km tiles, with both ellipsoidal and AHD heights
- digital elevation model (DEM) at 0.5 m resolution in 1×1 km tiles derived from points classified as ground
- digital surface model (DSM) at 1 m resolution in 1×1 km tiles derived from first return points
- lidar intensity images at 1 m resolution in 1×1 km tiles and as a mosaic from first return points
- RGB imagery acquired separately to the lidar data at 0.15 m resolution
- Flight lines and tile outlines as shapefiles

CSIRO undertook quality assurance on the supplied lidar data and derived a series of raster datasets to support that assessment.

Rasters derived by merging tiles delivered by the lidar supplier:

- Fitzroy_DEM_0m5.tif
- Fitzroy_DSM_1m.tif

Rasters derived from LAS points at 0.5 m resolution:

- MinZ – the minimum elevation of any point within each 1 m cell regardless of classification but excluding those classified as noise
    - Fitzroy_MinZ_0m5.tif

Rasters derived from LAS points at 1 m resolution:

- Ground count – the number of points classified as ground within each 1 m cell
    - Fitzroy_groundcount_1m.tif
- Pulse count – the number of last returns of any classification within each 1 m cell
    - Fitzroy_pulsecount_1m.tif
- The standard deviation of ground point heights within each 1 m cell
    - Fitzroy_stddev_1m.tif

Rasters calculated from other rasters:

- The MinZDOD rasters were calculated as MinZ - DEM and were used to detect the misclassification of points at abrupt edges, such as steep channel banks and the edges of gullies. A small positive value of MinZDOD occurs where the DEM is below the lowest lidar elevation and is a potential indication that points at the top of the bank have classified as vegetation instead of ground.
    - Fitzroy_MinZDOD.tif
- Hillshades were derived using illumination from two directions to support examination of the surface structure:
    - Fitzroy_SHD45_0m5.tif
    - Fitzroy_SHD315_0m5.tif

Positional accuracy:

The lidar data on which these products are based has a positional accuracy of better than +/-80 cm at 95% confidence interval. Comparison of points against surveyed building edges shows no detectable positional error.

Attribute accuracy:

The lidar data on which these products are based has a vertical accuracy of better than +/-20 cm at 95% confidence interval. Ground control survey determined the RMSE to be less than 5 cm.

Contact information

Technical contact:

Dr John Gallant
CSIRO Land and Water
GPO Box 1700
Canberra ACT 2600

Telephone: +61 2 6246 5734

Email: John.Gallant@csiro.au

Metadata information

Metadata date: 30 Sep 2019

Reef & Rainforest
RESEARCH CENTRE

www.nesptropical.edu.au